The Role of miR-155 in Myeloid cells during Experimental Autoimmune Encephalomyelitis

Thesis submitted to the

University of Dublin

For the

Degree of Doctor in Philosophy

By

Victoria Lyons

School of Biochemistry and Immunology

Trinity Biomedical Sciences Institute

Trinity College Dublin

Ireland

Word count 86238

Submitted 2020

Declaration

I declare that this thesis has not been submitted as an exercise for a degree at this or any other university and it is entirely my own work.

Or: for the exception of:

Figure 4.9 contained intracellular staining of BMDMs for iNOS and CD206. Dr. Natalie Payne contributed to experimental work and I performed FACs analysis.

Figures 5.15, 5.16, and 5.17 contained H&E and immunofluorescent staining on spinal cord sections which was performed by the Histology Platform at Monash University, however imaging and descriptive analysis were performed by Dr. Natalie Payne and myself.

I agree to deposit this thesis in the University's open access institutional repository or allow the library to do so on my behalf, subject to Irish Copyright Legislation and Trinity College Library conditions of use and acknowledgement.

Victoria Lyons

Acknowledgements

I would like to first and foremost acknowledge and thank my two supervisors Claire and Natalie for their dedicated time and guidance put into helping me complete this research project. Claire, thank you for offering me this amazing opportunity of undergoing a PhD candidature in the beautiful city of Melbourne and being such a supportive mentor. Natalie, thank you for taking me on as your student and always being available for encouragement. Thanks for all the hard work, time, and patience behind the making in this thesis, and for all the work that this thesis cannot translate. This project would not have been possible if it wasn't for the constant support and guidance from you both, and I couldn't have asked for better aspiring advisors that remind me of why I got into science to begin with.

I would like to thank everyone at the Hudson Institute of Medical Research past and present, Professor Bryan Williams, Tony, Howard, Die, Charlotte, Gen, Jonathon, Michael, Niamh, Nollaig, Dakang, Christy, and Xiao Fang, for making this journey so memorable. From gaining extremely helpful advice to helping me out during those chaotic experimental days and nights. I would also like to give a special thank you to Jen, for being there as mentor as much as friend who would make any stressful time seem better. I would additionally like to thank Dave at Trinity Biomedical Sciences Institute for being an available mentor for any inquires and support.

Although I spent the final parts of my PhD at ARMI, they are just as memorable to me as my time spent at the Hudson. Thank you to Professor Claud Bernard and Professor Andras Nagy for making my stay at ARMI possible. I would like to especially thank Guizhi for all your amazing work ethic and help with experiments, your amazing lab technique cannot be faulted, and any student would be lucky to shadow you. Thank you to the past Nagy lab members, Jean and Kathy, who were there for support during those final experimental days. While spending time writing this thesis in the office, I would like to thank the Nagy lab members that was there for me to simply chat, grab coffee, or laugh at the most ridiculous things, basically keeping me sane while writing! Laurie, Krystal, Mehri, Phuong, and Henry, thank you all!

I would next like to thank my family for their unconditional words of support and empowerment throughout this journey. Mam, Dad, Nanny, Grandad, thank you for being tech-savvy and calling me using your internet at all hours of the night, keeping me on track, and making sure I was still going to visit you that year. Thank you for giving me the courage to complete this Chapter in my life.

I would of course like to thank my biggest rock who I was lucky enough to meet after landing in this city only a couple of months. Nicholas, thank you for pushing me through times when I needed extra help, for putting up with me when I knew I was being unreasonable because my data wasn't perfect, and for the millions of phone call minutes during the commute and lunch runs. Your encouragement and support throughout this PhD helped me more than you know.

This research project was funded by the NHMRC, MS Research Australia, Health Research Board, and Marie Curie Cancer Care.

Summary

Multiple Sclerosis (MS) is a chronic autoimmune disease of the central nervous system (CNS) characterised by multifocal demyelinating lesions with associated neuronal damage. Although MS is a $CD4^+$ T cell-mediated disease, myeloid cells, including microglia and monocyte-derived macrophages, have recently garnered significant attention for their dual role in both sustaining chronic neuroinflammation and promoting tissue repair. Understanding the molecular mechanisms that regulate the plasticity of these cells is essential to exploiting their regenerative abilities in a therapeutic setting. The microRNA (miRNA) miR-155 has a known role in regulating macrophage plasticity through promoting a proinflammatory polarisation state, however its exact role in MS or its animal model is not yet fully elucidated. The aim of this project is to investigate the role of miR-155 in an animal model of MS and determine whether miR-155 deletion in macrophages skew their polarisation towards an anti-inflammatory phenotype with reparative abilities.

Experimental Autoimmune Encephalomyelitis (EAE) is a well-established murine model of MS used to investigate immunopathological mechanisms of disease. Findings from this research project using wild type (WT) EAE mice revealed an induction of miR-155 in myeloid cells, in particular macrophages, within the CNS. Importantly, miR-155 induction correlated with expression of inflammatory genes during the clinical onset of disease, suggesting miR-155 is required for polarisation towards a proinflammatory tissue-destructive phenotype.

To confirm miR-155 is required for proinflammatory polarisation of macrophages, novel miR-$155^{fl/fl}$ x LysMCre mice were generated where miR-155 was deleted in immune cells of the myeloid lineage. *In vitro* studies using two separate macrophage populations, bone marrow derived macrophages (BMDMs) and peritoneal macrophages, established that miR-155 deletion attenuated expression of the proinflammatory marker, iNOS, whilst promoting anti-inflammatory genes, such as ARG1 and ARG2. Collectively, *in vitro* findings indicated miR-155 deletion promoted macrophages exhibiting an anti-inflammatory phenotype.

The importance of miR-155 in myeloid cells during EAE was highlighted when miR-155$^{fl/fl}$ x LysMCre mice immunised with a reduced rMOG dose resulted in a delayed onset of clinical scores, reduced disease severity, atypical EAE, or in some cases disease resistance. Histological analysis of miR-155$^{fl/fl}$ x LysMCre spinal cords revealed immune cell accumulation surrounding the meninges with attenuated parenchymal infiltration, with infiltrating macrophages and activate microglia appearing to co-express iNOS and ARG1 at sites of spinal cord inflammation. Collectively, *in vivo* studies supported the potential of ameliorating EAE severity through deleting miR-155 from myeloid cells.

Overall, data generated in this research project supports a role for miR-155 in regulating macrophage plasticity by promoting a proinflammatory phenotype associated with CNS demyelination. Targeting miR-155 may therefore provide a novel strategy to promote CNS repair through harnessing reparative capabilities of macrophages.

Table of Contents

List of Figures

List of Tables

List of Abbreviations

α-HSCT	α-hematopoietic stem cell transplantation
APC	antigen presenting cell
ARG1	arginase 1
ARG2	arginase 2
BBB	blood brain barrier
BIC	B-cell integration cluster
BMDM	bone marrow derived macrophages
BSA	bovine serum albumin
CFA	complete Freund's adjuvant
CSF	cerebrospinal fluid
Ct	threshold cycle
Cy	cyanine
DC	dendritic cell
DMEM	dulbecco's modified eagle's medium
DMSO	dimethyl sulfoxide
DMT	disease modifying therapy
DNA	deoxyribonucleic acid
EAE	experimental autoimmune encephalomyelitis
EBV	Epstein-Barr virus
EDTA	ethylenediaminetetracetic acid
ELISA	enzyme-linked immunosorbent assay
EtBr	ethidium bromide
Ets	E-twenty six

FCS	foetal calf serum
FDA	food and drug administration
Fl	flox
FSC	forward scatter
GAPDH	glyceraldehyde 3-phosphate dehydrogenase
GWAS	genome-wide association study
HLA	human leukocyte antigen
IFN	interferon
Ig	immunoglobulin
IL	interleukin
iNOS	inducible nitric oxide synthase
KO	knockout
LPS	lipopolysaccharide
MBP	myelin basic protein
miRNA	microRNA
MOG	myelin oligodendrocyte protein
MRI	magnetic resonance imaging
mRNA	messenger RNA
MHC	major histocompatibility complex
MHV	mouse hepatitis virus
MS	multiple sclerosis
NO	nitric oxide
OPC	oligodendrocyte precursor cells
OL	oligodendrocytes

PAMP	pathogen associated molecular pattern
PBS	phosphate buffered saline
PCR	polymerase chain reaction
PE	phycoerythrin
PLP	proteolipid protein
PR	progressive relapsing
PP	primary progressive
qPCR	quantitative polymerase chain reaction
RISC	RNA induced silencing complex
RR	relapsing remitting
S1P	sphingsine-1-phosphate
SCFA	short-chain fatty acid
scRNA seq	single cell ribonucleic acid sequencing
SDS	sodium dodecyl sulphate
SEM	standard error of the mean
SHIP1	inositol polyphosphate 5-polyphosphatase 1
SnoRNA	small nucleolar RNA
SNP	single nucleotide polymorphism
SP	secondary progressive
SSC	side scatter
STAT3	signal transducer and activator of transcription-3
TCR	T cell receptor
TGF	tumour growth factor
Th	T helper

TLR	toll-like receptor
TMEV	Theilor’s murine encephalomyelitis virus
TNF	tumour necrosis factor
Treg	T regulatory cell
UTR	untranslated region
WT	wild-type

I dedicate this thesis to my parents,

thank you for your unconditional support.

Chapter 1

Introduction

1.1 Multiple Sclerosis

Multiple Sclerosis (MS) is an autoimmune disease of the central nervous system (CNS) mediated by infiltrating immune cells that cause chronic inflammation, demyelination, and neurodegeneration. It is the most common neurological disease amongst young adults, affects females to males at a 4:1 ratio, respectively (Farias *et al.*, 2014), and is associated with a significant socioeconomic burden. Symptoms of MS include intermittent or permanent neurological deficits related to impairment in motor, visual, and sensory abilities, such as numbness, tremors, fatigue and pain (Garg and Smith, 2015).

MS is a heterogeneous disease with respect to clinical course and symptoms. It is classified into four disease courses; relapsing remitting (RRMS), secondary progressive (SPMS), primary progressive (PPMS), and progressive remitting (PRMS) (Martin *et al.*, 2016a). The McDonald criteria is used to diagnose MS and is based on a clinical evaluation, the identification of number and location of CNS lesions as observed by magnetic resonance imaging (MRI), as well as the presence of oligoclonal bands or high immunoglobulin (IgG) in the cerebral spinal fluid (Thompson *et al.*, 2018). Most patients present with relapsing remitting MS (RRMS), a form of MS associated with intermittent relapses of clinical symptoms followed by remittance periods. To date, the majority of disease-modifying therapies (DMTs) are directed towards this form of MS (see Section 1.1.3 and Table 1.1). There are a large proportion of RRMS patients that gradually proceed towards secondary progressive MS (SPMS). Initial diagnosis of SPMS can be difficult, as patients proceeding towards a progressive stage may also be susceptible to relapses, and is usually made retrospectively after accumulation of disability (Lublin *et al.*, 2014). The percentage of RRMS patients proceeding towards SPMS increases with age and duration post RRMS diagnosis. Less frequently, patients are diagnosed with primary progressive MS (PPMS). This form generally affects <10% of MS patients and presents with consistent progressing clinical symptoms with no remittance or attenuating symptom phases. Lastly, the rarest form of MS is categorised as PRMS (progressive relapsing MS) which affects <5% of patients. This form of MS is also difficult to distinguish from other categories, however patients generally undergo infrequent remitting phases and overall present with a progressive disease course (Lassmann, 2017).

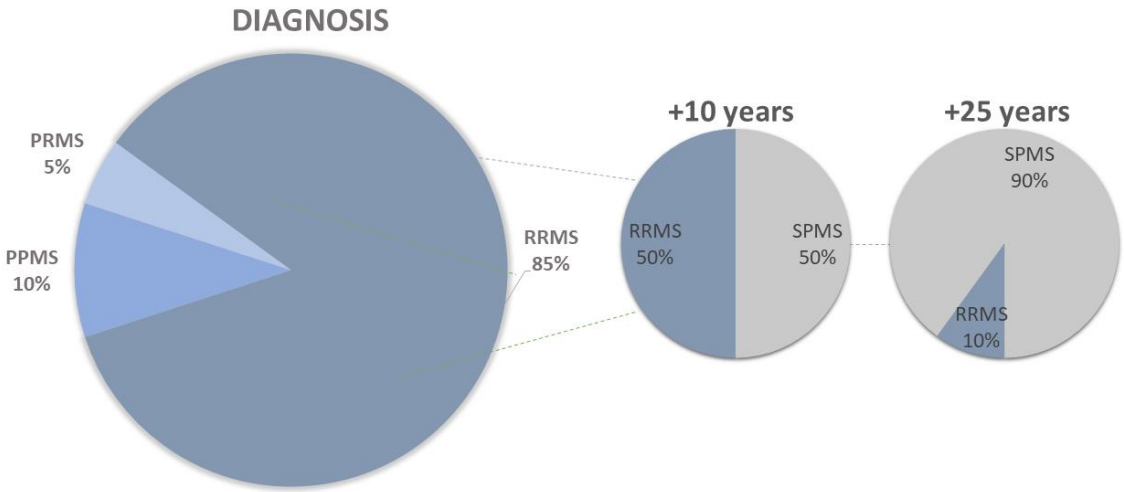

Figure 1.1 Proportion of patients diagnosed with different MS forms: PRMS, PPMS, RRMS, and SPMS. 50% of untreated RRMS patients develop SPMS within 10 years post diagnosis, this proportion increases to 90% within 25 years. Modified from: (Vukusic and Confavreux, 2003; McKay *et al.*, 2015).

1.1.1 MS Etiology

Although the exact etiology of MS is unknown, it is accepted that disease results from complex interactions between genetic and environmental factors (Baecher-Allan, Kaskow and Weiner, 2018).

The genetic basis of MS development is demonstrated by a 20-30% disease concordance in monozygotic twins, and 2-5% increased risk in first-degree relatives (Baecher-Allan, Kaskow and Weiner, 2018). The major histocompatibility complex (MHC) region encoding the human leukocyte antigen (HLA) molecules is the most prominent genetic risk factor in MS. The MHCII complex allele conferring the greatest risk is HL-DRB1*15:01 (Baranzini and Oksenberg, 2017). In contrast, there are known MHCI alleles associated with protection from MS such as; HLA-A*02, and HLA B*44 (Sawcer, Franklin and Ban, 2014), clearly highlighting the importance of MHC and antigen presentation in this inflammatory autoimmune disease. A genome wide association study (GWAS) based on a cohort of

>14,000 MS subjects discovered that there are a total of 110 non-MHC risk variants, including 18 MS risk variants relating to immune cell function outside the MHC loci (Beecham *et al.*, 2013). Low-frequency coding variants with roles in T cell homeostasis and innate immunity were also recently identified, further confirming the importance of the immune system in MS pathogenesis. T cell development was identifiably affected by the low-frequency variant histone deacetylase 7 (HDAC7), whereas innate immunity related low-frequency coding variants include protein activator of interferon induced protein kinase EIF2AK2 (PRKRA) and nod-like receptor family pyrin domain containing 8 (NLRP8), all of which incurred an amino acid change resulting in a missense mutation (Mitrovič *et al.*, 2018). These rare variants, not detectable in GWAS analyses, explain some of the missing heritability of MS and bring the total number of MS risk variants to almost 250. Understanding the effects of these variants and relevance to disease immunopathogenesis will facilitate the identification of disease biomarkers and development of more personalised MS treatments. For example, rs1800693 is a well characterised single nucleotide polymorphism (SNP) within the TNFRSF1A gene encoding tumour necrosis factor (TNF) receptor 1. This risk variant causes soluble TNF receptor production, which inhibits TNF signalling within cells and mirrors the surprisingly negative prognostic outcomes of TNF-blocking therapies (Gregory *et al.*, 2012).

Epidemiological evidence of MS distribution strongly supports the requirement of environmental factors to trigger MS in genetically predisposed individuals. Interestingly, further distances from the equator are associated with an increased risk of MS development. The observational association of latitudinal gradient on MS susceptibility is evident in countries distal from the equator i.e. Northern Europe, USA, and Australia (Hewer et al., 2013). This latitudinal gradient effect suggests MS development is associated with reduced UV exposure leading to vitamin D deficiency and reduced melatonin levels (Kawachi *et al.*, 2018). Since the 1960's, there has been accumulating evidence that higher UV exposure levels are associated with decreased MS risk and disease activity (Hart *et al.*, 2015), but this association could be linked with vitamin D deficiency and non-vitamin D dependent mechanisms. Vitamin D is proposed to assist in reducing the relapsing stages of MS by increasing T regulatory cells (Tregs) whilst inducing tolerogenic dendritic cells (DCs). UV exposure also increases vitamin D, but can additionally upregulate interleukin-10 (IL-10)

production and decrease inflammatory cytokines implemented in MS progression such as interferon-γ (IFN-γ), IL-17, and IL-23, (Hart *et al.*, 2015).

Viral infections are additional environmental risk factors associated with MS. Epstein Barr Virus (EBV) is the most documented infectious agent with the strongest correlation to MS development (Geginat *et al.*, 2017). Molecular mimicry is an established mechanism where pathogenic peptides exhibit similar components to host peptides to evade the immune response. Unfortunately, T cells against self-peptide components may become activated post exposure to pathogenic peptides, resulting in a breakdown of immune tolerance. Viral molecular mimicry has been strongly linked with MS and other autoimmune diseases. In the context of MS, the molecular mimicry between a latency antigen of EBV (EBNA-1) and host myelin sheath component, myelin basic protein (MBP), was established to induce $CD4^+$ T cell cross reactivity against self-myelin antigens (Geginat *et al.*, 2017). This mechanism of cross-reactivity was confirmed when $CD4^+$ T cells derived from MS CNS samples could identify B cells transformed with EBV (Holmøy, Kvale and Vartdal, 2004; Rojas *et al.*, 2018). Additionally, LMP1, an EBV secreted protein is a confirmed viral homologue of CD40, a cell surface protein found on DCs, T and B cells. CD40 is also an MS risk variant, thus highlighting another mechanism as to how EBV can manipulate the immune system and contribute to MS pathogenesis (Afrasiabi *et al.*, 2019).

The gut microbiome evidently plays a crucial role in maintaining a healthy status. Relapsing MS patients reportedly have microbiota dysbiosis, with selective enrichment and depletion of certain bacteria associated with metabolic pathways (Shahi, Freedman and Mangalam, 2017). Furthermore, the permeability of the blood brain barrier (BBB) and intestinal wall is influenced by gut metabolites such as short chain fatty acids (SCFAs). SCFAs are by-products from microbiota and play important roles in regulating immune cell gene expression and limiting oxidative stress (Ochoa-Repáraz, Kirby and Kasper, 2018). Studies using experimental autoimmune encephalomyelitis (EAE), a mouse model that recapitulates some of the autoimmune aspects of MS, have identified several gut microbes that influence disease severity. B. *fragilis* is a protective gut microbe that attenuates $CD4^+$ T cell activity and increases IL-10 producing cells via production of extracellular polysaccharide A, an

immune modulating polysaccharide identified by antigen presenting cells (Cohen-Poradosu *et al.*, 2011). In contrast, there are gut microbiota associated with enhancing the severity of EAE. Lipopolysaccharide (LPS) derived from P. *gingivalis* has been documented to promote neuroinflammation, and segmented filamentous bacterium (SFB) exacerbates EAE by promoting T helper 17 (Th17) cell activation (Nichols *et al.*, 2009). The increasing evidence surrounding the influential role of the gut microbiome on autoimmune diseases could provide novel avenues for microbiome biomarker development.

1.1.2 Immunopathology of MS

Under homeostatic conditions, the CNS is referred as a specialised niche where immune cell access is restricted. Leukocytes patrol the cerebrospinal fluid (CSF) or reside within the blood-CSF barrier and meninges but are absent from the healthy CNS parenchyma. The major CNS resident cell types include neurons, oligodendrocytes, astrocytes, and microglia. Neurons of the CNS comprise of a neuronal body, axon, branched dendrites, and are surrounded by a protective sheath comprising of myelin termed the myelin sheath. During autoimmune diseases of the CNS, neurons are often irreversibly damaged through demyelination processes leading to axonal loss and permanent neuron damage (K. Thompson and Tsirka, 2017). Oligodendrocytes are CNS resident cells that form the myelin sheath through extensions of their plasma membrane, hence its main functional attribute is to protect the axonal body of neurons. Protein components of these cells are targeted in demyelinating diseases resulting in cell death and exposing vulnerable neurons. Astrocytes are the most abundant glial family member and are mainly involved with synapse formation during homeostasis. In the context of MS, astrocytes exert critical functions during lesion development and glial scarring overall contributing to disease progression (Ponath, Park and Pitt, 2018). Microglia are considered the most unique glial cell member as they also are the only resident immune cell in the CNS parenchyma. The role of microglia during homeostatic and diseased states will be discussed further in section 1.3.6.

Immune cell infiltration, demyelinating lesions, axonal loss, neurodegeneration and glial scarring are pathological hallmarks of MS (Ghasemi, Nazemi, 2017., Lazibat, 2018). Current

understanding of lesion formation in MS is largely based on evidence from experimental animal models such as EAE and post-mortem samples from MS patients. The initiation of MS in genetically susceptible individuals is believed to occur when $CD4^+$ T cells are peripherally activated. This upregulates various adhesion molecules and therefore allows these cells to gain entry to the CNS at either subarachnoid vessels, post-capillary venules or the choroid plexus (Larochelle, Alvarez and Prat, 2011a). Antigen presenting cells (APCs) located at CNS borders re-activate $CD4^+$ T cells, a critical step that allows them to cross the glial limitans (Owens, Bechmann and Engelhardt, 2008). The release of inflammatory cytokines and changes in endothelial cells promotes breakdown of the blood brain barrier (BBB), leading to infiltration of peripheral immune cells of the innate and adaptive immune systems along with prolonged microglial activation and astrogliosis. The production of cytokines propagates recruitment and activation of additional inflammatory cells within the CNS parenchyma and establishment of inflammatory demyelinating lesions (Hunter, 2016). Chemotactic gradients allow targeted recruitment to lesion sites (Baecher-Allan, Kaskow and Weiner, 2018). Local inflammation is further promoted by cellular debris, which can result in *in situ* activation of polyspecific T cells recognising multiple antigens alongside epitope spreading leading to de novo priming of T cells (Ramadan *et al.*, 2016).

Demyelination heavily relies on peripheral immune cell infiltration into the CNS. The importance of peripheral immune cells during MS onset and progression is emphasised by histological evidence demonstrating abundant lymphocytes and myeloid cells at lesion sites. Although activated $CD8^+$ cells and B cells are present in lesions, myeloid derived cells such as macrophages and microglia substantially outnumber lymphocytes (Owens, Bechmann and Engelhardt, 2008). Distinct types of inflammation have been observed when comparing acute relapsing MS and patients with prolonged progressive disease duration (Lassmann, 2018). Acute and relapsing MS predominantly exhibits mass infiltration of T and B cells with prominent breakdown of the BBB causing acute and active plaques. In contrast, progressive MS patients predominantly demonstrate slow infiltration and accumulation of $CD8^+$ T cells and B cells with no prominent BBB breakdown, but instead results in formation of tertiary lymph follicle-like structures. CNS lesion types, locations, and inflammatory properties can also be used to distinguish RRMS and progressive MS (Lassmann, 2018). Due to the distinct types of inflammatory processes, it is not surprising that MS therapeutics

effective in RRMS are ineffective in patients with a progressive disease course. Collectively, neurodegeneration strongly correlates with MS patient clinical disability. There is also a direct association of MRI lesions and clinical relapses with enhanced disability in MS patients, however disability severity additionally relies on the location of lesions within the CNS (Goodin *et al.*, 2016). Lucchinetti et al. established a set of criteria utilising neurological markers within active MS lesion biopsies and autopsies, whereby destruction of oligodendrocytes, myelin loss, plaque distribution, and activation of the complement system were among strict criteria for establishing lesions amongst MS patients (Lucchinetti *et al.*, 2000).

Remyelination is the process of regenerating myelin sheaths surrounding axons to provide metabolic support and efficient transduction of signals amongst neurons within the CNS (Chari, 2007). The importance of remyelination is highlighted in a demyelinating disease such as a MS, whereby the accumulation of demyelinating processes and failure of remyelination during disease progression leads to neuronal loss, an occurrence that is strongly associated with enhanced clinical disability. Utilising animal models of MS has identified the critical role oligodendrocyte progenitor cells (OPCs) play in mediating remyelinating processes. OPCs have previously been reported to migrate towards an MS lesion through chemotaxis, prior to undergoing proliferation, differentiation, and maturation into mature oligodendrocytes. Upon transitioning into a mature oligodendrocyte, remyelination can occur around axonal bodies (Miron, Kuhlmann and Antel Jack P., 2011). As myelin sheaths are comprised of mature oligodendrocyte membrane extensions, current MS research and therapy directed towards CNS repair majorly focus on promoting proliferation and differentiation of oligodendrocytes. Several factors can facilitate remyelination, such as altering intrinsic signalling pathways in oligodendrocytes, promoting oligodendrocyte survival, and modulating the extracellular environment within MS lesions (Harlow, Honce and Miravalle, 2015). An example of a recently approved MS therapy previously marketed as an anti-histamine drug is Clemastine. Clemastine has demonstrated potential to assist remyelination through blocking histamine H1 receptor (Kremer *et al.*, 2019). Additional drugs demonstrating potential in promoting OPC differentiation in *in vitro* and *in vivo* studies include IRX4204. IRX4204 reportedly promoted OPC differentiation in addition to supressing CNS inflammation in an EAE model, enhancing the potential of this

drug due to its mechanisms affecting both gliogenesis and the immune response (Chandraratna, Noelle and Nowak, 2016). Collectively, the emergence of successful and promising therapeutics focusing on promoting remyelination holds promise in targeting remyelinating mechanisms mediated by oligodendrocytes.

Compensatory repair mechanisms do exist within the CNS spontaneously that can, to some extent, allow tissue recovery from acute inflammatory demyelinating events. Their failure over time as lesion burden increases leads to the accumulation of neurodegeneration and brain atrophy, and the acquisition of permanent neurological deficits during progressive disease. Repair mechanisms can be confirmed through visual identification of remyelinating lesion sites termed "shadow plaques". Shadow plaques can occur spontaneously in any form of MS, however there is a trend of more aged post-mortem MS samples containing higher proportions of remyelinating plaques. Overall, Patrikios et al. described spontaneous remyelination to be variable amongst MS patients, but estimated 20% of patients demonstrate shadow plaque regions covering 60-96% of total lesion area (Patrikios *et al.*, 2006). Failure to efficiently remyelinate lesions results in accumulative demyelination and axonal loss that collectively corresponds with enhanced clinical disability. Kuhlmann et al. describes acute axonal damage to occur predominantly at initial stages of MS, but APP-positive axons can also be confirmed throughout later stages of disease, highlighting the need to treat axonal damage as early as possible to limit clinical disability (Kuhlmann, 2002).

Ion channels such as sodium, potassium, and calcium, become disrupted during processes of demyelination, ultimately resulting in impaired neuronal signalling, and cell proliferation and differentiation. Due to the pivotal role ion channels play in maintaining CNS homeostasis, repair mechanisms post demyelinating processes include redistributing voltage-gated sodium channels (Chen, Yu and Wei, 2014). In the context of demyelinated neurons during EAE, sodium channels are upregulated which cause further axonal degeneration via disrupting the balance of the sodium-calcium exchanger (NCX) (Alizadeh, Dyck and Karimi-Abdolrezaee, 2015). Studies investigating neuroprotective effects utilising sodium blockers in EAE have generated optimistic results with drugs such as phenytoin, safinamide, flecainide, and lamotrigine. However, when translated into MS patients,

outcomes of using such mechanistic drugs have been limited and contradictory, hence studies targeting voltage-gated sodium channels require further investigation to confirm beneficial effects for MS patients (Zostawa *et al.*, 2017).

Recent studies have revealed the previously unrecognised heterogeneity of glial cells and have begun to more precisely define their role in neuroinflammatory and neurodegenerative diseases such as MS. Astrocytes and Oligodendrocytes are such CNS cell populations now recognised as important mediators during demyelinating diseases.

Astrocytes are abundant within the CNS and provide essential functions relating to neuronal trophic support and assisting with homeostatic maintenance (Liddelow *et al.*, 2017). Liddelow et al. describe the ability of astrocytes to polarise towards proinflammatory and anti-inflammatory phenotypes, similar to macrophages although not as complex or studied as thoroughly. Astrocytes demonstrating proinflammatory properties are described as A1, whereas astrocytes demonstrating anti-inflammatory and neuroprotective properties are termed A2. A1 astrocytes can exert direct neurotoxicity towards retinal ganglion cells, display a reduction in phagocytosis abilities, and most importantly decrease the rate of OPC proliferation and differentiation and facilitate neuronal death. Furthermore, reactive microglia have been documented to induce A1 astrocytes through production of proinflammatory cytokines TNF and IL-1α, and complement component C1q (Liddelow *et al.*, 2017). Collectively, Liddelow suggests A1 astrocytes assist in demyelinating processes and neuron death in neuroinflammatory diseases like MS, whilst highlighting the influential role of microglia in astrocyte mediated neurotoxicity. More specifically, Rothhammer et al. confirmed microglia production of TGF-β and VEGF-B by microbial metabolite exposure could modulate cytotoxic effects of astrocytes via aryl hydrocarbon receptor signalling in the context of EAE, overall attenuating inflammation (Rothhammer *et al.*, 2018).

Gene expression analysis focusing on astrocytes in a region-specific manner within the CNS using RiboTag technology determined cholesterol synthesis is potentially involved in the

pathogenesis of EAE, specifically within optic nerve regions as opposed to the spinal cord. This finding collectively emphasises that astrocytes exert different functions depending on their location, suggesting therapies targeting astrocytes should ideally be region specific (Itoh *et al.*, 2018). Genetic predisposition to MS susceptibility is known to comprise of risk variants within HLA allele regions. Recently, Poneth et al. confirmed an additional risk variant rs7665090^{G} located near the NFKB1 gene within astrocytes (Ponath *et al.*, 2018). This particular risk variant has reportedly positive associations with enhancing peripheral immune cell infiltrates into the CNS through skewing astrocyte function (Ponath *et al.*, 2018). Overall, Ponath demonstrates an astrocyte specific risk variant can impact lymphocyte recruitment into the CNS, lymphocyte proportions in MS lesions, and actual lesion size, highlighting the overlapping role of these CNS cells with peripheral leukocytes during immunopathogenic processes of MS.

Oligodendrocytes (OLs) are a post-mitotic differentiated glial cell type that play crucial roles in protecting neurons. Their development and differentiation from OPCs relies on multiple intrinsic and extrinsic signalling pathways (Galloway and Moore, 2016). During homeostatic conditions, they prevent axonal damage and maintain efficient signal conduction between neurons via formation of the myelin sheath (Biphenyls, 2015). In their mature and differentiated state, OLs have the ability of remyelination and repairing neuronal damage, however it has been shown post injury in adult CNS and during MS, remyelination is dependent on the migration of OLs precursor cells, oligodendrocyte progenitor cells (OPCs), to sites of inflammation or lesions. Migration is enhanced in acute lesions but is documented to be down-regulated in chronic inflammatory MS lesions (Antel *et al.*, 2018). Immune cell members of both the innate and adaptive immune system can influence the remyelination process by directly impacting OPC migration and OL differentiation. Microglial production of TNF-α reportedly affects human OPCs, resulting in neurotoxicity. Contrastingly, neurotrophic factors previously established to be produced by CNS resident cells, have now also been shown to be produced by infiltrating myeloid cells and lymphocytes (Rittchen *et al.*, 2015; Tsiperson *et al.*, 2015).

OLs have recently been identified to assist in providing metabolic support to axons in addition to facilitating saltatory production. In contrast, Flacao et al. additionally confirmed a novel subset of OLs and OPCs that may assist in activating of the adaptive immune response that facilitates demyelinating processes (Falcão *et al.*, 2018), overall identifying distinct subsets of OLs and OPCs involved in the pathogenesis of EAE. Jakel et al. further corroborated the diversity of oligodendrocytes by demonstrating the existence of a heterogeneous oligodendrocyte population in MS patients via single-nucleus RNA sequencing. Collectively, Jakel identified alterations to subpopulations of oligodendrocytes during MS, some of which show similar functionalities as mouse OLs. A loss of a specific mature oligodendrocyte population was observed whereas others were unaffected. Understanding oligodendrocyte heterogeneity and their functional differences will therefore be important for successful remyelinating MS therapies (Jäkel *et al.*, 2019). Furthermore, Yeung et al. strongly suggested existing mature oligodendrocytes are responsible for remyelinating processes as opposed to newly proliferative and differentiated OPCs. This suggestion was evidenced by the lack of new oligodendrocytes within shadow plaque regions in the majority of MS patients, whereby only a minority subcategory with aggressive MS displayed an increase of oligodendrocyte generation in white matter regions (Yeung *et al.*, 2019).

Detrimental roles of OPCs in promoting inflammation and immune cell infiltration into the CNS is highlighted by a study focusing on the involvement of the CNS vasculature system with OPCs. Nui et al. identified a defect in OPC migration towards lesion sites, an important process for remyelination to occur, and confirmed clustering of OPCs at perivascular regions within the parenchyma of MS patients, demonstrating an inability to detach from perivascular sites. Defective migration of OPCs from vascular regions towards lesion sites indirectly leads to enhanced BBB permeability, and failure to efficiently remyelinate lesion tissue. Furthermore, non-migratory clustered OPCs have shown to secrete Wif1, a molecule known to interfere with tight junction integrity, therefore further facilitating BBB breakdown and peripheral immune cell infiltration (Niu *et al.*, 2019).

Immune cells are not the only factors affecting OL differentiation and remyelination, as miRNAs such as miR-219 and miR-388 have recently emerged to play influential roles

within the CNS (Barca-Mayo and Richard Lu, 2012). MiRNAs such as the established innate immune cell mediator miR-146a, has increased expression levels within the brain post-stroke *in vivo* alongside being associated with promoting MBP+ OLs *in vitro* (Galloway and Moore, 2016). Although there is emerging literature discussing an array of miRNAs influential roles in promoting OL development and differentiation, there is limited information directly on miR-155 with OLs or OPCs in the context of MS or EAE.

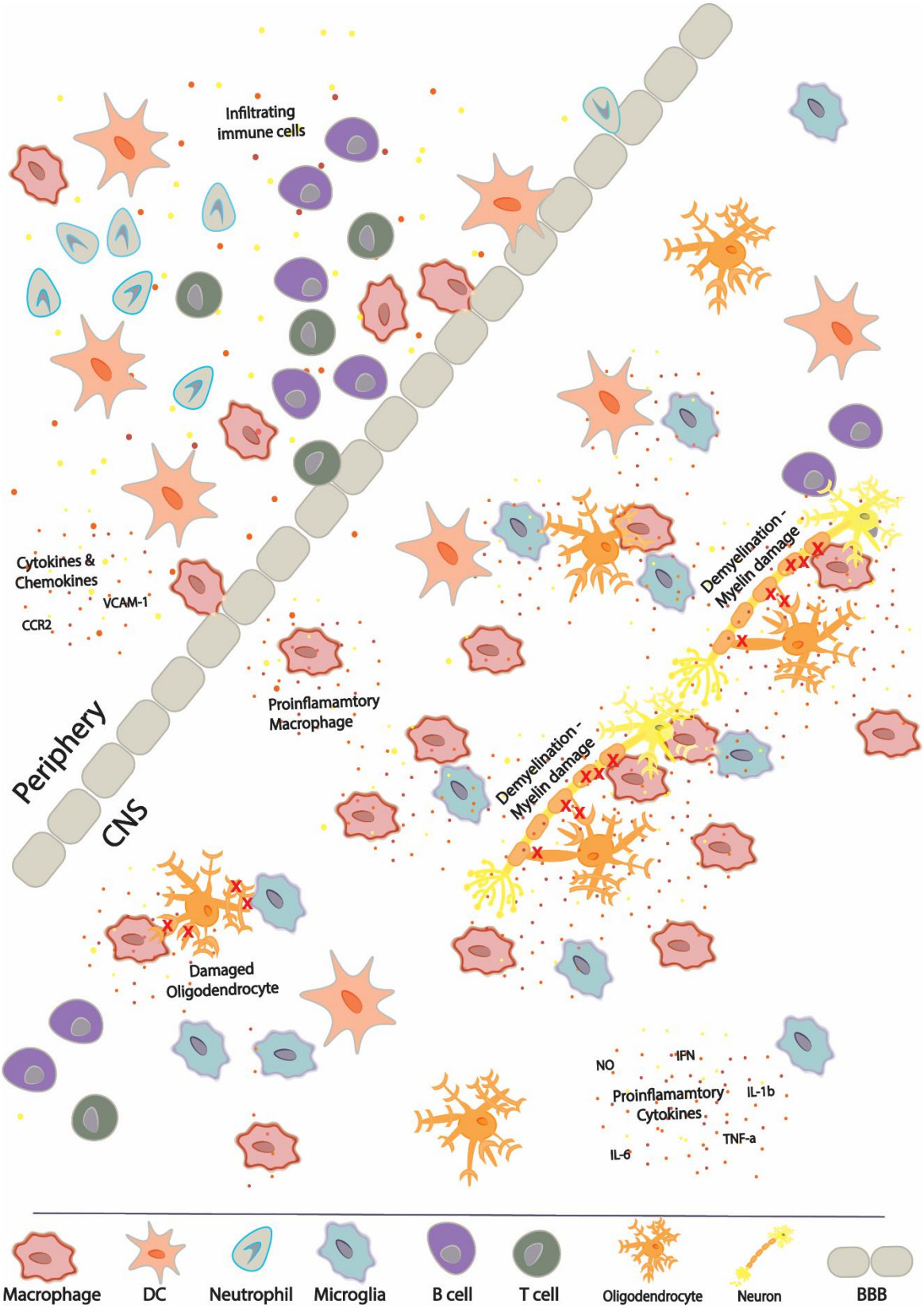

Figure 1.2 The immunopathology of MS. Peripheral immune cells infiltrate the CNS by breaching the BBB. Macrophages become polarised towards a proinflammatory phenotype, produce inflammatory cytokines and NO which ultimately contributes to oligodendrocyte loss, demyelinating processes, and lesion formation.

Although the etiology of MS is complex and much remains unelucidated, chronic inflammation mediated by immune cell activation within the CNS is a confirmed process for disease establishment. Immune cell populations are known to infiltrate the CNS from the periphery and cause demyelinating processes by either direct or indirect mechanisms, however whether MS is initiated by immune cell activation from within the CNS or initiated by periphery infiltrates is not yet understood (Dendroue CA, Fugger L, 2015). Specific mechanisms of infiltrating and CNS resident immune cell subsets involved in the immunopathogenesis of MS will be discussed in further detail in Section 1.3.

1.1.3 Current therapeutics for MS

Table 1.1 describes the mechanisms of action for the 12 Food and Drug Administration (FDA) approved disease-modifying therapeutics (DMTs) for MS. All current DMTs excluding Ocrelizumab are only appropriated for RRMS. These DMTs are mostly aimed at modulating or suppressing inflammation to preventing further relapses, by inhibiting immune cell infiltration into the CNS (Natalizumab, Fingolimod, Mitoxantrone, Siponimod), inhibiting immune cell activation (Glatiramer Acetate, IFN-β, Teriflunomide) or depleting T and B cell populations (Ocrelizumab, Cladribine, Alemtuzumab). However, most RRMS DMTs are ineffective in progressive forms of MS, highlighting the importance of elucidating immunopathological mechanisms driving progressive disease stages.

IFN-β was FDA approved and utilised as a first line treatment for MS since 1993. It was the first DMT approved for MS immunotherapy and elicits several non-specific target effects on immune cells. IFN-β has been noted to alter antigen presenting co-stimulatory molecules on myeloid cells and inhibit chemokine CCL7 and metallopeptidase 9 (MMP-9) on dendritic cells. Overall, this type 2 interferon prevents myeloid cell migration into the CNS and limits reactivation of encephalitogenic T cells (Martin *et al.*, 2016b).

Glatiramer acetate was first approved in 1996 for the treatment of RRMS (Weinstock-Guttman *et al.*, 2017). Glatiramer acetate appears to exhibit a strong binding affinity to MHC

molecules, resulting in a reduction in presentation of myelin specific components to T cells due to competition with glatiramer acetate. Upon binding of glatiramer acetate with MHC molecules, differentiation of Th2 responses and a reduction of TNF-α producing cells have also been recorded (Schrempf and Ziemssen, 2007).

Mitoxantrone is a synthetic anthracenedione that was FDA approved in 2000 for MS treatment. It was the first DMT directed towards treating SPMS along with attenuating relapsing forms of MS. The mechanism of action for mitoxantrone is quite broad compared to other approved DMTs, as it exerts anti-proliferative properties against T cells, B cells, and macrophages, and inhibits production of cytokines such as IFN-γ and TNF-α. Additionally, there have been reports of mitoxantrone supressing myelin destruction by macrophages, whilst supressing B cell function and promoting T cell differentiation towards suppressive phenotypes (Fox, 2004).

Natalizumab was approved for the treatment of MS in 2004 by the FDA. Natalizumab is a monoclonal antibody with binding affinity towards leukocyte integrins, α4β1 and α4β7. Through binding of natalizumab to α4β1 and α4β7, leukocyte adhesion and infiltration into the CNS is supressed, thus limiting immune cell tracking into the CNS to prevent neuroinflammation (Sellebjerg *et al.*, 2016).

Fingolimod was FDA approved for MS therapy in 2010 for adult use, and 2018 for children between the ages of 10 to 18 years old. Fingolimod is a synthetic compound analogue of sphingosine. Phosphorylated sphingosine activates sphingosine-1-phosphate (S1P) receptor signalling, a receptor family involved in facilitating leukocyte trafficking and neural cell proliferation. Therefore binding of phosphorylated fingolimod, fingolimod-phosphate, to S1P receptors in place of sphingosine leads to attenuation of S1P signalling and leukocyte migration (Chun and Hartung, 2010). Collectively, fingolimod notably hinders dendritic cell trafficking towards lymphoid organs and supresses lymphocytes from exiting lymph nodes, thus reducing relapsing stages of MS.

Teriflunomide was FDA approved in 2012. This MS DMT is a known dihydro-orotate dehydrogenase (DHODH) inhibitor, which ultimately results in selective impairment of activated lymphocyte proliferation. Collectively, it limits demyelination by preventing myelin-specific lymphocyte expansion within the CNS (Bar-Or *et al.*, 2014).

Dimethyl fumarate is a fumaric acid derivative that was FDA approved as an MS DMT in 2013. Oral administration of this molecule reportedly skews T cell differentiation from Th1 towards a Th2 phenotype with increased IL-4 and IL-5 production. Furthermore, dimethyl fumarate increases nuclear factor erythroid 2-related factor 2 (NRF2), a transcription factor responsible for attenuating oxidative stress and promoting neuron and oligodendrocyte protection (Bomprezzi, 2015). Overall, dimethyl fumarate promotes immunomodulatory properties within the peripheral immune system and CNS resident cells.

Alemtuzumab received FDA approval for relapsing forms of MS in 2014. Alemtuzumab is a monoclonal antibody that directly targets CD52 to induce antibody dependent cellular cytotoxicity (ADCC). As CD52 is a cell surface molecule found on the surface of T and B cells, with limited expression on monocytes/macrophages and natural killer cells, lymphocyte populations undergo induced apoptosis resulting in diminished cell proportions, and subsequently proinflammatory functions from these cells.

Ocrelizumab was FDA approved in 2017 to treat both relapsing forms of MS and PPMS. It is the first MS DMT appropriated for primary progressive forms of MS. Ocrelizumab is a monoclonal antibody targeting CD20, which is expressed on the surface of B cells but not plasma cells or pro-B cells. This anti-CD20 antibody assists in the prevention of clinical relapses along with supressing progressive MS symptoms. Ocrelizumab has been documented to promote cell-mediated cytotoxicity rather than complement mediated cytotoxicity *in vitro*. Furthermore, ocrelizumab appears to exert limited immunogenicity since it is a humanised antibody compared to rituximab, an alternative MS DMT (Mulero, Midaglia and Montalban, 2018). Collectively, ocrelizumab limits CNS inflammation through supressing CD20 mediated B cell antigen presentation.

Cladribine was originally FDA approved for the treatment of hairy cell leukaemia in the 1980's but is one of the most recent MS DMT to be approved for treating relapsing forms of MS in 2019. It is a synthetic analogue of deoxyadenosine. Upon administration of cladribine, there are documented events of declining circulatory T cell numbers, mainly affecting $CD4^+$ T cells rather than $CD8^+$ T cells. To a lesser extent, B cell and natural killer cell numbers were also affected by cladribine, via mechanisms of inducing cell death. Cladribine induces cell death through suppression of enzymes involved in DNA metabolism, overall causing breakage of DNA strands in selective cell subsets containing high deoxycytidine kinase ratios to 5'-nucleotidases, such as circulating lymphocytes (Leist and Weissert, 2011).

Siponimod is a synthetic derivative of fingolimod and one of the most recent DMT appropriated for MS. FDA approved in 2019, siponimod exerts higher specificity than fingolimod by preventing lymphocyte exit from lymph nodes via targeting S1PR1 and S1PR5 (Baecher-Allan, Kaskow and Weiner, 2018).

Table 1.1 Current FDA approved DMTs for MS.

DMT	Mechanism of Action	Route of Administration	MS category
IFNβ	Inhibition of inflammatory cytokines and T cell proliferation by binding IFNβ receptor	Injection Subcutaneous or Intramuscular	RRMS SPMS
Glatiramer Acetate	Competitively binds to MHC and skews Th1 towards Th2 response	Injection Subcutaneous	RRMS
Fingolimod	Prevents DC migration to lymphoid tissues and lymphocyte exit from lymph nodes	Oral	RRMS
Dimethyl fumarate	Activates the Nrf2 pathway which prevents oxidative damage	Oral	RRMS
Teriflunomide	Inhibits T cell activation and inflammatory cytokine production by sequestering dihydroorotate	Oral	RRMS SPMS
Cladribine	Induces apoptosis in T and B cells using adenosine deaminase	Oral	RRMS SPMS
Siponimod	Diminishes T and B cell migration from lymph nodes by targeting S1PR	Oral	RRMS SPMS CIS
Natalizumab	Prevents VLA4 binding to VCAM-1 and T and B cells infiltrating the CNS	Infusion Intravenous	RRMS
Ocrelizumab	Prevents B cell antigen presentation by blocking CD20	Infusion Intravenous	RRMS SPMS PPMS
Mitoxantrone	Inhibits: IFNγ, TNFα, IL-2, monocyte & lymphocyte migration via breaking DNA strands	Infusion Intravenous	RRMS SPMS
Alemtuzumab	T and B cells diminished via CD52 ab by activating complement system and ab dependent cellular cytotoxicity	Infusion Intravenous	RRMS SPMS

There are currently several DMTs in clinical trials for the treatment of MS. Secukinumab is a monoclonal antibody that neutralises IL-17A and used in the treatment of psoriasis and psoriatic arthritis. This potential DMT has been reported to reduce lesions in RRMS patients (Baecher-Allan, Kaskow and Weiner, 2018) and is currently in Phase III clinical trials for patients with RRMS . Laquinimod is an orally administered DMT in Phase III clinical trials for RRMS patients and Phase II for PPMS patients. Laquinimod is a compound that promotes Th2 and Treg responses and anti-inflammatory signalling. High doses of oral Biotin are in phase III clinical trials for RRMS and PPMS. This DMT aims to promote neuroprotective processes through the promotion of fatty acids and energy production for oligodendrocyte synthesis by Vitamin B7. Additionally, there has been reportedly improved disabilities in 30% of patients (Baecher-Allan, Kaskow and Weiner, 2018).

Bone marrow transplantation is an alternative off-label immunotherapy for suppressing relapses in RRMS and overall reducing the progression rate of disease (Baecher-Allan, Kaskow and Weiner, 2018). For example, non-myeloablative autologous hematopoietic stem cell transplantation (aHSCT) has been preliminarily documented to improve and reverse debilitating neurological symptoms in RRMS patients (Burt *et al.*, 2015), however it is considered more suited for treatment of aggressive forms of MS in patients where FDA approved DMTs like Natalizumab and Ocrelizumab have failed. This is due to the rigorous processes and risks involved with aHSCT, such as post transplantation infections and a 2% mortality rate. Although risks of aHSCTs appear high compared to available DMTs to treat RRMS, 83% of those with aggressive forms of MS displayed no disease progression 2 years post transplantation, which decreased to 67% post 5 years transplantation (Karceski, Frederick and Bourdette, 2017). Overall, aHSCT offers potential avenues for patients suffering fatal illnesses, but the risks involved for MS patients may outweigh the benefits when approved DMTs can be successful at preventing relapses.

Collectively it must be noted, the majority of FDA approved drugs are appropriated for RRMS and controlling relapses, but are mostly ineffective in progressive forms of MS, including patients that transition from RRMS to SPMS. The only FDA approved drug for

PPMS is Ocrelizumab. This limitation highlights the separate pathogenic pathways involved in different forms of MS and the need for more effective and personalised therapy.

Establishing successful MS DMTs that prevent disease progression with neuroprotective mechanisms have been challenging. DMTs aimed at dampening the immune response also attenuates essential repair processes within the CNS during remyelination phases (Yong *et al.*, 2019). Although excessive inflammation is detrimental to an immune-mediated disease like MS, it has beneficial effects for cell and myelin debris clearance, an important mechanism for remyelination (Neumann, Kotter and Franklin, 2009). Although all monoclonal antibody DMTs prevent inflammatory cascades, their mechanisms of action do not facilitate repair processes (Baecher-Allan, Kaskow and Weiner, 2018), unlike new potential therapies such as biotin (Phase III clinical trials for SPMS and PPMS) aimed at promoting oligodendrocyte synthesis with documented disability improvement. Additionally Clemistine, an over the counter antihistamine that is currently in Phase II clinical trials for RRMS, has been shown to both reduce immune cell activity as well as promote repair (Gallo, Centonze and Marrosu, 2017). Thus, identifying novel therapies that attenuate inflammation whilst promoting CNS repair is an important area for further research.

1.2 Animal models of Multiple Sclerosis

MS is a complex autoimmune mediated disease involving multiple mechanisms that influence disease onset and progression. Although there are no animal models available that recapitulate the entirety of cellular and molecular events involved in MS, there are established animal models proven useful in studying certain immunopathological mechanisms of MS as well as demyelination and remyelination. Animal models of MS have proven useful to further elucidate mechanisms of already approved drugs i.e. alemtuzumab, dimethyl fumarate, fingolimod, and natalizumab (Kipp *et al.*, 2017). Animal models of MS can generally be divided into: virus-induced, toxin-induced, and autoimmune-mediated, each representing distinct pathways to study different aspects of MS.

1.2.1 Virus-induced demyelination models

Viral infections with EBV and the JC virus are known risk factors associated with MS susceptibility and development (Kipp *et al.*, 2017). In animal models of MS, canine distemper virus, Theiler's murine encephalomyelitis virus (TMEV), and mouse hepatitis virus (MHV), can be used to induce neuroinflammatory and demyelinating processes within the CNS (Bjelobaba *et al.*, 2018). The most commonly used and characterised virus-induced model is picornavirus TMEV. Although demyelination from TMEV infection does not replicate the exact pathogenesis of MS, this model represents a chronic progressive form of disease with events of simultaneous demyelination and remyelination. During chronic stages of infection (<30 days), mass infiltration of immune cells occurs comprising mainly of monocytes, macrophages, and T cells within the white matter of the CNS, along with microglial proliferation within the brain stem. Additionally, phagocytic macrophages can be found in lesions during the demyelinating stages of infection (Bjelobaba *et al.*, 2018), an event observed at MS lesions sites in post mortem tissue (Grajchen, Jerome J. A. Hendriks and Bogie, 2018). In contrast to MS, epitope spreading is not considered to be involved in chronic stages of TMEV induced immune reactivity (Bjelobaba *et al.*, 2018).

1.2.2 Toxin-induced demyelination models

Toxin-induced models of demyelination are important to gain further understanding of the processes involved in demyelination and remyelination within the CNS. Ethidium Bromide (EtBr), Lysolecithin, and Cuprizone, are the most widely used models due to high reproducibility (Ransohoff, 2012). EtBr is a neurotoxic agent administered directly to site specific white matter regions, such as the spinal cord or cerebellar regions, to cause focal lesions. Peripheral immune cell infiltration is observed in this model due to toxin-induced astrocyte cell death and loss of BBB integrity (Bjelobaba *et al.*, 2018), unlike the Lysolecithin and Cuprizone models. Demyelination is caused by apoptosis of oligodendrocytes, while axons are not directly affected by this neurotoxin. The involvement of Schwann cells during remyelination processes at lesions has been reported in cats and rats injected with EtBr, a process also observed in human Devic's disease (Bjelobaba *et al.*, 2018).

Lysolecithin is a neurotoxic substance that selectively solubilises myelin producing cell membranes within the CNS. Remyelination is more rapid in this acute demyelination model (approximately 1 week post lysolecithin injection) compared to other toxin-induced models, potentially due to lysolecithin not targeting OPCs or astrocytes (Bjelobaba *et al.*, 2018). Oligodendrocytes are usually the main cell source for remyelinating lesions, but Schwann cells have been observed to assist in remyelination when lesions are of a larger size (Bjelobaba *et al.*, 2018). This model of demyelination and remyelination has provided great insight into the beneficial and detrimental attributes of microglia and macrophages during remyelination processes (Rawji and Yong, 2013a).

The cuprizone model is the most commonly used model to study demyelination and remyelination processes within white and grey matter regions of the CNS. Cuprizone is a copper chelator that induces oligodendrocyte apoptosis and subsequent astrocytic and microglial activation with no or little BBB breakdown or peripheral immune cell infiltration (Kipp *et al.*, 2017; Bjelobaba *et al.*, 2018). Its precise mechanism of action is not known but it is suggested to involve alterations in oligodendrocyte metabolism, mitochondrial stress and oxidative injury (Praet *et al.*, 2014a). Unlike other injectable toxin-induced models, the cuprizone model is induced by feeding a 0.2% w/w cuprizone-diet for 5-6 weeks. Spontaneous remyelination and repair is observed once the cuprizone-diet is removed (Hibbits *et al.*, 2009). Demyelination returns when cuprizone is re-introduced, while prolonged exposure for 12 weeks results in delayed and inefficient remyelination. This model thus provides access to explore time controlled remyelination and demyelination processes with great reproducibility and robustness (Kipp *et al.*, 2017). A study investigating the beneficial effects of vitamin D in CNS demyelination confirmed that a supplemented diet containing vitamin D caused a decrease in microglia activation and demyelination in EAE mouse models (Wergeland *et al.*, 2011; Rawji and Yong, 2013a). This study corroborated with MS clinical trials demonstrating how vitamin D supplementation is reportedly associated with reduced microglia activation and demyelination.

1.2.3 Autoimmune-mediated demyelination models

EAE is an autoimmune-mediated demyelinating animal model largely used to study immunopathological mechanisms involved in MS (Constantinescu *et al.*, 2011; Robinson *et al.*, 2014). Although this model of MS does not recapitulate every immunological and genetic aspect of disease, some of the current FDA approved MS therapies were based on promising results in this model e.g. Glatiramer acetate and Natalizumab (Robinson *et al.*, 2014). Although several laboratory animal species are susceptible to EAE, such as non-human primates and rats, inbred mouse strains are mainly used for this autoimmune-mediated model. EAE can be divided into two inducible models, either active or passive, and spontaneous models.

In contrast to virus and toxin-induced demyelination models, EAE is mediated by myelin-specific T cells and can be induced by two methods (Bjelobaba *et al.*, 2018). Direct immunisation with myelin specific antigens, termed active EAE, is the most commonly used model, while adoptive transfer of activated myelin-specific $CD4^+$ T cells, termed passive EAE, is an alternative method of disease induction (Robinson *et al.*, 2014).

Table 1.2 outlines susceptible mouse strains, immunising antigens, and the disease course used for EAE studies (Terry, Ifergan and Miller, 2016). C57Bl/6 and SJL/J mice are the most commonly used inbred mouse strains to study autoimmune-mediated demyelination. A chronic progressive course of EAE can be observed when C57Bl/6 mice are immunised with rMOG, $MOG_{35-55,}$ rPLP, and $PLP_{180-199}$. In contrast, SJL/J mice display a relapsing-remitting disease course of EAE when immunised with MOG, PLP, and MBP (Terry, Ifergan and Miller, 2016; Kipp *et al.*, 2017).

Table 1.2 Inducible mouse models used to study EAE disease courses.

Mouse Strain	Myelin Antigen	Disease Course
C57BL/6	$MOG_{35-55,}$ rPLP, $PLP_{180-199}$	Chronic progressive
SJL/J	MOG_{92-106}, rMBP, MBP_{84-104}, MBP_{89-101}, rPLP, PLP_{57-70}, $PLP_{104-117,}$ $PLP_{139-151}$, $PLP_{178-191}$, $PLP_{180-199}$	Relapsing-Remitting
BALB/c	rPLP, $PLP_{180-199}$	Chronic progressive
ABH	rMOG, MOG_{8-22}, PLP_{56-70}	Chronic relapsing
PL/J, B10.PL	rMBP, $MBP_{Ac1-11,}$ MBP_{34-47} MOG_{35-55}, PLP_{43-64}	Chronic and acute monophasic

Active EAE involves direct immunisation with myelin components emulsified in Complete Freunds Adjuvant (CFA) containing *Mycobacterium tuberculosis*, and additional adjuvant injections of *pertussis toxin* (Terry, Ifergan and Miller, 2016). Active immunisation with myelin antigens causes peripheral APCs to phagocytose injected myelin antigens before migrating to lymph nodes and spleen to present these myelin antigens to resident lymphocytes. This induces myelin-specific Th1 and Th17 cells in peripheral secondary lymphoid organs, which facilitates encephalitogenic Th1 and Th17 cell infiltration of the BBB and inflammation within the CNS (O'Neill *et al.*, 1998; Kipp *et al.*, 2017). Since this form of EAE involves $CD4^+$ T cell activation in the periphery, induction and effector stages of EAE are possible to study (Bjelobaba *et al.*, 2018).

Passive EAE involves isolating activated $CD4^+$ T cells from lymph nodes and spleen of immunised mice, re-stimulating and activating $CD4^+$ T cells *in vitro* with the myelin component, and adoptively transferring activated myelin-specific $CD4^+$ T cells into naïve recipient mice (Terry, Ifergan and Miller, 2016). Passive EAE induction is more complex and time consuming but has certain benefits compared to active EAE. Since passive EAE does not require adjuvants to induce disease like active EAE induction, it bypasses priming

phases of EAE and allows specific interrogation of the effector without activating TLR signalling with microbial agonists. Additionally, during *in vitro* T cell stimulation stages of passive EAE, T cells may be skewed with specific cytokines or blocking antibodies to manipulate their phenotype and functional activity. T cells can also be labelled *in vitro* for *in vivo* tracking purposes to identify myelin-specific T cells within the CNS during EAE (Stromnes and Goverman, 2006).

Although inducible EAE models are invaluable tools for elucidating much information surrounding MS, there are limitations and discrepancies between EAE and MS. These limitations are evident when successful amelioration of EAE with specific therapeutics does not translate into beneficial effects in MS. Indeed, MS symptoms may remain unchanged or have even been exacerbated in some instances, as observed with TNF-α and IFN-γ supressing treatments (Vickers, Jackson and Cheetham, 2011; Baecher-Allan, Kaskow and Weiner, 2018). Other discrepancies have emerged using chemokine and cytokine mediated treatment, where there is limited success in MS treatment compared to EAE (Vickers, Jackson and Cheetham, 2011), collectively highlighting EAE does not recapitulate every pathogenic aspect of MS. Physical limitations of actively inducing EAE include the actual administration of substances. There are evident increased risks of adverse reactions occurring such as reports of granuloma formation at injection sites (Bjelobaba *et al.*, 2018).

A noted limitation of EAE models is that the autoimmune response is directed again myelin antigens within white matter regions and consequently they fail to model grey matter atrophy, which is involved in MS progression. β-Synuclein is a neuronal protein identified as a component in plaque development during brain degenerative diseases such as Alzheimer's disease. A previous study identified that immunisations of Lewis rats with β-Synuclein peptide caused typical EAE symptoms and uveitis, possibly due to this protein also being a component of myelin (Cohen *et al.*, 2003). Building upon this study, it was recently shown that β-Synuclein-reactive T cells specifically infiltrated grey matter regions where β-Synuclein is highly expressed in neuronal processes and synapses. Furthermore, grey matter invading T cells specific for β-Synuclein promoted local inflammation and

enhanced peripheral immune cell infiltration, which ultimately resulted in brain atrophy (Lodygin *et al.*, 2019).

Overall, spontaneous EAE models provide great aspects to study the immunopathogenesis of EAE without intervening procedures, however the limited success in clinical trials using EAE models suggests the need for more translational models. Development of new EAE models recapitulating neurodegenerative aspects of MS may enhance therapeutic options that suppress and reverse demyelination damage in MS patients.

1.3 Immune cell subsets implicated in MS

MS is a multi-faceted autoimmune-mediated disease of the CNS. Although MS is referred to as a $CD4^+$ T cell mediated disease, the heterogeneous immunopathological mechanisms underlying this disease involve both the innate and adaptive immune branches. Elucidating the mechanisms by which pathological immune cell players drive inflammation against myelin-specific antigens may lead to the development or repurposing of DMTs, which may act to block critical inflammatory pathways or skew immune cells towards a phenotype that promotes CNS repair. In addition to $CD4^+$ T cells, $CD8^+$ T cells, B cells, macrophages, dendritic cells, and neutrophils, are important in disease pathogenesis. The beneficial and detrimental roles of these immune subsets, which have been elucidated predominantly using the EAE model, are discussed in the following paragraphs.

1.3.1. The role of T cells

T cells are a diverse group of adaptive immune cells that recognise specific antigens when presented in the context of MHC by antigen presenting cells. Upon recognition of their cognate antigen and the provision of co-stimulatory signals, naïve T-cells undergo differentiation into subsets depending on the transcription factors they express and the cytokine signals from the surrounding microenvironment. Each of these subsets play distinct roles in promoting or attenuating inflammation. Current evidence supports MS as being a $CD4^+$ T cell mediated disease (Fletcher *et al.*, 2010). Th1, Th17, Th2, and T regulatory (Treg) cells play an important role in the EAE model of MS and will be discussed further.

Additionally, $CD8^+$ T cells are cytotoxic T cells, which are found in active MS lesions, are likely to contribute to disease pathogenesis and will also be discussed.

1.3.1.1 Th1 cells

Th1 cells were the first proinflammatory $CD4^+$ T cell subset associated with MS pathogenesis. In EAE, these effector T cells arise within peripheral lymphoid tissues after immunisation with myelin-specific antigens. The transcription factor T-bet was identified to control Th1 differentiation and production of signature Th1 cytokines IFN-γ, TNFα, and IL-2 (Belinda J. Kaskow and Baecher-Allan, 2018). Additionally, the importance of Th1 cells in driving EAE is highlighted by the requirement of essential transcription factor T-bet that causes encephalitogenic Th1 and Th17 cells (Yang *et al.*, 2009). Moreover, during T cell recruitment from the periphery to the CNS, a predominant Th1 phenotype is evident, collectively emphasising the critical contributing role of T-bet during the pathogenesis of disease. TNF-α, an inflammatory cytokine produced by Th1 cells, has also been associated with allowing $CD4^+$ T cell to transmigrate from the perivascular space to the parenchyma. Furthermore, its relevance in MS is emphasised by the presence of TNF-α at active lesion sites, within MS patient serum samples, and within the CSF of MS patients (Kawakami *et al.*, 2004; Göbel, Ruck and Meuth, 2018a).

IFN-γ, the hallmark cytokine produced by Th1 cells, is associated with promoting inflammation and reactivity against myelin components. Not only can Th1 producing IFN-γ cells be found at MS lesions, but the presence of this inflammatory cytokine correlates with an active and relapsing stage of disease (Legroux and Arbour, 2015). Furthermore, IFN-γ producing $CD4^+$ T cells have been documented to increase chemokines such as CCR6 to permeate the blood-CSF barrier, and activate other infiltrating and CNS resident cells (Goverman, 2009). Overall, IFN-γ producing Th1 cells contribute to the complex understandings of MS and EAE. Despite recognising IFN-γ as a critical cytokine for disease progression, EAE was exacerbated in IFN-γ deficient or STAT1 deficient mice (Ferber *et al.*, 1996; Bettelli *et al.*, 2004). Moreover, patients administered IFN-γ to treat MS displayed enhanced clinical symptoms of disease (Panitch *et al.*, 1987). These findings highlight the contrasting roles Th1 cells and their cytokines exhibit during MS and EAE, highlighting the

importance of studying other immune cell subsets to further elucidate the relationship amongst immune cell population during MS and EAE.

1.3.1.2. Th17 cells

Th17 cells were identified as a distinct Th cell subset largely based on evidence in autoimmune models such as EAE, where IL-17 secreting cells were found to display a transcriptional signature unique to that of Th1 and Th2 cells (Harrington *et al.*, 2005; Heon Park *et al.*, 2005). The transcription factor RORγt drives the differentiation of Th17 cells that, in addition to IL-17, produce signature cytokines such as IL-21, IL-22, IL-23, IL-9, and TNF-α (Fletcher *et al.*, 2010). IL-12 is a heterodimeric cytokine containing a p40 subunit, it was only when this p40 subunit was also found in a separate heterodimer molecule, now referred to IL-23, when Th17 cells were discovered (Basso, Cheroutre and Mucida, 2009). IL-23 is critical for the development of Th17 cell. Moreover, IL-23 deficient mice are resistant to EAE development (Thakker *et al.*, 2014). Other cytokines proven to contribute to Th17 differentiation include: TGF-β, IL-6, IL-1, and IL-21 (Chung *et al.*, 2009). Although IL-23 is not responsible for the production of IFN-γ producing Th1 cells, it is crucial for the expansion of pathogenic $CD4^+$ T cells during EAE (Langrish *et al.*, 2005).

Interestingly, adoptive transfer of myelin-specific Th17 cells resulted in a relapsing-remitting EAE disease course in SJL/J mice but failed to induce EAE clinical signs in C57Bl/6 mouse strains (O'Connor *et al.*, 2008). Furthermore, mice exhibited enhanced EAE severity upon adoptively transferring Th17 cells compared to Th1 cells (Langrish *et al.*, 2005). The presence of elevated IL-17 and IFN-γ are both positively associated with active stages of MS (Fletcher *et al.*, 2010), however the pathogenic importance of Th17 cells is further highlighted by being directly located within active MS brain lesions rather than inactive lesion sites (Tzartos *et al.*, 2008).

The translational importance of IL-17 in MS and EAE progression is highlighted with Secukinumab, an MS DMT currently in Phase III clinical trials which blocks IL-17 signalling. Even though there is evidence towards the presence and expansion of Th17 cells

in MS and EAE, their exact mechanisms of action in contributing to disease progression has yet to be fully understood.

1.3.1.3. Th2 and Tregs

Th2 and Tregs are $CD4^+$ T cell subsets unrelated to promoting inflammation like Th1 and Th17 cells but involved in resolving inflammation and dampening the immune response. Th2 cells are differentiated upon exposure to IL-4 and identified by their transcription factor GATA-3. They produce anti-inflammatory cytokines such as IL-4, IL-5, and IL-10 to attenuate inflammation and reduce activation of proximal immune cells (Belinda J Kaskow and Baecher-Allan, 2018). A cohort of RRMS patients were studied to identify a predominant Th1/Th2 cytokine profile when treated with MS DMTs, Glatiramer Acetate and Natalizumab. Glatiramer Acetate appeared to skew the T cell response towards a Th2 response, which would be beneficial in MS patients, however larger cohorts would be needed to confirm (Oreja-Guevara *et al.*, 2012).

Tregs are another categorised anti-inflammatory $CD4^+$ T cell subset documented in MS and EAE. Tregs are differentiated from naïve $CD4^+$ T cell by the presence of co-stimulatory factor IL-2. FoxP3 is the distinguishable transcription factor responsible for Treg cytokine production of IL-10, TGF-β, and IL-5 (Kitz, Singer and Hafler, 2018). MS onset is associated with a breakdown of self-tolerance resulting in activation of myelin-specific encephalitogenic T cells, Tregs are associated with maintaining peripheral tolerance in healthy conditions by negatively regulating inflammatory $CD4^+$ T cell subset immune responses (Danikowski, Jayaraman and Prabhakar, 2017). Therefore, it is unsurprising that the downregulation of suppressive Treg phenotypes are associated with promoting the pathogenesis of MS. Due to the suppressive functional characteristics of Tregs, they provide opportunities to harness anti-inflammatory cytokine to attenuate inflammatory signalling in auto-immune mediated diseases like MS (Danikowski, Jayaraman and Prabhakar, 2017).

The importance of Th2 and Treg roles in attenuating inflammation is corroborated in preclinical studies. IL-10, a critical regulatory cytokine produced by Th2 cells and Tregs, was found to positively correlate with reduced incidence and severity of EAE (Klose *et al.*,

2013; Payne *et al.*, 2013; Winger and Zamvil, 2016). Moreover, Laquinimod is a potential MS DMT in clinical trials with reported decreases in relapse rates in RRMS patients. This potential DMT promotes Treg and Th2 cells and their corresponding cytokines such as TGF-β to promote a neuroprotective microenvironment (Comi *et al.*, 2012).

1.3.1.4. Cytotoxic $CD8^+$ cells

Although MS is referred as a $CD4^+$ T cell mediated disease, $CD8^+$ T cells have emerged as critical pathogenic players during disease progression. Although, effector $CD8^+$ T cells do not exhibit the same cytokine profiles as $CD4^+$ T cells, they elicit direct cytotoxicity within the CNS (Belinda J Kaskow and Baecher-Allan, 2018). Furthermore, these cytotoxic cells outnumber $CD4^+$ T cells within lesions of MS patients (Goverman, Perchellet and Huseby, 2005). Additionally, $CD8^+$ T cells appear to undergo greater levels of clonal expansion compared to $CD4^+$ T cells *in vitro* when derived from MS CSF and blood (Crawford *et al.*, 2004).

In EAE, $CD8^+$ T cells can only infiltrate the CNS when exposed to stimuli that result in activated effector $CD8^+$ T cells. Unlike $CD4^+$ T cells, $CD8^+$ T cells can only recognise myelin-specific antigens when presented in an MHCI molecule not MHCII. However, since MHCI molecules do not usually present exogenous antigens, it is proposed cross-presentation occurs during inflammatory stress whereby myelin antigens can be processed through MHCI presentation pathways (Fletcher *et al.*, 2010). Viral infections in MS patients result in exacerbated MS disease severity. It is believed virally infected $CD8^+$ T cells with MHCI molecules containing viral peptides are responsible for enhancing disease activity during relapsing stages as opposed to mechanisms exerted by $CD4^+$ T cells (Winger and Zamvil, 2016). Once $CD8^+$ T cells acquire myelin-specificity, their main pathogenic mechanism mediates cytotoxicity through release of granules targeting oligodendrocytes and axons (Goverman, Perchellet and Huseby, 2005). $CD8^+$ T cells has also been reported to mediate demyelination within the CNS through cell-cell mediated lysis (Friese *et al.*, 2008).

Potential DMTs for MS highlight the pathological roles of $CD8^+$ T cells in MS progression, whereby monoclonal antibody treatment aimed to deplete only $CD4^+$ T cells (cM-T412)

caused no improvement in MS (van Oosten *et al.*, 1997). However, DMTs aimed at depleting both $CD4^+$ and $CD8^+$ T cells resulted in reduced disease severity and becoming FDA approved (Alemtuzumab) (Coles *et al.*, 2006). Despite the collective evidence of $CD8^+$ T cells contributing to disease severity in MS and EAE, there is also suggestive evidence of a beneficial role where MHCI molecule HLA-A2 (A*0201) is associated with MS protection (Burfoot *et al.*, 2007). Complex findings from CD8 TCR spontaneous EAE models suggest further investigation into the role of effector $CD8^+$ T cells in EAE could enhance the potential for future MS DMTs.

1.3.2 B cells

Unlike T cells, B cell receptors are comprised of immunoglobulins (Igs). When B cells become activated, they have the ability to become myelin-specific memory cells and are capable of differentiation into plasma cells to secrete Igs which contributes to disease progression (Van Kaer *et al.*, 2019).

There is substantial evidence surrounding the immunopathological roles of B cells during MS and EAE. The relevance of B cells in MS is emphasised by the presence of Igs in MS patients CSF. Intrathecal oligoclonal Igs are often used as a biomarker of disease incidence and progression (Mitsdoerffer and Peters, 2016; Sospedra, 2018). Additionally, patients have been reported to present with distinct Oligoclonal band (OCB) patterns when CSF samples are examined by electrophoresis with Coomassie-blue staining.

Studies surrounding EAE in B cell deficient mice concluded B cells were not crucial for the development of EAE but did contribute to disease severity. This was evidenced by decreased levels of demyelination within the CNS of B cell deficient mice compared to controls (Svensson *et al.*, 2002). Moreover, reduced incidence rates of passive EAE were observed in B cell deficient mice (Emily R Pierson, Stromnes and Goverman, 2014). During EAE, memory B cells mediate demyelination through production of anti-myelin antibodies (Monica K Mann *et al.*, 2012). During inflammatory stages of MS, B cells are documented to undergo clonal expansion within the CNS and are recognised infiltrates within MS lesions (Sospedra, 2018). Inflammatory B cells also mediate disease progression through secretion

of cytokines that result in activation of other immune cells such as: IL-6, TNF-α, and GM-CSF. Furthermore, B cells have been reported to uptake myelin antigens and migrate to lymphoid organs to facilitate myelin-specific T cell activation during EAE (Mitsdoerffer and Peters, 2016). B cells are also theorised to undergo maturation and differentiation within the meninges of MS patients. This is due to evident B cell aggregates occurring within the CNS which resemble tertiary lymphoid organs (TLOs) with germinal centre-like structures (Mitsdoerffer and Peters, 2016).

The diverse functions of B cells add gravity to the complexities of MS and EAE. In addition to promoting demyelination via antigen presentation and Ig and inflammatory cytokine production, B cells also exhibit immunoregulatory effects when differentiated into a Breg phenotype. IL-10, IL-38, and TGF-β are established anti-inflammatory cytokines produced by Bregs (Van Kaer *et al.*, 2019). IL-10 and TGF-β are known mediators of EAE amelioration, furthermore, TGF-β producing B cells reportedly limit EAE disease severity through attenuating Th1 and Th17 immune responses by decreasing antigen presentation of myelin antigens (Bjarnadóttir *et al.*, 2016).

The dual roles of effector memory B cells and Bregs are highlighted by clinical outcomes of B cell mediated MS immunotherapies. Previous DMTs targeting specific B cell receptors were ineffective at reducing disease severity, and in some instances displayed evident exacerbations of disease. A potential DMT which targets BAFF, a selective B cell survivor factor, evidently accelerated EAE clinical scores. This event appeared to be unique to EAE since targeting this molecule in a separate autoimmune disease, systemic lupus erythematosus (SLE), has proven beneficial (Vincent *et al.*, 2014; Sospedra, 2018). Another DMT termed Atacicept, diminished B cell and plasma cell functions via targeting BlyS/April receptors on mature B cells, despite proven benefits in SLE and rheumatoid arthritis (RA), this too resulted in exacerbated RRMS disease severity (Kappos *et al.*, 2014). In contrast, Rituximab is an FDA approved DMT which targets $CD20^+$ B cells to reduce B cell antigen presentation. It reportedly reduces relapse stages in RRMS, however due to evidence of off-target effects of decreasing T cell numbers, the efficacy of Rituximab cannot be confirmed to be solely B cell dependent (Hauser *et al.*, 2008). Other studies carried out on MS patients observed a correlation of disturbed Breg populations with disease progression (Van Kaer *et*

al., 2019), this observation would corroborate with findings suggestive of the immunoregulatory effects IL-10 producing B cells elicit, and could account for failed DMTs targeting B cell specific receptors. Accumulating findings on B cell targeted therapy in MS remain complicated to date, suggesting humoral immunity in EAE should have a greater focus to understand how B cells may be harnessed for their benefits.

1.3.3 Dendritic cells

Dendritic cells (DCs) are recognised as key professional antigen presenting cells of the innate immune system. During homeostatic conditions, DCs constitutively express MHCI and MHCII molecules containing self-antigens in the periphery to maintain peripheral tolerance, and educate lymphocytes within the thymus to maintain central tolerance (Hopp, Rupp and Lukacs-Kornek, 2014). In contrast, during periods of inflammatory stress, DCs are rapid responders and swiftly present antigens to activate lymphocytes to mount an inflammatory immune response. Due to distinct effector functions, DCs are categorised into 3 subclasses: plasmacytoid DC (pDC), conventional DC1 (cDC1), and conventional DC2 (cDC2) (Lévesque *et al.*, 2016). pDCs are generally associated with peripheral tolerance and antiviral responses, and therefore express TLR7 and TLR9. This DC subset can also produce inflammatory cytokines such as: IL-6, IFN-γ, and TNF-α to assist in promoting inflammation. Conventional DCs exhibit a separate immune role, where they are involved in promoting inflammatory Th1/2/17 and $CD8^+$ T cell responses alongside modulating the immune system. They can be identified by their profiles of TLRs: TLR-1-6, and TALR-8, and produce an array of cytokines: IL-8, IL-12p70, CCL3/4, IFN-γ, and TNF-α (Xie *et al.*, 2015).

DCs exhibit differential roles during EAE progression depending on whether they are mature DCs in the initial stages of disease, or whether they are steady-state DCs. Although mature DCs during EAE initiation are detrimental to EAE disease progression, steady state DCs prove important to induce immunotolerance in peripheral T cells. Due to the presence of steady state DCs, exacerbated EAE has been previously recorded in mouse models containing Cre recombinase technology to deplete $CD11c^+$ cells. Enhanced disease severity appeared to be caused by hindered steady-state DC mediated PD-1 induction as this subgroup population was depleted (Sagar *et al.*, 2012). Immunomodulatory functions of

pDCs were also demonstrated in EAE mice treated with anti-mPDCA-1, an agent to deplete pDCs. Exacerbation of clinical disease and increased IL-17 and IFN-γ producing Th cells within the CNS were observed in anti-mPDCA-1 treated EAE mice (Miller *et al.*, 2008), overall suggesting a protective role of pDCs in EAE. Although complete deletion of DCs subsets in animal models of EAE failed to attenuate clinical disease activity and CNS inflammation, DCs remain critical contributors that assist in demyelination processes.

During EAE, DCs are pivotal in activating encephalitogenic Th1 and Th17 cells in the periphery via presenting myelin-specific antigens to naïve lymphocytes (Diebold, 2008). Furthermore, DCs within the perivascular space reactivate encephalitogenic T cells to assist the migration of T cells into the neural parenchyma (David A. Giles *et al.*, 2018). In contrast, despite the inflammatory role of DCs in disease progression, DCs also negatively regulate T cell activity by inducing programmed death ligand (PD-1) to promote Tregs (Yogev *et al.*, 2012). In order to elicit their functions, DCs must be recruited to the CNS through a CCL2 mediated chemotactic gradient (Sagar *et al.*, 2012). It's additionally reported that EAE mouse models displayed a direct correlation between disease activity and DC infiltration. Furthermore, ERK activation was noted to support DC paracellular infiltration into the CNS (Sagar *et al.*, 2012).

In EAE, DCs are further involved in promoting disease progression by reactivating T cells with myelin-specific antigens once inside the CNS. Giles et. Al. performed a study focussing on a subclass of immune cells with phenotypic markers indicative of DCs present within the CNS of EAE mice during non-inflammatory conditions, termed CNS resident DCs (David A. Giles *et al.*, 2018). It is strongly suggested these CNS resident DCs within the perivascular space and the plexus stroma are causative mediators in reactivating T cells *in situ*, thus promoting infiltrating T cells to reach the parenchyma (David A. Giles *et al.*, 2018; Waisman and Johann, 2018). Collectively, the antigen presenting role of DCs prove critical in promoting the infiltration of T cells into the parenchyma of EAE mice where demyelination and oligodendrocyte loss occur.

In the context of MS, the predominant phenotype and functions of DCs exhibit inflammatory properties (Nuyts *et al.*, 2013). Infiltrating pDCs and cDCs are both present within MS demyelinating lesions and in the CSF, pDCs can be additionally found within the leptomeninges of MS patients (Huang *et al.*, 1999; Aung *et al.*, 2010), hence the presence of high population proportions of these cells may be utilised as a biomarker of MS progression (Pashenkov *et al.*, 2002). During the pathogenesis of MS, DCs are heavily involved in presenting myelin-specific antigens to T cells within the periphery which ultimately leads to T cell recruitment to the CNS.

Although the first MS FDA approved drug, IFN-β, has been successful in reducing MS relapses, the exact mechanisms of how this DMT affects the immune response is not fully understood. One study aimed at further understanding the mechanistic approach of this DMT uncovered useful information relating to DCs. Aung et. al. confirmed the ability of DCs to express CCL3-5 was reduced, which subsequently decreased TLR9 and increased IFN-α and CCR7, overall attenuating the inflammatory response (Aung *et al.*, 2010). Fingolimod is another approved DMT that, in addition to preventing egress of lymphocytes from the lymph nodes, also limits the effector function of DCs (Thomas *et al.*, 2017). The mechanisms of action during long term Fingolimod treatment reportedly interfered with the antigen presentation and migratory abilities of DCs when targeting S1PR. Overall, Fingolimod treatment exerted suppressive functions to not only lymphocytes but also DCs, whereby they were documented to exhibit reduced antigen presentation to lymphocytes within lymph nodes and reduced migration into the CNS (Thomas *et al.*, 2017).

DCs are important immune cells that provide a bridge between the innate and adaptive immune systems through their professional APC functions that facilitate peripheral T cell activation and reactivation of T cells within the CNS. DCs are the most studied innate cell in relation to MS and EAE, yet there is still potential for future DMTs to directly target these innate cells to limit Th1 and Th17 immune responses.

1.3.4 Neutrophils

Neutrophils are the first responders of the innate immune system. They require the presence of IL-6, TNF-α, and GM-CSF to be released from the bone marrow into the bloodstream (Pierson, Wagner and Goverman, 2018), then require further inflammatory signals to invade tissues and elicit their effector functions. The specific signals to release and activate neutrophils are stringently controlled due to the inability of these innate cells to be target specific. In the context of autoimmune diseases, neutrophils cannot distinguish between their targets, therefore invasion into tissues whilst activated results in non-specific tissue destruction and cell death (Bardoel *et al.*, 2014). The effector functions of neutrophils include antigen presentation, production of inflammatory cytokines, reactive oxygen species (ROS), as well as the unique ability to release neutrophil extracellular traps (NETs) (Mantovani *et al.*, 2011). NETs are comprised of chromatin structures that resemble a web-like structure which is released from activated neutrophils. NETs have abilities to physically capture antigens and cytokines to mediate direct cell damage, a process associated with multiple autoimmune diseases (Papayannopoulos, 2018).

The importance of neutrophils in EAE is highlighted with depleted peripheral neutrophil populations prior to clinical onset of EAE causing ameliorated disease outcomes (Fordham *et al.*, 1998; Neumann *et al.*, 2013; Pierson, Wagner and Goverman, 2018). Additionally, depleting neutrophils with anti-Ly6G during preclinical stages of EAE impaired maturation of dendritic cells, macrophages, and microglia (Neumann *et al.*, 2013). In contrast, impediment to EAE disease progression was not confirmed in mice who have depleted neutrophil populations after onset of clinical disease but rather no significant clinical changes were observed compared to controls (Neumann *et al.*, 2013). Collectively, neutrophils appear to exert functional roles during the course of EAE. They are important mediators of proinflammatory cytokines and facilitate the increased permeability of the BBB integrity, overall proving to be a causative agent in promoting CNS inflammatory stress in animal models of EAE.

Neutrophils can be distinguished from other innate immune cells by their surface expression of Ly6G, however they can be further categorised by their expression of ICAM1 during the progression of EAE (Hawkins *et al.*, 2017). ICAM1 is believed to identify extravascular

neutrophils from intravascular neutrophils within the CNS, these two subpopulations of neutrophils appear to exert differential functions during the course of EAE. Transcriptomic analyses of these populations determined extravasated neutrophils to exhibit more macrophage-like functions, such similar properties include MHCII dependent antigen presentation and activation of other immune cells (Hawkins *et al.*, 2017). Selectin molecules were confirmed to facilitate neutrophil recruitment and extravasation into spinal cord parenchyma regions. In particular, P-selectin was shown valuable for brain parenchyma invasion during stages of acute inflammation, but there were additional adhesion molecules shown important for the extravasation including E-selectin and L-selectin, ICAM-1, and VCAM-1 (Bernardes-Silva *et al.*, 2001).

During EAE, neutrophils have been documented to play pivotal roles during the effector phases of disease, rather than promoting myelin-specific and encephalitogenic T cells. It is suggested that neutrophils facilitate immune cell infiltration into the CNS during EAE via activating APCs (Julie M Rumble *et al.*, 2015a) and producing an inflammatory cytokine milieu of: IL-1β, IL-6, IL-12, IL-23, IFN-γ, and TNF-α (Lévesque *et al.*, 2016; Pierson, Wagner and Goverman, 2018). Furthermore, ROS production by neutrophils contributes to BBB permeability (Larochelle, Alvarez and Prat, 2011b). Studies surrounding the role of neutrophils in EAE confirmed neutrophils are involved in promoting infiltration of peripheral lymphocytes and myeloid cells into the CNS (Pierson, Wagner and Goverman, 2018).

In the context of MS, small numbers of neutrophils are found within chronic CNS lesions (Julie M Rumble *et al.*, 2015a), however the precise role of neutrophils in MS is not fully elucidated. During homeostatic environments within the bloodstream, neutrophil functions are limited against antigens and therefore require priming to become activated. Exposure to molecules such as inflammatory cytokines and chemokines act as priming agents that cause neutrophil activation. Once neutrophils are primed, they exhibit activated phenotypes and are no longer functionally limited against antigens (Yao *et al.*, 2015; Silva *et al.*, 2017). Neutrophils derived from the circulation of MS patients exhibited inflammatory neutrophil phenotypes with increased expression of MHCII, TLR2, and elastase/protease activity (Woodberry *et al.*, 2018). It has been noted that neutrophils exhibit a longer half-life with

increased levels of degranulation in RRMS patients compared to healthy controls. Additionally, the production of ROS and NETs have been associated with the pathogenesis of MS, whereby increased levels are present in RRMS patient whole blood and serum samples that correlate with disease activity (Naegele *et al.*, 2012).

Currently, there are no FDA approved DMTs that specifically target neutrophils, but MS patients treated with Ocrelizumab, Ofatumumab, Fingolimod, and Rituximab have been reported to exhibit decreased neutrophil cell counts. Moreover, Alemtuzumab and IFN-β have been suggested to indirectly affect neutrophil functions (Woodberry *et al.*, 2018), suggesting non-specific suppression of neutrophil activity in EAE. Collectively, current evidence suggests a pathogenic role for neutrophils in MS however further research is required to understand how neutrophil effector functions may be inhibited to limit demyelination and overall tissue damage.

1.3.5 The role of monocytes/macrophages

Monocytes and macrophages are innate immune cells derived from hematopoietic stem cells (HSCs). Monocytes are circulatory residents of the blood vascular system with abilities to differentiate and morphologically change into macrophages under conditions that require extravasation from blood into tissues, usually during inflammatory stresses.

Monocyte infiltration into the CNS is positively associated with EAE disease severity. Caravagna et al. described monocyte infiltration into the spinal cord as early as 10 days post immunisation. Infiltration into spinal cord parenchyma regions is confirmed to occur through the meninges as opposed to monocytes extravasating blood vessels. It is within parenchymal regions where monocytes become differentiated into either monocytic derived macrophages or DCs (Caravagna *et al.*, 2018). Monocytes have further been described to accumulate in surrounding regions of demyelinating spinal cord lesions in EAE rats (Eltayeb *et al.*, 2007).

$CCR2^{+}Ly6C^{hi}$ monocytes have been described essential players for promoting demyelination during the effector stages of EAE. Monocytes are known to become recruited

towards the CNS during EAE further facilitating in the proinflammatory stress within the CNS environment. Studies have shown that EAE mice with depleted monocyte recruitment chemokine, CCR2, have significantly reduced disease activity (Izikson *et al.*, 2000; Mildner *et al.*, 2009).

IL-1β has been recognised as a critical mediator of facilitating monocyte recruitment into the CNS (Paré *et al.*, 2018a). Pare et al. demonstrated the transmigration of infiltrating monocytes relied on IL-1β to enter the spinal cords of EAE mice. Furthermore, GM-SCF production from endothelial cells in response to IL-1β was identified as the causative agent to induce monocyte differentiation into professional APCs. Monocytic derived cells have strong associations of further promoting proinflammatory $CD4^+$ T cells, in addition to causing neurotoxicity within the CNS (Paré *et al.*, 2018a). Collectively, IL-1β signalling alone and IL-1β mediated GM-CSF production proves essential for monocyte infiltration and differentiation within the CNS which ultimately leads to enhanced EAE disease severity.

The presence of monocytes in perivascular regions of active MS lesions highlight the critical role of monocytes in MS activity. Monocytes can be divided into two main categories: classical monocytes ($CD14^+CD16^-$) and nonclassical monocytes ($CD14^+CD16^+$). Blood samples derived from MS patients were confirmed to have significantly higher proportions of nonclassical monocytes compared to controls. Additionally, MS patients exhibited decreased expression of scavenger receptor CD163, suggestively correlating with the increase of nonclassical monocytes phenotype (Carstensen Gjelstrup *et al.*, 2018). As nonclassical monocytes are not considered proinflammatory like their counterpart classical monocytes, these immune cell subsets appear to exert functions distinct from classical monocytes. Blood derived monocytes of MS patients are also confirmed to express higher IL-6 levels compared to controls, but did not show different expression levels of IL-10 or TNF-α (Kouwenhoven *et al.*, 2001; Waschbisch *et al.*, 2016).

Overall, monocyte recruitment into the CNS is a prominent immunopathogenic event during MS and EAE. The prevention of monocyte infiltration into the CNS during disease models of MS results in disease resistance or significantly reduced disease severity. Although

monocyte differentiation within the CNS of EAE models leads to enhanced inflammatory stress, there are nonclassical monocyte populations with opposing effects. Therefore, further studies into monocyte differentiation and the ability to skew their functions could provide invaluable information surrounding their role in MS.

The prominent role for macrophages in the pathogenesis of EAE was initially confirmed in 1984 by Craggs et al. (Craggs, King and Thomas, 1984). Craggs et al. proved the depletion of macrophage populations in EAE induced Lewis rats significantly reduced the severity of disease. Administering intraperitoneal (IP) injections of silica dust to selective diminish macrophage populations prior to clinical signs of disease demonstrated an attenuation of clinical scores and a delayed onset of disease. Furthermore, providing a second IP injection of silica dust at day 11 post immunisation prevented further disease progression for 4 weeks (Craggs, King and Thomas, 1984). Interestingly, the prevalence of macrophages within the CNS during EAE progression surpasses all other infiltrating peripheral immune cell subsets by comprising of approximately 50% of the entire infiltrating population (Huitinga, van Rooijen, C. J. de Groot, *et al.*, 1990). Huitinga et al. further corroborated the pathogenic role of macrophages in EAE by demonstrating intravenous injections of liposomes containing dichloromethylene diphosphate to deplete spleen and liver macrophages resulted in a reduction of EAE clinical signs (Huitinga, van Rooijen, C. J. . de Groot, *et al.*, 1990). More recently, inducing apoptosis of phagocytic monocyte derived populations using clodronate caused an overall reduction of $CD4^+$ T cells, but within $CD4^+$ T cell subpopulations, clodronate caused decreased Th17 cells and increased Th1 cells. Most importantly, clodronate treated mice exhibited reduced severity of EAE progression compared to controls (Moreno *et al.*, 2016).

Macrophages evidently play a critical role in the immunopathogenesis of EAE, however they are also implemental players for disease regression at later stages of EAE. Even though their depletion demonstrates an alleviation of clinical disease, there are evidence that illustrates an important role for macrophages in CNS debris clearance and resolving stages of MS. The beneficial importance of macrophages in attenuating disease activity lies in their ability to express anti-inflammatory molecules and tissue repair mechanisms (Jiang, Jiang and G. X. Zhang, 2014). Alternatively activated macrophages demonstrate disease attenuating abilities

by dampening the proinflammatory cytokine cascade through IL-10 production, along with expressing the mannose receptor and metalloproteinase 9 (MMP-9) (Jiang, Jiang and G. X. Zhang, 2014) and is discussed further in section 1.3.5.4.

Overall, the heterogenicity of macrophage polarisation is an important feature of these immune cells during disease progression of demyelinating disorders. It is known that both proinflammatory and immunoregulatory phenotypes of macrophages co-exist during MS and EAE, hence these cells are not solely detrimental during disease progression but most importantly assist with tissue repair.

1.3.5.1 Factors regulating macrophage phenotypes

Macrophages have abilities of polarising from proinflammatory to anti-inflammatory phenotypes, and vice versa, under appropriate environmental conditions. Upon inflammatory insults, macrophage phenotypes exhibit increased expression of GM-CSF, IFN-γ, IL-1β, and TNF-α. In contrast, macrophages may alter their phenotypes and exhibit immunomodulatory molecules such as upregulated IL-10 expression. These polarisation factors will be discussed further in the following paragraphs.

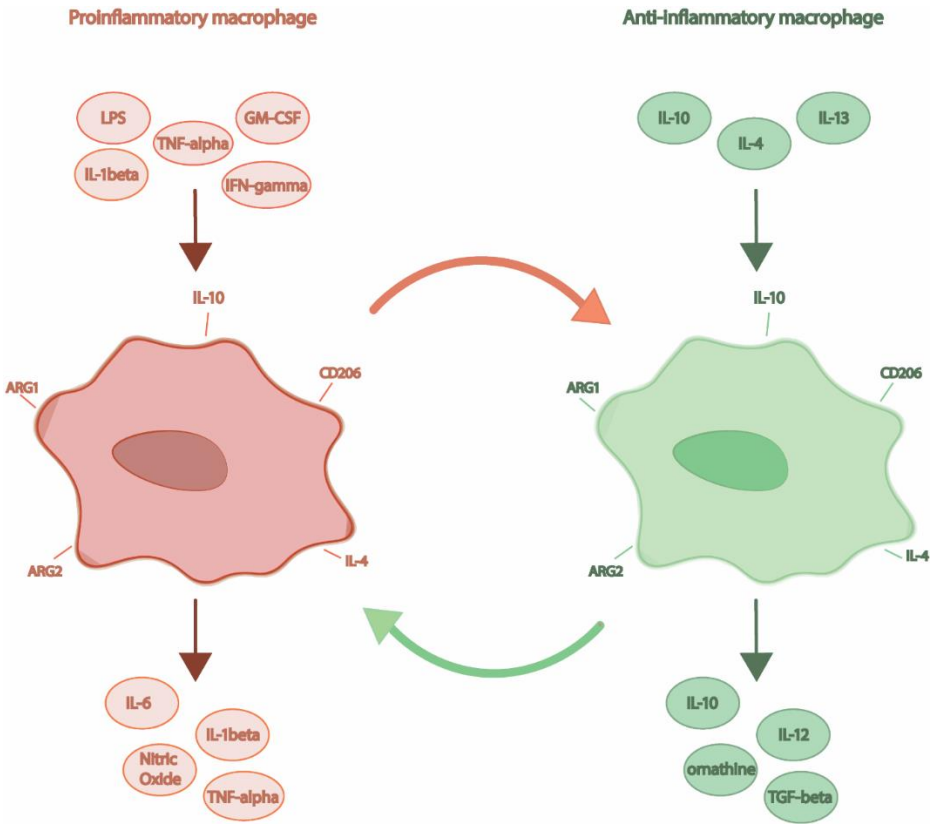

Figure 1.3 Macrophage Polarisation. Macrophage plasticity abilities to polarise from a proinflammatory phenotype towards an anti-inflammatory phenotype, and vice versa, depending on their exposure to agonists.

Granulocyte macrophage colony-stimulating factor (GM-CSF) is a proinflammatory hematopoietic growth factor involved in governing the expansion of bone marrow derived macrophages under inflammatory conditions. Under homeostatic conditions, GM-CSF promotes monocyte/macrophage maturation, and has the ability to differentiate myeloid derived cells under inflammatory environments and as previously mentioned, GM-CSF is critical for differentiating $CCR2^{+}Ly6C^{hi}$ infiltrating monocytes during EAE (Croxford, Spath and Becher, 2015b). Moreover, GM-CSF evidently plays a critical role in EAE development as GM-CSF deficient mice are resistant to disease. Additionally, administration of rGM-CSF to EAE mice resulted in enhanced disease severity (Jonathan L. McQualter, et. al, 2001). A separate study focusing on the role of GM-CSF in CNS inflammation observed alterations to the quantity and locations of myeloid cell infiltrates within the CNS when GM-CSF levels were disrupted in EAE Csf^{CD4} mice (Spath *et al.*, 2017), suggesting GM-CSF is involved in maintaining the macrophage infiltrate population within the CNS. The inflammatory role of GM-CSF is translational from EAE to MS to a certain extent, whereby

elevated levels of GM-CSF are present within the CSF but not serum of MS patients during disease progression (Spath *et al.*, 2017). Although the role of GM-CSF in MS is understood to promote proliferation and expansion of macrophages within the CNS, there is additional interest of this cytokine in relation to T cell pathogenesis in MS and EAE (Kostic *et al.*, 2018).

IFN-γ is generally referred as a proinflammatory cytokine strongly associated with Th1 cells, however it additionally mediates essential anti-inflammatory mechanisms within the CNS during EAE (Miller *et al.*, 2015). Whilst exploring the role of IFN-γ during EAE, mice injected with systemic IFN-γ or directly into the CNS exhibited attenuated clinical disease scores, yet MS patients administered with IFN-γ as a therapeutic based upon the beneficial role observed in animal models presented with drastically enhanced disease severity. These contrasting outcomes emphasised the duel effector function IFN-γ exerts on immune cells within settings of autoimmune mediated neurodegenerative diseases. IFN-γ reportedly induces both a pathogenic and protective role in macrophages during the progression of EAE (Arellano *et al.*, 2015). Macrophage production of NO in response to IFN-γ has shown to not only cause direct neuron toxicity but also directly supresses $CD4^+$ T cell proliferation. In contrast, IFN-γ plays a pathogenic role in macrophages by increasing CCL2 expression and thereby facilitating $CCR2^+$ macrophage migration into the spinal cord during typical EAE (E. H. Tran, Prince and Owens, 2000; Elise H Tran, Prince and Owens, 2000).

IL-1β is considered a hallmark for CNS inflammation and a potent inflammatory cytokine critical for EAE. It is mainly produced by monocyte derived macrophages and CNS resident macrophages (microglia) (Liu and Quan, 2018). Studies investigating the importance of IL-1β in the context of EAE have verified IL-1β and IL-1R deficient mice exhibit resistance or severely impacted EAE clinical scores (Lin and Edelson, 2017). One study confirmed IL-1β facilitates the migration of periphery monocytes to infiltrate the spinal cord prior to onset of clinical scores. Additionally, IL-1β deficient mice exhibited reduced neutrophil levels within the periphery and reduced abilities of monocytes and neutrophils to migrate into the CNS during disease progression (Paré *et al.*, 2018b). The extent of CNS inflammation in EAE contributed to monocyte derived macrophages is highlighted as these cell subsets are

important sources of IL-1β (Lin and Edelson, 2017), a crucial cytokine for disease development.

TNF-α is another inflammatory cytokine heavily involved in promoting inflammatory cytokine cascades during autoimmune diseases. Macrophages are not only a major source of TNF-α production, but they are highly receptable to TNF-α signalling. It is a pivotal player of causing further inflammatory signalling cascades, and has abilities of sustaining IFN-β <48 hours post TLR agonist treatment through an autocrine feedback loop (Parameswaran and Patial, 2010; Valentin-Torres *et al.*, 2016). In the context of EAE, blocking TNF-α with anti-TNF-α treatment resulted in a delayed onset of clinical disease and a reduction of EAE incidence (Batoulis *et al.*, 2013). Although EAE mice exhibited ameliorated clinical scores initially, there were no confirmed alterations to Th1/Th17 activity in the CNS. However, there was an evident increase of Th1/Th17 immune responses in the periphery (Batoulis *et al.*, 2013), emphasising the multifunctional role of TNF-α in EAE. Moreover, a protective role of TNF-α is highlighted during a randomised clinical trial for MS utilising an anti-TNF-α agent, Lenercept. Lenercept surprisingly opposed expectations whereby MS patients displayed exacerbated clinical scores with more severe neurological deficits compared to placebo controls ('TNF neutralization in MS: results of a randomized, placebo-controlled multicenter study. The Lenercept Multiple Sclerosis Study Group and The University of British Columbia MS/MRI Analysis Group.', 1999). After Lenercept was concluded to exacerbate MS severity, Taoufik et. al, confirmed protective roles for TNF-α in relation to EAE (Taoufik *et al.*, 2011). It was reported that blocking only the soluble form of TNF-α and not the transmembrane form led to decreased inflammatory cytokine cascades within the CNS. Furthermore, inhibiting solely soluble TNF-α increased glial fibrillary acidic protein, a neuroprotective agent within the spinal cord, and decreased phosphorylation levels of NFκB (Taoufik *et al.*, 2011).

IL-10 is a well established anti-inflammatory cytokine with great influence on attenuating a mounted immune response. Macrophages are considered the main recipient affected by IL-10 signalling (Minton, 2017). IL-10 severely impacts macrophage activation states by signalling through Stat1 and Stat3, signalling in this Stat dependent manner allows IL-10 inhibition of inflammatory molecules such as: IL-1β, IL-6, TNF-α, IFN-γ, and CD86 (Liu,

WMoore and L-FMui, 1998). IL-10 was additionally proven to be involved in targeting macrophage metabolism, whereby IL-10 deficient bone marrow macrophages presented with altered mitochondrial functions, decreased autophagy levels, and increased IL-1β production when challenged *in vitro* with LPS (Minton, 2017). One of the immunoregulatory effects of macrophages include debris clearance of apoptotic cells, it is strongly suggested IL-10 producing macrophages prominently facilitate the clearance of early apoptotic cells (Xu *et al.*, 2006). IL-10 is one of the select cytokines produced by Th2 cells, a differentiated T cell phenotype associated with attenuated inflammation in EAE. Furthermore, IL-10 transgenic mice exhibited resistance to EAE disease development, whereas IL-10 deficient mice exhibited increased severity of clinical scores (Bettelli *et al.*, 1998). Although IL-10 is considered the most effective anti-inflammatory molecule, harnessing these anti-inflammatory properties into an MS therapeutic is evidently difficult and has not yet been efficiently achieved. There are plausible reasonings behind the failure to achieve an effective IL-10 targeted DMT in MS such as, the potential of increasing MHCII expression on B cells, and delivery methods of administrating IL-10 (Saxena *et al.*, 2015).

1.3.5.2 Macrophages and their role in CNS damage

Monocytic derived macrophages facilitate neurotoxic processes within the CNS through several mechanisms. Macrophages are reported to exert classical activation functions during early stages of EAE prior to repolarising towards their anti-inflammatory phenotype. During the proinflammatory classically activated state, macrophages have abilities to promote demyelination by antigen presentation to T cells via MHCII, CD40, and CD86 (Girvin, Dal Canto and Miller, 2002; Bartholomäus I, Kawakami N, Odoardi F, Schläger C, Miljkovic D, Ellwart JW, 2009). Macrophages additionally upregulate proinflammatory cytokines that enhance inflammatory stress within the CNS and further facilitates the clinical progression of early stage EAE. They also release neurotoxic gases including NO and reactive nitrogen species (RNS) which has a direct negative impact on remyelination processes (Jiang, Jiang and G.-X. Zhang, 2014).

Inducible nitric oxide synthase (iNOS) is an inflammatory gene mediator classically used to identify the polarisation phenotypes of macrophages. INOS competes with anti-inflammatory gene ARG1 to convert L-arginine that results in NO production, a potent

cytotoxic agent. Multiple inflammatory agonists (IFN-γ, TNF-α) have been confirmed to induce iNOS, which in turn causes NO production and direct CNS tissue toxicity (Farias *et al.*, 2007). INOS has been strongly implicated with promoting chronic inflammation in diseases such as EAE, furthermore, increased NO levels in the CSF of MS patients are evident which additionally correlates with disease severity (Sonar and Lal, 2019). Therefore, it was surprising to confirm NOS2 deficient mice displayed exacerbated EAE clinical scores (Jeffrey Weidner *et al.*, 1998). Further studies aimed to understand why this outcome occurred suggesting the role of iNOS in EAE is more complex than originally hypothesised. Weidner et. al, performed a study focussing on the impact of iNOS depletion at separate clinical stages of EAE (Sonar and Lal, 2019). It appeared iNOS regulated immune cell infiltration into the CNS during distinct stages of disease but did not alter lymphocyte priming of myelin-specific antigens during preclinical stages. Depletion of iNOS during antigen-priming stages of EAE resulted in an influx of granulocytic myeloid cells into the brain only, whereas depletion of iNOS in the effector stages of disease promoted increased cellular infiltration into the spinal cord only (Sonar and Lal, 2019). The complex interplay between iNOS and EAE activity is complicated, but emerging studies are beginning to elucidate the mechanisms of this classical inflammatory mediator. Future studies separating distinct stages of EAE may underpin not only how but at which timepoint is important for mediators of inflammation to exert their pathogenic functions.

1.3.5.3 Macrophage repair mechanisms

Macrophages exhibit a vast array of functional characteristics, including resolution of inflammation and promotion of tissue repair. Macrophages are strong mediators of producing anti-inflammatory cytokines and debris clearance, pivotal processes for facilitating tissue repair (Oishi and Manabe, 2018), so their importance within a chronically inflamed environment is critical for limiting tissue destruction.

Macrophage polarisation within an *in vivo* environment is considered to comprise of a spectrum of heterogenous phenotypes rather than entirely proinflammatory or anti-inflammatory states. Furthermore, macrophages have been documented to undergo an intermediate transition phase whereby they exhibit a differential shift in iNOS expression to ARG1 expression during disease resolving stages in EAE (Locatelli, Theodorou, Kendirli,

Jordão, *et al.*, 2018). There are additional known markers to identify repair states, for instance Ly6C^{hi} macrophage populations appear to diminish whilst predominantly Ly6C^{low} populations emerge during reparative processes within the CNS (Oishi and Manabe, 2018).

ARG1 is a gene marker of anti-inflammatory polarisation of macrophages. It is involved in competitively binding with iNOS to convert L-arginine to ornithine and urea (Xu *et al.*, 2003). It is a metabolic enzyme that tightly regulates nitrogen metabolism within the cell. The relevance of ARG1 in EAE is highlighted when its expression levels were drastically upregulated during EAE progression, specifically within spinal cords of EAE mice. More importantly, inhibiting arginase activity with ABH resulted in attenuating EAE clinical scores (Xu *et al.*, 2003). As ARG1 is associated with an anti-inflammatory macrophage phenotype, its inhibition leading to disease alleviation is unexpected, therefore perhaps the unspecificity of ABH eliminating all arginase activity is detrimental, as ARG2, an isoform of ARG1, would also be non-specifically targeted. Although there is an evident involvement of ARG1 negatively regulating iNOS and NO production by binding to L-arginine, there is contrasting data supporting an overall pathogenic role of ARG1 in neurological autoimmune diseases such as EAE (Caldwell *et al.*, 2015). Further research into the exact mechanisms of classical anti-inflammatory macrophage marker ARG1, and its isoform ARG2 during specific stages and timepoints of disease could expand insights to how these arginase enzymes function, as their roles do not appear to be fully elucidated, as evidenced by inconsistent literature (Yang and Ming, 2013; Ahmad, Shah and Doré, 2016; Choudry *et al.*, 2018a; Fouda *et al.*, 2018).

Debris clearance through phagocytosis is an essential process for remyelination to occur. Macrophages play crucial roles in clearing dead cell and myelin debris during neuroinflammation. Macrophages have been visualised to phagocytose myelin debris in active MS lesions since the 1970's, however the exact functional role of macrophages during this occurrence remained unelucidated until more recent studies on macrophage phenotypes during myelin phagocytosis emerged. Uptake of myelin debris within the CNS has since been documented to cause alterations to macrophage phenotypes and functional abilities (Kopper and Gensel, 2018). One study demonstrated how phagocytosed myelin can cause morphological changes in macrophages towards a 'foamy' appearance, due to increased lipid

content within the macrophage membrane. Myelin is a highly concentrated lipid containing material, which also consists of cholesterol and protein, but it is the lipid component that creates the foamy-like appearance of macrophages when it is phagocytosed (Jiang, Jiang and G. X. Zhang, 2014; Grajchen, Jerome J.A. Hendriks and Bogie, 2018). Although internalisation of myelin has previous associations with facilitating CNS inflammation, foamy macrophages have been documented to express anti-inflammatory and neuroprotective properties such as IL-10, TGF-β, and IL-4 at the centre of MS lesions (Boven *et al.*, 2006; Grajchen, Jerome J. A. Hendriks and Bogie, 2018). Furthermore, foamy macrophages have been described to follow three distinct phases which includes tissue repair activity, these include: receptor signalling, intracellular processing, and aging (Henderson *et al.*, 2009; Grajchen, Jerome J.A. Hendriks and Bogie, 2018). During the receptor signalling phase, foamy macrophages exhibit a proinflammatory phenotype with increased expression of TNF-α, IL-1β, IL-6 and NO production, along with decreased expression of ARG1 and the mannose receptor. Foamy macrophages then appear to transition into an intracellular processing stage whereby myelin is internalised and associated with a reparative phenotype. This reparative phenotype consists of increased IL-10, IL-1RA, and peroxisome proliferator activated receptors (PPAR). The inflammatory signature of macrophages is supressed due to the activation of these nuclear receptors. The final aging stage of foamy macrophages exhibit a proinflammatory phenotype with increased IL-1β expression and activation of the NOD-like receptor protein 3 (NLRP3) inflammasome. Inflammasome activation arises from the inability to efficiently process the phagocytosed myelin material containing high levels of cholesterol (Grajchen, Jerome J.A. Hendriks and Bogie, 2018). A separate study surrounding myelin-laden macrophages demonstrated a reduction in IFN-γ production from T cells when exposed to myelin-laden macrophages compared to controls (van Zwam *et al.*, 2011). This study additionally outlined how myelin-laden macrophages retained the capacity to cause T cell proliferation but not differentiation towards a Th1 phenotype. Most importantly, even though there were no alterations to IL-10 and IL-17 production, myelin-laden macrophages could attenuate clinical scores of EAE (van Zwam *et al.*, 2011).

Accumulating evidence suggests iron as an important factor for macrophage uptake of myelin within the CNS (Schonberg *et al.*, 2012; Gillen *et al.*, 2018). Iron uptake in macrophages during MS has strong associations with proinflammatory macrophage phenotypes. Gillen at al. strongly suggested iron uptake further enhances proinflammatory

phenotypes. Additionally, it is proposed that iron containing macrophages and microglia are persistent for long periods of time within chronic inflammatory MS lesion sites, outlining iron as a potential biomarker of chronic inflammatory lesions (Gillen *et al.*, 2018). In contrast, there are noted benefits of iron/ferritin towards repair and oligodendrocyte replacement within the CNS. Schonber et al. acknowledged the harmful effects of excessive iron and ferritin in macrophages and how it can contribute to oxidative stress, and neuron and oligodendrocyte cell death. However, it was also noted CNS tissue repair relies on iron and ferritin for remyelination and axon restoration processes (Schonberg *et al.*, 2012). Overall, these studies highlight how macrophages can be skewed to a reparative phenotype to facilitate remyelination by iron/ferritin, however they may also be negatively influenced to cause damage. Therefore, further insights to how metabolic mechanisms appropriate macrophages towards repair need to be elucidated.

It is understood macrophages contain the ability to regenerate myelin within the CNS (Rawji, Mishra and Vw, 2016). Remyelinating capacities of macrophages was highlighted in studies that depleted macrophages in focal demyelination animal models and observed limited remyelination and failure to successfully clear myelin debris (Kotter *et al.*, 2005). Macrophages have been documented to directly promote oligodendrocyte proliferation through their production of TNF-α, and further promote oligodendrocyte differentiation through their secretion of activin A, IGF-1, endothelin-2, and trophic factors. Macrophages additionally promote remyelination by remodelling the extracellular matrix and supressing molecules that inhibit oligodendrocyte differentiation such as chondroitin sulfate proteoglycans (CSPGs) (Rawji, Mishra and Vw, 2016).

1.3.5.4 Current therapeutics and macrophages

Potential MS therapeutics targeting macrophages are not as established as DMTs targeting the adaptive immune system, yet emerging preliminary findings from macrophage targeted therapies hold promise. In addition to supressing proinflammatory aspects of these innate players, repolarisation and repair abilities appear an opportunistic avenue that minimises neuroinflammation whilst promoting remyelination.

The phagocytic ability of macrophages and their recruitment across the BBB into the CNS during EAE allows for transport and nanoparticle (NP) delivery systems for therapeutic use (J. Wang *et al.*, 2019). Montes-Cobos et al. attempted to improve current approved glucocorticoid (GC) therapy to limit unwanted side effects. These studies confirmed GCs with inorganic hybrid nanoparticles (i.e. BMP-NP) exhibited preferential uptake by phagocytic macrophages while also exerting immunomodulatory functions, overall limiting systemic side effects (Montes-Cobos *et al.*, 2017).

Zhang et al. performed studies targeting a proinflammatory transcription factor in macrophages, c-Rel, via siRNA to supress targets of NFκB activation and limit the overall inflammatory response. Collectively, Zheng confirmed that suppression of IL-12, IL-23, and IL-1β through c-Rel inhibition ultimately led to downregulated IFN-γ and IL-17A production *in vitro* from macrophages cultured with MOG-specific T cells. When Zhang translated c-Rel depletion in macrophages *in vivo* using an EAE model via a nanoparticle delivery system, Th1/Th17 immune responses were attenuated along with reduced T cell infiltration into the CNS, ultimately resulting in ameliorated EAE clinical scores (H. Zhang *et al.*, 2017).

Fumaric acid esters (FAE) have previously been used for the treatment of psoriasis and is further suggested to play a beneficial role in MS. Schilling et al. confirmed beneficial findings utilising FAE in the context of EAE through mechanisms mediated by the infiltration of macrophages. Schilling et al. demonstrated a reduction of macrophage infiltration in the spinal cord post FAE treatment that strongly correlated with disease course amelioration (Schilling *et al.*, 2006). Furthermore, another compound termed forskolin caused attenuated disease severity in EAE. This event was confirmed to occur from increased ARG1 and downregulated CD86 in macrophages (J. Wang *et al.*, 2019).

Collectively, emerging preliminary data focusing on targeting macrophages for alleviating disease activity proves optimistic. Macrophages have many functions which may be skewed for potential therapeutic effects. Moreover, utilising phagocytic abilities of macrophages to deliver compounds via a nanoparticle delivery system when being recruited directly into the

CNS through their chemotactic gradient offers invaluable potential that has yet to be fully explored.

1.3.6 Microglia

Microglia are members of the glial cell family found within the CNS. They are classically known as resident innate immune cells involved in surveying the CNS during healthy states with reactive abilities during neuroinflammation (Wlodarczyk et al. 2015, Graeber & Streit 2010). Although they are referred to as resident innate immune cells of the CNS, their origin is quite different by commencing in the embryonic yolk sac during development as opposed to being derived from a haemopoietic lineage like blood born innate immune cells (Graeber and Streit, 2010; Amici, Dong and Guerau-de-Arellano, 2017). Additionally, microglia reportedly share cell surface markers as infiltrating bone marrow derived macrophages, CNS border resident macrophages, and dendritic cells. It is proposed these immune cell subsets co-exist simultaneously during homeostatic conditions and undergo phenotypic changes during inflammation. Elucidating phenotypes and functions of these cells prove critical to understand disease mediating mechanisms during autoimmune mediated demyelinating diseases. Mrdjen et, al. demonstrated these cell populations can be delineated utilising single cell RNA sequencing (sc-RNAseq). Transcriptional analysis can be performed from sc-RNAseq samples to distinguish microglial transcriptional profiles (Mrdjen *et al.*, 2018), an invaluable tool for mapping which cell type is responsible for underlying disease related mechanisms. Additionally, microglia may be identified simply by their cell surface markers, as transcriptional analysis of microglia reveal they share surface markers with peripheral immune cells it is vital these cells are recognised by more than one marker, in mice some include: $CD45^{int/low}$, CX3CR1, and Tmem119 (Sousa, Biber and Michelucci, 2017).

Microglia exhibit abilities to alter their morphology and transcriptional profile depending on their environment and signalling molecules (Song and Colonna, 2018). During homeostatic conditions, microglia behave as sensors by surveying their environment through extending and morphing their processes around other glial cells and neurons removing cell debris and monitoring neuron activity (K. K. Thompson and Tsirka, 2017). During these roles, microglia are termed ‘resting’ in an anti-inflammatory neuroprotective polarisation stage. Resting microglia are also recognised as patrolling microglia and are described to exert

higher motility compared to activated microglia. Additionally, resting microglia may be distinguished from their activated state by the profile of the molecules they express and secrete such as: IL-10, ARG1, CCL22, and CD206 (Luo *et al.*, 2017a).

There is accumulating evidence of microglia playing both neuroprotective and neurodegenerative roles during neuroinflammation. Research groups have proposed the outcome of neuronal health during CNS inflammatory diseases is dependent on timing, duration of insult, morphological state, and localisation of microglia (Patel *et al.*, 2013; Konishi and Kiyama, 2018; Trotta *et al.*, 2018). During early stages of EAE, microglia are considered to transition from a surveying and resting phenotype into an activated proinflammatory mediator of neurodegeneration. It is believed the apolipoprotein (APOE) pathway is responsible for the phenotypic switch of microglia in separate mouse models of neurodegeneration. Microglia was further confirmed to exhibit a proinflammatory phenotype upon phagocytosing apoptotic neurons (Krasemann *et al.*, 2017).

Microglia depletion studies have unveiled differential findings depending on the animal model of disease under investigation. For instance, Macp-1 saporin depletion of microglia populations with an approximate 50% efficacy caused enhanced myeloid derived cell infiltration into the CNS in post ischemic CNS inflammation (Jin *et al.*, 2017). Additionally, decreased neuron lesions were observed in mice deficient in microglia via inhibiting CSF-1R after brain injury (Rice *et al.*, 2017). In the context of EAE, Hepner et al. utilised bone marrow chimeric tg620^{chi} mice to investigate the suppression of microglia activation during EAE progression. Collectively, this study confirmed inhibiting microglia activation and production of NO and cytokines was critical in attenuating EAE disease severity (Heppner *et al.*, 2005).

Similar to monocyte derived macrophages, microglia are receptive to a multitude of cytokines and are additional secretors of proinflammatory and anti-inflammatory molecules proven to intervene with the disease course of EAE and MS. IFN-γ and Heat shock protein 5 (HSPB5) production by infiltrating T cells are confirmed causative agents in microglia polarisation to elicit an inflammatory phenotype, ultimately assisting demyelinating

processes (Voß *et al.*, 2012). When polarised to an inflammatory phenotype microglia produce an array of proinflammatory cytokines such as; TNF-α, IL-6, and Il-1β, alongside antigen presenting and co-stimulatory molecules MHCII and CD40 to present to $CD4^+$ T cells (K. K. Thompson and Tsirka, 2017). The production of TNF-α by microglia has been considered a representative marker of disease progression and demyelination in both MS and EAE (Hanisch, 2002a; Voß *et al.*, 2012; Hirbec, Noristani and Perrin, 2017; Savarin, Dutta and Bergmann, 2018). IL-17 producing cells are critical players in driving neuroinflammation, they are confirmed to interact with microglia resulting in IL-6 induction and NO production (Graeber & Streit 2010). Microglia additionally express chemokine receptors on their surface to attract lymphocytes into the CNS and promote inflammatory stress leading to neuron damage. Such chemokines include CCR3, CCR5, CXCR3, and CX3CR1 (Hanisch, 2002b).

Recently, proinflammatory microglia have been documented to facilitate remyelination from undergoing necroptosis mediated by type-1 IFN signalling. Remyelination appears to occur post necroptosis as microglia repopulate towards a neuro-regenerative phenotype within white matter regions with supressed proinflammatory activation states (Lloyd *et al.*, 2019). In contrast, IFN signalling has previously been documented to contribute to a neurotoxic microglia activation state within grey matter regions, whereby microglia adopt ataxia characteristics that ultimately lead to acute neurodegeneration in EAE (Rubino *et al.*, 2018). These two studies collectively emphasise locational importance of microglia within the CNS, where microglia exert contrasting functions upon exposure to type-1 IFN signalling dependent on their resident region.

Macrophages have been documented to cross-talk with microglia directly by antigen presenting, and indirectly through producing inflammatory and anti-inflammatory molecules (Luo *et al.*, 2017c). Macrophages and microglia co-exist during events of immune mediated CNS inflammation and exert similar functionalities despite their fluctuating cell proportions and heterogenous gene transcriptional profiles throughout disease progression (Chu *et al.*, 2018a; Savarin, Dutta and Bergmann, 2018). Reactive microglia can be found alongside infiltrating macrophages at sites of active lesions in MS releasing NO and chemokines to

recruit lymphocytes, emphasising how these cells play important roles at the centre of ongoing inflammation (Savarin, Dutta and Bergmann, 2018).

In the context of MS, microglia are noted to exert proinflammatory properties in early stages of disease prior to phenotypically switching towards an anti-inflammatory phenotype post-acute stages of disease (Chu *et al.*, 2018b). Within MS lesions, microglia have been observed in active states along the perimeter of lesions in addition to normal appearing white matter regions (Airas, Nylund and Rissanen, 2018). Furthermore, RRMS patients undergoing relapse phases do not exhibit substantial immune cell infiltration into the CNS, suggesting CNS inflammation is driven locally by CNS resident APCs such as microglia (Luo *et al.*, 2017b).

Overall, microglia is strongly suggested to play a double-edged sword in neuroinflammatory diseases (K. K. Thompson and Tsirka, 2017). Those that cause intraneuronal damage seem to elicit reactive microglia that promote further damage to neurons, whereas diseases associated with lipid and protein debris such as the cuprizone mouse model exhibit more of a neuroprotective phenotype, where microglia phagocytose extracellular debris (Song and Colonna, 2018).

1.4 microRNAs

MicroRNAs (miRNAs) are small endogenous non-coding RNA molecules usually comprising of 18-24 nucleotides in length (Bartel, 2004). MiRNAs play fundamental roles as regulatory molecules within all cellular pathways. These regulatory molecules supress gene expression on a post transcriptional level by binding to 3' untranslated regions (3'UTR) on target messenger RNA (mRNA) to induce targeted gene silencing or degradation (Vidigal and Ventura, 2015).

Their biogenesis consists of multiple processes and relies on enzymes and transport proteins for successful synthesis of a mature miRNA (Gebert and MacRae, 2019). Biogenesis is initiated within the nucleus through a transcription process performed majorly by RNA

polymerase II at the miRNA gene site to produce primary miRNA (pri-miRNA) with a structure that resembles a hairpin (Faraoni *et al.*, 2009). Pri-miRNA is cleaved at the base of the hairpin by an endonucleolytic enzyme called Drosha (RNAse III enzyme) within a microprocessor complex. The functional relevance of the mammalian microprocessor complex is to act as a catalytic processor to yield precursor miRNAs (pre-miRNAs). The two main proteins within this complex include Drosha and Di George Syndrome critical region gene 8 (DGCR8). DGCR8 positions the hairpin structure of pri-miRNAs for Drosha to exert its enzymatic mediated cleavage. The microprocessor additionally comprises of several other proteins including p68 and p72 subunits, helicase enzymes responsible for efficient cleavage of certain pri-miRNAs (Treiber, Treiber and Meister, 2012, 2019). Cleavage by Drosha results in pre-miRNAs containing hairpin structures of approximately 70 nucleotides with a 2-nucleotide overhang (Gebert and MacRae, 2019).

Exportin-5 is a transport protein that recognises the 2-nucleotide overhang and enables the export of pre-miRNA from the nucleus into the cytoplasm. It is within the cytoplasm where Dicer (an RNAse III enzyme) processes pre-miRNA via cleavage to result in a mature miRNA duplex of approximately 22 nucleotides consisting of another nucleotide overhang structure. A singular strand from the mature miRNA duplex, termed the guide strand, enters an Argonaute (AGO) protein within an RNA induced silencing complex (RISC), whilst the second strand from the miRNA duplex, termed the passenger strand, is degraded. miRNAs are mature at this stage and can exert their regulatory functions from within the RISC (Gebert and MacRae, 2019).

MiRNA biogenesis dependent on Drosha and Dicer are considered to follow the canonical pathway of mature miRNA development, however there are documented miRNAs that do not require Drosha or Dicer and follow a non-canonical pathway of biogenesis, these include 2 classes of miRNAs that are termed mirtrons or tailed mirtrons (Treiber, Treiber and Meister, 2019). Microprocessor-independent miRNAs are initially derived from splicing, they bypass Drosha processing but are exported into the cytoplasm by the exportin 1 pathway and cleaved by Dicer. It is noted that miRNAs derived from canonical pathways are more conserved to those of microprocessor-independent pathways. In contrast to multiple miRNAs synthesised via a microprocessor-independent manner, there is currently only 1

known Dicer-independent miRNA, this is the miR-451 biosynthesis pathway. MiR-451 undergoes Drosha mediated cleavage within the microprocessor but is also processed by highly conservative AGO slicer abilities. Although miR-451 is too short to be processed by Dicer, the poly(A)-specific ribonuclease is further trimmed before entering the RISC complex to exert its regulatory functions (Treiber, Treiber and Meister, 2019).

Mature miRNAs contain a region of 2-8 nucleotides at the end of their hairpin loop termed a seed region, it is this region that is directly involved in gene regulatory processes by binding complementarily to 3' untranslated regions of target mRNA gene sites. Binding of miRNA seed regions to 3' target mRNA gene sites causes translational repression or degradation (RAMESH S. PILLAI, 2005; Vidigal and Ventura, 2014), overall negatively regulating gene expression at a translational level.

Mature miRNAs found in vertebrates are predicted to target approximately 200 target mRNA transcripts each (Friedman *et al.*, 2009). MiRNAs can achieve target mRNA suppression by complimentary binding of their seed sequences either through canonical (exact sequence pairing) or non-canonical manners (incomplete match pairing between miRNA seed sequence and mRNA sequence) (Agarwal *et al.*, 2015). MiRNA targets can be experimentally validated by Northern/Western blot, immunoprecipitation, mass spectrometry, and RNA sequencing. Northern and western blots would be efficient to measure RNA and protein expression of target mRNAs, respectively (Pasquinelli, 2012).

Computational algorithms have been generated to predict a multitude of miRNA targets however the focus of these computational algorithms is mainly towards canonical binding sites rather than non-canonical predicted miRNA binding sites. Most commonly used computational target algorithms include TargetScan, miRbase, ElMMO, and CLIP (Hausser and Zavolan, 2014). TargetScan was developed as a statistical analysis tool for measuring miRNA target sites individually utilising the probability rates of preferentially conserved targeting (P_{ct}) sites (Friedman *et al.*, 2009). In contrast, miRBase is considered the primary public database of miRNA products. It is a registry of all published miRNA sequences

generated through experiments and deep sequencing that yields highly stringent confident miRNA annotations (Kozomara and Griffiths-Jones, 2014). EIMMO is a computational database focused on predicted interactions between miRNA and complimentary target mRNA. EIMMO can predict seed sequence conservation amongst 4 species including humans and mice, and uses Bayesion phylogenetic models to identify predicted miRNA target sites (Gaidatzis *et al.*, 2007). Crosslinking and immunoprecipitation (CLIP) is another method to predict miRNA target sites through identifying AGO-binding sites. Some limitations that apply to computational algorithms include false positive or false negative miRNA prediction sites due to the incomplete complementary sequence binding. Additionally, computational algorithms may not include all deciding factors of complimentary sequence binding and therefore overestimate target predicting sites *in vivo* (Brodersen and Voinnet, 2009). Improvements to assist overcoming these challenges include combination techniques of existing computational prediction programs such as combining CLIP with high-throughput sequencing (HITS), termed HIT-CLIP (Pasquinelli, 2012).

1.4.1. miRNAs involvement with the immune system

MiRNAs are known fine tuners of the immune response that regulate both innate and adaptive immune cell gene expression (O'Neill, Sheedy and McCoy, 2011; Baulina, Kulakova and Favorova, 2016). They play a role in all aspects of immune cell function ranging from immune cell development and differentiation, to immune cell activation and functional responses (Lindsay, 2009). Table 1.3 outlines mRNA targets of influential miRNAs and their involvement in autoimmune mediated diseases.

Table 1.3 miRNAs involved in regulating the immune system.

MiRNA	MiRNA Targets	Immune cells impacted	Autoimmune disease associations	References
miR-21	SPRY1, PDCD4, PTEN	T cells, B cells, DCs, macrophages, neutrophils	MS, SLE, RA, IBD, Psoriasis.	(Wang, Wan and Ruan, 2016)
miR-124	TRAF6, MCP1, STAT3, MyD88	T cells, DCs, macrophages	EAE, IBD, RA, Alzheimer's disease	(Pizzorusso *et al.*, 2015; Qin *et al.*, 2016)
miR-125a/b	TNF-α, IRF4, Akt, 5-LO, KLF13, UVRAG	T cells, B cells, DCs, macrophages, NK cells	MS, Alzheimer's disease, SLE, Crohn's disease	(Lindsay, 2009; Lee, Kim and Jo, 2016)
miR-146	IRAK1/2, TRAF6, STAT1, ICOS, PKCε, IRF3	T cells, B cells, DCs, macrophages, NK cells	EAE, SLE, RA, Sjögren's syndrome,	(Xu *et al.*, 2012; Testa *et al.*, 2017)
miR-155	SOCS1, p27, KPC1, JARID2, S1pr1, SHIP1, MAF8, Rac1, TSPAN14	T cells, B cells, DCs, macrophages, neutrophils, NK cells	MS, EAE, SLE, RA, UC, IBD, Psoriasis, Alzheimer's disease	(Rui-Xue Leng, Hai-Feng Pan and Wei-Zi Qin, Gui-Mei Chen, 2011; Testa *et al.*, 2017)

Numerous miRNAs play a regulatory role in both myeloid and lymphoid development and differentiation. For instance, MiR-17-5p, miR-20a, and miR-106a has been documented to target acute myeloid leukaemia-1 (AML-1) mRNA at the 3' untranslated region within monocytes to supress proliferation, maturation, and differentiation (Lindsay, 2009; Tsitsiou and Lindsay, 2009). Upon targeting AML-1, M-CSF receptor has been reported to decrease which leads to suppression of monocyte maturation and differentiation along with enhanced blast proliferation (Fontana *et al.*, 2007). To further highlight the influential role of these miRNAs in monocytopoiesis, anti-miRs of miR-17-5p, miR-20a, and miR-106a have proven to cause reversable outcomes leading to upregulation of M-CSF receptor, increased macrophage development, and decreased blast cell proportions (Fontana *et al.*, 2007).

The miR-17-92 cluster is an example of how miRNA clusters are involved in cell differentiation (Tsitsiou and Lindsay, 2009). MiR-17-92 acts as a finetuner to myeloid cells, and also T, B, and NK lymphocytes (Kuo, Wu and Yang, 2019). In macrophages, miR-17-92 reportedly downregulates monocyte maturation and differentiation, in addition to upregulation of blast cell proliferation. B cells are functionally affected by this miRNA through promoting germinal centre B cell proportions whilst hindering the presence marginal zone B cells. Additionally, miR-17-92 has shown to enhance early B cell development. T cell differentiation is mainly regulated by this miRNA cluster, whereby Treg differentiation is supressed and Th1 and Th17 responses are enhanced. Furthermore, miR17-92 notably promotes T follicular helper cell migration and differentiation (Kuo, Wu and Yang, 2019).

MiR-155 is another miRNA with functional roles of skewing lymphoid and myeloid cell proliferation and differentiation. Within B cells, miR-155 has been recorded to interfere with B cell Ig class switching from IgM to IgG by targeting transcription factor PU.1. MiR-155 has also been shown to skew T cell subsets. It appears in the absence of miR-155, T cells have a majorly skewed Th2 phenotype compared to Th1 phenotypes, suggestively mediated through targeting transcription factor musculoaponeurotic fibrosarcoma (c-Maf) (Lindsay, 2009). MiR-155 has additional functions in myeloid cell proliferation, it has been recorded that miR-155 promotes the expansion of monocytes and granulocytes post exposure to TLR agonist LPS. Furthermore, the involvement of miR-155 in immune cell expansion is highlighted with the strong association of overly expressed miR-155 in acute myeloid leukaemia (AML), with the presence of myeloid neoplasia characteristics (Lindsay, 2009).

Innate immune cells are the first line of defence when confronted with antigens, they have rapid abilities to promote an inflammatory response by signalling through TLRs to activate transcription factors when challenged by an agonist (Kiyoshi Takeda and Shizuo Akira, 2005; Baulina, Kulakova and Favorova, 2016). MiRNAs are confirmed to regulate innate immune responses by finetuning TLR signalling pathways. For example, proinflammatory miR-146a becomes upregulated in response to TLR2/3/4/5 agonists such as LPS, retinoic

acid-inducible gene 1 (RIG-1), and IL-1β (X., Z. and G., 2014). Mir-146a positively regulates the MyD88 and NFκB signalling pathway within macrophages, DCs, T cells, neural cells, and epithelial cells (O'Neill, Sheedy and McCoy, 2011; X., Z. and G., 2014). MiR-155 is another inducible miRNA upon recognition of TLR2/3/4/9 agonists such as LPS, EBV, and *Helicobacter pylori*. MiR-155 has shown to positively regulate MyD88, TRIF, AP1, and NFκB signalling cascades within monocytes/macrophages, DCs, Tregs, and B cells for the promotion of proinflammatory molecules (O'Neill, Sheedy and McCoy, 2011; X., Z. and G., 2014). In contrast, miR-125b is a miRNA that negatively regulates the TLR signalling pathway upon exposure to TLR4 agonists such as LPS. MiR-125b has been shown to attenuate NFκB and AKT1 signalling in macrophages, DCs, and splenocytes and directly target TNF to supress proinflammatory immune responses (O'Neill, Sheedy and McCoy, 2011; X., Z. and G., 2014).

Whilst mRNA expression downstream of TLR signalling pathways are finetuned by miRNAs, cytokine production is also influenced (Mccoy, 2011; Baulina, Kulakova and Favorova, 2016). Certain miRNAs act to inhibit the secretion of cytokines by targeting the components of the secretion pathway. For example, miR-9 targets TLR signalling transcription factor NFκB in response to IL-1 to inhibit the IL-1 response. MiR-155 also participates in a negative feedback loop in response to TNF by targeting Fas-associated protein with death domain (FADD) to mediate TNF-induced apoptosis (Mccoy, 2011). In other cases, miRNAs directly bind to the 3'UTR of cytokine mRNA to cause degradation. For instance, let-7e is an upregulated miRNA in EAE shown to directly target IL-10 mRNA to cause T cell differentiation towards a Th1 and Th17 phenotype (Baulina, Kulakova and Favorova, 2016). IL-10 is also targeted by miR-106a and miR-4661 in response to IL-10 itself for its own stabilisation (Mccoy, 2011). In contrast, miR-26a is a downregulated miRNA found in brain cells during EAE. MiR-26a is shown to target IL-6 mRNA expression for enhancement of Th17 cytokine production (Baulina, Kulakova and Favorova, 2016).

Adaptive immune cell members are dependent on antigen presentation from innate immune cells for recognition of antigens to undergo differentiation, proliferation, and exert their effector functions. Therefore, miRNAs regulate adaptive immune responses quite differently

compared to innate cells. MiRNAs reportedly finetune mRNA expression associated with the development, maturation, and differentiation of T cell subsets and B cells (Baulina, Kulakova and Favorova, 2016). This is most definitively highlighted in Dicer deficient mice, which have profound deficits in B cell differentiation, antibody class production, and interference of B cell VDJ recombination (O'Carroll *et al.*, 2007; Chernajovsky and Robbins, 2010).

In B cells, miRNAs have been identified to play a prominent regulatory role in their development, Ig class switching, proliferation and even cell death. MiR-181a was amongst the first miRNAs identified to play a key role in B cell development (de Yébenes, Bartolomé-Izquierdo and Ramiro, 2013). MiR-181a was found involved in regulating B cell development and differentiation by targeting Bcl-2 like protein 11 (BIM) to prevent BIM mediated apoptosis, thus increasing the proportions of B-lineage cells (Danger *et al.*, 2014). MiR-24 is another miRNA which targets BIM along with caspase-9 to achieve PU.1 mediated suppression of B cell development (Li *et al.*, 2013). MiR-155 is essential for B cell development with extensive studies surrounding the role of this miRNA in B cells. The importance of miR-155 in B cells is highlighted in miR-155 deficient mice, whereby there is an evident lack of germinal centre B cell proportions with a severe reduction of secreted Ig class switching. Furthermore, PU.1 and activation-induced cytidine deaminase (AID) are established targets of miR-155 in B cells, these molecules are confirmed to play an important role in B cell class-switch recombination (CSR) and somatic hypermutation (SHM) (de Yébenes, Bartolomé-Izquierdo and Ramiro, 2013).

Within T cells, multiple miRNAs are confirmed to regulate T cell differentiation, proliferation, and clonal expansion abilities. For example, miR-125b participates in negatively regulating T cell differentiation through interfering with the mTOR and MYC signalling pathway via targeting PR/SET Domain 1 (PRDM1), IFN-γ, and IL1RB (Baumjohann and Ansel, 2013). Correlating with negative regulation of T cell development, miR-146a is involved in inhibiting T cell clonal expansion. NFκB is responsible for inducing this miRNA but in turn miR-146a targets TRAF6 and IRAK1 in a negative feedback loop to suppress T cell clonal expansion (Baumjohann and Ansel, 2013). In contrast, the miR-17-92 cluster is involved in positively promoting T cell proliferation and survival. MYC has been

shown to induce miR-17-92 cluster expression through targeting phosphatase and tensin homolog (PTEN) and BIM, known associators of cell division (Baumjohann and Ansel, 2013).

1.4.2 MiR-155

1.4.2.1 Discovery of miR-155

The B-cell integration cluster (BIC) was initially recognised as an activated gene post promoter insertion at a retroviral integration site of avian leukosis virus (AVL) induced B cell lymphoma. *Bic* expression appeared driven by AVL mediated B cell lymphomas, and was thought to work with c-myc for immune cell activation (Tam *et al.*, 1997). MiR-155 was among 1 of 34 novel miRNA sequences to be discovered in a study using tissue-specific cloning techniques. MiR-155 was excised from mouse colon tissues and was derived from noncoding *BIC* RNA, which was found to exhibit a 78% conservative rate between human, mouse, and chicken cDNA (Lagos-Quintana *et al.*, 2002). Several years after discovering *BIC*, Eis et al. confirmed the positive association of induced miR-155 expression in B cell lymphomas compared to control circulatory B cells and therefore suggested that miR-155 drove the pro-oncogenic activity of *BIC*. Furthermore, miR-155 was associated with activated B cell phenotypes in B cell lymphomas rather than germinal centre B cells (Eis *et al.*, 2005). *BIC* was soon after recognised as pri-miR-155, the precursor of mature miR-155. In a study utilising a Burkett lymphoma cell line named Ramos, B cell receptor induced pri-miR-155/*BIC* expression firstly identified the involvement of NFκB and PKC signalling with miR-155 induction (Kluiver *et al.*, 2007).

1.4.2.2 MiR-155 biogenesis

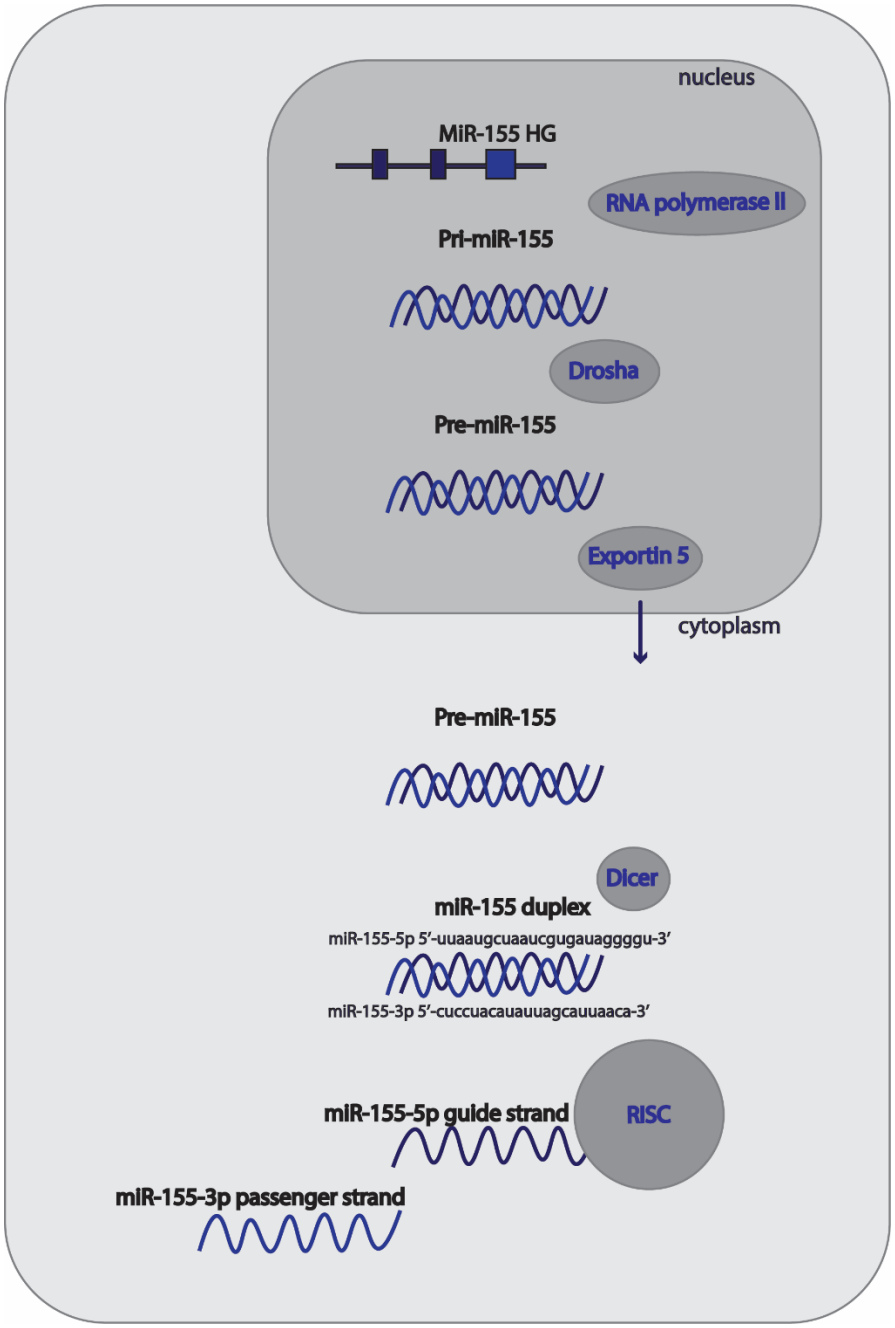

Figure 1.4 The biogenesis of miR-155 including mature sequences of miR-155-5p (uuaaugcuaaucgugauaggggu) and miR-155-3p (cuccuacauauuagcauuaaca) post dicer processing.

MiR-155 is synthesised from the canonical pathway of miRNA biogenesis. The miR-155 house gene is found encoded within the 2nd exon of the *BIC* gene region and transcribed by RNA polymerase II. Once pri-miR-155 is processed by Drosha to pre-miR-155, the miR-155 duplex consists of 2 nucleotide strands with incomplete complimentary sequence

binding structurally resembling a hairpin loop. Pre-miR-155 5' end of the hairpin loop (cuguuaaugcuaaucgugauaggggguuuuugc) is termed miR-155-5p, and pre-miR-155 3' end of the hairpin loop (gacaauuacgauuauacauccucagucaaccu) is termed miR-155-3p (Alivernini *et al.*, 2018). Usually, the passenger strand of the miRNA duplex is discarded as the guide strand enters into the RISC complex to target mRNAs, however there is evidence that both miR-155-5p and miR-155-3p are involved in mRNA targeting. Even though miR-155-3p is generally regarded as the passenger strand and the fold induction is approximately 20-200-fold less compared to miR-155-5p, it appeared functional in DCs when exposed to TLR7 agonists (Zhou *et al.*, 2010).

1.4.2.3 Evolution of miR-155

Evidence of high conservation levels within the *BIC* region amongst a multitude of species heavily implies miR-155 is a highly conservative miRNA. Xie et al. performed a comparative genomics study on the miR-155 family comparing an array of species (Xie *et al.*, 2014). Outcomes from this comparative study confirmed the miR-155-5p arm to be highly conserved among vertebrates, but the miR-155-3p arm appeared to contain nucleotide changes. Usually, it is the miR-155-3p arm which contains the most conserved sequences, hence Xie et al. suggested that miR-155 underwent arm switching at some point. Due to the highly conserved target binding seed sequences in miR-155-5p, its functional mechanisms may also be highly in comparison to miR-155-3p (Xie *et al.*, 2014; Zhuang *et al.*, 2017). Collectively, current evident indicates miR-155 as evolutionary conserved as opposed to evolutionally diverse, this is further highlighted by the consistency of dysregulated miR-155 levels in an array of diseases.

1.4.2.4 Tissue Distribution

MiR-155 is a known miRNA involved in many aspects of cell development and function. Landgrat et al. performed the first survey atlas of miRNAs in humans and mice using an RNA library sequencing approach. This atlas determined miR-155 in humans may be found in respiratory, reproductive, and nervous systems, along with being identified in the kidneys, connective tissues, and embryos. Most importantly, miR-155 was found ubiquitously in the haemopoietic system, indicating a prominent role for miR-155 in immune cells derived from

haematopoiesis. In contrast, miR-155 distribution in mice was less broad, it is mainly identified in the haemopoietic system with less abundance in the liver, reproductive, and respiratory systems (Landgraf *et al.*, 2007). Furthermore, a separate research group that identified the presence of miR-155 in extracellular vesicles in mice, determined extracellular miR-155 may be taken up by cells of the kidney, liver, muscle, lung, and adipose tissue (Bala *et al.*, 2015). The ability of various tissue specific cells to uptake extracellular miR-155 further highlights the broad spectrum of cells and biological systems this multifunctional miRNA can impact and why miR-155 is implemented in an array of various disease states.

1.4.2.5 MiR-155 targets

MiR-155 is known to play a pleotropic role in gene regulatory pathways in all immune cell subsets. TargetScan estimates 4174 genes are targeted by miR-155 in humans, with 918 of these target genes found in mice. However, most computational analysis studies focus on miRNA target binding in a canonical manner rather than non-canonical binding mechanisms. A study performing a large transcriptome-wide identification screen determined approximately 40% of miR-155-dependent AGO binding sites does not have complete complementary seed region binding, suggesting only 60% of miR-155 mediated gene regulation was accountable using software algorithms solely based on canonical binding (Loeb *et al.*, 2012). However, this study additionally confirmed that non-canonical binding of miR-155 to target mRNA did not cause significant gene regulation compared to exact seed region binding, but just attenuated mRNA expression by approximately 2-fold (Loeb *et al.*, 2012). A more recent study utilising differential iCLIP, 3'UTR usage analysis, along with RNA-sequencing, investigated the dependent role of miR-155 mediated gene regulation in T cells, B cells, DCs, and macrophages (Hsin *et al.*, 2018). MiR-155 was confirmed to differentially control gene regulation by preferential 3' UTR binding to transcripts based on the cell type as opposed to an alternative cleavage and polyadenylation (ApA) dependent manner. Furthermore, a miR-155 regulatory map was generated in mentioned four immune cell subsets for in depth analysis of important immune cells from the lymphoid and myeloid immune system. This regulatory map identified 352 miR-155 dependent iCLIP sites in macrophages, 99 of which were also co-expressed in T cells, B cells, and DCs (Hsin *et al.*, 2018), highlighting that miR-155 has the ability to commonly and differentially influence distinct immune cell subsets.

1.4.2.6 The first genetic models of miR-155

The first genetic models of miR-155 deficient mice confirmed the importance of miR-155 in providing an effective immune response. Rodriguez et al. determined a null mutation in the bic/miR-155 gene caused immunodeficiency, along with further observed alterations to the structural composition of lung airways (Rodriguez *et al.*, 2007a). MiR-155 deficient mice demonstrated a decrease in proliferation in response to LPS, in addition to downregulated production of IL-2 and IFN-γ in response to a tetracycline resistance gene (TetC). Furthermore, miR-155 deficient mice presented with increased collagen thickness within the respiratory airways, suggesting a remodelling role for miR-155 within the lungs in the absence of inflammatory agonists (Rodriguez *et al.*, 2007a).

Subsequent studies focusing on miR-155 deficient mice determined the crucial regulatory role for miR-155 in T and B lymphocytes (Vigorito *et al.*, 2013). MiR-155 was proven essential for infection clearance when challenged with attenuated *Salmonella*, although miR-155 deficient mice could clear the *Salmonella* infection, their efficiency was impaired with decreased antibody and cytokine production against the pathogen. The stark efficiency of infection clearance between WT and miR-155 deficient mice was highlighted when this same research group challenged miR-155 deficient mice with a live attenuated strain of *Salmonella*. The causative result for this defective clearance was suggestively related to germinal centre (GC) impairment and not VDJ recombination of GC B cells. Additionally, TNF and Lymphotoxin-α (LT-α) production was notably reduced by B cells of miR-155 deficient mice compared to controls (Thai *et al.*, 2007; Vigorito *et al.*, 2013).

Since miR-155 is a known contributor during pathological conditions, the majority of research focusses on miR-155 in the context of infections, inflammatory diseases, and cancers. However, less is known about miR-155 during homeostatic conditions. Zhang et al. focused on determining the role of miR-155 under normal conditions utilising a miR-155 deficient mouse strain derived from CRISPR/CAS9 technology. Collectively, Zhang determined there were no significant differences between controls and mice deficient for miR-155 in relation to growth and physiological appearances of kidneys and livers. Zhang

confirmed miR-155 to not be involved in mouse development during the initial 8 weeks (42 days) post birth (D. Zhang *et al.*, 2017).

1.4.2.7 The role of miR-155 in haematopoiesis

MiR-155 plays a prominent role in haematopoiesis during both pathological and homeostatic conditions. Due to associations of miR-155 with lymphomas, it was amongst the first miRNAs to be identified in the haematopoietic system (O'connell, Zhao and Rao, 2011). Haematological malignancies strongly associated with prolonged miR-155 expression include B cell lymphoma, Hodgkin's lymphoma, and acute myeloid leukaemia (AML). MiR-155 expression levels are usually low during homeostatic conditions, however there is noted differences in its expression between cells. For instance, miR-155 expression appears lower in mature bone marrow cells compared to HSPCs, and higher in GM-CSF derived DCs compared to M-CSF derived macrophages (O'Connell, Zhao and Rao, 2011).

The importance of miR-155 in haematopoiesis is further highlighted by the abundance of myeloproliferative disorders correlating with prolonged miR-155 expression. MiR-155 within bone marrow samples was found to expand granulocytes and monocytes in response to LPS (O'Connell *et al.*, 2008). Expanded granulocytes and monocytes through miR-155 induction appeared to resemble myeloid neoplasia and contained an array of repressed genes associated with haematopoietic development (O'Connell *et al.*, 2008). Transcription factor PU.1 is essential for immune cell development. This stringently controlled transcription factor is a known target of miR-155 and shown to repress myeloid and lymphocyte differentiation (Prajnya Ranganath, 2015), further demonstrating how miR-155 regulates immune cell differentiation.

The influence of miR-155 in myelopoiesis was determined when homeobox protein 9 (HOXA9) appeared to closely mimic miR-155-5p expression. HOXA9 is an essential protein for haematopoiesis and found in bone marrow, HOXA9 deficient marrow cells were found to display decreased levels of miR-155 expression. HOXA9 also has the ability to induce myeloid colony formation, an ability which appears to diminish in miR-155 deficient mice, indicative of miR-155 being involved in regulating the functions of HOXA9 (Elton *et al.*,

2013). MiR-155 has also been identified to control the development of Tregs. Treg homeostasis was confirmed to rely on miR-155 mediated target binding of SOCS1 to attenuate IL-2 (Elton *et al.*, 2013).

1.4.2.8 The role of miR-155 in disease

Infectious and autoimmune mediated diseases often involve many aspects of the immune system that display deregulated miRNA profiles. MiR-155 is a particularly known miRNA involved in an array of diseases and considered a biomarker of inflammatory stress. Infectious diseases with strong associations of elevated miR-155 expression include those mediated by both bacterial and viral agents. In the context of bacterial infections, miR-155 usually recognises agonists through the TLR pathway, however miR-155 has also been reported to recognise bacterial cell wall component peptidoglycan through NOD2 receptor signalling (Staedel and Darfeuille, 2013). *Mycobacterium tuberculosis* (TB) and *Mycobacterium bovis* (M. *bovis*) are two highly infectious bacterial agents that affect humans and animals, respectively. MiR-155 is notably induced in macrophages post TB and M. *bovis* infection, leading to elimination of the mycobacterium pathogen through altering macrophage phagocytosis processes to facilitate ROS production (Zhou, Li and Wu, 2018). MiR-155 deficient mice further proves the importance of miR-155 during TB infection by representing a higher mortality rate with higher quantities of colony forming units within their lungs compared to WT controls (Zhou, Li and Wu, 2018). In the context of viral infections, miR-155 has been identified as one of the most implemented miRNAs in latent EBV associated B cell lymphomas (Lu *et al.*, 2008). As previously mentioned, EBV protein LMP1 has the ability to upregulate miR-155 expression to modulate the immune response (Di Lisio *et al.*, 2012).

Autoimmune mediated diseases such as MS, RA, and SLE, have strong correlations with upregulated miR-155 expression. During MS, miR-155 upregulation is confirmed in demyelinating plaques and mononuclear cells derived from whole blood samples (Leng *et al.*, 2011a; Baulina, Kulakova and Favorova, 2016). In RA, miR-155 expression was found at higher levels within synovial fluid, tissue, and fibroblasts compared to osteoarthritis (OA) patients, suggesting a more prominent role for miR-155 in RA than OA. Considering the multifaceted mechanisms of SLE, it is unsurprising the exact role of miR-155 has yet to be

fully understood in this autoimmune disease. Even though miR-155 is considered a proinflammatory miRNA, its expression in serum samples of patients with SLE is significantly lower compared to healthy controls, further, urine samples exhibited relatively the same miR-155 expression between SLE patients and controls. Further highlighting the importance of miR-155 in these mentioned autoimmune diseases, miR-155 deficient mouse models of MS and RA are resistant or display autoimmune impairment of disease (Leng *et al.*, 2011a).

Overall, the prominent role of miR-155 in infectious and autoimmune mediated diseases stresses the need to tightly regulate this miRNA. Due to the widespread presence of deregulated miR-155 in diseases, it has become of interest to companies who wish to harness its master regulatory abilities over the immune response for potential DMTs.

1.4.2.9 MiR-155 Therapeutic approaches

The mass library of miRNA networks illustrates the extensive regulation these molecules exert during homeostatic and disease states, hence their widespread regulatory properties hold promise for intervening therapeutics. There are currently over 20 miRNA-based therapeutics involved in clinical trials, with mechanisms spanning from miRNA delivery systems to siRNA-based drugs. Cancer appears to hold the most abundant miRNA based therapy patents, with autoimmune diseases holding the third most abundant patents (Chakraborty *et al.*, 2017).

Immunopathogenic mechanisms mediated by miRNAs during disease states may be supressed via multiple methods. Such methods are currently in preclinical or clinical trials as potential DMTs for autoimmune diseases and cancers. Some of which include: small molecule inhibitors of miRNAs (SMIRs), miRNA mimics, antisense oligonucleotides targeting miRNAs (AMOs), LNA anti-miRs, miRNA sponges, and antagomirs (Shah *et al.*, 2016).

MRG-106 is an LNA based anti-miR of miR-155 that is currently synthesised by miRagen Therapeutics Inc for clinical trials. MRG-106 is currently in phase II clinical trials for Mycosis Fungoides/cutaneous T cell lymphoma (CTCL). Collectively, this study observed beneficial clinical changes in MRG-106 treated patients, along with no significant differences between the MRG-106 monotherapy group and the MRG-106 in conjunction with the stable therapy group (Foss *et al.*, 2018). The overall positive outcome from MRG-106 Phase I clinical trial has suggested MRG-106 to be trialled for additional miR-155 implemented diseases such as chronic lymphocytic leukemia (CLL), and adult T-cell leukemia/lymphoma (ATLL).

Overall, MRG-106 appears to be a promising candidate to ameliorate clinical outcomes of Mycosis Fungoides/CTCL patients. In the context of MS, miR-155-based therapies have not yet emerged but seems optimistic when considering the prominent proinflammatory role miR-155 exerts during MS and EAE disease progression.

1.4.3 miR-155 in Macrophages

1.4.3.1 miR-155 agonists and antagonists in macrophages

In 2007, O' Connell et. al, confirmed miR-155 as a highly inducible miRNA in mouse macrophages when exposed to TLR agonists (O'Connell *et al.*, 2007). MiR-155 was one of three miRNAs found upregulated in THP-1 monocytes in response to TLR4 agonist LPS and the TLR3 agonist, Poly I:C. MyD88, JNK, and TRIF signalling were deemed essential for miR-155 induction in response to TLR agonists. IFN-β was additionally identified to cause upregulation of miR-155 expression, however this was confirmed to rely on TNF-α autocrine signalling to successfully induce miR-155 (O'Connell *et al.*, 2007). Further studies demonstrated that IFN could induce different immune cell activation states based on miR-155 induction.

Proposedly, if IFN induces miR-155 expression prior to TLR activation, miR-155 regulates the immune cell to become an IFN-mediated protective phenotype. In contrast, if TLR signalling is activated when IFN induces miR-155 expression, miR-155 is confirmed to

inhibit SOCS1 for further enhancement of IFN signalling (Loeb *et al.*, 2012; Forster, Tate and Hertzog, 2015), therefore mediating further inflammatory processes.

IL-1β signals through the IL-1R signalling pathway in myeloid cells and downstream signalling molecules that are essential for IL-1β production include TRAF6 and TAK1. MiR-155 binding of TAK1 and TAB2 has also been shown to modulate IL-1R signalling (O'Neill, Sheedy and McCoy, 2011). Ceppi et al. illustrated a TLR/IL-1 signalling pathway that directly affected miR-155 expression when exposed to bacterial pathogens. MiR-155 also appeared to directly target TAB2 in human monocytic derived DCs and involved in a negative feedback loop to hinder proinflammatory cytokine production (Ceppi, P. M. Pereira, *et al.*, 2009a).

TNF-α has been documented to promote proinflammatory miRNAs including miR-146a in HDLECS *in vitro*, but miR-155 was the highest miRNA induced by TNF-α in these primary cells. Moreover, IFN-γ was recorded to further enhance TNF-α mediated miR-155 induction (Yee *et al.*, 2017a).

IL-10 is confirmed to suppress miR-155 expression when challenged with LPS in primary macrophages *in vitro*. The mechanism of how IL-10 elicits its inhibition on miR-155 was determined through inhibition of BIC transcription in a STAT3-dependent fashion (Claire E McCoy *et al.*, 2010a). Additionally, it was reported IL-10 inhibition on miR-155 depended on the presence of SHIP1 to an extent, for SHIP1 deficient macrophages had impaired miR-155 induction in the presence of LPS (Cheung *et al.*, 2013).

1.4.3.2. Transcriptional regulation of miR-155 in macrophages

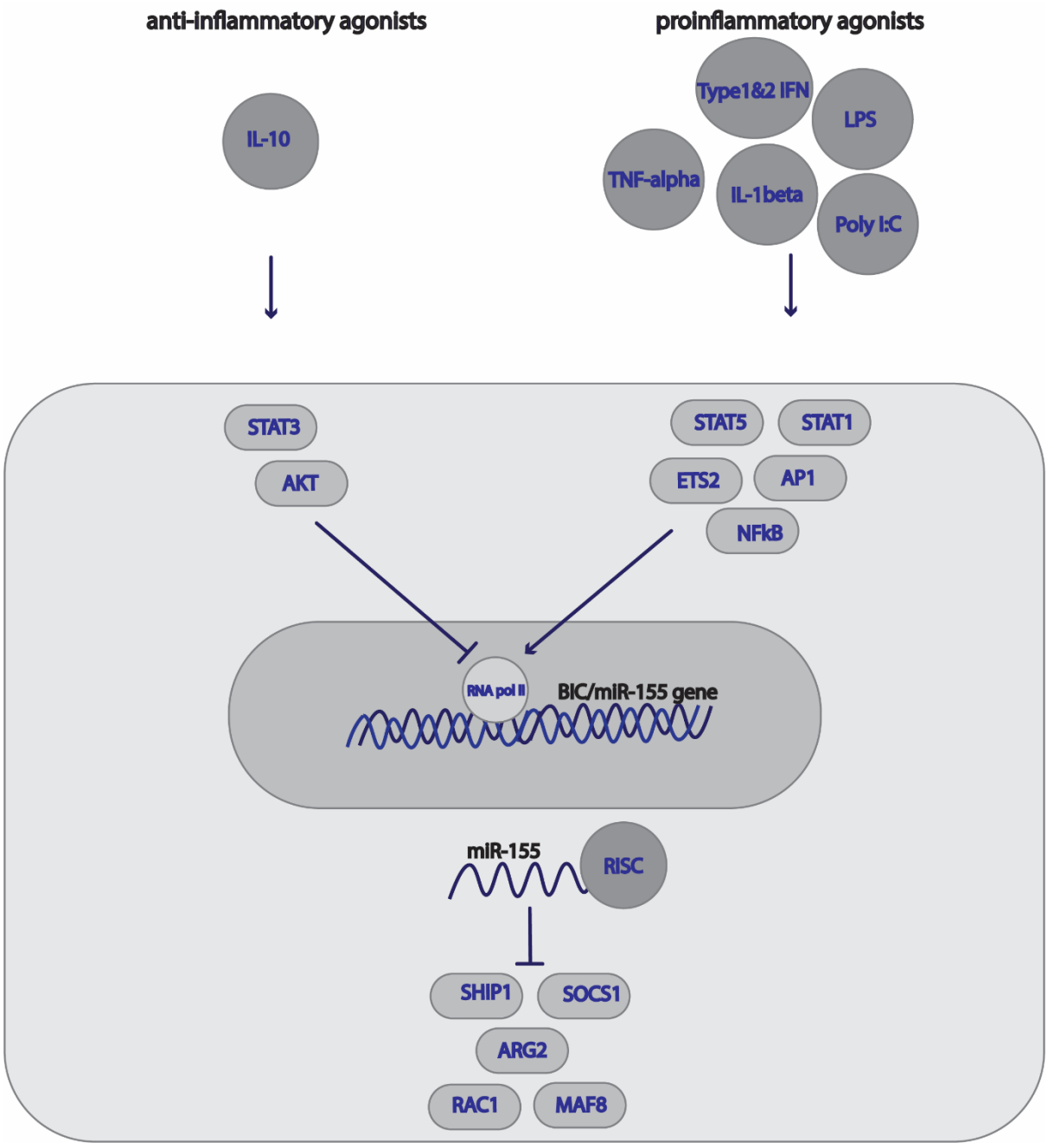

Figure 1.5 Proinflammatory and anti-inflammatory miR-155 agonists and targets within an immune cell.

NFκB is a transcription factor considered to be a major regulatory transcription factor implemented in an array of inflammatory diseases. It shares a network with miR-155 by promoting miR-155 expression to regulate the extent of inflammatory activity. It is unsurprising NFκB shares a correlative relationship with miR-155 as NFκB DNA binding sites have been confirmed within the BIC promoter region, alongside the presence of AP1 and ETS2 DNA binding sites (Yin *et al.*, 2008; Claire E McCoy *et al.*, 2010b; Thompson, Vardinogiannis and Gilmore, 2013). In addition to positively regulating miR-155, NFκB is also impacted by this miRNA by initiating a proinflammatory signalling cascade. The NFκB-miR-155 positive feedback loop is reportedly initiated within 12 hours post TLR exposure and positively enhances inflammation through miR-155 targeting SHIP1 thus activating inhibitor of IκB kinase (IKK) (Markopoulos *et al.*, 2018).

AP1 is a transcription factor that facilitates macrophage production of IL-12 and IL-23 upon exposure of TLR4 agonists. AP1 consists of a dimeric structure comprising of Fos and Jun proteins. In addition to AP1 containing direct DNA binding sites in BIC (Yin *et al.*, 2008), miR-155 is confirmed to directly target c-fos, a member of the Fos family, a regulatory process confirmed essential for DC differentiation and maturation (Yin *et al.*, 2008; Dunand-Sauthier *et al.*, 2011).

Ets2 belongs to one of the largest transcription factor families that are involved in regulating genes within signalling pathways (Oikawa and Yamada, 2003). Ets2 has been identified as a key transcription factor for the regulation of miR-155 expression within macrophages by directly binding to the BIC promoter. To confirm the importance of Ets2 in miR-155 regulation, Ets2 deficient mice exhibited impaired miR-155 induction when challenged with LPS (Quinn *et al.*, 2014). A separate study confirmed a pathogenic role for Ets2 in liver fibrosis, whereby transgenic mice containing a mutated form of Ets2 were protected from disease (Baran *et al.*, 2011), further implicating the involvement of Ets2 in promoting an inflammatory disorder.

MiR-155 transcription is regulated by multiple members of the STAT family of transcription factors (Kohanbash and Okada, 2012). STAT1 and STAT5 are known transcription factors

that positively regulate miR-155 expression, conversely miR-155 has additionally been shown to positively regulate STAT1 and STAT5 expression. Proinflammatory IFN signalling cascades can become initiated by miR-155 mediated activation of STAT1, furthermore IFN related genes are proposedly increased up to 30% through STAT activation. MiR-155 binding of SOCS1 has also been recorded to cause phosphorylation of both STAT1 and STAT3. In contrast to STAT1 and STAT5, STAT3 negatively regulates miR-155 expression by directly supressing its transcription (Kohanbash and Okada, 2012). McCoy et al. determined STAT3 was essential for anti-inflammatory cytokine IL-10 to mediate its suppression of miR-155 transcription within the BIC gene (Claire E McCoy *et al.*, 2010), collectively highlighting how the STAT family play a duel role in the transcriptional regulation of miR-155 expression.

1.4.3.3 Key miR-155 targets in macrophages

MiR-155 targets include proteins that have been identified in cytosolic, nuclear, and membrane regions of immune cells. Some characterised targets within cytosolic regions include: SHIP1 and SOCS1, nuclear proteins targeted by miR-155 include: PU.1, Fos, and those that reside within the span of cell membranes include: CTLA-4 and S1PR1 (Mashima, 2015).

PU.1 is a transcription factor found in lymphoid, myeloid, and tissue specific cells (Umazume *et al.*, 2018). PU.1 is referred to play an important role in macrophages regarding their effector function towards other immune cells. It was further confirmed to influence the expression of antigen presenting molecules on DCs, and positively correlates with enhanced macrophage and DC inflammation in a mouse model of autoimmune uveitis (Umazume *et al.*, 2018). Using PU.1$^{155-/155-}$ chimera mice to study the relationship between miR-155 and PU.1 in the context of adaptive immunity, PU.1 was identified as a direct target of miR-155. Lu et al. determined miR-155 inhibition of PU.1 subsequently led to a reduction in Pax5 expression, which demonstrated a profound effect on B cell differentiation (Lu *et al.*, 2014).

CTLA-4 is a negative regulator of T cell activation and responsible for attenuating an immune response mediated by T cell binding of co-stimulatory molecules on the surface of

APCs. Competitive binding is strongly suggested to occur between CTLA-4 and CD28 for the stimulation of CD80 and CD86, whereby CTLA-4 binding of CD80/86 dampens a proinflammatory response compared to CD28 binding to CD80/86 (Rowshanravan, Halliday and Sansom, 2018). A study surrounding the role of miRNAs in atopic dermatitis confirmed CTLA-4 as a direct target of miR-155. Collectively, Sonkoly et al. identified CTLA-4 suppression mediated by miR-155 overexpression led to enhanced $CD4^+$ T cell proliferation which assisted inflammation (Sonkoly *et al.*, 2010).

S1PR1 is one of five members of the G couple protein receptors with strong influences towards myeloid cell polarisation and migration during CNS autoimmune processes (Tsai *et al.*, 2019). S1P1 signalling has confirmed associations with myeloid cell activation and more importantly was proven influential in the context of myeloid cell involvement during EAE pathogenesis. This signalling receptor could interfere with the clinical outcome of EAE as LysMCre mice deficient in S1P1 presented with atypical clinical scores of disease (Tsai *et al.*, 2019). S1PR1 was identified as a target of miR-155 in the context of allergic and helminth-induced immune responses. Along with facilitating myeloid cell differentiation, S1PR1 is additionally involved in T cell egression from lymphoid organs. Okoye et al. confirmed S1PR1 downregulation through miR-155 overexpression assisted T cell egression from lymphoid organs and interfered with Th2 immunity during allergic airway responses (Okoye *et al.*, 2014).

SHIP1 is a phosphoinositide phosphatase involved in modulating the immune system by negatively regulating immune cell activation and cytokine signalling (Mccoy, 2011; Pauls and Marshall, 2017). Increased levels of SHIP1 have been associated with dampening the immune response by inhibiting NFκB and MAPK activation upon exposure to TLR agonists (Pauls and Marshall, 2017), overall exhibiting functions to attenuate inflammatory environments. SHIP1 has been identified as a direct target of miR-155 (O'connell *et al.*, 2009). MiR-155 has been confirmed to directly bind to the 3' UTR for inhibition of SHIP1 expression to enhance immune cell activation. Furthermore, a direct relationship between miR-155 and SHIP1 can be recognised when miR-155 deficient macrophages present with increased SHIP1 expression levels. Interestingly, depletion of SHIP1 exhibited similar functional outcomes to those of increased expression of miR-155, whereby alterations to

germinal centre formations, hematopoietic processes, and decreases in lymphocyte populations were observed. These occurrences also appeared to affect T cell differentiation by skewing phenotypes towards Th1 rather than Th2, and further influenced B cell function by promoting alternative Ig class switching (O'connell *et al.*, 2009).

SOCS1 is considered to be the most critical family member of Suppressors of Cytokine Signalling (SOCS) (Liau *et al.*, 2018). Playing a crucial role in supressing the activity of Janus Kinases (JAK), a family of receptor kinases involved in cytokine signalling, SOCS1 attenuates an inflammatory immune response through ubiquitin ligase activity or directly binding to JAK1 and JAK2 (Liau *et al.*, 2018), collectively supressing proinflammatory processes. Furthermore, SOCS1 is a critical modulator of inflammatory cytokines TNF-α and IL-1β (Sun *et al.*, 2018). SOCS1 is a target of miR-155. Elevated miR-155 expression has shown to correlate with increased SOCS1 expression and vice versa during inflammatory stress (Sun *et al.*, 2018). During viral infections, miR-155 has been documented to promote anti-viral mechanisms by facilitating type IFN-α/β signalling through negatively regulating SOCS1 expression in a feedback loop process (Li *et al.*, 2019). SOCS1 expression has been reportedly differentially expressed in EAE, and predominantly found in macrophages during early stages of disease, additionally, administration of SOCS1-mimetic peptide ameliorates disease activity in a chronic EAE mouse model (Berard *et al.*, 2010).

TAB2 is an essential adaptor protein for the IL-1β signalling pathway, and a confirmed target of miR-155. Importantly, miR-155 suppression of TAB2 has been associated with modulating IL-1β signalling cascades (Virtue, Wang and Yang, 2012). MiR-155 inhibition of TAB2 has been confirmed in human monocyte derived DCs in a separate study, where miR-155 inhibited TAB2 to regulate IL-1β signalling in response to LPS *in vitro* (Ceppi, P. M. Pereira, *et al.*, 2009).

1.4.3.4 Functional outcome

The ability of miR-155 to control plasticity switches between macrophage phenotypes have also been documented (Cai *et al.*, 2012). One study focussing on the polarisation role miR-155 exerts on tumour associated macrophages (TAMs) proposed miR-155 re-educates

macrophages from pro-inflammatory phenotypes to anti-inflammatory states, and vice versa. Cai et. al, used anti-miR-155 antisense oligonucleotides to deplete miR-155 in IFN-γ and LPS treated macrophages and determined an alternatively activated phenotype, consisting of decreased TNF-α, iNOS, and IL-12, with increased IL-10 and ARG1. Furthermore, alternatively activated TAMs (IL-4 exposure) treated with overexpression of miR-155 repolarised macrophages towards a proinflammatory phenotype by displaying increased TNF-α, iNOS, IL-12, increased toxicity against tumours, with decreased IL-10 and ARG1 (Cai *et al.*, 2012). Overall, this study emphasised how tightly miR-155 can regulate macrophage polarisation, skewing macrophage phenotypes in both inflammatory directions, and how macrophage functions may be altered for either proinflammatory or anti-inflammatory purposes.

A separate study was carried out surrounding the role of miR-155 in classically activated macrophages upon treatment with IFN-γ and LPS. Jablonski et al. performed this study in genetically miR-155 deficient macrophages to examine the extent of miR-155 control over the macrophage transcriptional signature (Kyle A. Jablonski *et al.*, 2016). Findings from this study determined classically activated miR-155 deficient macrophages exhibited hindered iNOS, IL-1β, and TNFα gene expression, with limited NO production compared to WT controls. Additionally, classical anti-inflammatory gene marker ARG1 was not significantly altered amongst the two mouse strains when treated with IL-4, suggesting miR-155 is involved in supressing investigated pro-inflammatory genes but not alternatively activated macrophage expression of ARG1. Overall, Jablonski et al. concluded the pro-inflammatory macrophage signature is dependent on miR-155, where miR-155 deficiency in classically activated macrophages results in increased alternatively activated macrophage signatures (Kyle A. Jablonski *et al.*, 2016).

1.4.4 miR-155 in microglia

MiR-155 additionally plays a proinflammatory role in microglia by supressing immunoregulatory genes and transcription factors. *In vitro* studies reveal reactive microglia treated with LPS or IFN-γ have increased miR-155 expression levels which correlate with decreased immunoregulatory transcription factor SOCS1 (Cardoso *et al.*, 2012). Separate *in vitro* studies using microarray expression profiling of microglia confirmed miR-155 was the

strongest induced miRNA upon LPS treatment (Freilich, Woodbury and Ikezu, 2013). Translationally, *in vivo* studies investigating familial and sporadic amyotrophic lateral sclerosis (ALS) in SOD1 mice found miR-155 upregulated in microglia isolated from spinal cords, with an overall loss of homeostatic microglial molecular signature (Butovsky *et al.*, 2015). Similarly, *in vivo* studies investigating ALS, PD, brain injury following ischemic stroke, and AD, correlate reactive and pathogenic microglia with induced miR-155 expression (Pareek *et al.*, 2014; Butovsky *et al.*, 2015; Pena-Philippides *et al.*, 2016; Thome *et al.*, 2016; Caldeira *et al.*, 2017; Henry *et al.*, 2018).

1.4.5 miR-155 in MS/EAE

MiRNA profiling of MS lesions suggests a broad network of immune cell signalling pathways are finetuned by these small conservative regulators. One study confirmed distinct differentially expressed miRNA profiles in MS patients compared to healthy controls (Jr *et al.*, 2013). MiR-155 is one of many miRNAs found differentially expressed in MS lesions, however miR-155 is quite unique, as it was confirmed elevated in multiple cell types including: astrocytes, $CD4^+$ T cells, macrophages, and microglia. Moore et. al, has proven miR-155 to play a pathogenic role in MS by associating the presence of elevated miR-155 expression within proinflammatory macrophage and microglia phenotypes in MS lesions (Moore, Vijayaraghava T.S. Rao, *et al.*, 2013; Mohammed, 2019). Due to the presence of miR-155 in MS lesions and serum samples, studies have suggested the potential for miR-155 as a biomarker of MS activity. One study focusing on a cohort of RRMS patients, and patients undergoing a post-acute stage of remission, a stage of MS with increased neuroinflammatory activity, has determined a correlation of miR-155 expression levels with disease activity. MiR-155 derived from MS serum was confirmed highest during the post-acute stage of remission compared to RRMS patients who have been in remittance for 2+ years, suggesting elevated miR-155 is associated with higher disease severity (Niwald *et al.*, 2017). Moreover, a separate study has demonstrated strong evidence of miR-155 interfering with CD47 expression within MS lesions. Macrophages are proposed to facilitate demyelination processes via miR-155 by indirectly supressing CD47, a macrophage phagocytosis inhibitor, thereby indirectly promoting macrophage phagocytosis of myelin antigens and enhancing neuroinflammatory processes (Junker *et al.*, 2009; Jr *et al.*, 2013).

There is approximately 50% of differentially expressed miRNA profiles that are conserved from MS patients to EAE mouse models. Although the most potently upregulated miRNA in human MS samples (miR-650) is not found in EAE, the highly elevated miR-155 signature is prominently translational from MS to EAE in multiple cell types during disease progression (Jr *et al.*, 2013; Mohammed, 2019). Furthermore, the importance of miR-155 in EAE is highlighted by reproducible reports of total miR-155 deficient mice exhibiting resistance to disease induction (O'Connell, *et al.*, 2010; G. Murugaiyan *et al.*, 2011; Mycko *et al.*, 2015). O' Connell et. al, was the first research group to establish inducible EAE resistance in total miR-155 deficient mice. Collectively, EAE induced miR-155$^{-/-}$ mice resulted in decreased numbers of splenic IFN-γ producing Th1 cells, reduced IL-17A mRNA, hindered DC antigen presentation to lymphocytes, and reduced footpad inflammation 48 hours post keyhole limpet hemocyanin (KLH) (O'Connell *et al.*, 2010a). Shortly after the emergence of miR-155 dependence for EAE pathogenesis, Murugaiyan et al demonstrated miR-155 deletion caused alterations to CD4^{+} T cell cytokine profiles whereby there were decreased amounts of IFN-γ and IL-17, further highlighting a critical role for miR-155 in Th1 and Th2 differentiation. Additionally, treatment of WT mice with anti-miR-155 during preclinical stages of disease (day 5 post immunisation) resulted in significantly attenuated clinical scores (Gopal Murugaiyan *et al.*, 2011).

Considering the role of miR-155 may slightly differ in each immune and CNS resident cell it regulates, and the unpredictable phases of inflammatory flare ups in MS, caution should be taken regarding the administration of a miR-155 inhibitor such as MRG-106. Perhaps it would be more beneficial to appropriate a location or cell-type specific anti-miR for miR-155 in the context of MS. Therefore, further understanding miR-155 in all implicated cell types during preclinical and demyelination phases in animal models of MS is required for achievement of a miR-155 based DMT.

Collectively, there is irrefutable evidence suggesting the prominent role of infiltrating macrophages and CNS resident microglia in contributing towards the immunopathogenesis and repair mechanisms of MS and its mouse model EAE. Moreover, there is extensive evidence to suggest miR-155 dysregulation is a deleterious factor in MS disease progression and EAE disease models, whereby miR-155 genetic deletion and/or inhibition leads to

enhanced clinical outcomes in EAE. This thesis will explore the relationship between miR-155 and macrophages in a model of EAE.

1.5 Project Aims and Objectives

The role of myeloid cells in experimental autoimmune encephalomyelitis (EAE) has garnered great research interest in recent times. Yet, the role of miR-155 in macrophages has not yet been explored in the context of EAE. This study aims to focus on understanding the role of miR-155 in macrophages throughout a primary progressive EAE time course.

The hypothesis is that miR-155 deletion will promote an alternatively activated macrophage phenotype with anti-inflammatory/immunoregulatory properties, thus attenuating inflammation during EAE disease progression.

This was investigated in the following aims:

1. To determine the expression of miR-155 in immune cell subsets throughout an EAE time course in C57BL/6 wild-type mice.
2. To assess the impact of miR-155 deletion using macrophages from miR-155$^{fl/fl}$ x LysM^{Cre} mice *in vitro.*
3. To investigate the role of miR-155 deletion in an EAE model using miR-155$^{fl/fl}$ x LysM^{Cre} mice.

Chapter 2

Materials and Methods

2.1 Materials

2.1.1 General laboratory equipment and materials

All centrifuges were obtained from Agilent Technologies. Flow cytometry analysers (FACS CANTO II, BD LSRFortessa) were obtained from BD Biosciences. 7900HT Fast Real-Time PCR System was obtained from Thermo Fisher. Tissue culture materials including: 5 ml, 10 ml, 25 ml Stripette serological pipettes, tissue culture treated plates (6, 12, 24, 48, 98 well plates), cell scrapers, 175 cm vented cap tissue culture flasks, 10 cm and 6 cm culture dishes, were purchased from Corning Costar and Sigma-Aldrich (Merck). Pasteur pastettes, surgical scalpel blades, pipette tips, 1.75 ml Eppendorf tubes, 27 G and 15 G needles were purchased from Thermo Fisher Scientific.

2.1.2 General laboratory reagents

TRIzol and Glycogen (RNA grade) were purchased from ThermoScientific. BD CBA inflammation kit was purchased from BD Biosciences. Ethanol, methanol, and isopropanol were purchased from stores in the Hudson Institute of Medical Research. MyTaq red mix was purchased from Bioline. RNeasy mini kit was purchased from Qiagen. Recombinant IL-10 was purchased from R&D Systems. Chloroform, red blood cell lysis buffer, Complete DMEM media, RPMI-1640 media, and Dulbecco's Phosphate Buffered Saline were purchased from Sigma Aldrich. RNase and DNase free water were purchased from Promega. FBS was purchased from Gibco.

2.1.3 Animal husbandry

C57BL/6 mice were obtained from either Monash Animal Research Platform (MARP) or Monash Health. MiR-155 Tm1.1 Gard/j (miR-155 floxed mice) were purchased from The Jackson Laboratories. MiR-155 floxed mice were crossed with $LysM^{Cre}$ strains (donated by Professor. Paul Hertzog) to generate an experimental mouse strain (miR-$155^{fl/fl}$ x $LysM^{Cre}$) lacking miR-155 in immune cells derived from the myeloid lineage. All naïve mice were housed at Monash Animal Research Platform, and those induced with EAE were housed at Animal Research Laboratories on Monash University campus. All animal protocols used in this research project were in accordance with the Monash Medical Centre 'A' (MMCA)

animal ethics committee approval, or Animal Research Laboratory animal ethics committee approval.

2.1.4 PCR reagents

High Capacity cDNA Reverse Transcription Kit, Taqman microRNA reverse transcription kit, and SYBR safe DNA gel stain were purchased from Thermo Fisher Scientific. All PCR primers for gene expression analysis were purchased from IDT. Mmu-miR-155, mmu-snoRNA202, mmu-miR-191, and U6 Taqman primers for miRNA expression analysis were purchased from Applied Biosystems. GoTaq Green master mix was purchased from Promega. SensiFast Probe HiRox kit and protein ladder (10-250kDa) were purchased from Bioline.

Table 2.1 List of primers and primer sequences for Real Time PCR.

Primer name	Primer sequence (forward)	Primer sequence (reverse)
iNOS	CAGCTGGGCTGTACAAACCTT	CATTGGAAGTGAAGCGTTTCG
ARG1	GCAGTGGCTTTAACCTTGGC	TGGCGCATTCACAGTCACTT
ARG2	GGATCCAGAAGGTGATGGAA	AGAGCTGACAGCAACCCTGT
TNF-α	CAAATTCGAGTGACAAGCCTG	GAGATCCATGCCGTTGGC
IL-10m	GGTTGCCAAGCCTTATCGGA	ACCTGCTCCACTGCCTTGCT
ETS2	CAGAGGCCTAATCCTCAGTC	GGCCAAATTACAAAACCTTC
SHIP1	GGTGGTACGGTTTGGAGAGA	ATGCTGAGCCTCTGTGGTCT
M18s	GTAACCCGTTGAACCCCAT	CCAAATCGGTAGTAGCG
GAPDH	TTCACCACCATGGAGAAGGC	GGCATGGACTGTGGTCATGA

2.1.5 Flow cytometry reagents

Flow cytometry antibodies utilised in this research project were purchased from eBiosciences.

Table 2.2 List of cell surface markers used for phenotyping by flow cytometry.

Cell surface marker	Fluorescent tag	Clone
CD45	PerCPCy5.5, APC-Cy7	30-F11
CD11b	APC	M1/70
CD11c	BV605	HL3
F480	FITC, BV711	BM8, T45-2342
MHCII	BV510	M5/114.15.2
Ly6C	BV421	AL-21
Ly6G	PE-CY7	1A8
CX3CR1	FITC	SA011F11
CCR2	PE	575301
CD8	PerCPCy5.5	53-6.7
CD4	PE, Pacific Blue	GK1.5
B220	PE-Cy7, PerCPCy5.5	RA3-6B2
PI	PerCPCy5.5	-

Table 2.3 List of intracellular markers used for phenotyping by flow cytometry.

Intracellular marker	Fluorescent tag	Clone
NOS2/iNOS	PE	CXNFT
CD206	PE-CY7	MR6F3

2.1.6 Immunofluorescent staining reagents

Immunofluorescent antibodies utilised in this research project were purchased from Thermo Fisher Scientific.

Table 2.4 List of primary antibodies used for immunofluorescent staining.

Immunofluorescent marker	Host/isotype	Clone
CD68	Rat/IgG2a	FA-11
iNOS	Rabbit/IgG	-
ARG1	Rabbit/IgG	-

Table 2.5 List of secondary antibodies used for immunofluorescent staining.

Immunofluorescent tag	Host/isotype	Class
Alexa Fluor 488	Goat IgG	Polyclonal
Alexa Fluor 647	Goat IgG	Polyclonal

2.2 Methods

2.2.1 Mouse Strains

C57BL/6 mice were used throughout this project for *in vitro, in vivo,* and *ex vivo* studies. All animal experiments were performed in accordance with animal ethics guidelines, as set out by the relevant Monash University Animal Ethics Committee.

Table 2.6 miR-155$^{fl/fl}$ x LysM^{Cre} mouse strains and corresponding group name.

Mouse Strain	Group
miR-155$^{fl/fl}$ x LysMCre$^{+/-}$	Experimental
miR-155$^{fl/fl}$ x LysMCre$^{+/+}$	Experimental
miR-155$^{fl/fl}$	Control
LysMCre$^{+/+}$	Control

Figure 2.1 outlines the breeding strategy used to generate LysM^{Cre} controls and miR-155$^{fl/fl}$ x LysM^{Cre} mice. Breeding strategy stage 1 involves breeding miR-155 floxed mice with LysMCre to obtain heterozygous miR-155 floxed x LysM^{Cre} mice. These offspring are bred in stage 2 to generate both homozygous and heterozygous miR-155 floxed x LysM^{Cre} mice. Stage 3 breeding strategy involves continuously breeding homozygous and heterozygous miR-155 floxed x LysM^{Cre} mice to generate LysMCre controls and homozygous miR-155 floxed x LysM^{Cre} mice for *in vitro* and *in vivo* experiments outlined in Chapter 4 and Chapter 5, respectively.

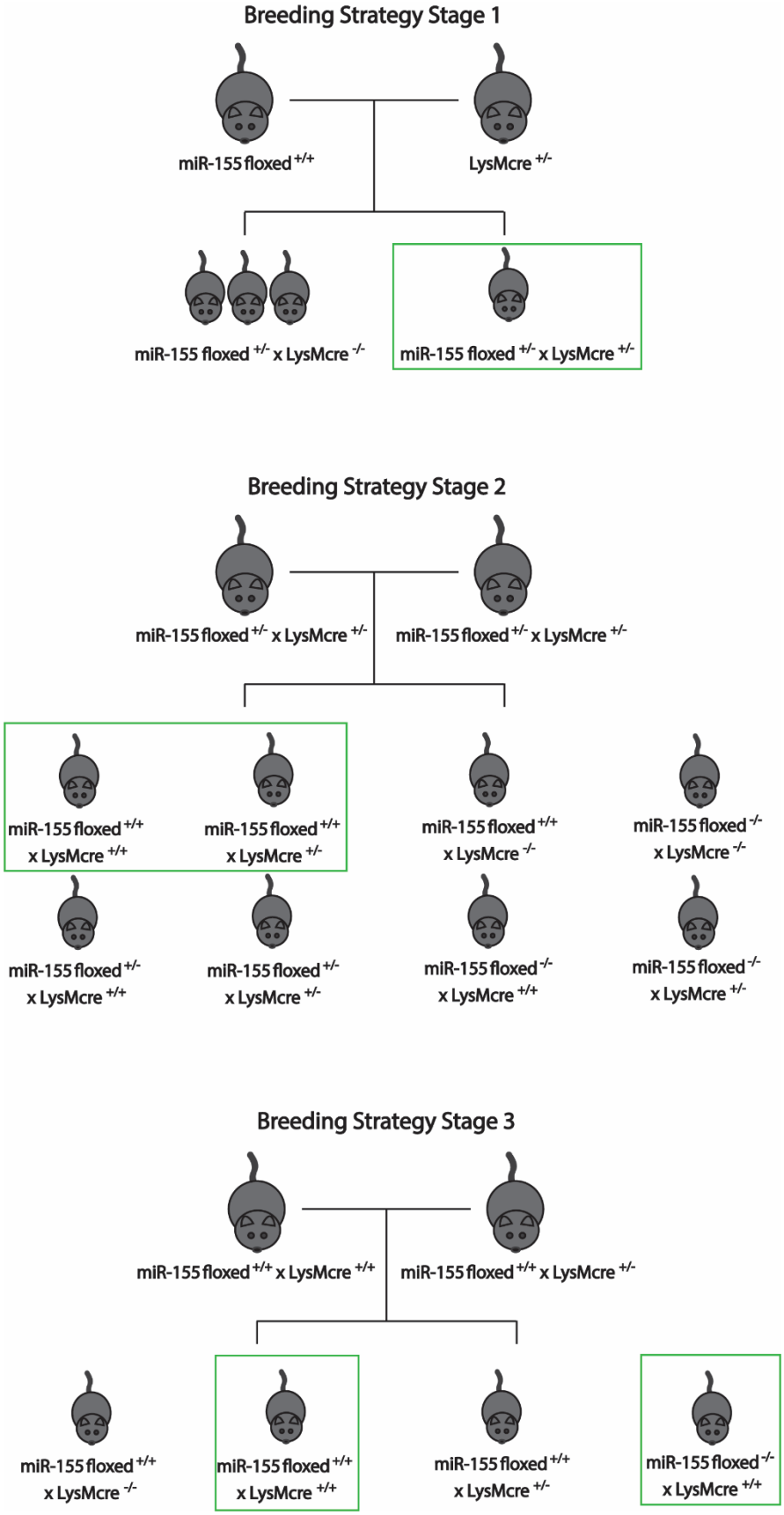

Figure 2.1: Breeding strategy of miR-155$^{fl/fl}$ x LysM^{Cre} mice.

2.2.1.1 Genotyping

Genotyping was carried out on three mouse strains to verify experimental and control groups: miR-155$^{fl/fl}$, LysMCre, and miR-155$^{fl/fl}$ x LysMCre. It involved a 3 step process; DNA extraction from tail clippings, PCR, and agarose gel electrophoresis. Initially genotyping was performed in-house at the Hudson Institute of Medical Research before being outsourced to a DNA genotyping service, TransnetYX.

2.2.1.2 DNA Extraction

Each tail clipping was incubated with 300µl of 50Mm NaOH. Samples were incubated for 45-50 minutes at 95°C and vortexed to ensure dissolvement of tail tissue. The NaOH reaction was stopped with the addition of 25µl Tris-HCl pH 8.0. Samples were vortexed and centrifuged at 13,000rpm for 1 minute.

2.2.1.3 PCR for amplification of flox and LysMCre regions

PCR was carried out using DNA of tail clippings to amplify miR-155 floxed and/or LysMCre regions.

2.2.1.4 MiR-155 flox PCR

2µl of DNA sample was added to 8µl of PCR master mix outlined in table 2.7 to create a total volume of 10µl. Samples were gently vortexed and briefly centrifuged before entering the PCR machine under the following cycling conditions:

Step 1. 94°C, 2 minutes. **Step 2.** (94°C 20 seconds, 65°C 15 seconds, 68°C 10 seconds) x 10**. Step 3.** (94°C 15 seconds, 60°C 15 seconds, 72°C 10 seconds) x 28. **Step 4.** 72°C 2 minutes. **Step 4.** 12°C overnight.

Table 2.7 Reagents and corresponding volumes for miR-155 flox PCR.

Reagent	Volume (µl/sample)
MyTaq (Bioline)	5
DNA sample	2
22862 (10µM)	0.5
22863 (10µM)	0.5
H_2O	2

2.2.1.5 LysMCre PCR

2µl of each DNA tail sample was added to 8µl of PCR master mix outlined in table 2.3 to create a total volume of 10µl. Samples were gently vortexed and briefly centrifuged before entering the PCR machine under the following cycling conditions;

Step 1. 94°C 2.5 minutes. **Step 2.** (94°C 1 minute, 63°C 1 minute, 72°C 1.5 minute) x 35. **Step 3.** 72°C, 10 minutes. **Step 4.** 12°C overnight.

Table 2.8 Reagents and corresponding volumes for LysMCre PCR.

Reagent	Volume (µl/sample)
GoTaq (Promega)	5
DNA sample	2
LysM1 (10µM)	0.25
LysM2 (10µM)	0.25
H_2O	2.25
Cre8 (10µM)	0.25

2.2.1.6 Gel Electrophoresis

Gel electrophoresis was performed using a 2% Agarose gel to visualise the presence of floxed and LysMCre regions. Agarose gels underwent an electric current of 95V for 25 minutes. The following images represent samples that were wild-type (WT), heterozygous (H), or homozygous (Fl) for (A) floxed miR-155 sites and (B) LysMCre regions.

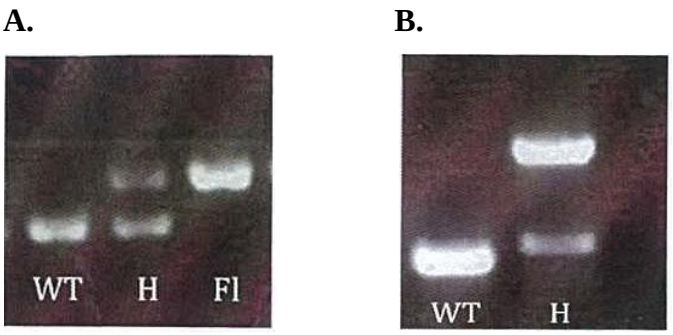

Figure 2.2: A. miR-155 flox PCR on a 2% agarose gel representing a WT mouse with no miR-155 floxed sites in lane 1, a Het mouse with one allele positive for floxed sites and one allele negative in lane 2, and a homozygous floxed mouse in lane 3. B. LysMCre PCR on a 2% agarose gel demonstrating a WT mouse negative for LysMCre in lane 1, and a Het mouse with one allele positive for LysMCre and one allele negative in lane 2.

2.2.2 EAE Induction

EAE was actively induced in 9-12 week old female C57BL/6 mice by Dr. Natalie Payne and Dr. Guizhi Sun at the Australian Regenerative Medicine Institute. Mice were immunised by subcutaneous injection of between 32.5 and 65µg recombinant MOG (rMOG, produced in-house) emulsified in Complete Freund's Adjuvant (CFA) supplemented with 400µg Mycobacterium tuberculosis into both hind flanks. An intraperitoneal injection of 200ng pertussis toxin was administered immediately after rMOG (day 0) and day 2 post immunisation (Payne *et al.*, 2013).

2.2.3 Clinical Scoring and Monitoring of Mice

Mice were monitored daily for EAE disease progression by observing clinical symptoms and paralysis. The following assigned scoring system was used to grade stages of paralysis; 0 – no disease visible, 0.5 – partial tail paralysis, 1 – complete tail paralysis, 1.5 – loss of righting

reflex, 2 – hind limb weakness or partial paralysis, 2.5 – one hind limb paralysis, 3 – complete hind limb paralysis, 4 – forelimb weakness and hind limb paralysis, and 5-moribund state. Due to ethical reasons, mice were humanely sacrificed upon reaching a clinical score of 4. When mice reached a clinical score of 3, their housing contained nectar, sunflower seeds, absorbent bedding, water bottles with extended nozzles, and a camera monitoring system was in place to monitor EAE mice remotely.

2.2.4 Isolation of Primary Cells

2.2.4.1 CNS Leukocyte Isolation

The entire CNS (brain and spinal cord) was harvested and placed in 6cm^2 petri dishes containing DMEM on ice. CNS samples were then transferred to 6cm^2 petri dishes containing freshly prepared digestion buffer (25ng/ml DNase and 1mg/ml Collagenase D). CNS samples were thoroughly diced using a scalpel blade within 6cm^2 petri dishes and incubated for 30 minutes at 37˚C for tissue digestion to occur. 5ml of PBS containing FBS was added to stop this enzymatic reaction. Digested CNS samples were pressed through a 70µm filter using a Pasteur pipette and the back of a 1ml syringe with FACS buffer (DPBS containing 2% FBS, 5mM EDTA) to a total volume of 15ml. CNS samples were centrifuged at 4˚C for 5 minutes at 2,000rpm. Supernatants were decanted and 8ml of 40% Percoll was added to each sample to resuspend the pellet. Each cell suspension was gently layered on the surface of 3ml of 70% Percoll within a 15 ml Falcon tube. Layered suspensions were centrifuged at room temperature for 25 minutes at 2,000rpm with no brake activation. After centrifugation, between the interface of the 40% and 70% Percoll layers, a buffy coat layer is present which contains CNS leukocytes. CNS leukocytes located at the buffy coat layer were transferred to a clean 15ml Falcon tube using a Pasteur pipette. 10ml of FACS buffer was added to each sample and centrifuged at 4˚C for 5 minutes at 1,500rpm. CNS leukocytes were resuspended in 1ml of FACS buffer and counted using a Neubauer Haemocytometer in a dilution of 1:2 with Trypan Blue. CNS Leukocytes were Fc blocked and cell surface stained for either phenotypic analysis or cell sorting via flow cytometry.

2.2.4.2 Spleen Leukocyte Isolation

Spleen samples were harvested and placed in Falcon tubes containing 5ml of chilled RPMI media on ice. Spleen samples were pressed through 70µm filters into 6cm^2 petri dishes using the back of a 1ml sterile plastic syringe. 5ml of RPMI was pipetted through these 70µm filters to ensure entire collection of splenocytes. Suspended spleen cells within 6cm^2 petri dishes were transferred to a 15ml Falcon tube. Cells were centrifuged at 4˚C for 5 minutes at 1,200rpm. Supernatants were decanted and cell pellets were re-suspended in 1ml Red Blood Cell (RBC) lysis buffer. Each Falcon tube was flicked or gently pipetted to ensure thorough mixing of lysis buffer with cells. Cell suspensions mixed with RBC lysis buffer were incubated for 3 minutes before 12ml of complete RPMI was added to neutralise the lysis buffer reaction. Cells were centrifuged at 4˚C for 5 minutes at 1,200rpm. Falcon tubes were decanted and re-suspended in 12ml of RPMI and passed through a second 70µm filter into 15ml Falcon tubes and centrifuged at 4˚C for 5 minutes at 1,200rpm. Supernatants were decanted and cell pellets were re-suspended in 5ml of FACS buffer. Spleen leukocytes were counted using a Neubauer Haemocytometer at a dilution of 1:10-1:50 with Trypan Blue. An additional wash step with FACS buffer was carried out to ensure entire removal of RPMI. Spleen leukocytes were analysed immediately by flow cytometry (Section 2.2.7) or qPCR (Section 2.2.9, 2.2.10).

2.2.4.3 Whole blood leukocyte Isolation

Whole blood was harvested from mouse hearts using a 5ml syringe and 27G needle immediately after mouse culling in CO_2 chamber. Prior to blood harvesting, syringes and Eppendorf tubes were lined with Heparin to prevent blood samples from clotting. Once blood samples were harvested, they were immediately placed within Heparin lined Eppendorf tubes on ice. Blood samples were transferred from Eppendorf tubes into 15ml Falcon tubes by continuously rinsing samples with FACs buffer using a Pasteur pipette until no visible blood remained inside the Eppendorf tube. Falcon tubes were then centrifuged at 300G for 5 minutes at 4°C. Supernatants were aspirated and 3ml of red blood cell (RBC) lysis buffer was added for 5 minutes at room temperature. This step is the most crucial due to potentially damaging leukocyte viability if lysis buffer is not neutralised in 5 minutes by the presence of FBS found in FACS buffer. 10ml of FACS buffer was added to each sample to neutralise the RBC lysis reaction. Samples were centrifuged at 300G for 5 minutes at 4°C

and supernatants were aspirated. Cell pellets within the 15ml Falcon tube were then resuspended gently in 1ml of FACS buffer for cell counting. Blood samples were centrifuged once more at 300G for 5 minutes at 4°C and supernatants were aspirated. Leukocytes were Fc blocked and cell surface stained for either phenotypic analysis or cell sorting via flow cytometry.

2.2.4.4 Peritoneal macrophage isolation

Peritoneal macrophages were isolated within the animal housing facility using sterile materials and reagents. PBS was loaded into a 10ml syringe with a 27G needle attached. Male C57BL/6 mice were culled within a CO_2 chamber. Fur from each mouse was removed around the abdomen to expose the peritoneal cavity. Approximately 4-5ml of PBS was injected into the peritoneal cavity with the needle bevel facing upwards. Abdomens were massaged to ensure complete circulation of PBS within the cavity and detachment of macrophages from organ epitheliums. A 27G needle was inserted into the peritoneal cavity with its bevel facing downwards to extract peritoneal macrophages suspended in PBS. Samples were transferred to 50ml Falcon tubes on ice. An incision of 3mm was made in the abdomen using a scissors to further expose the peritoneal cavity. The area of incision was placed over a 50ml Falcon tube to allow drainage of remaining PBS. Samples within 50ml Falcon tubes were centrifuged for 5 minutes at 1,200rpm and the cell pellet resuspended in 1ml complete DMEM containing 10% FBS, 100U/ml penicillin, 100µg/ml streptomycin for cell counting using a Neubauer Haemocytometer. Peritoneal cavity cells were then plated at 3×10^5 cells per 24 well plate for 2-3 hours to enable adherence of macrophage-like cells in Complete DMEM. Complete DMEM was gently removed and replaced with fresh medium. Cell were then stimulated with 100ng/mg LPS for 24 hours for either qPCR (Section 2.2.9, 2.2.10) or flow cytometry analysis (Section 2.2.7).

2.2.4.5 Bone Marrow Derived Macrophage (BMDM) isolation

BMDM's were harvested within the animal housing facility using sterile materials. Femurs were removed from male C57BL/6 mice and placed in 5 ml of complete DMEM on ice. Within a biological safety cabinet, intact femur surfaces were washed by being placed in 80% ethanol, followed by PBS, and complete DMEM. A sterile scalpel was used to cut both

ends of the femur within an empty sterile 6cm^2 petri dish to expose the bone marrow. Using a forceps to position the femur over a 50ml Falcon tube, 5ml of complete DMEM was plunged through the bone marrow using a 30G needle attached to a 10ml syringe. Samples within 50ml Falcon tubes were centrifuged for 5 minutes at 12,000rpm to pellet bone marrow cells and resuspended in complete DMEM. Bone marrow cells were maintained in 10cm^2 petri dishes at 37ºC with 5% CO_2 and cultured for a total of 7 days to allow for macrophage differentiation and maturation. BMDM culture medium consisted of 80% complete DMEM supplemented with 20% L929 medium. BMDM culture medium was replaced on days 3 and 6. On day 6, cells were either scraped using a cell scraper or trypsinised with 1.5 ml of TrypLE^{tm} to suspend adherent BMDM's for cell counting (Figure 3.44). Cells were diluted 1:2 with Trypan Blue to check their viability. BMDM's were plated at a concentration of 3-5 x 10^5 cells/ml in a 24 well plate for 18-24 hours. BMDM's were stimulated with numerous agonists including; 100ng/ml LPS, 20ng/ml IL-10, and 20ng/ml IFN-γ. BMDM's were either lysed for qPCR analysis (Section 2.2.9, 2.2.10) or flow cytometry (Section 2.2.7), and supernatants were analysed by ELISA (Sections: 2.2.11, 2.2.12).

2.2.5 Cultured cell lines

2.2.5.1 L929 cell maintenance

L929 cells were cultured to provide L929-condtioned medium essential for the differentiation and maturation of macrophages from bone marrow cells. Constituents of this medium responsible for cell differentiation include; GM-CSF, IL-3, and Flt3L. L929 cells were cultured in 10 cm^2 petri dishes in RPMI culture medium at 37ºC in 5% CO_2 for approximately 10 days. Once cells reached confluency (90-100%), usually occurring on day 3, PBS was used to gently wash non adherent cells and media. Cells were trypsinised using 1ml of Trypsin and passaged into 3x 10cm^2 petri dishes. Once 3x 10cm^2 petri dishes reached confluency, 2x 10 cm^2 petri dishes containing L929 cells were washed with PBS and trypsinised before being pooled together and resuspended in 50ml of complete RPMI medium. L929 cells within the 50ml suspension were evenly inoculated into 5x T175 flasks. L929 cells within the remainder 10 cm^2 petri dish were cryopreserved and stored at -80°C. Cells within the 5x T175 flasks were incubated at 37ºC in 5% CO_2 for a further 5 days. Supernatants from all 5x T175 flasks were pooled together and sterile filtered using a Corning 500ml bottle-top vacuum filter system. L929 supernatants were aliquoted in 15ml

Falcon tubes with a total volume of 12ml per tube and stored at -80°C. Once supernatants were thawed, they were stored at 4°C for a maximum of 2 weeks.

2.2.5.3 Cryopreservation of cells

DMSO acts as a cryoprotectant by reducing the risk of cell lysis and preventing the formation of ice crystals on cell surfaces. Cells were suspended in Freeze Mix in cryovials and stored at -80°C. Freeze mix consisted of 70% complete DMEM cell medium, 20% foetal bovine serum (FBS), and 10% dimethyl sulfoxide (DMSO). Freeze mix was prepared and aliquoted in cryovials prior to cells being resuspended and added drop-wise to each cryovial to a total volume of 1ml. Cells were placed in either Mr. Frosty freezing containers or placed in polystyrene packaging and stored immediately at -80°C. Mr Frosty freezing containers contains isopropanol which decreases its temperature by 1ºC per minute. This slow incremental temperature decrease prevents shock to cells undergoing cryopreservation.

2.2.6 Cell counting

Cells were counted manually using a haemocytometer. The haemocytometers coverslip was firmly attached ensuring all squares were covered. Cell samples were suspended and thoroughly mixed in 1ml of either FACS buffer or appropriate cell culture medium. Cell suspensions were diluted with Trypan Blue stain in a 96 well plate to identify cell viability. 10µl of stained cells were pipetted under the cover slip attached to the haemocytometer. A brightfield microscope was used to view cells. If the cell count was too high or low to obtain a confirmatory cell count, a higher or lower dilution was of cell suspension in Trypan Blue stain was used. Viable cells were identified by an absence of blue as they have an intact cell membrane and non-viable cells appeared blue. Dying cells were excluded from the viable cell count. All 4 large corner (4 x 4) squares (figure 2.3) were counted and an average cell number was taken. This average was then multiplied by the dilution factor (Trypan Blue ratio to cell suspension), and by a factor of 10^4. The resultant number is equal to the cell count per ml of original cell suspension.

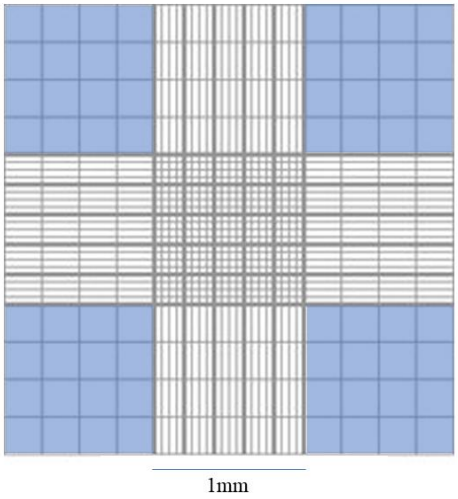

Figure 2.3: Haemocytometer counting chamber. Cells within the 4 corner squares (highlighted blue) are counted and an average cell count is recorded before calculations of cells/ml are performed.

2.2.6.1 Cell concentration guidelines

Table 2.9 Guidelines of tissue culture plates used with according cell concentrations and volumes. In certain cases, where cell concentrations could not meet above guidelines, all samples within experiment were normalised to the lowest cell concentration to prevent sample variability.

Tissue Culture Plate	Cell concentration per well	Medium volume per well
6 well plate	1×10^6	2ml
12 well plate	5×10^5	1ml
24 well plate	$3\text{-}5 \times 10^5$	500µl
48 well plate	$1\text{-}2 \times 10^5$	300µl
96 well plate	1×10^5	200µl

2.2.7 Flow Cytometry

For this research project, flow cytometry was used for isolating immune cell populations by cell sorting, and phenotyping immune cells by cell surface staining and intracellular staining. FACS CANTO II and BD LSRFortessa from BD Biosciences were utilised to acquire samples.

2.2.7.1 Cell surface staining of immune cells

Total immune cells from CNS, spleen, and blood samples were Fc blocked at a 1:150X dilution in FACS buffer to prevent unspecific binding of FACS antibodies. Samples were incubated for 30 minutes at 4°C and washed with 1ml of FACS buffer. Samples were aliquoted into FACS tubes at cell concentrations according to Table 2.10.

Table 2.10 Cell concentration used for cell sorting and phenotyping within CNS, spleen, and blood samples

	CNS	**Spleen**
Cell Sorting	Entire sample	1 x 107
Phenotyping	2 x 10^5	5 x 10^5
Single Stains/Controls	-	2 x 10^5

Samples were centrifuged at 1200rpm for 5 minutes and supernatants were decanted. 50µl of phenotyping antibody cocktail, or 100µl of cell sorting antibody cocktail (refer to Table 2.2), or 50µl of single stains (1:400) were added to each corresponding FACS tube. Samples were incubated for 30 minutes in the dark at 4°C. Samples were washed with 1ml of FACS buffer and centrifuging at 1,200rpm for 5 minutes. Supernatants were decanted and resuspended in 180µl of FACS buffer for cell sorting and phenotypic analysis.

2.2.7.2 Intracellular staining of immune cells

Primary cells were transferred to FACS tubes and Fc blocked using anti-mouse FcR antibody (CD16/CD32) for 15 minutes at 4°C in FACS buffer (5µl/ml). For cell surface staining, cells were washed in FACS buffer and stained with diluted antibodies for 15 minutes at 4°C. eBioscience fixation/permeabilisation buffer was used to wash cells 3x times at 1,200rpm for 5 minutes. Cells were then fixed using fixation/permeabilisation buffer for 40 minutes at 4°C and washed 3 times in 1X eBioscience permeabilisation buffer. For intracellular staining, cells were blocked using anti-mouse FcR antibody (CD16/CD32) for 45 minutes at 4°C in 1X permeabilisation buffer (5µl/ml). Cells were then washed in 1X permeabilisation buffer before intracellularly staining for 45 minutes at 4°C. Finally, cells were washed 3 times in 1X permeabilization buffer before being resuspended in FACS buffer and acquired on BD FACSCanto II.

2.2.7.3 Data collection

Samples used for cell sorting and phenotyping were analysed using FlowJo Vx 10.0 software. Gating strategies outlined in section 3.2 were derived from FlowJo Vx 10.0 software layout editor.

2.2.8 RNA Extraction

2.2.8.1 Modified TRIzol protocol for low cell counts

RNA was extracted from sorted immune cell populations using a modified TRIzol (ThermoScientific) protocol. This protocol was optimised to investigate both miRNA and gene expression in low cell number populations. Samples were lysed in 1ml of TRIzol Reagent and incubated for 5 minutes in Eppendorf tubes within a fume hood. 200µl of chloroform was added to samples before 30 seconds of vigorous shaking and 10 minutes of incubation at room temperature. Cell lysates were centrifuged at 12,000rpm for 15 minutes at 4°C. After centrifugation samples were separated into 3 phases; an organic phase (containing proteins and lipids), an interphase (containing DNA), and the desired aqueous phase (containing RNA). A total of 400µl of the aqueous phase was carefully pipetted into a clean Eppendorf tube containing 500µl of Isopropanol. Samples were centrifuged for 12,000rpm for 10 minutes at 4°C and supernatants were carefully decanted. Samples were

resuspended in 1ml 80% Ethanol and centrifuged at 7,500rpm for 5 minutes at 4°C. Supernatants were decanted and samples were air dried for 5-10 minutes by inverting Eppendorf tubes onto clean tissue. Samples were resuspended in 30µl of DNase and RNase free H_2O and heated at 55-60°C on a heating block for 5-10 minutes. Samples were placed immediately on ice for further analysis (section 2.2.9) or stored at -80°C indefinitely.

2.2.8.2 Modified Qiagen kit for abundant cell numbers

The Qiagen kit protocol was used for BMDM's due to their abundant cell numbers. This technique is optimised from the manufacturers protocol to investigate both miRNA and gene expression. Modification in this protocol includes using additional alcohol washing steps and resuspending RNA pellets in lower volumes of RNase/DNase free water.

2.2.9 Real-time PCR (RT-PCR) for gene expression analysis

2.2.9.1 Amplicons

qPCR amplicons were used to generate a specific product for each gene of interest being analysed. This ensured that primer pairs for each gene of interest were working efficiently. Amplicons enabled the generation of a standard curve to determine exact copy numbers in final stages of gene data analysis. Preparation of qPCR amplicons consisted of several steps: cDNA generation, agarose gel electrophoresis, DNA extraction, purification from agarose gels, and a serial dilution of determined DNA concentrations. These dilutions were used to generate standard curves in the final RT-PCR reaction for analysis of gene expression (section 2.2.9.3).

RNA (80ng/µl) from unstimulated BMDM's was used to generate cDNA as outlined in Table 2.8.

Table 2.11 Reagents and volumes used to generate qPCR amplicons from synthesised cDNA for mRNA.

Reagent	Volume (µl/sample)
MyTaq2x	10
Forward primer (5µl)	0.8
Reverse primer (5µl)	0.8
RNase/ DNase free H_2O	7.4
cDNA (80 ng/ µl)	1

Samples were gently vortexed and briefly centrifuged before entering PCR machines under the following cycling conditions;

Step 1. 95°C, 2 minutes. **Step 2.** 95°C, 15 seconds**. Step 3.** 60°C, 15 seconds. **Step 4.** 72°C, 10 seconds. **Step 5.** GOTO Step 2, 35x. **Step 6.** 72°C, 2 minutes. **Step 7.** 12°C, overnight.

2% agarose gels were comprised of the following reagents and volumes in table 2.9. Samples were loaded onto 2% agarose gels and run for 25 minutes at 95V.

Table 2.12 Reagents and volumes/weights used to generate 2% agarose gels.

Reagent	60ml total volume
Molecular grade agarose	0.9g
50x TAE buffer	1.2ml
Deionised H_2O	Up to 60ml
SybrSafe DNA gel stain	6µl

DNA extraction and purification from agarose gels was carried out using Biolines "Isolate II PCR and Gel Kit". A scalpel was used to excise the visible band of DNA in the agarose gel and placed into an Eppendorf tube. 200µl of Binding Buffer CB was added per 100mg of DNA band. Samples were incubated for 5-10 minutes at 50°C with intermittint vortexing until the agarose gel was visibly dissolved. Samples were loaded in "Isolate II PCR" gel columns within collection tubes and centrifuged at 11,000rpm for 30 seconds. Flow-through in the collection tube was discarded and samples were loaded with 700µl Wash Buffer CW. Samples were centrifuged at 11,000rpm for 30 seconds and the previous wash step was repeated to reduce chaotropic salt carry-over. Samples were centrifuged at 11,000rpm for 60 seconds with no substances on the column to dry the silica membrane within the column. Columns were placed in a 1.7ml Eppendorf tube and loaded with 30µl of Elution Buffer C directly onto the silica membrane. Samples were incubated for 1 minute at room temperature before being centrifuged at 11,000rpm for 1 minute. Purified DNA was now eluted into Eppendorf tubes and samples were paced immediately on ice.

Purified DNA samples were nanodropped at 280 nm to determine DNA concentrations (ng/µl). Using the following equation: *C1V1=C2V2*, the desired standard concentrations could be acquired. DNA standards (amplicons) were labelled as follows:

Table 2.13 Standard/ amplicon labels with corresponding concentrations (ng/µl).

Standard/Amplicon	Concentration (ng/µl)
A	0.1
B	0.001
C	0.00001

2.2.9.2 cDNA generation for gene expression

RNA generated from section 2.2.8.1 (TRIzol) was measured using a NanoDrop 1000 spectrophotometer and normalised with RNase/DNase free H_2O to generate a stock RNA

concentration of 50-80 ng/µl. A master mix was generated using a high capacity cDNA reverse transcription kit (ThermoFisher) according to Table 2.15.

Table 2.14 Reagents and volumes used to generate cDNA for mRNA.

Reagent	Volume (µl/sample)
dNTP	0.8
10x Buffer	2
RNase inhibitor	0.2
RT enzyme	1
Random Primers	2

14µl of RNA samples were added to 6µl of above PCR master mix in PCR strip tubes to create a total volume of 20µl. Samples were gently vortexed and centrifuged before entering the PCR machine under the following cycling conditions;

Step 1. 25°C, 10 minutes. **Step 2.** 37°C, 2 hours**. Step 3.** 85°C, 5 minutes. **Step 4.** 12°C overnight.

2.2.9.3 RT-PCR for gene expression

Master mixes comprising of below reagents in table 2.15 were prepared for each gene of interest.

Table 2.15 Reagents and volumes used to determine gene expression using qPCR. Each volume represents cDNA samples in duplicate.

Reagent	Volume (µl/sample)
Forward Primer (5 µM)	0.4
Reverse Primer (5 µM)	0.4
HiRoxSybr	10
H2O	7.2

8.9µl of each gene of interest master mix was added per well of a 384 well TRLA plate. 1µl of synthesised cDNA was added to each correlating master mix creating a total volume of 10µl per well. Samples were sealed using appropriate plate cover slips and centrifuged at 10,000rpm for 1 minute to remove residual volume from plate edges before the qPCR machine cycle commenced.

2.2.9.4 Data analysis

Data derived from the 7900HT Fast Real-Time PCR system was analysed via the ΔΔCt fold induction method. This method represented the fold change of each gene of interest against unstimulated conditions and house-keeping genes. The Cycle Threshold (Ct) values obtained from the completed RT-PCR run was used to subtract each gene of interest from selected housekeeping genes. The average of this subtracted value was then added to the Ct values of each gene of interest (ΔCt). Lastly, ΔCt values are doubled to achieve ΔΔCt values that represent the fold change of gene expression.

2.2.10 RT-PCR for miRNA expression

2.2.10.1 miR-155 Oligo

A miR-155 oligo was used to determine absolute values of miR-155 expression by creating a miR-155 standard curve. This standard curve was generated from the following mature mmu-miR-155 sequence;

5’- rUrUrA rArUrG rCrUrA rArUrU rGrUrG rArUrA GrGrG rGrU - 3’

A top standard of 32.8pM was generated from 1nM stock followed by 7 serial 4-fold dilutions, the 8th tube was used as a non-template control which contained only H_2O. These serial dilutions underwent cDNA generation (section 2.2.10.2) and RT-PCR (section 2.2.10.3) in parallel with experimental RNA samples, and were used in the same master mixes to control cycle variability.

2.2.10.2 cDNA generation for miRNA expression

RNA generated from section 2.2.8.1 (TRIzol) was measured using a NanoDrop 100 spectrophotometer and normalised with RNase/DNase free water to generate a stock RNA concentration of 50-80ng/µl. A master mix containing Taqman primers (Applied Biosystems) was generated using a reverse transcription kit according to table 2.16.

Table 2.16 Reagents and volumes used to generate miRNA cDNA. A maximum of 8 miRNA primers could be included per reaction.

Reagent	Volume (µl/sample)
dNTP	0.125
10x Buffer	1.5
RNase inhibitor	0.18
RT enzyme	1
Primer(s)	0.375 (per miRNA)
DNase/RNase free H_2O	variable

DNase/RNase free H_2O volumes varied in above rtPCR master mix to create a total volume of 12µl master mix for each normalised RNA sample. 3µl of normalised RNA was added to 12µl rtPCR master mix in PCR strip tubes to create a total volume of 15µl. Samples were

gently vortexed and centrifuges before entering the PCR machine under the following cycling conditions;

Step 1. 16°C, 30 minutes. **Step 2.** 42°C, 30 minutes. **Step 3.** 85°C, 5 minutes. **Step 4.** 15°C overnight.

2.2.10.3 RT-PCR for miRNA expression

RNA generated from section 2.2.8.1 (TRIzol) was measured using a NanoDrop 100 spectrophotometer and normalised with RNase/DNase free water to generate a stock RNA concentration of 10ng/µl. Master mixes were generated according to table 2.17 utilising 2x Sensifast HiRox (Bioline) and Taqman primers (Applied Biosystems).

Table 2.17 Reagents and volumes used to determine miRNA expression using qPCR. Each volume represents cDNA samples in duplicate.

Reagent	Volume (µl/sample)
2x Sensifast HiRox	10.13
miRNA Pimer	0.58
DNase/RNase free H_2O	8.13

8.9µl of each miRNA of interest master mix was added to each well of a 384 well TRLA plate. 1µl of synthesised miRNA cDNA was added to each correlating master mix creating a total volume of 10µl per well. Samples were sealed using appropriate plate cover slips and centrifuged at 10,000rpm for 1 minute to remove residual volume from plate edges before the qPCR machine cycle commenced.

2.2.10.4 Data Analysis

MiRNA were analysed using 2 different qPCR normalisation methods; ΔΔCt fold change (section 2.2.9.4) or miR-155 absolute copy number. MiR-155 absolute copy number involved plotting miR-155 Ct values against values of synthetic miRNA oligo that generated a standard curve. From this standard curve, the equation of the line could be used to identify endogenous miR-155 copy numbers within biological samples.

2.2.11 ELISA (Enzyme Linked Immunosorbent Assay)

Supernatants from BMDM's and peritoneal macrophages were analysed for mIL-10 production using a sandwich ELISA system. This assay used capture and detection rabbit anti-mouse antibodies specific for mIL-10. 96 well Nunc plates were coated with capture antibody for 24 hours at 4°C. Blocking buffer was added to prevent non-specific binding of antibodies. Sample supernatants and standards were added to corresponding wells and incubated for 2 hours at room temperature. Detection antibody was added according to the manufacturers guidelines for 1 hour at room temperature in the dark. H_2SO_4 was used as a stop solution to end the enzymatic reaction occurring with the detection antibody and samples. A coloured product was produced if the cytokine of interest was present in sample supernatants and standards. The concentration of cytokine present correlated with colour intensities. FLUOstar OPTIMA plate reader was used to obtain the absorbance of light at 450 nm and analyse samples in Nunc plates.

2.2.12 BD™ Cytometric Bead Array (CBA)

Supernatants from stimulated BMDM's and peritoneal macrophages were analysed for cytokine production using a BD™ CBA mouse inflammation kit. Six cytokines could be detected simultaneously within each sample by measuring fluorescence intensities of bead populations coated with capture antibodies correlating with different cytokines. PE-conjugated detection antibodies were added to each sample containing sample supernatant and capture beads. In parallel with samples, a serial dilution of recombinant standards was prepared to generate a standard curve. A sandwich complex formed when capture beads, PE-conjugated antibodies, recombinant standards, and samples were incubated for 2 hours at room temperature in the dark. PE, FITC, and "Set Up Bead" controls were incubated for 30

minutes at room temperature in the dark and washed with Reagent Diluent alongside samples and recombinant standards. Sample data was acquired using a CANTO flow cytometer following the recommended voltage settings for PE and APC-Cy7. Results were analysed using the FCAP Array™ Software and generated in a tabular and graphical format in Excel or PDF formats.

2.2.13 CNS processing for histological and immunofluorescent staining

2.2.13.1 CNS perfusion and OCT embedding

Female C57BL/6 mice were culled using a CO_2 chamber and prepared immediately for whole body perfusion. Mice were perfused by incising the vena cava and inserting a 25G needle attached to a mechanical pump into the bottom left ventricle of the heart. 50ml PBS was mechanically pumped throughout the whole body before switching to 50ml of 4% PFA. Once perfusions were complete, CNS samples were harvested intact brains were cut into pieces to allow thorough fixation of CNS tissues. Brains were cut for coronal sectioning and spinal cords were cut for transverse sectioning. CNS pieces were placed in 5ml tubes containing 4% PFA overnight at 4°C. CNS sections were then rinsed with PBS using a Pasteur pipette and placed in 5ml tubes containing 30% sucrose for 1-2 days at 4°C. Ice boxes were filled with dry ice and 70ml of 2-butanol was poured in a weigh boat and placed on top of the dry ice. OCT was poured in $10mm^2$ TissueTeq cassettes and CNS pieces were carefully positioned upright in cassettes using forceps. Cassettes containing CNS pieces were placed inside ice boxes on weigh boats containing 2-butanol until the OCT compound changed from clear to white. Cassettes were then transferred to -80°C until cryosectioning occurred.

2.2.13.2 Immunofluorescent staining of OCT embedded frozen sections

Frozen CNS sections embedded in OCT were brought to room temperature for 30-60 minutes before 3x 5 minute washes were performed using 1x PBS in a staining rack. Once the final PBS wash was complete, slides were tapped at 90° angles to remove excess PBS. A liquid blocker pen was used to draw a barrier around samples to be immunostained for CD68 and iNOS or CD68 and Arg1. A blocking solution (10% BSA, 0.3% Triton X-100, 1x PBS, 10% NGS) was added to samples to prevent non-specific binding of antibodies and

slides were incubated at room temperature for 30 minutes. Primary antibodies were prepared fresh during this incubation period in blocking solution at a 1:400 dilution. Slides were tapped at 90° angles to remove excess blocking buffer and placed in the humidified chamber. 80µl of each desired primary antibody solution was added to samples ensuring sections are entirely covered to prevent sections from drying out. The humidified chamber containing sections was gently placed at 4°C overnight. Sections were then transferred from 4°C to room temperature. Slides were gently tapped on paper towels at 90° angles to discard primary antibody solutions before being placed in a staining rack to be washed with 1x PBS 3x times at 5 minute intervals. During PBS washing intervals, secondary antibody solutions were prepared in blocking solution at a 1:400 dilution. Once the final PBS wash was complete, slides were gently tapped at 90° angles to remove excess PBS and placed in the humidified chamber where 80µl of secondary antibody solutions were added onto sections ensuring complete coverage. Slides were incubated at room temperature for 2 hours in complete darkness. Slides were gently tapped at 90° angles to remove excess secondary antibody solutions before being placed in a staining rack to be washed with 1x PBS 3x times at 5 minute intervals. During these PBS washes, DAPI nuclear stain was prepared in 1x PBS at a dilution of 1:2000. Slides were gently tapped at 90° angles to remove excess PBS before being placed in a humidified chamber to be stained with 80µl of DAPI nuclear stain at room temperature for 15 minutes in complete darkness. Slides were gently tapped at 90° angles to remove excess DAPI solution before being placed in a staining rack to be washed with 1x PBS 3x times at 5 minute intervals. Slides were gently tapped at 90° angles to remove excess PBS prior to mounting medium and coverslips being added to slides. Bubbles created by mounting medium were removed via applying pressure on coverslips with forceps. Slides were incubated overnight to allow drying at room temperature covered in aluminium foil. Brightfield/Immunofluorescent Microscopy was carried out the following day.

2.2.13.3 Haematoxylin and Eosin staining of OCT embedded frozen sections

Frozen spinal cord sections were thawed from -80°C at room temperature and stained with haematoxylin and Eosin (H&E) at the Monash University Histology platform according to a standard protocol. Briefly, spinal cord sections of EAE mice were stained with Haematoxylin for 7 minutes prior to rinsing 3x times with tap water. Sections were dipped once in acid-alcohol and rinsed 3x times with tap water prior to a 10 second alkaline wash.

Sections were then rinsed 3x times with tap water before stained with Eosin for 8 minutes. Sections were transferred into 3 ethanol containers for 10 seconds each for alcohol washing before being transferred into 3 xylene containers for 10 seconds each prior to cover slip adhesion with mounting media. Sections were left at room temperature in the fume hood for drying and kept indefinitely at room temperature for slide scanning and image analysis using image analysis software ImageScope.

2.2.14 Statistical analysis

All statistical analyses performed in the following results chapters were based on the standard error mean of minimum 2 independent experiments. In Chapter 3, One-way ANOVA with Bonferroni's correction was applied to data, unless otherwise stated. Data analysis in Chapter 4 utilised two-way ANOVA with Bonferroni's correction, unless otherwise indicated. In Chapter 5, two-way ANOVA with Bonferroni's correction and unpaired t-test with Welch's correction were performed to appropriate data sets, unless otherwise indicated. All statistical analyses were performed using PRISM software. Levels of statistical data significance were represented by star symbols: * $P<0.05$, ** $P<0.01$, *** $P<0.001$, **** $P<0.0001$.

2.2.15 Experimental design for sample cohorts in EAE studies

EAE was induced in C57BL/6 female mice over a maximum duration of 28 days. Generally, a cohort of 12-15 mice were immunised with rMOG and pertussis toxin simultaneously to induce an EAE time-course, prior to culling approximately n-3 mice per timepoint of interest (days 7, 14, 21, 28). Due to animal ethical restrictions and clinical outcomes of mice, certain EAE timepoints warranted further investigation and EAE induction required to be repeated to gain sufficient sample numbers at specific timepoints (minimum n-3 per data set). Therefore, certain EAE timepoints may represent variable independent experimental repeats and sample numbers to achieve a minimum of n-3 per EAE timepoint.

Chapter 3

The role of miR-155 in Wild Type mice in EAE

3.1 Introduction

MiR-155 is a widely studied proinflammatory miRNA involved in regulating and fine-tuning immune cell function (Sonkoly, Ståhle and Pivarcsi, 2008; Mashima, 2015). Although miR-155 is an essential miRNA for successful clearance of pathogens, chronically elevated miR-155 expression in immune cells is implicated in an array of cancers and autoimmune diseases such as Rheumatoid Arthritis, MS, and its murine model EAE (Blüml *et al.*, 2011; Leng *et al.*, 2011; Moore, Vijayaraghava T.S. Rao, *et al.*, 2013). Even though there are strong associations of increased miR-155 expression with autoimmune pathologies, its full mechanisms and roles within individual immune cell subsets remain elusive.

EAE is an animal model of MS in which the innate and adaptive immune systems are involved in promoting a chronically inflamed CNS environment. The T cell mediated attack in EAE is directed towards the myelin sheath surrounding neuronal axons, causing demyelination sporadically within the CNS (Miller, Karpus and Davidson, 2007; Ben-Nun *et al.*, 2014). The contribution of miR-155 to EAE pathogenesis has been confirmed in miR-155$^{-/-}$ mice, which are resistant to disease induction. Specifically, these studies revealed total miR-155 deficient mice had impaired development of Th1 and Th17 cells during the induction phase of EAE, along with decreased inflammatory cytokine production (IL-17, IFN-γ), and reduced infiltration of peripheral CD4^{+} T cells into the CNS, subsequently alleviating disease severity (Connell *et al.*, 2010). Moreover, the miR-155 antagomir, LNA-anti-miR-155, attenuated the clinical signs of EAE when administered intravenously at preclinical stages of disease (from day 5 post immunisation). Additionally, LNA-anti-miR-155 administration post onset of EAE clinical scores resulted in a more rapid clinical recovery of mice (Gopal Murugaiyan *et al.*, 2011)

Although considered a CD4^{+} T cell mediated disease, the role of myeloid cells in MS has garnered recent attention. In particular, macrophages derived from CNS infiltrating monocytes have the potential to either promote disease progression or facilitate repair depending on their polarisation state (Mishra and Wee Yong, 2016). These divergent activation states have been identified in MS animal models through expression of the markers iNOS and ARG1, which appear to define the metabolic state of inflammatory and anti-inflammatory macrophages, respectively (Veronique E Miron *et al.*, 2013; Locatelli,

Theodorou, Kendirli, Jordão, *et al.*, 2018). Although miR-155 has been identified to regulate the polarisation state of macrophages (Kyle A Jablonski *et al.*, 2016), and its upregulation has been confirmed in myeloid cells derived from MS patients (Moore, Vijayaraghava T S Rao, *et al.*, 2013), analysis of miR-155 expression in myeloid cell lineages during EAE has not been thoroughly explored.

Most studies surrounding the immunopathogenesis of MS utilise the EAE mouse model to elucidate important mechanisms driving CNS inflammation. However, these studies mainly use linear encephalitogenic peptides such as MOG_{35-55} to induce autoreactivity against myelin, which lack conformation-dependent epitopes and fail to activate autoantigen specific B cells. In contrast, immunisation of C57BL/6 mice with recombinant MOG protein, comprising the extracellular region that is exposed to the immune system, activates MOG-specific B cells and therefore more closely recapitulates the human disease (Emily R. Pierson, Stromnes and Goverman, 2014). Therefore, this research project investigating the involvement of miR-155 in numerous immune cell subsets in EAE will utilise the recombinant MOG protein for disease induction in order to capture mechanisms of disease pathogenesis that may be missed with EAE induction using MOG_{35-55} peptide.

Overall, this Chapter investigates miR-155 expression in individual lymphocyte and myeloid cell populations within the CNS of WT female C57BL/6 mice with rMOG-EAE. The objective of this study is to determine whether miR-155 expression in myeloid cell subsets contribute to EAE development and progression. This will be determined in the following experimental aims:

1. To determine which immune cell subset expresses the greatest levels of miR-155 during an EAE disease course.
2. To assess the expression of miR-155 transcription factors and target genes.
3. To investigate if elevated miR-155 correlates with myeloid polarisation states.

3.2 Results

3.2.1 Clinical scores of WT mice during EAE.

To investigate the role of miR-155 in EAE, female C57BL/6 mice were induced with chronic progressive EAE by immunisation with recombinant rodent MOG protein (rMOG) emulsified in Complete Freund's adjuvant. Immunising mice with rMOG instead of the immunodominant encephalitogenic peptide MOG_{35-55} activates MOG specific-B cells, thus closer recapitulating the pathology of human MS (Weber MS, 2011, Biochima et Biophysica Acta). Initial studies surrounding this murine model of MS involved daily observations of mouse paralysis throughout an EAE disease time course. Mice were observed by grading levels of paralysis using the following clinical scoring system: 1. Limp tail 2. Weak hind legs 3. Paralysed hind limbs 4. Weak forelimbs 5. Moribund/ dead. Figure 3.1 represents clinical scores of EAE induced mice over a 28 day period. Clinical disease onset was identified by limp tail/paralysis and occurred on day 13.2 (S.E.M ± 0.32), after which EAE symptoms progressed sharply between days 12-16, with scores ranging from 0.5 to 2.5. Clinical scores plateaued at day 18 and during the chronic stages of EAE (days 20-28), clinical scores slightly regressed with observations of spontaneous remission. Overall, these results displayed a chronic progressive clinical course of EAE with a mean clinical score of 2.05 (S.E.M ± 0.31), and cumulative score of 15.82 (S.E.M ± 4.91).

3.2.2 Immune cell populations increase within the CNS during EAE.

To investigate changes in immune cell populations within the CNS during EAE, CNS tissues were collected from naïve mice and at 7-day intervals following EAE induction. These represent key time points during the clinical course of EAE: day 7, pre-clinical stage; day 14, clinical onset of disease; day 21, plateauing of clinical scores/ onset of spontaneous recovery; day 28, chronic stage and end point of EAE. Figure 3.2A demonstrates the gating strategy used to delineate and sort immune populations within the CNS. All immune cells were initially derived from singlets followed by intact cells, before subsequently being sorted into specific immune cell subsets based on cell surface marker expression. Myeloid cells/microglia were identified as $CD11b^{+}F4/80^{+}$ cells, B cells were derived from $CD11b^{-}F4/80^{-}B220^{+}$ cells, and $CD4^{+}$ and $CD8^{+}$ T cells were derived from $CD11b^{-}F4/80^{-}B220^{-}CD4^{+}$ and $CD11b^{-}F4/80^{-}B220^{-}CD8^{+}$ cells, respectively.

As shown in Figure 3.2B, the proportion of myeloid cells/microglia significantly increased within the CNS from 7.52% in naïve mice to 38.40% at day 7 of EAE (P value 0.0023). This proportion of myeloid cells/microglia was maintained at day 14 (37.44%) before decreasing slightly at day 21 (25.73%), although this was not significant. At day 28, the average proportion of myeloid cells/microglia increased to 38.66% (P value 0.0007 vs naïve).

Figure 3.2C demonstrates that the proportion of $CD4^+$ T-cells steadily increased in naïve mice (0.55%) to day 7 EAE (4.01%) before plateauing at day 14 (13.63%) and day 21 (14.98%) ($p<0.01$ vs naive). The proportion of $CD4^+$ T cell then slightly decreased at day 28 to 7.98% (not significant).

Figure 3.2.D shows that $CD8^+$ T cell proportions increased at a later stage in EAE compared to other immune cell populations analysed. $CD8^+$ T cell proportions were maintained at 0.23% and 1.46% in naïve mice and at day 7 EAE, respectively. At day 14, $CD8^+$ T cells increased to 6.15% and further increased at day 21 to 11.55% ($P<0.001$ vs naïve and day 7). At day 28, $CD8^+$ T cells significantly decreased to 4.45% (P value 0.0179).

Analysis of B cell populations during EAE (Figure 3.2E) revealed a different trend compared to other immune cells examined due to no significant increases in cell proportions between days 14-28 EAE. B cell proportions significantly increased from 0.91% in naïve mice to 14.49% at day 7 EAE (P value 0.0027). At days 14 and 21, B cell proportions significantly decreased to 4.47% and 4.39% ($p<0.01$ vs day 7), before slightly decreasing further to 1.72% (P value 0.0022 vs day 7).

Overall, these data represent a higher proportion of $CD11b^+F4/480^+$ cells and $CD4^+$ T cells present within the CNS during clinical onset of disease (day 14) and later chronic stages of EAE (days 21-28) compared to $CD8^+$ T cells and B cells. The proportion of $CD11b^+F4/480^+$ cells is higher at all EAE time points analysed in comparison to $CD4^+$ T cells, which is not unexpected as this population includes microglia, the resident immune cells of the CNS.

3.2.3 Lymphocyte populations decline within the spleen during EAE.

Analysis of immune cell populations within the spleen was carried out alongside analysis of CNS tissue in Section 3.2.2. Figure 3.3A demonstrates the gating strategy used to delineate and sort immune cell populations within the spleen. All immune cells were firstly derived from singlets followed by intact cells, and then immune cells were sorted into the same four

immune cell subsets as in Section 3.2.2: $CD11b^{+}F4/80^{+}$ myeloid cells, $CD11b^{-}F4/80^{-}B220^{+}$ B cells, $CD11b^{-}F4/80^{-}B220^{-}CD4^{+}$ and $CD11b^{-}F4/80^{-}B220^{-}CD8^{+}$ $CD4^{+}$ and $CD8^{+}$ T cells respectively.

Figure 3.3B demonstrates that myeloid cell proportions remained relatively low throughout EAE, consistent with this population being predominantly tissue resident macrophages. Myeloid cell proportions in naïve mice (1.95%) did not significantly increase during EAE at day 7 (2.47%). There was relatively no change in myeloid cell proportions at days 14 and 21 (2.69% and 3.07%), before slightly decreasing to 2.2% at day 28, chronic stages of EAE (not significant).

As shown in Figure 3.3.C, $CD4^{+}$ T cell proportions declined at certain timepoints during disease progression. $CD4^{+}$ T cell proportions significantly decreased from 18.01% in naïve mice to 9.26% (P value 0.0002) at day 7 EAE, and further decreased to 7.94% at day 14 ($P<0.0001$ naïve vs day 14). $CD4^{+}$ T cells slightly increased at day 21 to 13.41% (not significant) before decreasing once more at day 28 to 11.98% (P value 0.0091 naïve vs day 28).

Figure 3.3D represents the proportion of $CD8^{+}$ T cells within the spleen during EAE. $CD8^{+}$ T cell proportions significantly decreased from 14.78% in naïve mice to 9.08% (P value 0.0318) at day 7 EAE, and further decreased at day 14 to 3.92% (P value 0.0001 naïve vs day 14). $CD4^{+}$ T cell proportions then slightly increased at day 21 to 8.65% and remained relatively constant at day 28 at 6.08%.

B cell proportions are shown in Figure 3.3.E. B cell proportions significantly and sharply declined in naïve mice from 63.75% to 41.44% (P value 0.0037) at day 7 EAE. B cell proportions further decreased significantly at day 14 to 19.79% (P value 0.0078) before slightly increasing at day 21 to 33.22% and day 28 to 35.54% (not significant).

Overall, these data indicate that $CD11^{+}F4/80^{+}$ myeloid cell proportions did not significantly change within the spleen throughout EAE. Furthermore, lymphocyte population studies investigating $CD4^{+}$ T cells, $CD8^{+}$ T cells, and B cells demonstrated that these cell proportions significantly decreased within the spleen at days 7 and 14 EAE, coinciding with their recruitment to the CNS, but slightly increased during chronic stages of disease at days 21 and 28.

3.2.4 miR-155 induction is highest in myeloid cells/microglia within the CNS during EAE.

Initial population studies within the CNS throughout EAE suggest that all investigated immune cells are involved in disease progression. However, in order to investigate if miR-155 plays a role in these immune cell subsets, miR-155 expression was measured in sorted immune cells (derived from Section 3.2A). Data was then analysed using the ΔΔCT method so that the fold-change of miR-155 at each 7-day interval was assessed, thereby enabling visualisation of any miR-155 induction or reduction throughout an EAE time course. This would establish which immune cell subsets had the greatest induction of proinflammatory miR-155 and at which stage of disease.

Figure 3.4A illustrates miR-155 induction in myeloid cells/microglia. There was relatively no fold change of miR-155 between naïve mice and day 7 EAE at 0.99 and 0.32-fold respectively, but miR-155 was relatively induced to 5.07-fold at day 14 (not significant P value 0.0770). MiR-155 decreased at day 21 to 3.06-fold before increasing once more at day 28, end stage of EAE, to 5.95-fold (P value 0.0210, day 7 vs day 28). Notably, myeloid cells/microglia displayed miR-155 induction at different stages of EAE: clinical onset of disease and chronic stage/end point of EAE, this further correlated with increased myeloid cells/microglia proportions within the CNS at days 14 and 28.

As shown in Figure 3.4B, there was little miR-155 induction in $CD4^+$ T cells between naïve mice at 0.76-fold and at day 7 EAE at 0.88-fold. MiR-155 induction was significantly increased to 3.91-fold at day 14 (P value 0.0204 naïve vs day 14), before slightly decreasing to 2.22-fold at day 21 and 2.14-fold at day 28.

MiR-155 fold-changes in $CD8^+$ T cells are shown in Figure 3.4C. Similarly shown in myeloid cells/microglia and $CD4^+$ T cells, miR-155 induction in $CD8^+$ T cells did not change in naïve mice (0.78-fold) when compared to day 7 EAE (0.95-fold change). However, there was a significant decrease at day 14 to 0.27-fold (P value 0.0264 naïve vs day 14), this decrease was further evident at day 21 to 0.06-fold (P value 0.0110 naïve vs day 21), whereas day 28 had significantly induced miR-155 expression to 1.19-fold (P value 0.0120).

MiR-155 fold-change in B cells is represented in Figure 3.4D. Overall, there was no evident miR-155 induction at any stage of EAE. However, a slight decrease of miR-155 expression was observed between naïve mice (0.87-fold) and days 7-14 EAE (0.48-0.22-fold), before

miR-155 increased slightly and decreased once more at days 21-28 respectively (0.89 to 0.56-fold).

Collectively, these data showed miR-155 induction was maximal at 5.95-fold in myeloid cells/microglia compared to $CD4^+$ (3.91-fold), $CD8^+$ (1.19-fold) and B cells (0.89-fold) during EAE progression. Furthermore, this induction was only significant during stages of clinical onset of disease or end stage of EAE.

3.2.5 miR-155 absolute levels are highest in myeloid cells/microglia within the CNS during EAE.

MiR-155 expression was next analysed using an absolute quantification method that determines the exact copy number of miR-155 in a given cell, thereby allowing direct comparison between immune cell subsets. Sorted immune cells (derived from Section 3.2.2A) from the CNS were assessed.

Figure 3.5A represents miR-155 expression in myeloid cells/microglia. In myeloid cells/microglia from naïve mice, the expression of miR-155 was 53.58 x 10^4, which significantly increased to 458.53 x 10^4 by day 28 (P value 0.0230). As shown in Figure 3.5B, the expression of miR-155 in $CD4^+$ T cells was increased from naïve mice at 34.42 x 10^4 to 195.88 x 10^4 at day 14 EAE, miR-155 expression did not significantly change from days 21 to 28, with expression levels at 170.42 x 10^4 and 132.59 x 10^4, respectively. Figure 3.5C demonstrates how miR-155 expression levels in $CD8^+$ cells decreased at days 14 (61.62 x 10^4) and 21 (49.18 x 10^4) EAE compared to naïve mice (292.22 x 10^4). Figure 3.5D represents miR-155 expression levels in B cells. MiR-155 expression was significantly decreased at day 14 EAE at 26.66 x 10^4 compared to naïve mice with 207 x10^4 (P value 0.0247).

In conclusion, this set of data suggests that the absolute level of miR-155 expression was greatest in myeloid cells/microglia at 458.53 x 10^4 compared to any other immune cell population in the CNS.

3.2.6 miR-155 induction within splenic immune cells during EAE.

miR-155 induction studies within the CNS provided useful information by identifying involvements of key immune cell subsets during disease progression. To further investigate the involvement of these immune cells at the same key timepoints outside the inflammatory CNS environment, miR-155 induction was measured in sorted splenic immune cells (derived from Section 3.2.3).

As shown in Figure 3.6A, miR-155 was not induced in $CD11b^{+}F4/80^{+}$ myeloid cells within the spleen. All EAE timepoints had no significant induction of miR-155 compared to naïve splenic $CD11b^{+}F4/80^{+}$ myeloid cells, reaching a maximum fold change of 0.74.

In contrast, Figure 3.6B represents a significant increase of miR-155 induction in $CD4^{+}$ T cells at day 14 EAE to 2.65-fold in comparison to naïve and day 7 samples at 1.05 and 0.63-fold (P values<0.0001). This increase interestingly coincided with development of clinical onset of disease. Following this induction, miR-155 was significantly decreased at day 21 to 0.70-fold (P<0.0001) before slightly increasing once more to 1.52-fold at day 28 (P value 0.0093, day 14 vs day 28).

Figure 3.6C examines miR-155 induction in $CD8^{+}$ T cells. Overall, miR-155 expression did not significantly increase throughout EAE, although a slight trend of increased and decreased fold changes were observed from days 7 to day 28 with ranging fold differences between 0.92 to 2.71-fold.

Figure 3.6D represents miR-155 induction in splenic B cells during EAE. As observed in $CD8^{+}$ T cells, miR-155 expression did not significantly change between naïve and EAE splenic B cells (fold changes remained between 0.53 and 1.50-fold).

Overall, these data showed miR-155 expression was only significantly induced in splenic $CD4^{+}$ T cell during EAE progression. Interestingly, miR-155 expression was not induced in $CD11b^{+}F4/80^{+}$ splenic myeloid cells, despite results in Section 3.4A suggesting miR-155 could be playing a specific role in $CD11b^{+}F4/80^{+}$ cells within the CNS.

3.2.7 miR-155 absolute values increased in splenic $CD4^{+}$ T cells in EAE.

MiR-155 copy numbers were next analysed in immune cell subsets derived from the spleen during EAE. Sorted immune cells (derived from Section 3.2.3A) were assessed for miR-155 absolute levels.

Figure 3.7A outlines miR-155 expression levels in myeloid cells. In myeloid cells derived from naïve mice, the expression of miR-155 was 163.85 x 10^4, which relatively did not change by day 28 at 136.53 x 10^4. As shown in Figure 3.7B, the expression of miR-155 in $CD4^+$ T cells was significantly increased from naïve mice at 125.72 x 10^4 to 332.92 x 10^4 at day 14 EAE (P value 0.0225). From days 14 to 21 EAE, miR-155 expression significantly decreased from 332.92 x 10^4 to 111.49 x 10^4 (P value 0.0276). Figure 3.7C represents miR-155 expression levels in $CD8^+$ cells. MiR-155 expression slightly increased at days 14 (314.12 x 10^4) and 21 (446.22 x 10^4) EAE compared to naïve mice (160.17 x 10^4). As demonstrated in Figure 3.7D, miR-155 expression levels in B cells remained relatively unchanged throughout EAE.

In conclusion, this set of data suggests that the absolute level of miR-155 expression increased only in splenic CD4+ T cells to 332.92 x 104 compared other immune cell subsets investigated, consistent with previously published studies revealing a role during T-cell priming during EAE (O'Connell, Kahn, William S.J. Gibson, *et al.*, 2010a).

3.2.8 Inflammatory and anti-inflammatory gene expression in myeloid cells/microglia during EAE.

Within the CNS, miR-155 expression was induced in myeloid cells/microglia in EAE, suggesting this miRNA plays an important and previously unidentified role in this immune cell population during disease. To further understand whether induction of miR-155 was associated with an inflammatory phenotype that promotes neuroinflammation, gene expression studies were carried out using RNA samples generated from sorted myeloid cells/microglia (Section 3.2.2A). The classical pro-inflammatory markers, iNOS and TNFα, classical anti-inflammatory and immunoregulatory markers, IL-10m and ARG1 (Mosser and Edwards, 2008), were first analysed to determine how expression of these genes correlated with induction of miR-155 expression in myeloid cells/microglia during EAE.

As shown in Figure 3.8A, myeloid cells/microglia displayed significantly induced iNOS gene expression at day 14 EAE compared to naïve and day 7 EAE mice by 5.26-fold (P values<0.01), before iNOS significantly decreased at days 21 and 28 to 2.33 and 0.69-fold respectively (P values 0.0134/0.0038, day 14 vs 21/28). Figure 3.8B represented there was no significant induction of TNFα gene expression during EAE. Despite lack of statistical

significance, there was a subgroup of mice with high TNFα gene expression. This could be due to certain mice displaying different stages of clinical scores at the day 14 EAE timepoint.

Whilst investigating anti-inflammatory IL-10m gene expression (Figure 3.8C), a significant reduction between naïve myeloid cells/microglia at all timepoints during the EAE disease course to below 0.2-fold was observed (P values<0.001/<0.01, naïve vs days 7-21/28). Interestingly, there was a trend towards increased expression of ARG1 at day 14 (4.8-fold) compared to naïve and day 7, with a further increase to 8.43-fold at day 21. At this latter time point, ARG1 expression is significantly increased compared to naïve, day 7, and day 28 of EAE (P<0.01, naïve/day 7 vs day 21, P<0.05, day 21 vs day 28), coinciding with spontaneous recovery of clinical disease (Fig 3.1).

Overall, inflammatory genes iNOS and TNFα are evidently induced at day 14 as mice develop clinical signs of disease, suggesting myeloid cells/microglia exist in an inflammatory functional state. In contrast, immunoregulatory genes IL-10m and ARG1 are either significantly down regulated (IL-10m) throughout EAE or become significantly induced at day 21 when EAE symptoms plateau or slightly regress, suggesting a potential switch to an anti-inflammatory functional phenotype.

3.2.9 Gene expression of miR-155 targets throughout EAE

Correlating miR-155 expression with inflammatory and immunoregulatory gene expression in myeloid cells/microglia provided insight to their characteristics and behaviour during EAE. To further confirm a role for miR-155 in $CD11b^{+}F4/80^{+}$ cells within the CNS during EAE, gene expression of ETS2, a transcriptional regulator of miR-155, as well as miR-155 targets: SHIP1 and ARG2 were assessed.

ETS2 is a known transcriptional inducer of miR-155 (Quinn et el, 2014). Figure 3.9A shows ETS2 expression was significantly induced to 4.66-fold at day 14 EAE (P<0.001, naïve/day 7 vs day 14), consistent with miR-155 expression data in fig.3.4A, before expression levels significantly decreased at days 21 and 28 to 2.10 and 0.91-fold (P<0.01, day 14 vs day 21, P<0.0001, day 14 vs day 28).

Figure 3.9B represents gene expression data for SHIP1, a known immunoregulatory target of miR-155 (O' Connell et el, 2009). SHIP1 expression was significantly increased to 8.13-fold at day 7 (P value 0.0004) before gene expression significantly decreased to less than 1-

fold from days 14-28. Interestingly, SHIP1 expression inversely mirrors that of miR-155 in fig3.4A and has a pattern that is consistent with its repression by miR-155.

ARG2 expression, a novel miR-155 target (Dunand-Sauthier et el, 2014) and isoform of the classical anti-inflammatory marker ARG1 (Nicholas Ah Mew et el, 2015), is shown in Figure 3.9C. ARG2 induction was significantly reduced throughout days 7-21 of EAE in comparison to naïve mice (P>0.01), displaying a similar pattern to the anti-inflammatory cytokine IL-10m (Fig.3.8C).

In summary, these data are consistent with the induction of miR-155 observed in Fig.3.4A whereby ETS2 correlated with miR-155 induction at day 14 EAE, and immunoregulatory genes SHIP1 and ARG2 were repressed during stages of EAE when miR-155 levels are high.

3.2.10 Ly6C, MHCII, and CCR2 expression on myeloid cells/microglia in EAE.

To further investigate the characterisation of myeloid cells/microglia within the CNS during EAE, immune cells from the CNS were cell surface stained for phenotypic markers indicative of inflammatory states in naïve mice, and mice at 7-day intervals throughout EAE. Figure 3.2A demonstrates the gating strategy used to delineate myeloid cells/microglia within the CNS for phenotypic analysis for surface Ly6C, MHCII, and CCR2. All surface marker proportions were derived from intact $CD45^{+}CD11b^{+}$ cells.

As shown in Figure 3.10B, the proportion of Ly6C significantly increased on $CD45^{+}CD11b^{+}$ cells at day 7 EAE at 39.92% from 12.01% in naïve samples (P value 0.0410). This proportion of myeloid cells/microglia steadily increased further at day 14 (44.72%) and 21 (71.57%), before significantly decreasing at day 28 to 34.17% (P value 0.0266).

Figure 3.10C represents the proportion of $MHCII^{+}$ myeloid cells/microglia. The proportion of MHCII significantly increased from naïve samples at 0.90% to 14 at 43.80% (P<0.0001), before slightly increasing further to 51.95% at day 21 (not significant), lastly, MHCII remained relatively stable at 47.57% at day 28 EAE.

Figure 3.D shows CCR2 proportions in naïve mice and at day 14 EAE. CCR2 significantly increased from naïve mice at 6.67% to day 14 EAE at 38.43% (P value 0.0002).

Collectively, these data represent Ly6C, MHCII, and CCR2 were all significantly increased at certain stages of EAE. Ly6C, an inflammatory marker, was significantly increased from

day 7-21 EAE, indicative of an inflammatory myeloid cells/microglia phenotype. MHCII, an antigen presenting molecule, was significantly increased from day 14-28 EAE, proposing increased antigen presenting at this timepoint. Lastly, CCR2, a chemokine, was significantly increased at day 14 EAE, suggesting increased chemoattractive recruitment into the CNS.

3.2.11 Myeloid cells/microglia expression of iNOS and CD206 in EAE.

Myeloid cells/microglia underwent further phenotypic analysis to investigate intracellular iNOS and cell surface CD206 (mannose receptor) to determine if this immune cell population displayed characteristic inflammatory (iNOS) or immunoregulatory (CD206) phenotypic markers.

Figure 3.11A represents the gating strategy used to determine iNOS and CD206 proportions in myeloid cells/microglia. Myeloid cells/microglia represented $CD45^{+}CD11b^{+}$ cells and were derived from singlets and intact cells.

Figure 3.11B demonstrates the proportions of intracellular iNOS in naïve CNS myeloid cells/microglia and at day 14 EAE. iNOS was significantly increased from 0.15% in naïve samples to 13.37% at day 14 EAE (P value 0.0106). Figure 3.11C represents a histogram of the shift of iNOS expression between naïve and day 14 EAE samples normalised to mode.

Figure 3.11D shows the proportions of CD206 on naïve and day 14 EAE myeloid cells/microglia from the CNS. The proportions of CD206 did not significantly change between samples and remained relatively stable at 9.91% (naïve) and 7.99% (day 14). Figure 3.11E represents no change in CD206 expression via overlapping histograms normalised to mode in naïve and day 14 EAE samples.

In summary, these data show increased inflammatory phenotype marker, iNOS, during a peak incline of clinical scores at day 14 EAE, and correlate with iNOS gene expression shown in Figure 3.8A. Opposingly, CD206, an anti-inflammatory scavenger receptor shows no significant change at this timepoint of EAE compared to naïve mice.

3.2.12 Clinical scoring of mice at day 14 EAE.

Following initial analysis of the 28-day EAE time course, day 14 EAE emerged as a key timepoint of interest to study in greater detail due to the significant increase of myeloid

cells/microglia population proportions, induction of miR-155 expression, and inflammatory gene expression within the CNS, which additionally coincided with the clinical onset of disease. To investigation this timepoint further, a separate cohort of C57BL/6 mice were immunised with rMOG and daily observations of mouse paralysis were carried out over a period of 14 days. Figure 3.12 represents clinical scores of EAE induced mice over a 14-day period. Clinical disease onset occurred on day 12.88 (S.E.M ± 0.39) before EAE symptoms progressed sharply between days 12-14 to scores 0.5 to 2.5.

Overall, these results were consistent with previous clinical score data (Figure 3.1) and displayed a progressive clinical course of EAE with a mean clinical score of 1.94 (S.E.M ± 0.23), and a mean cumulative score of 3.81 (S.E.M ± 0.86).

3.2.13 Macrophage and neutrophil populations increase during EAE.

As day 14 EAE was established as a key timepoint of interest for this research project, a further detailed analysis of immune cell populations within the CNS were carried out. Specifically, the myeloid cells/microglia immune cell population was further analysed by subdividing these immune cells into macrophages, neutrophils and microglia. These 3 immune cell subsets were chosen for further investigation due to miR-155 and inflammatory gene expression data, and increased interest in the role of myeloid cell subsets and microglia in EAE pathogenesis (Liu *et al.*, 2014; Lévesque *et al.*, 2016; Herz *et al.*, 2017). C57BL/6 mice immunised in Section 3.2.12 were culled at day 14 EAE and immune cell subsets were isolated from CNS tissue for further analysis. Naïve CNS samples were obtained from C57BL/6 mice not immunised with rMOG.

Figure 3.13A demonstrates the gating strategy used to delineate and sort macrophages, microglia, neutrophils from other immune cells within the CNS. All populations of interest were initially derived from singlets, intact cells, and viable cells. Immune cells were then sorted into further subsets using cell surface markers; macrophages: $CD45^{hi}Ly6G^{-}CD11b^{+}F4/80^{+}$, microglia: $CD45^{int}Ly6G^{-}CD11b^{+}CX3CR1^{+}$, and neutrophils: $CD45^{hi}Ly6G^{+}CD11b^{+}$ cells.

As shown in Figure 3.13B, the proportion of macrophages significantly increased from approximately 2.12% in naïve mice to 12.17% at day 14 EAE (P value 0.0270), consistent with the infiltration by peripheral immune cells (Figure 3.2). Figure 3.13C demonstrated that

microglia proportions significantly decreased during EAE with cell proportions at 59.09% in naïve mice and 24.33% at day 14 (P value 0.0106). As shown in Figure 3.13D, the proportion of neutrophils within the CNS remained relatively the same at 18.32% in naïve mice to 18.30% at day 14 EAE.

Overall, these population studies were consistent with known roles of these immune cells in EAE, whereby peripheral myeloid cells invade the CNS to mediate tissue damage, thus leading to the clinical onset of disease.

3.2.14 miR-155 is significantly induced in macrophages in EAE

As shown in Figure 3.4, a mixed myeloid/microglia population ($CD11b^{+}F4/80^{+}$) had the highest induction of miR-155 within the CNS during EAE. Therefore, to characterise the role of miR-155 in more specific cell subsets when EAE symptoms progressed sharply, miR-155 induction was measured in macrophages, microglia, and neutrophils at day 14 of disease.

As shown in Figure 3.14A, miR-155 expression in macrophages was significantly induced at day 14 EAE (6.75-fold) when compared to naïve samples (1.16-fold) (P value 0.0244). Figure 3.14B represents miR-155 expression in microglia. Despite a lack of statistical significance, there was an evident trend of increased miR-155 expression at this timepoint (10.36-fold) compared to naïve samples (1.40-fold). Figure 3.14C examines miR-155 induction in neutrophils within the CNS. As similarly observed in microglia, neutrophils had no significant induction of miR-155 at day 14 EAE. Overall, neutrophils had a miR-155 induction to 8.06-fold at day 14 EAE.

Collectively, there were evident trends of increased miR-155 expression at day 14 EAE in all immune subsets examined: macrophages, microglia, and neutrophils. However, miR-155 induction was only significantly induced in macrophages, indicating this pro-inflammatory miRNA has more influence in macrophages during EAE.

3.2.15 miR-155 absolute values significantly increased in macrophages in EAE.

Absolute quantification of miR-155 was performed to determine the exact copy number of miR-155 in myeloid derived cells and CNS resident cells at day 14 EAE. Sorted

macrophages, microglia, and neutrophils (derived from Section 3.2.13) from the CNS were assessed.

Figure 3.15A represents miR-155 expression in macrophages. Macrophages derived from naïve mice contained miR-155 expression levels of 6.67 x 10^4, which significantly increased to 64.74 x 10^4 by day 14 (P value 0.0354). As shown in Figure 3.15B, miR-155 expression levels in microglia was increased from naïve mice at 31.75 x 10^4 to 205.78 x 10^4 at day 14 EAE (not significant). Figure 3.15C demonstrates how miR-155 expression levels in naïve neutrophils are higher than naïve macrophages and microglia miR-155 levels at 97.89 x 10^4. miR-155 expression then increased to 589.64 x 10^4 at day 14 EAE, although no significance could be determined.

Collectively, these data suggest the absolute level of miR-155 expression was increased in all immune cell subsets within the CNS at day 14, but absolute miR-155 levels were only significantly increased in macrophages at day 14 compared to naïve samples.

3.2.16 miR-155 is not induced in blood monocytes at day 14 EAE.

MiR-155 expression levels within the CNS during EAE suggest that macrophages and neutrophils are involved in EAE disease activity. Therefore, in order to investigate if miR-155 plays a role in these immune cell subsets within the circulation prior to entering the CNS, miR-155 expression was measured in sorted immune cells derived from the blood. Data was then analysed using the ΔΔCT method so that the fold-change of miR-155 could be determined in naïve samples and at day 14 EAE.

Figure 3.16A demonstrates the gating strategy used to delineate and sort monocytes and neutrophils from other immune cells within the bloodstream of naïve and day 14 EAE samples. All immune subsets were initially derived from singlets, intact cells, and viable cells. Immune cells were then sorted into further subsets using cell surface markers; monocytes: $CD45^{hi}CD11b^{+}Ly6G^{-}Ly6C^{+}$ and neutrophils: $CD45^{hi}Ly6G^{+}CD11b^{+}$ cells.

Figure 3.16B illustrates miR-155 induction in circulating inflammatory monocytes. There was interestingly a decreased fold change of miR-155 between naïve mice and day 14 EAE at 1.06 and 0.24-fold (not significant). Although miR-155 increased in myeloid derived macrophages within the CNS at this timepoint, miR-155 was not induced in monocytes, perhaps suggesting miR-155 induction requires signals from the CNS microenvironment.

MiR-155 fold-changes in blood neutrophils are shown in Figure 3.16C. In contrast to blood monocytes, miR-155 induction in blood derived neutrophils increased from naïve mice (1.30-fold) to day 14 EAE (6.85-fold change), although this was not significant. This result correlates with miR-155 induction in CNS neutrophils indicating miR-155 induction is maintained in neutrophils prior to and after entering the CNS during EAE.

In summary, these data showed miR-155 induction was not evident in blood monocytes but rather exhibited a relative decrease in fold-change. Moreover, miR-155 induction was found highest in neutrophils within the blood at day 14 EAE.

3.2.17 miR-155 absolute levels decreased in blood monocytes at day 14 EAE.

MiR-155 expression was next analysed using an absolute quantification method which determines the exact copy number of miR-155 in monocytes and neutrophils derived from blood. Sorted immune cells (derived from Section 3.2.16) were assessed.

Figure 3.17A represents miR-155 expression in blood derived monocytes. MiR-155 expression levels decreased from 26884.32 x 10^4 in naïve samples to 9739.33 x 10^4 at day 14 EAE (not significant). As shown in Figure 3.17B, the expression of miR-155 in neutrophils was increased from naïve mice at 1294.22 x 10^4 to 13135.84 x 10^4 at day 14 EAE (not significant).

To summarise, this set of data suggests that the absolute level of miR-155 expression was increased in neutrophils, whereas miR-155 expression levels in monocytes appeared to decrease at day 14 EAE compared to naïve samples. Interestingly, miR-155 expression levels in monocytes are higher during naïve states compared to neutrophils, and higher than macrophages within the CNS at day 14 EAE (Figure 3.15A).

3.2.18 Ly6C, MHCII, and CCR2 expression is increased on macrophages within the CNS in EAE.

To investigate the polarisation states of macrophages within the CNS at day 14 EAE, immune cells were cell surface stained for phenotypic markers. Macrophages were delineated from other immune populations by; $CD45^{hi}Ly6G^{-}CD11b^{+}F4/80^{+}$, and investigated for surface Ly6C, MHCII, and CCR2.

Figure 3.16A demonstrates the proportion of Ly6C expression found on the surface of macrophages in naïve and day 14 EAE samples. The proportion of macrophages expressing Ly6C was significantly increased at day 14 to 92.6% (P<0.0001). Figure 3.16B represents the expression of Ly6C in an overlapping histogram format, where there was an evident increase of $Ly6C^+$ macrophages at day 14 EAE relative to naive macrophages.

As shown in Figures 3.18C and 3.18D, the proportion of macrophages expressing MHCII significantly increased from approximately 10.85% in naïve mice to 70.68% at day 14 EAE (P<0.0001).

Figures 3.18E and 3.18F CCR2 expression on macrophages within the CNS. CCR2 expression significantly increased on macrophages at day 14 EAE compared to naïve samples from 36.70% to 77.34% (P<0.0001).

In summary, macrophages within the CNS at day 14 EAE showed high cell surface expression of the inflammatory markers Ly6C and CCR2 markers, as well as upregulation of MHCII. This concurs with phenotypic analysis of myeloid cells/microglia, portraying macrophages as inflammatory drivers during neuroinflammation in EAE.

3.2.19 Ly6C and MHCII expression is increased on microglia in EAE.

To investigate microglial polarisation states during EAE coincidingly with macrophages, phenotypic analysis was also performed on microglia for surface Ly6C and MHCII expression. Microglia were delineated from other immune populations by; $CD45^{int}Ly6G^-CD11b^+CX3CR1^+$ cells, before being investigated for surface Ly6C and MHCII.

Figure 3.19A represents the Ly6C expression on microglia in naïve and day 14 EAE samples. Ly6C expression was notably variable among biological replicates but was found significantly increased at day 14 to 24.63% compared to naïve microglia at 0.07% (P value 0.07). Figure 3.17B shows a representative overlapping histogram format of Ly6C expression on microglia in which increased Ly6C expression was observed.

Figure 3.19C showed the proportion of microglia expressing MHCII significantly increased from approximately 0.17% in naïve mice to 53.94% at day 14 EAE (P value 0.0003). Figure 3.17D represents MHCII expression as an overlapping histogram normalised to mode to represent the shift positive shift of MHCII expression at day 14 EAE.

Overall, microglia from EAE samples demonstrated significantly increased Ly6C and MHCII expression. Microglia data correlated with macrophage phenotypes, indicative of an inflammatory phenotype. However, microglia expressed Ly6C and MHCII to a lesser extent corroborating with separate studies.

3.2.20 MHCII and CCR2 expression is increased on neutrophils within the CNS in EAE.

Neutrophils were the final immune cell subset to be investigated for phenotypic analysis. This infiltrating myeloid cell was analysed alongside macrophages and microglia within the CNS of naïve and day 14 EAE mice for characterisation of their polarised state. Neutrophils were delineated from other immune populations by; $CD45^{+}Ly6G^{+}CD11b^{+}$ cells, prior to being investigated for surface Ly6C, MHCII, and CCR2.

Figure 3.20A represents Ly6C expression on neutrophils in naïve and day 14 EAE samples. Unlike other analysed immune cell subsets, neutrophils had significantly decreased Ly6C expression at day 14 EAE (89.5%) compared to naïve samples (94.15%) (P value 0.0416). This decrease is seen in Figure 3.20B as an overlapping histogram normalised to mode.

As shown in Figure 3.20C, MHCII expression was significantly increased at day 14 EAE to 10.26% compared to naïve samples at 0.16% (P value 0.008). This was visually evident in Figure 3.20D via overlapping histogram normalised to mode.

Figure 3.20E demonstrated how CCR2 expression significantly increased at day to 18.36% compared to naïve samples at 0.31% (P value 0.0003). Figure 3.20F mirrored this significant increase of CCR2 expression in a histogram normalised to mode.

Collectively, these data portrayed neutrophils having increased antigen presenting and chemoattractant abilities due to their increased MHCII and CCR2 expression, respectively. However, inflammatory marker Ly6C expression was significantly decreased, opposing other immune cells examined at day 14 EAE

(A)

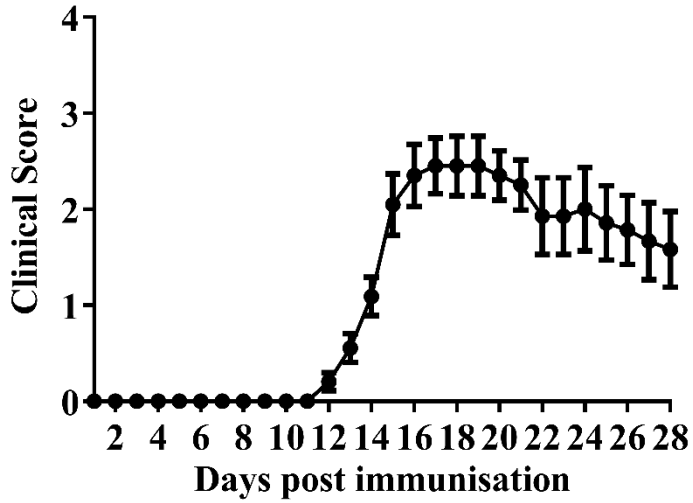

(B)

Day of disease onset	13.2 ± 0.32 (12-15)
Mean clinical score	2.05 ± 0.31 (0.5-3.5)
Cumulative score	15.82 ± 4.91 (1-43)

Figure 3.1 Clinical scores of WT mice during EAE.

C57BL/6 WT mice were actively induced with EAE using 65 µg rMOG on day 0 and 200 ng Pertussis toxin as an adjuvant on days 0 and 2. EAE was carried out for a total of 28 days. (A) Clinical scoring was carried out daily by measuring grade of paralysis. (B) Day of disease onset, mean clinical score, and cumulative score were derived from daily clinical scores. Data represents mean ± S.EM. (n=10-30, 3-4 independent experiments).

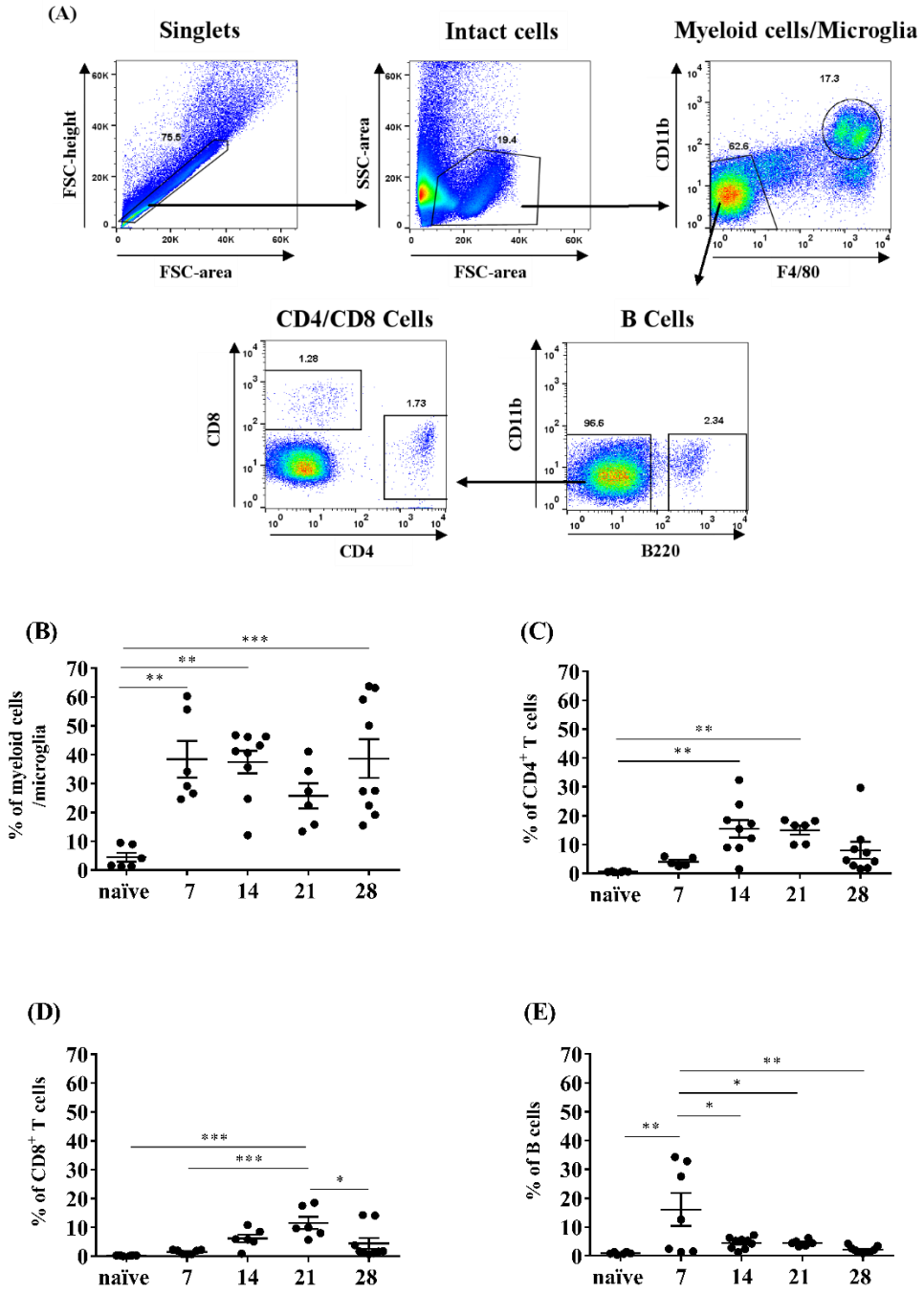

Figure 3.2 Immune cell populations increase within the CNS during EAE.

CNS samples from naïve and EAE induced C57BL/6 WT mice underwent immune cell isolation and cell sorting using flow cytometry. Cells were stained for surface CD11b, F4/80, CD4, CD8, and B220. (A) Representative gating strategy for immune cell population isolation. (B-E) Population proportions of myeloid cells/microglia (B), $CD4^+$ T cell (C), $CD8^+$ T cell (D), and B cells (E), throughout EAE at 7-day intervals. Data represents the percentage of immune cells relative to intact cells and expressed as mean ± S.EM. (n=6-9, 2-3 independent experiments). *P<0.05, ** P<0.01, ***P<0.001; one-way ANOVA with Bonferroni's correction.

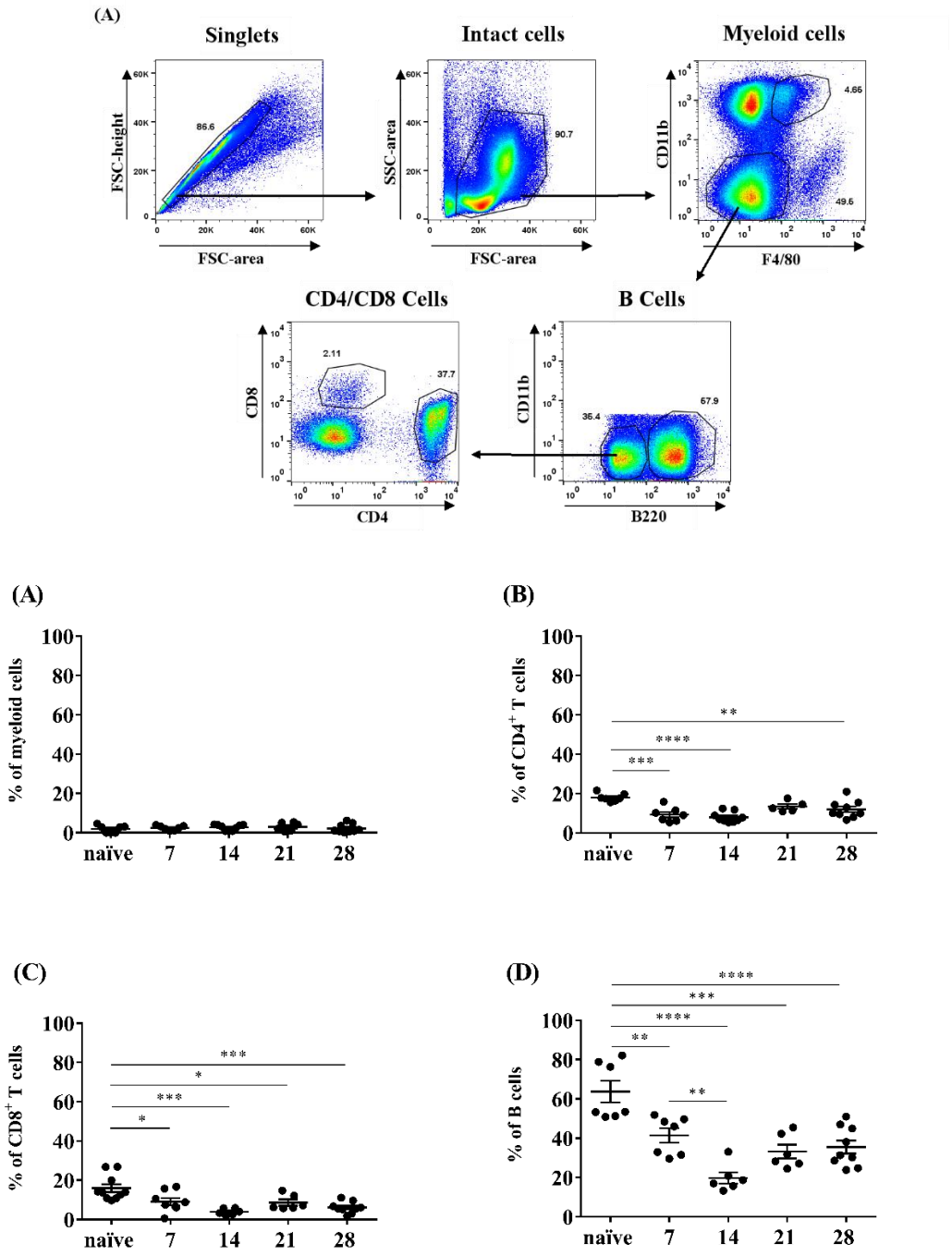

Figure 3.3 Lymphocyte populations decline within the spleen during EAE.

Spleen samples from naïve and EAE induced C57BL/6 WT mice underwent immune cell isolation and cell sorting using flow cytometry. Cells were stained for surface CD11b, F4/80, CD4, CD8, and B220. (A) Representative gating strategy for immune cell population isolation. (B-E) Population proportions of myeloid cells (B), $CD4^+$ T cell (C), $CD8^+$ T cell (D), and B cells (E), throughout EAE at 7-day intervals. Data represents the percentage of immune cells relative to intact cells and expressed as mean ± S.EM. (n=6-9, 2-3 independent experiments). *P<0.05, ** P<0.01, ***P<0.001, ****P<0.0001; one-way ANOVA with Bonferroni's correction.

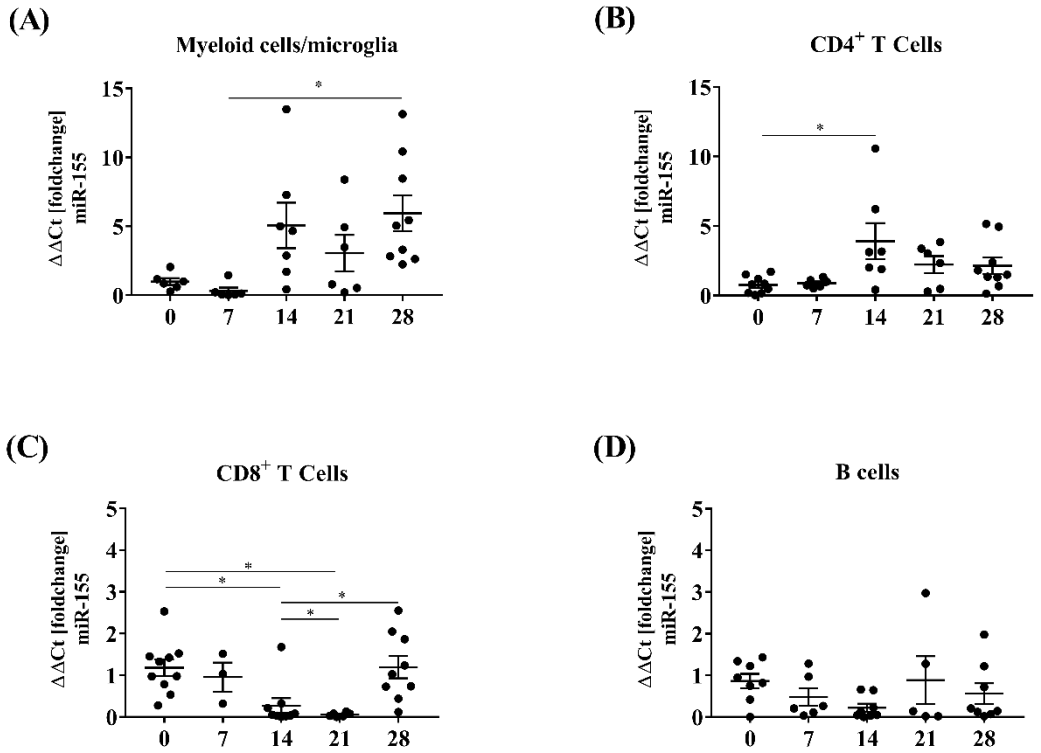

Figure 3.4 miR-155 induction is highest in myeloid cells/microglia within the CNS during EAE.

CNS immune cells of naïve and EAE C57BL/6 WT mice were sorted at 7-day intervals throughout EAE into 4 immune cell populations and lysed in TRIzol for total RNA isolation. Total RNA was extracted and rtPCR and qPCR was performed using Taqman probes to determine miR-155 expression in myeloid cells/microglia (A), $CD4^+$ T cells (B), $CD8^+$ T cells (C), and B cells (D). Data represent the ΔΔCT fold induction of miR-155 relative to naïve samples, normalised against the average of three housekeeping genes sno-202, miR-191, and snU6, and expressed as mean ± S.EM. (n=3-10, 1-3 independent experiments). *P<0.05; one-way ANOVA with Bonferroni's correction.

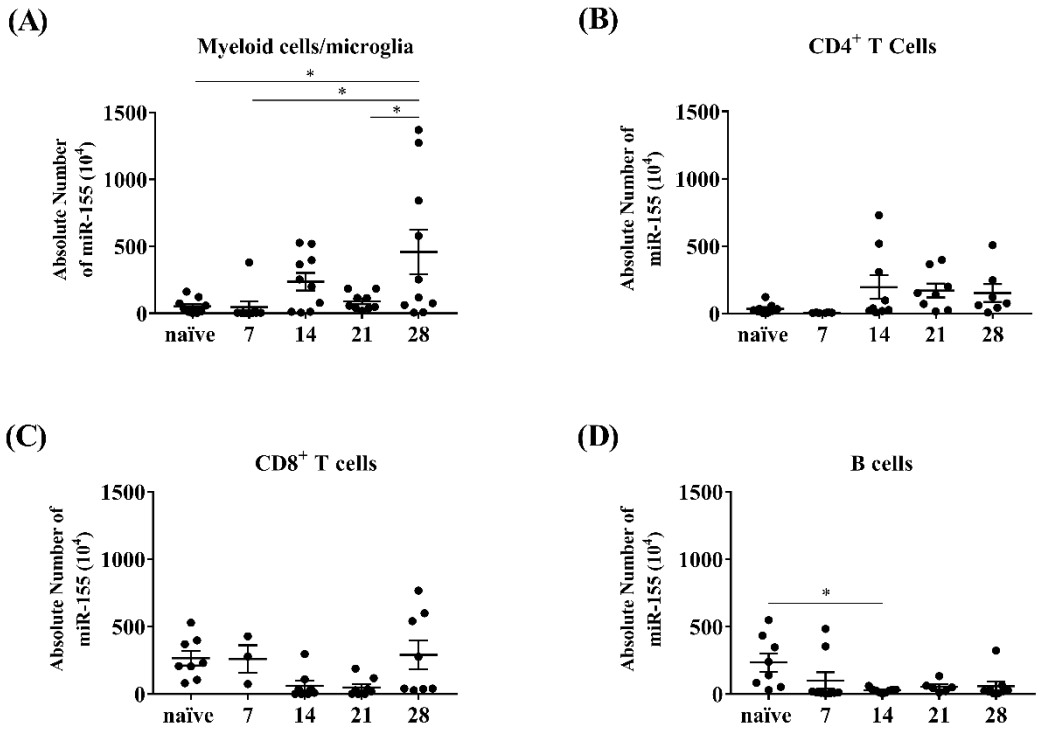

Figure 3.5 miR-155 absolute levels are highest in myeloid cells/microglia within the CNS during EAE.

CNS immune cells of naïve and EAE C57BL/6 WT mice were sorted at 7-day intervals throughout EAE into 4 immune cell populations and lysed in TRIzol for total RNA isolation. Total RNA was extracted and rtPCR and qPCR was performed using Taqman probes to determine miR-155 expression in myeloid cells/microglia (A), $CD4^+$ T cells (B), $CD8^+$ T cells (C), and B cells (D). Data represent the absolute values of miR-155 normalised against the average of three housekeeping genes sno-202, miR-191, and snU6, and expressed as mean ± S.EM. (n=3-10, 1-3 independent experiments). *P<0.05; one-way ANOVA with Bonferroni's correction.

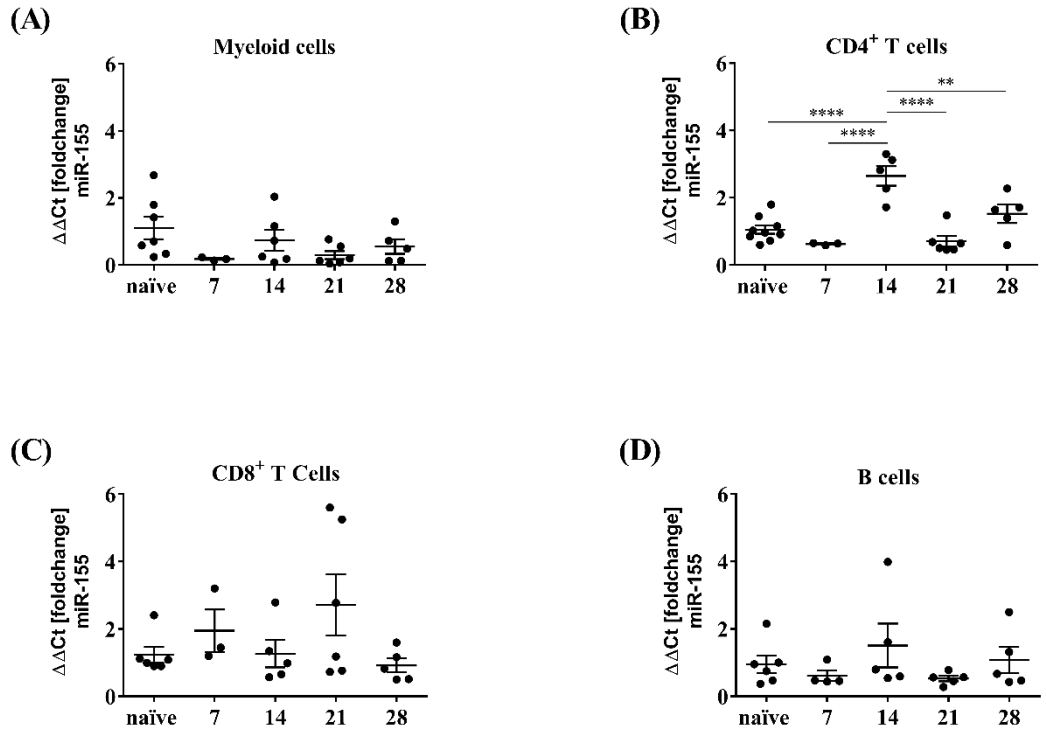

Figure 3.6 miR-155 is induced within splenic CD4$^+$ T cells in EAE.

Spleen immune cells of naïve and EAE C57BL/6 WT mice were sorted at 7-day intervals throughout EAE into 4 immune cell populations and lysed in TRIzol for total RNA isolation. Total RNA was extracted and rtPCR and qPCR was performed using Taqman probes to determine miR-155 expression in myeloid cells (A), CD4$^+$ T cells (B), CD8$^+$ T cells (C), and B cells (D). Data represents the ΔΔCT fold induction of miR-155 relative to naïve samples, normalised against the average of three housekeeping genes sno-202, miR-191, and snU6, and expressed as mean ± S.EM. (n=3-9, 1-3 independent experiments). **P<0.05, ****P<0.0001; one-way ANOVA with Bonferroni's correction.

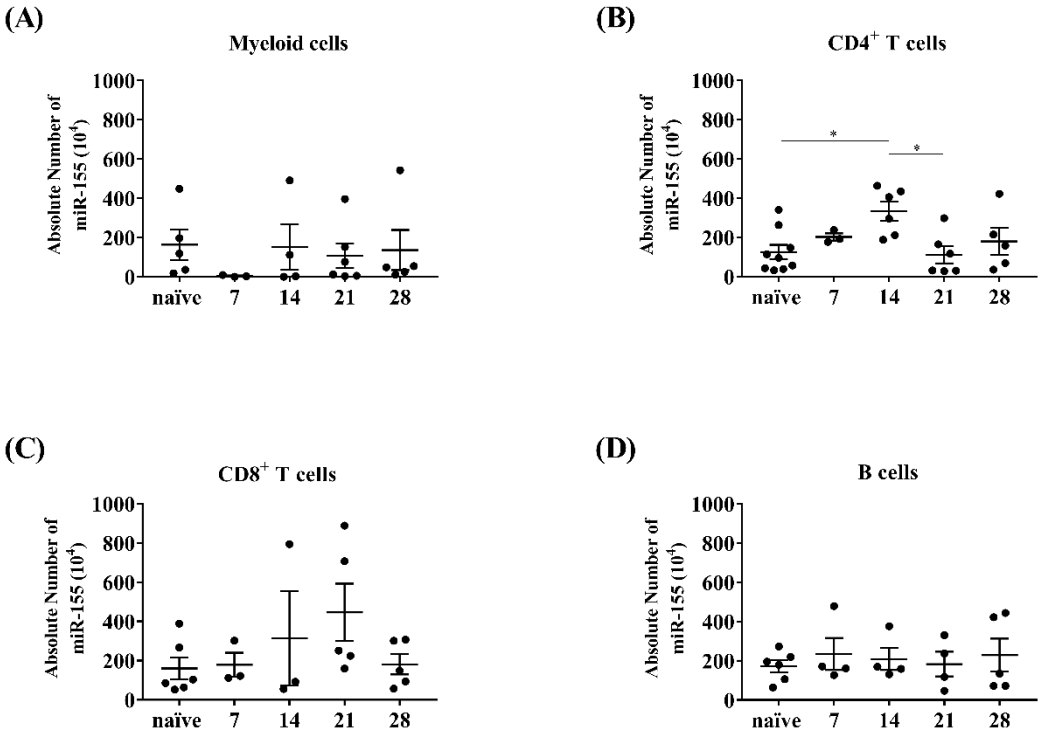

Figure 3.7 miR-155 absolute values increase in splenic CD4$^+$ T cells in EAE.

Spleen immune cells of naïve and EAE C57BL/6 WT mice were sorted at 7-day intervals throughout EAE into 4 immune cell populations and lysed in TRIzol for total RNA isolation. Total RNA was extracted and rtPCR and qPCR was performed using Taqman probes to determine miR-155 expression in myeloid cells (A), CD4$^+$ T cells (B), CD8$^+$ T cells (C), and B cells (D). Data represents the absolute values of miR-155 normalised against the average of three housekeeping genes sno-202, miR-191, and snU6, and expressed as mean ± S.EM. (n=3-9, 1-3 independent experiments). *P<0.05; one-way ANOVA with Bonferroni's correction.

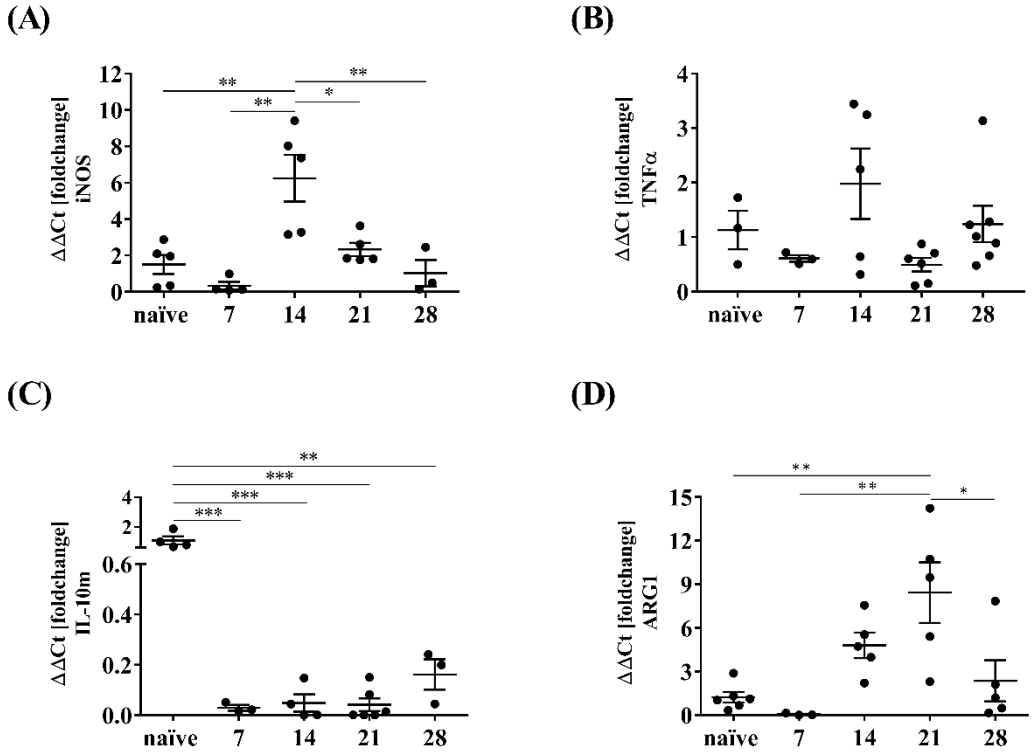

Figure 3.8 Inflammatory and anti-inflammatory gene expression in myeloid cells/microglia during EAE.

Myeloid cells/microglia of naïve and EAE C57BL/6 WT mice were sorted at 7-day intervals throughout EAE for 28 days and lysed in TRIzol for total RNA isolation. Total RNA was extracted and rtPCR and qPCR was performed to determine *inos* (A), *tnfα* (B), *il10m* (C), and *arg1* (D). Data represents the ΔΔCT fold induction of gene expression relative to naïve samples, normalised against the average of two housekeeping genes *m18s*, and *gapdh*, and expressed as mean ± S.EM. (n=3-7, 1-3 independent experiments). *P<0.05, **P<0.01, ***P<0.001; one-way ANOVA with Bonferroni's correction.

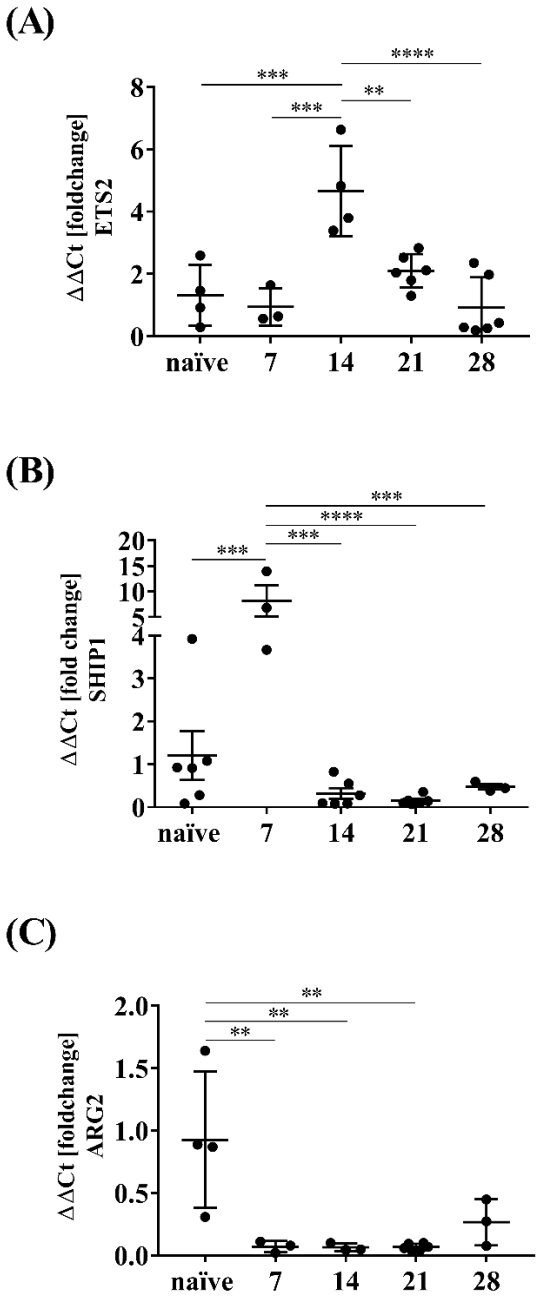

Figure 3.9 Gene expression of miR-155 targets throughout EAE.

Myeloid cells/microglia of naïve and EAE C57BL/6 WT mice were sorted at 7-day intervals throughout EAE for 28 days and lysed in TRIzol for total RNA isolation. Total RNA was extracted and rtPCR and qPCR was performed to determine *ets2* (A), *ship1* (B), and *arg2* (C). Data represents the ΔΔCT fold induction of gene expression relative to naïve samples, normalised against the average of two housekeeping genes *m18s*, and *gapdh*, and expressed as mean ± S.EM. (n=3-7, 1-3 independent experiments). **P<0.01, ***P<0.001, ****P<0.0001; one-way ANOVA with Bonferroni's correction.

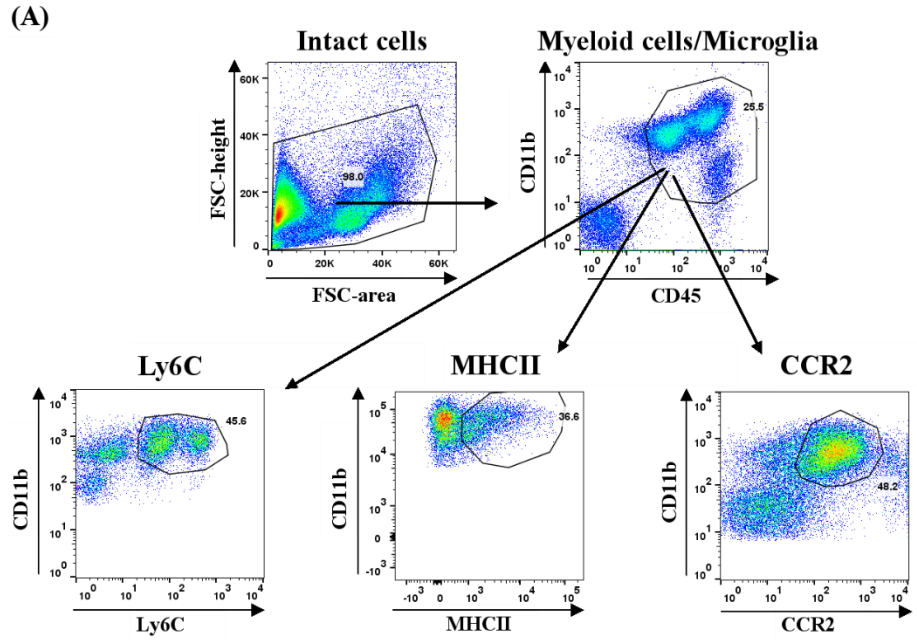
(A)
Intact cells
Myeloid cells/Microglia
FSC-height
FSC-area
98.0
CD11b
CD45
25.5
Ly6C
MHCII
CCR2
45.6
36.6
48.2
CD11b
Ly6C
MHCII
CCR2

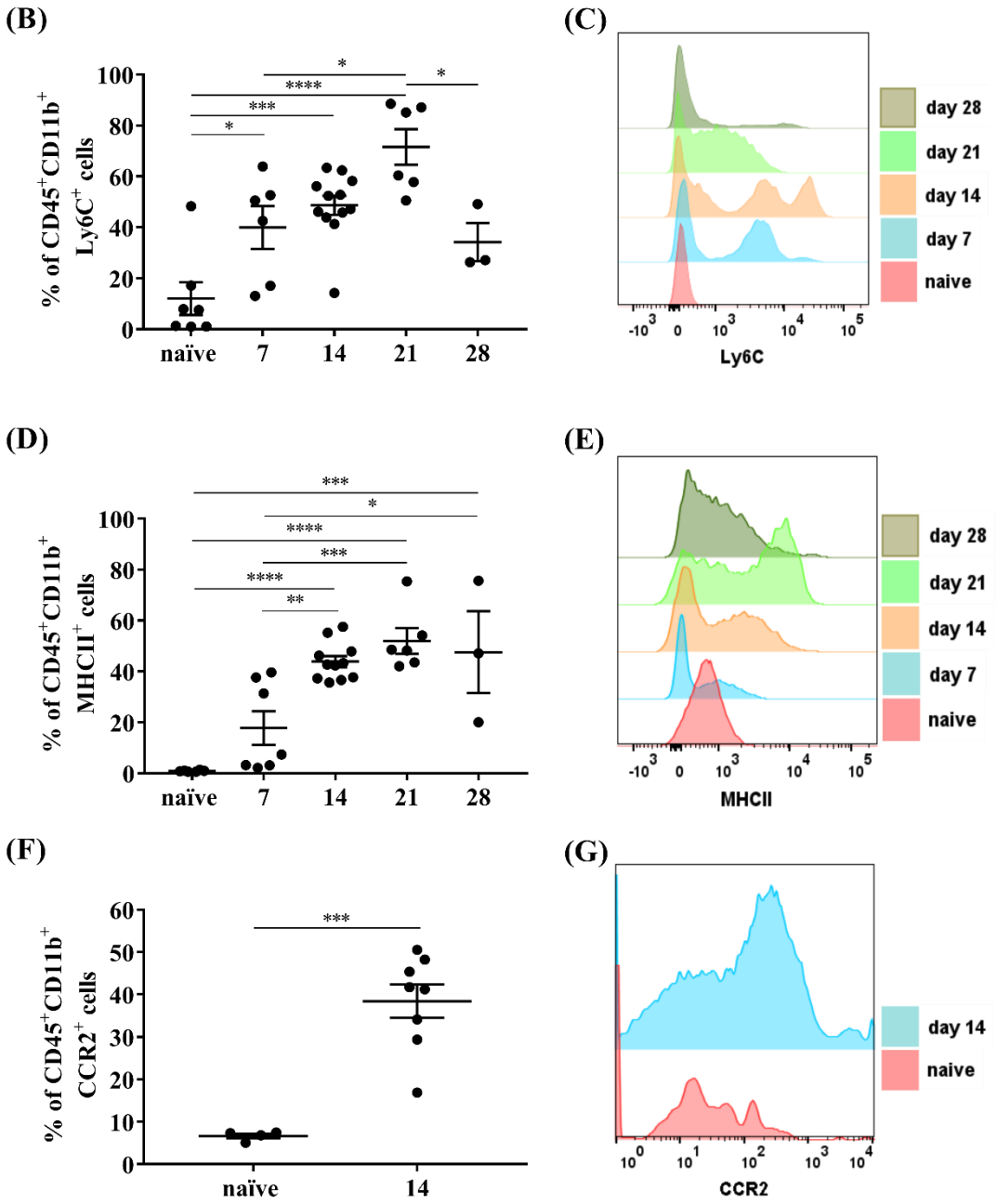

Figure 3.10 Ly6C, MHCII, and CCR2 expression on myeloid cells/microglia in EAE.

CNS samples from naïve and EAE induced C57BL/6 WT mice underwent immune cell isolation and cell sorting using flow cytometry. Cells were stained for surface CD11b, CD45, Ly6C, MHCII, and CCR2. (A) Representative gating strategy for phenotypic analysis of myeloid cells/microglia. (B-E) Quantification of the proportion of $CD45^+$ $CD11b^+$ myeloid cells/microglia expressing Ly6C (B,C), MHCII (D,E), and CCR2 (F,G). Data represents mean ± S.EM. (n=3-12, 1-3 independent experiments). *P<0.05, ** P<0.01, ***P<0.001, ****P<0.0001; one-way ANOVA with Bonferroni's correction.

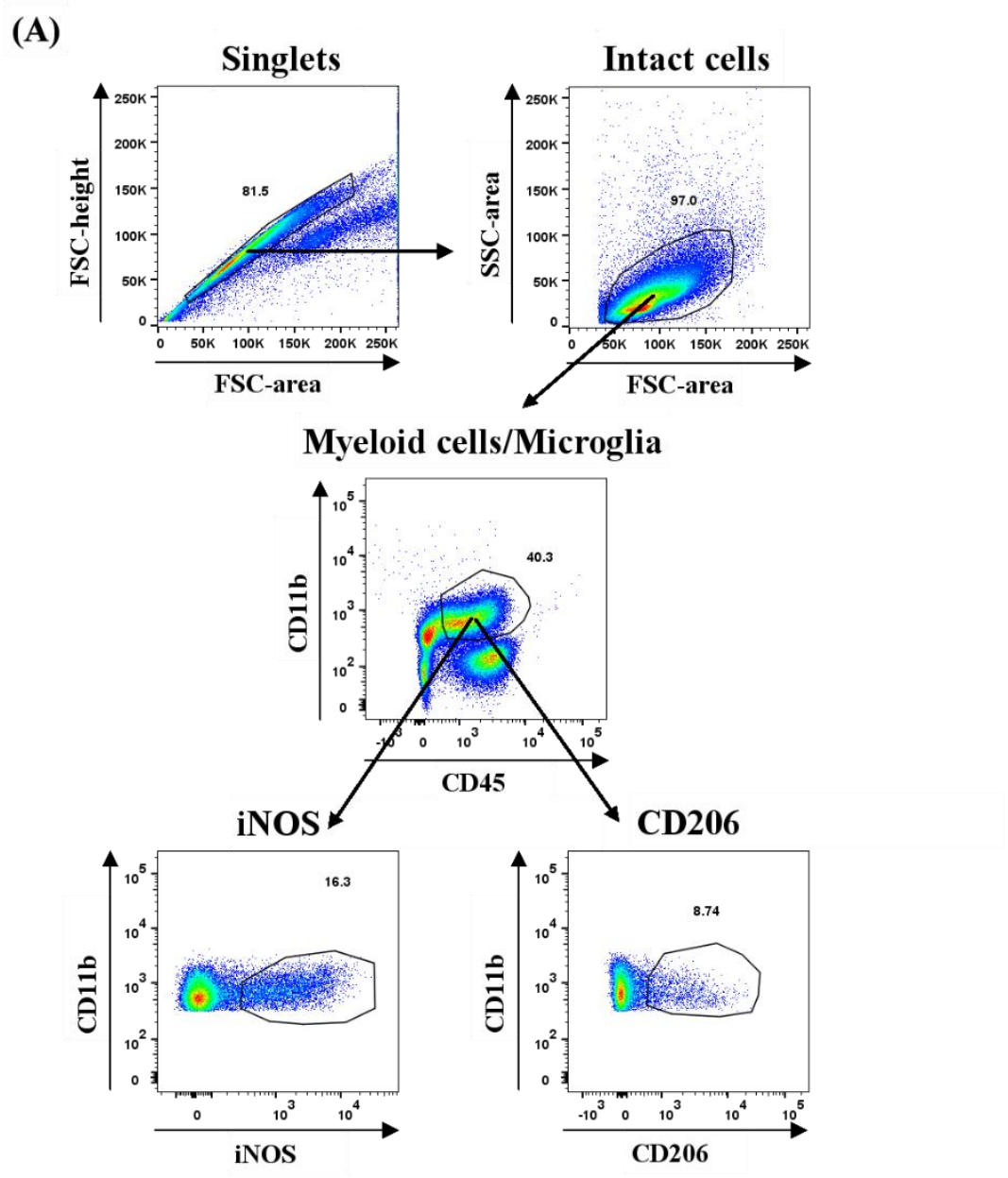
(A)
Singlets
FSC-height
FSC-area
81.5
Intact cells
SSC-area
FSC-area
97.0
Myeloid cells/Microglia
CD11b
CD45
40.3
iNOS
CD206
16.3
8.74

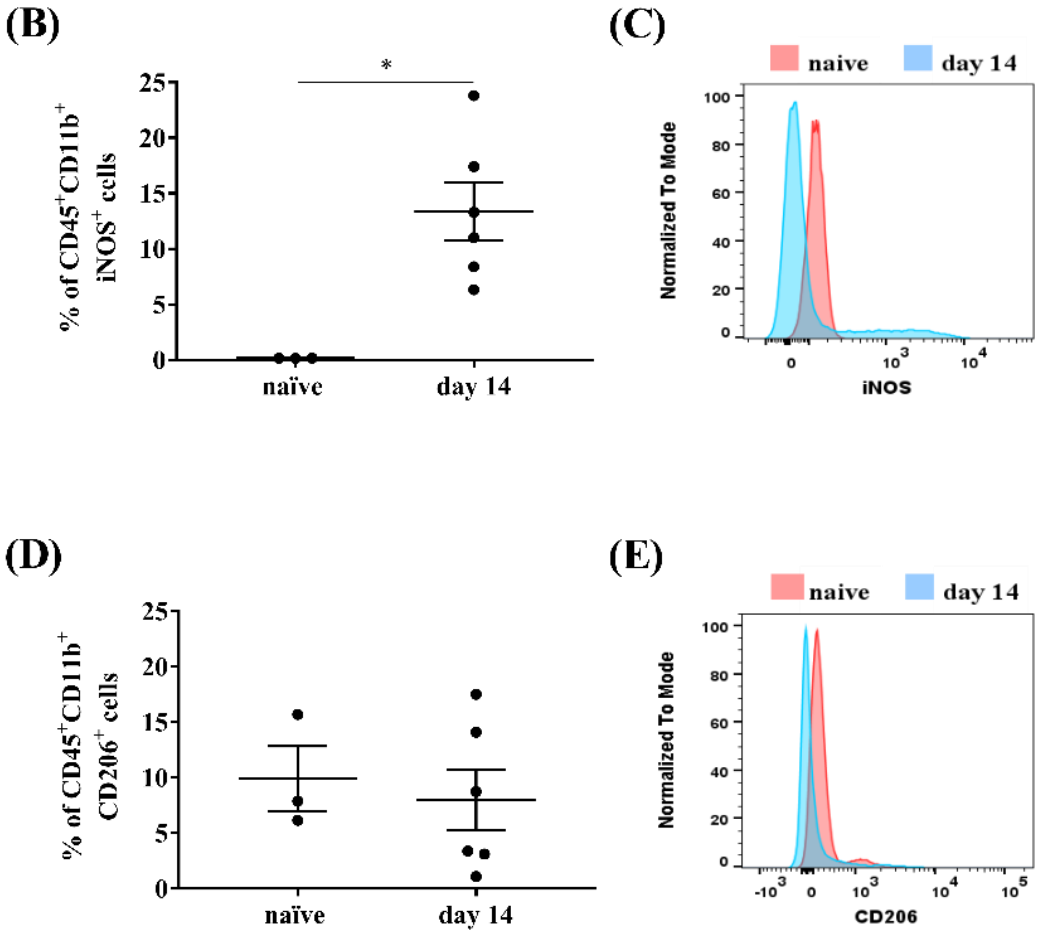

Figure 3.11 Myeloid cells/microglia expression of iNOS and CD206 in EAE.

CNS samples from naïve and EAE induced C57BL/6 WT mice underwent immune cell isolation and cell sorting using flow cytometry. Cells were stained for surface CD11b, CD45, iNOS, and CD206. (A) Representative gating strategy for phenotypic analysis of myeloid cells/microglia. (B-E) Quantification of the proportion of $CD45^+$ $CD11b^+$ myeloid cells/microglia expressing iNOS (B,C), and CD206 (D,E). Data represents mean ± S.EM. (n=3-6, 1-2 independent experiments). *P<0.05; unpaired t-test with Welch's correction.

(A)

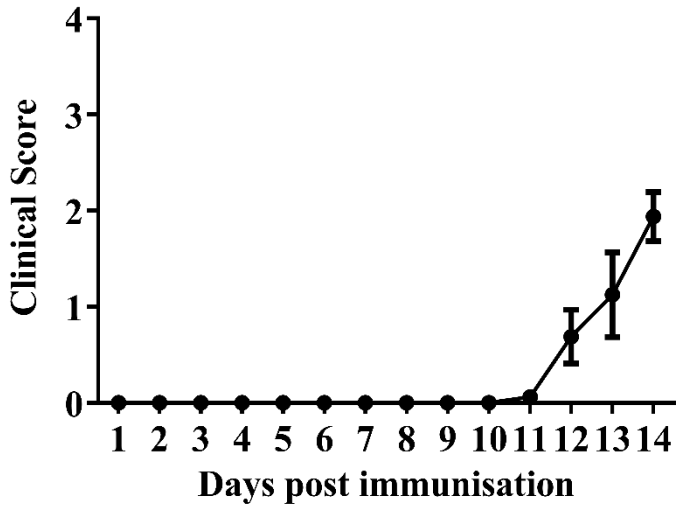

(B)

Day of disease onset	12.88 ± 0.39 (11-14)
Mean clinical score	1.94 ± 0.23 (0.5-3.5)
Cumulative score	3.81 ± 0.86 (1-5.5)

Figure 3.12 Clinical scoring of mice at day 14 EAE.

C57BL/6 WT mice were actively induced with EAE using 65 µg rMOG on day 0 and 200 ng Pertussis toxin as an adjuvant on days 0 and 2. EAE was carried out for a total of 14 days. (A) Clinical scoring was carried out daily by measuring grade of paralysis. (B) Day of disease onset, mean clinical score, and cumulative score were derived from daily clinical scores. Data represents mean ± S.EM. (n=11, 2 independent experiments).

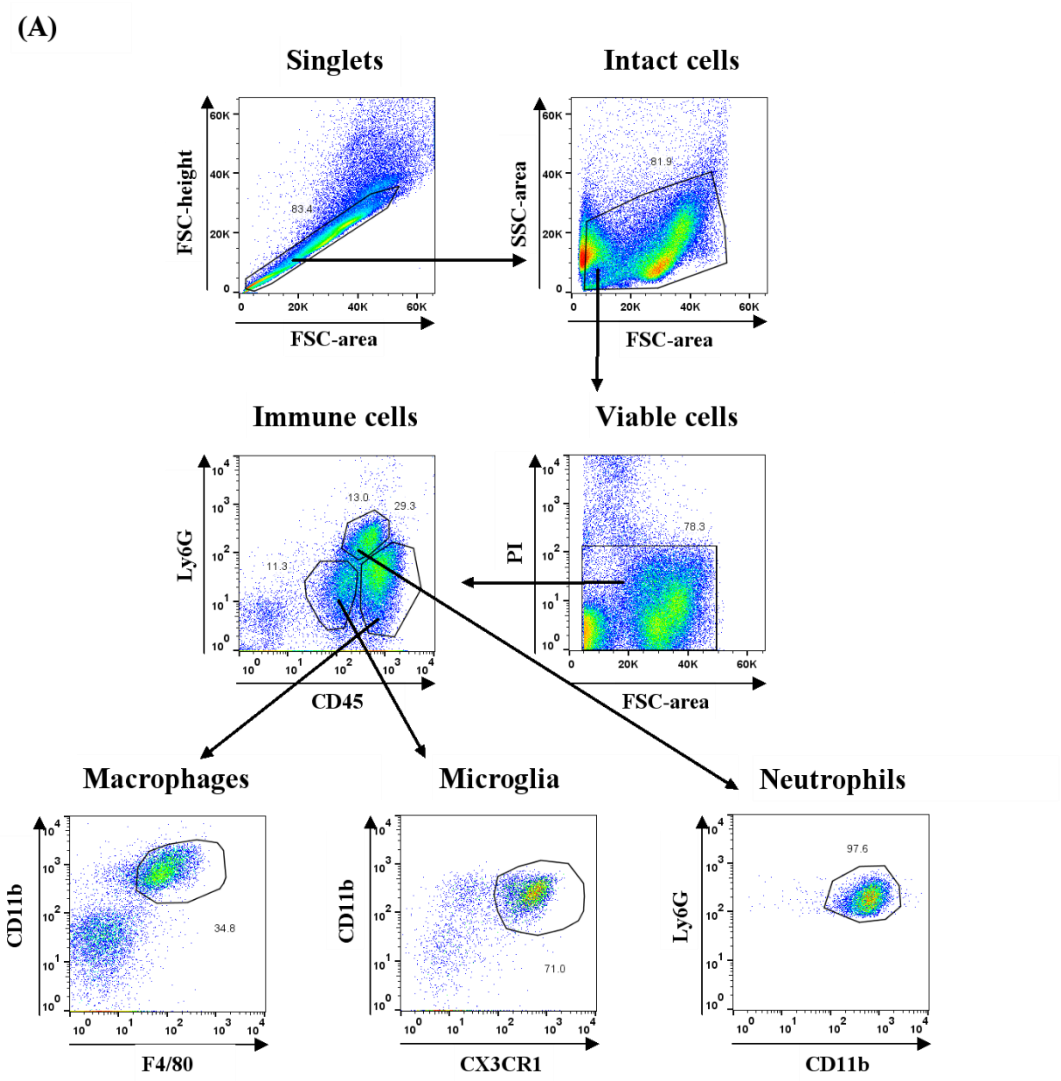
(A)
Singlets
Intact cells
FSC-height
FSC-area
SSC-area
FSC-area
83.4
81.9
Immune cells
Viable cells
Ly6G
CD45
PI
FSC-area
13.0
29.3
11.3
78.3
Macrophages
Microglia
Neutrophils
CD11b
F4/80
CD11b
CX3CR1
Ly6G
CD11b
34.8
71.0
97.6

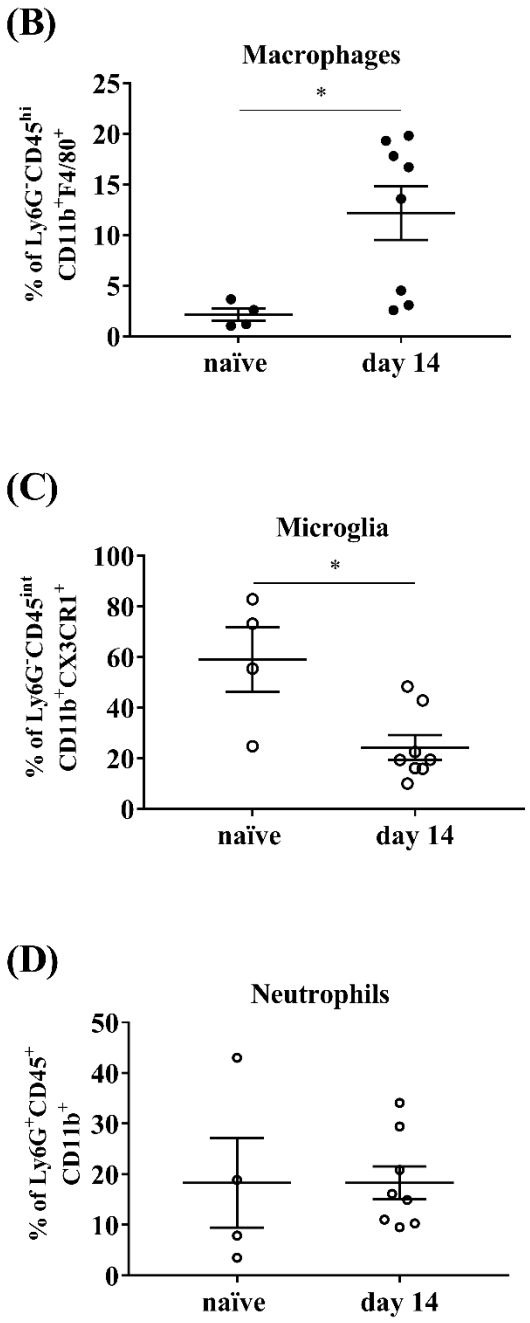

Figure 3.13 Macrophage and microglia proportions change in EAE.

CNS samples from naïve and day 14 EAE C57BL/6 WT mice underwent immune cell isolation and cell sorting using flow cytometry. Cells were stained for surface CD45, CD11b, F4/80, CX3CR1, and Ly6G. (A) Representative gating strategy for immune cell population isolation. (B-D) Population proportions of macrophages (B), microglia (C), and neutrophils (D). Data represents the percentage of immune cell s relative to $CD45^+$ cells and expressed as mean ± S.EM. (n=4-8, 2 independent experiments). * $P<0.05$; one-way ANOVA with Bonferroni's correction.

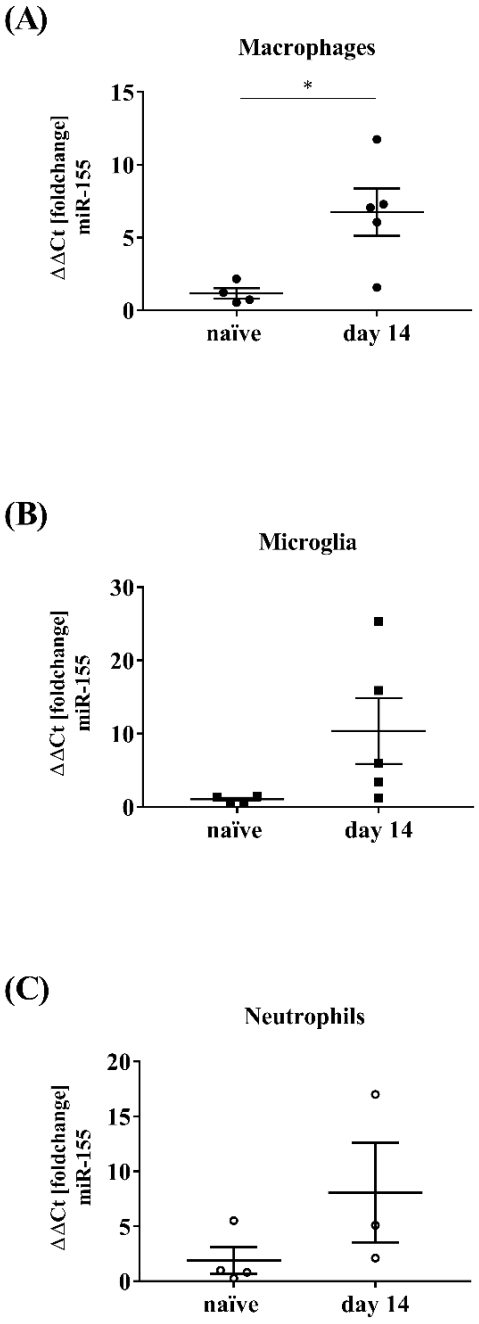

Figure 3.14 miR-155 is significantly induced in macrophages in EAE.

CNS samples from naïve and day 14 EAE C57BL/6 WT mice underwent immune cell isolation, cell sorting using flow cytometry into 3 immune cell populations, and lysis in TRIzol for total RNA isolation. Total RNA was extracted and rtPCR and qPCR was performed using Taqman probes to determine miR-155 expression in macrophages (A), microglia (B), and neutrophils (C). Data represent the ΔΔCT fold induction of miR-155 relative to naïve samples, normalised against the average of three housekeeping genes sno-202, miR-191, and snU6, and expressed as mean ± S.EM. (n=3-5, 2 independent experiments). *P<0.05; one-way ANOVA with Bonferroni's correction.

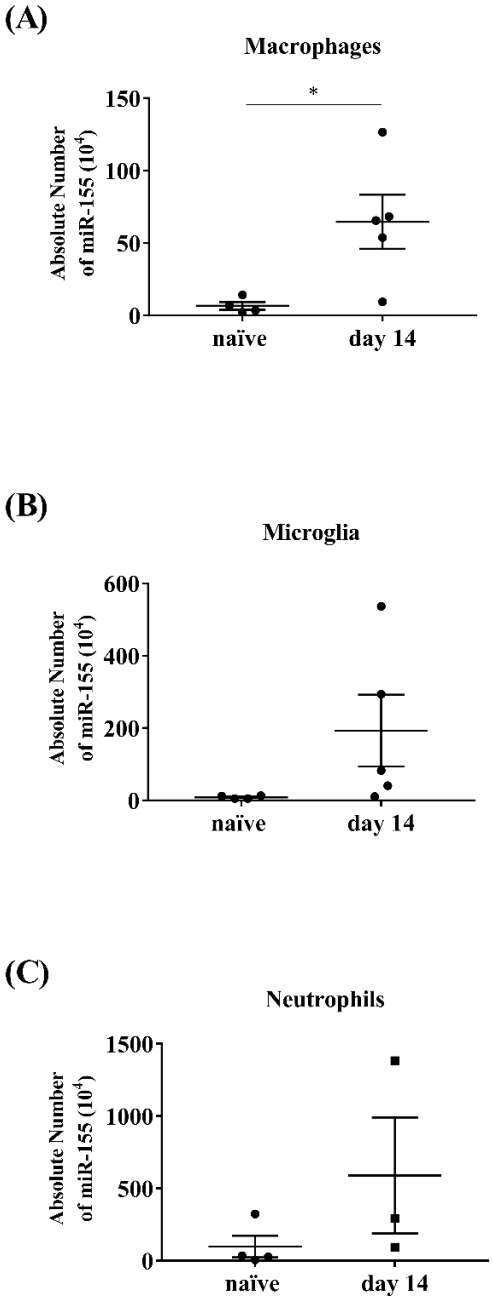

Figure 3.15 miR-155 absolute levels significantly increased in macrophages in EAE.

CNS samples from naïve and day 14 EAE C57BL/6 WT mice underwent immune cell isolation, cell sorting using flow cytometry into 3 immune cell populations, and lysis in TRIzol for total RNA isolation. Total RNA was extracted and rtPCR and qPCR was performed using Taqman probes to determine miR-155 expression in macrophages (A), microglia (B), and neutrophils (C). Data represent the absolute values of miR-155 normalised against the average of three housekeeping genes sno-202, miR-191, and snU6, and expressed as mean ± S.EM. (n=3-5, 2 independent experiments). *P<0.05; one-way ANOVA with Bonferroni's correction.

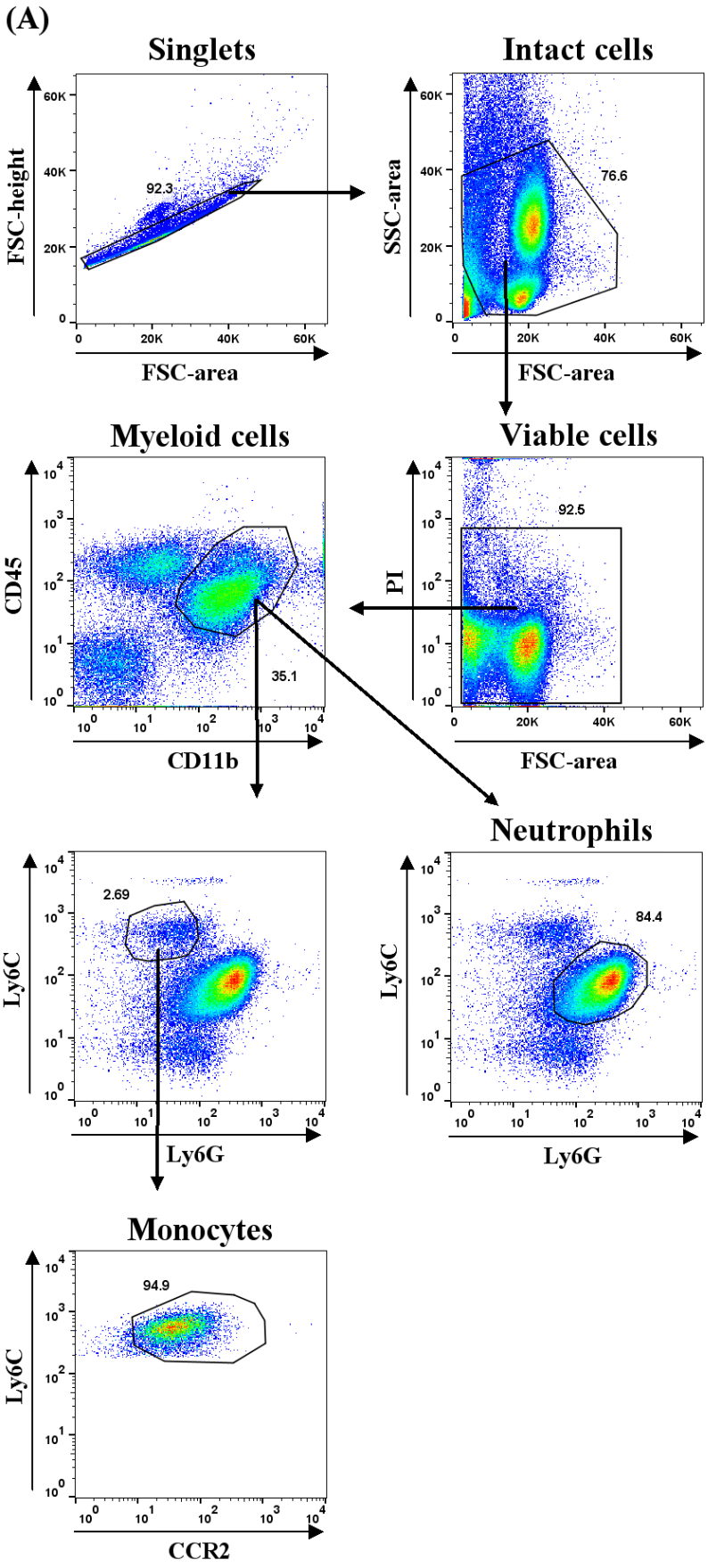
(A)
Singlets
FSC-height
FSC-area
92.3
Intact cells
SSC-area
FSC-area
76.6
Myeloid cells
CD45
CD11b
35.1
Viable cells
PI
FSC-area
92.5
Neutrophils
Ly6C
Ly6G
2.69
Ly6C
Ly6G
84.4
Monocytes
Ly6C
CCR2
94.9

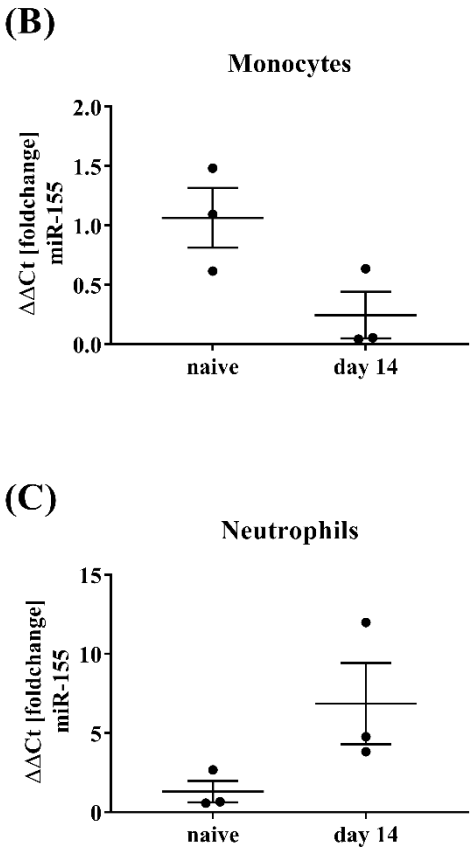

Figure 3.16 miR-155 is not induced in blood monocytes at day 14 EAE.

Blood samples from naïve and day 14 EAE C57BL/6 WT mice underwent immune cell isolation and cell sorting using flow cytometry into 2 immune cell populations. Cells were stained for surface CD45, CD11b, Ly6C, Ly6G, and CCR2. (A) Representative gating strategy for immune cell populations. Sorted cells were then lysed in TRIzol for total RNA isolation. Total RNA was extracted and rtPCR and qPCR was performed using Taqman probes to determine miR-155 expression in monocytes (B) and neutrophils (C). Data represent the absolute values of miR-155 normalised against the average of three housekeeping genes sno-202, miR-191, and snU6, and expressed as mean ± S.EM. (n=3, 1 independent experiment).

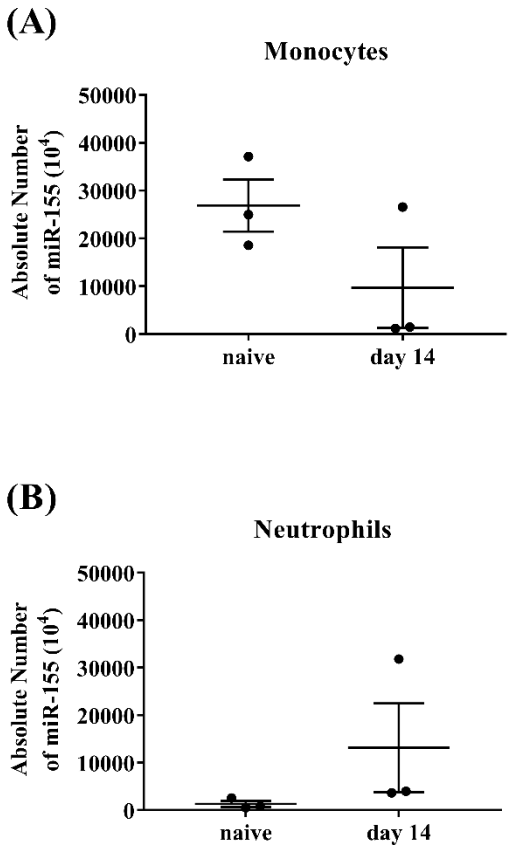

Figure 3.17 miR-155 absolute levels decreased in blood monocytes at day 14 EAE.

Blood samples from naïve and day 14 EAE C57BL/6 WT mice underwent immune cell isolation, cell sorting using flow cytometry into 2 immune cell populations, and lysis in TRIzol for total RNA isolation. Total RNA was extracted and rtPCR and qPCR was performed using Taqman probes to determine miR-155 expression in monocytes (A) and neutrophils (B). Data represent the absolute values of miR-155 normalised against the average of three housekeeping genes sno-202, miR-191, and snU6, and expressed as mean ± S.EM. (n=3, 1 independent experiment).

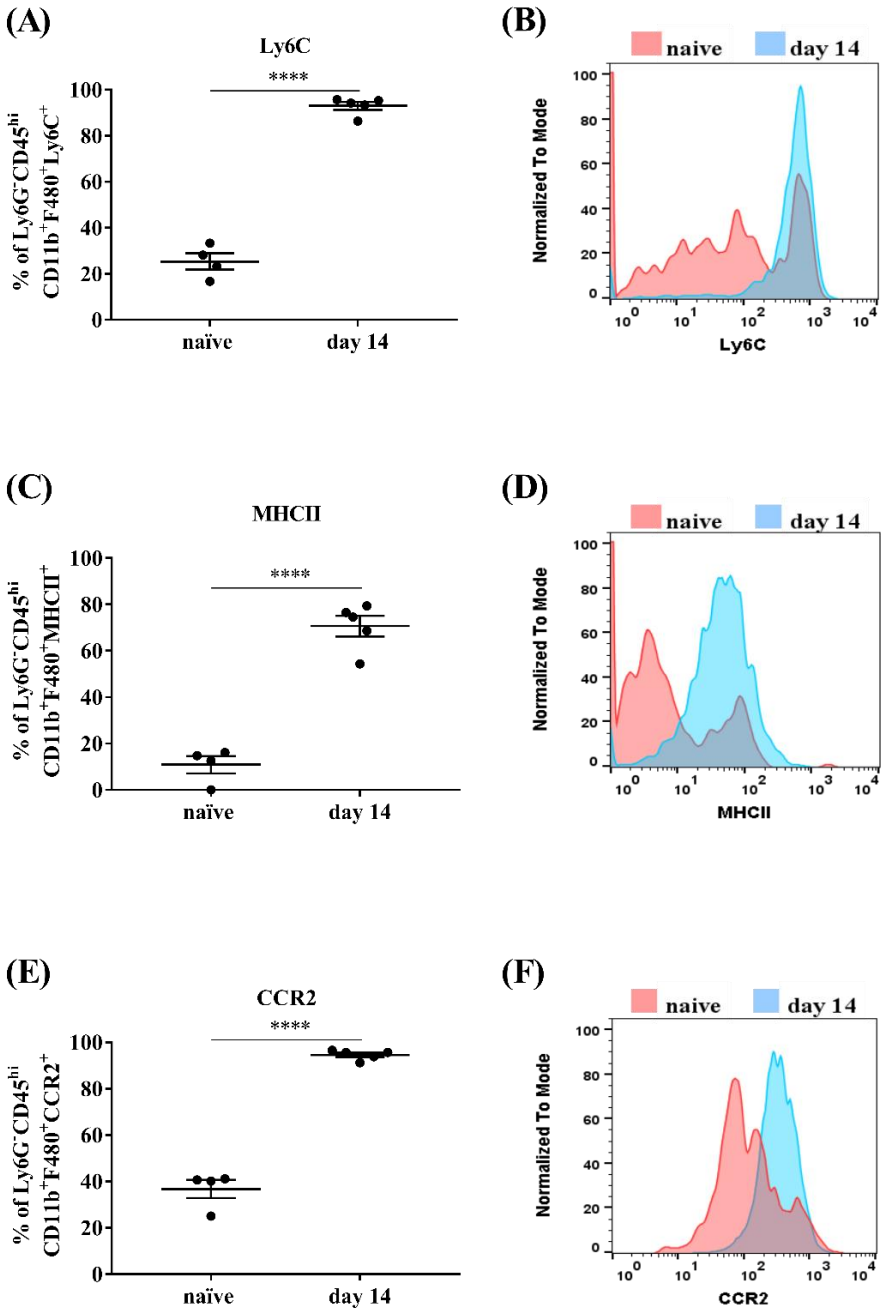

Figure 3.18 Ly6C, MHCII, and CCR2 expression is increased on macrophages within the CNS in EAE.

CNS samples from naïve and day 14 EAE C57BL/6 WT mice underwent immune cell isolation and cell sorting using flow cytometry. Cells were stained for surface $CD45^{hi}$, $CD11b^{+}$, $F4/80^{+}$, and $Ly6G^{-}$ to delineate macrophages for phenotypic analysis. (A-F) Quantification of the proportion of macrophages expressing Ly6C (A,B), MHCII (C,D), and CCR2 (E,F). Data expressed as mean ± S.EM. (n=4-5, 2 independent experiments). ****P<0.0001; unpaired t-test with Welch's correction.

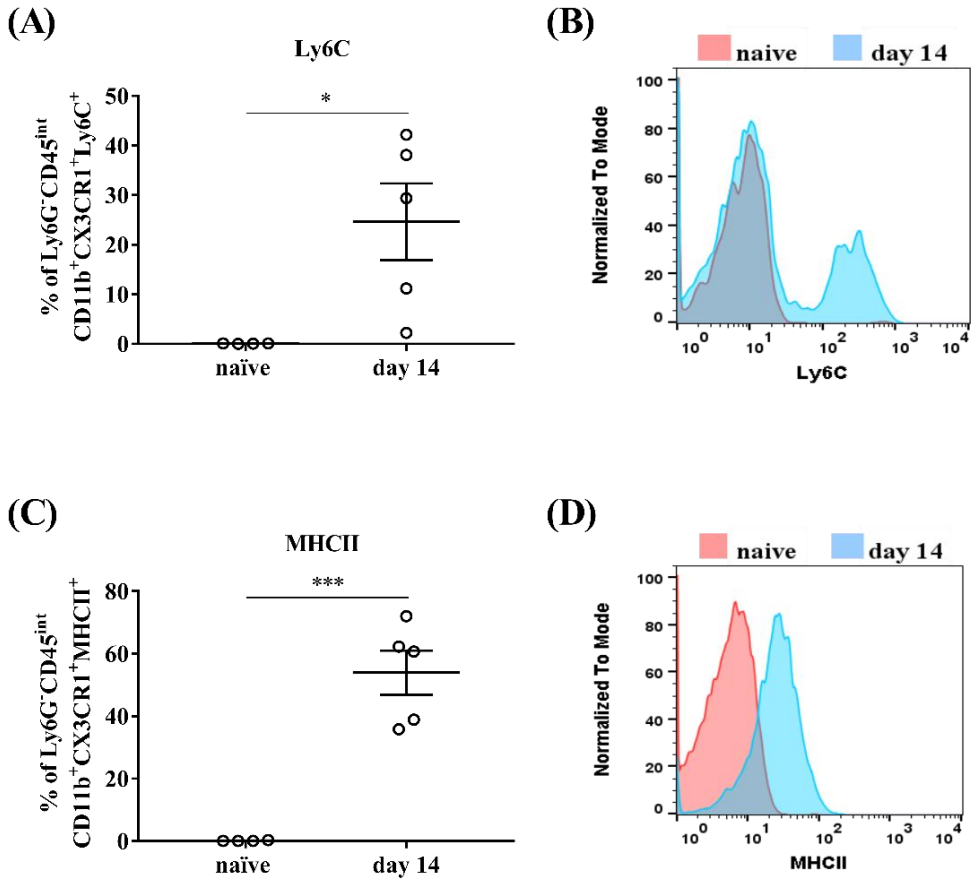

Figure 3.19 Ly6C and MHCII expression is increased on microglia in EAE.

CNS samples from naïve and day 14 EAE C57BL/6 WT mice underwent immune cell isolation and cell sorting using flow cytometry. Cells were stained for surface $CD45^{int}$, $CD11b^{+}$, $CX3CR1^{+}$, and $Ly6G^{-}$ to delineate microglia for phenotypic analysis. (A-F) Quantification of the proportion of microglia expressing Ly6C (A,B), MHCII (C, D). Data expressed as mean ± S.EM. (n=4-5, 2 independent experiments). *P<0.05, ***P<0.001, ****P<0.0001; unpaired t-test with Welch's correction.

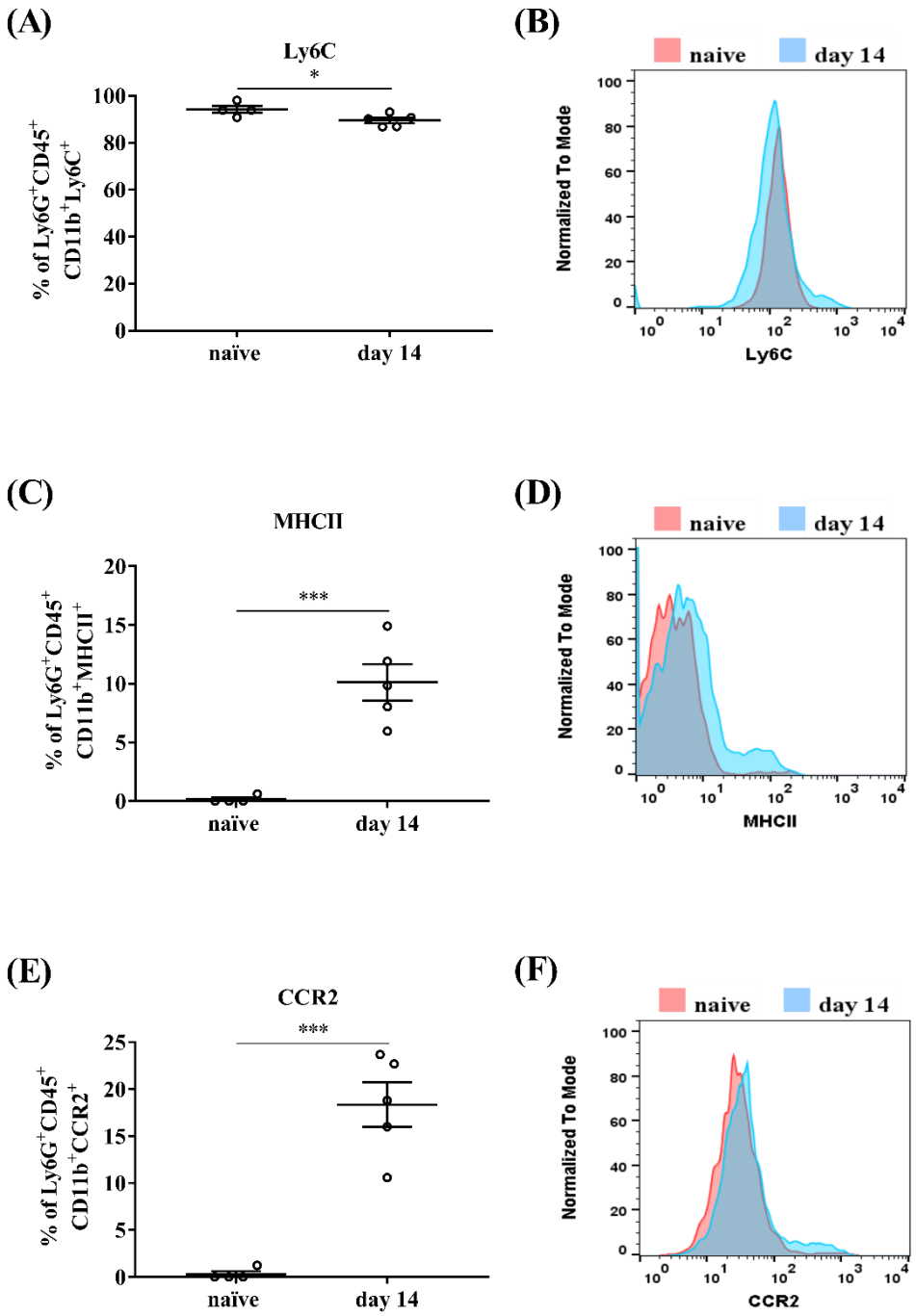

Figure 3.20 MHCII and CCR2 expression is increased on neutrophils within the CNS in EAE.

CNS samples from naïve and day 14 EAE C57BL/6 WT mice underwent immune cell isolation and cell sorting using flow cytometry. Cells were stained for surface $CD45^+$, $CD11b^+$, and $Ly6G^+$ to delineate neutrophils for phenotypic analysis. (A-F) Quantification of the proportion of neutrophils expressing Ly6C (A,B), MHCII (C,D), and CCR2 (E,F). Data expressed as mean ± S.EM. (n=4-5, 2 independent experiments). *P<0.05, ***P<0.001; unpaired t-test with Welch's correction.

3.3 Discussion

MiR-155 is a pivotal inflammatory regulator of the immune system (Vigorito *et al.*, 2013). Due to its prominent involvement in all immune cells, it is not unexpected that elevated miR-155 is associated with numerous diseases, such as MS (O'Connell, Kahn, William S J Gibson, *et al.*, 2010; G. Murugaiyan *et al.*, 2011; Gopal Murugaiyan, Beynon, Mittal, Joller and Howard L. Weiner, 2011; Jevtić *et al.*, 2015). The importance of this proinflammatory miRNA is exemplified in EAE studies using miR-155 knockout mice. These studies highlight the crucial role of miR-155 by unequivocally demonstrating amelioration of clinical disease or disease resistance in miR-155 deficient mice (O'Connell, Kahn, William S J Gibson, *et al.*, 2010; G. Murugaiyan *et al.*, 2011; Seddiki *et al.*, 2014).

Analysis of the regulatory effects of miR-155 in lymphocytes during EAE has yielded invaluable information on mechanisms of disease immunopathogenesis (O'Connell, Kahn, William S J Gibson, *et al.*, 2010; G. Murugaiyan *et al.*, 2011). However, there has recently been a shift in EAE/MS research by directing focus from T cells towards the innate immune system, particularly macrophages. Growing evidence of the importance of macrophage polarisation states has since emphasised that these cells may be potentiated for immunotherapy and tissue regeneration (Moore, Vijayaraghava T S Rao, *et al.*, 2013; Locatelli, Theodorou, Kendirli, Joana, *et al.*, 2018). Although miR-155 is known to be a key driver of inflammatory macrophage polarisation (Kyle A Jablonski *et al.*, 2016), information regarding the role of miR-155 in macrophages during EAE is lacking. Additionally, a complete comparative analysis of miR-155 in myeloid and lymphoid immune cell subsets throughout an EAE time course remains unexplored. Understanding the role of miR-155 in relevant multiple cell subsets during EAE could reveal critical information as to how miR-155 elicits fine-tuning of inflammatory responses at the molecular and cellular level. These mechanisms could be targeted to not only prevent induction of an inflammatory phenotype, but also to promote CNS repair through inducing a switch from an inflammatory to a regenerative activation state.

This Chapter explored immune cell subsets from both myeloid and lymphoid lineages throughout a progressive EAE time course. Comparative analysis of miR-155 expression between myeloid cells/microglia, $CD4^+$/$CD8^+$ T cells, and B cells within the CNS and

spleen identified key players influenced by miR-155. Collectively, this Chapter confirmed key immune cell populations within CNS throughout timepoints of EAE, and more importantly, which of these immune cells had the highest induction of miR-155. Additionally, $CD11b^{+}F4/80^{+}$ cell gene profiles were analysed for proinflammatory and anti-inflammatory markers along with miR-155 target gene expression to map polarisation phenotypes with miR-155 induction and population proportions during EAE.

This Chapter determined that almost half of immune cell proportions within the CNS during EAE are $CD11b^{+}F4/80^{+}$ cells. $CD11b^{+}F4/80^{+}$ does not identify a specific immune cell subpopulation, but rather captures a heterogeneous population recognised to predominantly comprise of mononuclear phagocytes. Within the CNS, this includes infiltrating macrophages derived from infiltrating $Ly6C^{hi}$ inflammatory monocytes, and tissue resident populations derived from the yolk sac such as microglia and non-parenchymal macrophages (Arcuri *et al.*, 2019; Hume, Irvine and Pridans, 2019). This data corroborates previous studies surrounding EAE, which highlights macrophages as one of the most prolific immune cell populations within the CNS during disease progression. Further, macrophage infiltration has reported to correlate with disease progression (Bruck *et al.*, 1995; Bahareh Ajami, Jame L Bennett, Charles Krieger, Kelly M McNagny, 2011). Abundant peripheral myeloid cell infiltration seen in EAE is consistent with MS, where the most predominant infiltrating peripheral immune cell in MS lesions, highlighting the relevance of macrophages in disease immunopathogenesis. Moreover, macrophages are confirmed to express both acute and chronic inflammatory markers: MRP14, 27E10, and 25F9 in active MS lesions, and notably sustained chronic inflammatory marker 25F9 expression within inactive lesions (Bruck *et al.*, 1996; Bitsch *et al.*, 2000; Lucchinetti *et al.*, 2000).

The first miR-155 knockout study using EAE induced C57Bl/6 mice was performed in 2010 by O'Connell's research group (O'Connell, Kahn, William S J Gibson, *et al.*, 2010). This study proved miR-155 was pivotal for EAE development through $miR\text{-}155^{-/-}$ mice exhibiting mechanisms of impaired inflammatory T cell function and a reduced ability of dendritic cells to present antigens to $CD4^{+}$ T cells. This Chapter is consistent with O' Connell's findings as significant induction of miR-155 was determined in $CD4^{+}$ T cells within both the spleen and CNS during EAE. Moreover, these findings further correlates

with Murugaiyan's study by demonstrating increased relative miR-155 expression in the CNS, spleen, and another periphery lymphoid tissue, lymph nodes (G. Murugaiyan *et al.*, 2011). Overall, these findings align with literature describing the initial activation of $CD4^+$ T cells occurring in the periphery, prior to recruitment to the CNS and reactivation, suggesting the inflammatory role of miR-155 in this immune cell subset initiates in the periphery. Additionally, this Chapter reported no significant changes in miR-155 expression in $CD8^+$ T cells and B cells within the spleen, but there was a reduction in fold change of miR-155 in $CD8^+$ T cells along with decreased miR-155 expression levels in B cells within the CNS at clinical stages of disease. Although $CD8^+$ T cells and B cells have a recognised role in the pathogenesis of EAE, they additionally provide regulatory roles that facilitate disease amelioration (Monica K. Mann *et al.*, 2012; Arbour *et al.*, 2015). These dual abilities of $CD8^+$ T cell and B cells prove these cells are not persistently inflammatory during EAE progression, and perhaps miR-155 does not play a proinflammatory role in these lymphocyte populations during certain EAE timepoints.

Although significant induction of miR-155 expression in $CD4^+$ T cells was determined, this Chapter excitingly demonstrated the highest induction of miR-155 occurred in myeloid cells/microglia within the CNS. This finding suggested a prominent regulatory role for miR-155 in this immune cell population during the clinical onset of EAE. Furthermore, miR-155 induction was not evident within tissue resident macrophages in the spleen. Moreover, data from this Chapter indicate the regulatory role of miR-155 in macrophages occurs within the CNS, as it was not upregulated in circulating monocytes. This is unique compared to other immune cells, such as neutrophils and $CD4^+$ T cells, which have upregulated miR-155 expression in both the periphery and CNS. In contrast, Mycko et al. documented findings surrounding the failure of miR155-5p induction in myeloid cells during EAE (Mycko *et al.*, 2015). Findings generated from this Chapter contrasts with this study, which could be due to several differences in experimental designs. In this Chapter, EAE induction was performed using rMOG which closer recapitulates human disease in addition to involving B cell pathogenesis within the CNS, as opposed to MOG_{35-55} (Häusler *et al.*, 2018). Furthermore, Mycko categorises all $CD11b^+$ cells as macrophages, however several other immune cells have abilities to express this marker, also known as integrin alpha M, such as monocytes, neutrophils, granulocytes, natural killer cells and microglia (Springer, 1990). This Chapter used an

array of macrophage markers to specifically categorise infiltrating macrophages within the CNS ($CD45^{hi}Ly6G^{-}CD11b^{+}F4/80^{+}$) to exclude other immune cell infiltrates and CNS resident cells. Additionally, Mycko investigated miR-155 within brains of EAE mice and did not include analysis of the spinal cord regions. In EAE mouse models immunised with $MOG_{35-55,}$ the majority of lesions are localised within spinal cords as opposed to brain regions (Lassmann and Bradl, 2017), therefore perhaps findings focussing on brain samples solely do not collectively represent miR-155's global role in EAE. Mycko also utilised SmartFlares to investigate miRNA expression levels within immune cell populations instead of qPCR. SmartFlares have been reported as an unreliable tool since there is documented failure of correlation between probe fluorescent intensity using flow cytometry and RNA transcripts analysed using qPCR (Czarnek and Bereta, 2017). Additional gene expression data from this Chapter supports a role for miR-155 in macrophages during EAE. An increase in transcription factor *Ets2* mimicking miR-155 induction provided additional evidence miR-155 was driving proinflammatory macrophage polarisation. Furthermore, immunoregulatory miR-155 target *Ship1* was supressed entirely throughout EAE upon clinical onset of disease, indicating anti-inflammatory abilities of macrophages mediated by *Ship1* were prevented by miR-155. Additionally, miR-155 target *Arg2* was downregulated throughout EAE until day 21, once more indicative of a proinflammatory macrophage undergoing a polarisation phenomenon towards an anti-inflammatory state at later stages of EAE progression.

Initial analysis of $CD11b^{+}F4/80^{+}$ cells throughout EAE provided a global overview of miR-155 expression in phagocytic cells, revealing induction occurs specifically within the CNS. Using a more defined sorting strategy, it was identified that miR-155 induction is significantly highest in $CD45^{hi}CD11b^{+}F4/80^{+}$ macrophages compared to neutrophils and CNS resident microglia. In accordance with infiltrating macrophages inducing high levels of miR-155, Moore et al. confirmed increased miR-155 expression in $CD68^{+}$ cells within brain lesions of MS patients compared to healthy controls (Moore, Vijayaraghava T.S. Rao, *et al.*, 2013a). Collectively, this implicates miR-155 as playing a proinflammatory role in myeloid derived macrophages at lesion sites. Interestingly, this research group identified a change in miR-155 expression the parenchyma and perivascular regions within the brain of healthy controls (Moore, Vijayaraghava T S Rao,

et al., 2013). These findings highlight the importance of locating and tracking miR-155 expression within the CNS environment. Visibly tracking the exact timing and localisation of miR-155 expression in infiltrating macrophages by in situ hybridisation could address important questions relating to how miR-155 finetunes infiltrating myeloid cells, and at which stages of EAE. Questions surrounding the correlation of miR-155 and macrophage polarisation properties during distinctly separate phases of EAE (progressive, remitting, and relapsing) could be addressed and help target crucial moments when miR-155 is most influential in EAE.

This Chapter demonstrated macrophage induction of miR-155 appeared after gaining entry into the CNS but was not induced in splenic macrophages. To address the hypothesis that miR-155 is only induced upon entering the CNS, analysis of bloodborne monocytes and neutrophils was performed. Surprisingly, circulating monocytes could not induce miR-155 expression in EAE, unlike neutrophils. This data concurs with Locatelli et al. by suggesting the CNS microenvironment promotes polarisation properties of macrophages (Locatelli, Theodorou, Kendirli, Jordão, *et al.*, 2018). This finding additionally aligns with studies surrounding characteristic alterations to macrophages upon exposure to molecules within the CNS. For instance, GM-CSF is expressed by many CNS specific cell subsets, such as microglia and oligodendrocytes in humans and astrocytes in mice (Aram *et al.*, 2019) but also by pathogenic Th17 cells that infiltrate the CNS during EAE (Komuczki *et al.*, 2019). EAE resistance observed in genetically deficient GM-CSF mice proves it is an essential factor for disease development (McQualter *et al.*, 2001). As miR-155 is not induced in bloodborne inflammatory monocytes, even though inflammatory cytokines such as IFN-γ and TNF-α are upregulated (Yee *et al.*, 2017), it suggests that either opposing signals are present, miR-155 is involved in a negative feedback loop prior to CNS entry, or a maturation step is required to induce miR-155 after entry into the CNS. A rat model of MS confirmed the presence of both anti-inflammatory and proinflammatory cytokines within the bloodstream at 8 days post immunisation of MOG peptide (Borjini *et al.*, 2016). IL-10, a known suppressor of miR-155 induction, was amongst those investigated. As such, collective exposure of monocytes to contrasting signals within the bloodstream may exert a significant influence on miR-155 induction. Moreover, the hypothesis that miR-155 is only induced post CNS entry and differentiation into macrophages is consistent with recent evidence on the interaction between monocyte-derived cells with endothelial cells

upon CNS entry, and with CD4 T cells in the parenchyma, which is largely mediated by inflammatory cytokines GM-CSF and IL-1β (Paré *et al.*, 2018). Further studies exposing monocytes with different stimuli *in vitro,* or utilising tissue engineered BBB models could be insightful to examine miR-155 induction (Komuczki *et al.*, 2019).

Emerging studies surrounding EAE supports a pathogenic role of neutrophils by confirming their involvement in CNS infiltration into the parenchyma, production of proinflammatory cytokines such as TNF-α and IL-1β, and strong associations of their presence with BBB breakdown (Pierson, Wagner and Goverman, 2018). Moreover, their pathogenic role is evident in the context of MS, where levels of neutrophil elastase significantly correlates with MS lesion volumes (Julie M. Rumble *et al.*, 2015). Although neutrophils are recognised to assist in CNS autoimmunity in both EAE mouse models and MS, the role of miR-155 in these cells during these disease contexts are less understood. This Chapter identified induction of miR-155 in circulating neutrophils at day 14 EAE, suggesting a role for miR-155 in neutrophils at the mean day of disease onset. A separate study identified a role for miR-155 in neutrophil migratory regulation in Myelodysplastic Syndromes (MDS). Cao et al. demonstrated by introducing miR-155 ectopically resulted in decreased neutrophil trafficking along a chemotactic gradient (Cao *et al.*, 2017). Perhaps further studies surrounding miR-155's role in neutrophil migration during EAE would be insightful to understand how miR-155 may impact neutrophil infiltration into the parenchyma.

Results from this Chapter confirmed that macrophage induction of miR-155 within the CNS during EAE correlated with increased Ly6C, MHCII, and CCR2 expression. These proinflammatory and antigen presenting molecules aligns with studies demonstrating the existence of proinflammatory macrophages within the CNS during disease progression. Ly6C expression is known to correlate with proinflammatory activity in mouse monocytes/macrophages. Monocytes/macrophages can be further divided into low, intermediate, or high expressing cells, the latter recognised to additionally be associated with phagocytic abilities (Jiyeon Yang, Lixiao Zhang, Caijia Yu, 2014), a process involved in demyelination during EAE progression (Grajchen, Jerome J. A. Hendriks and Bogie, 2018). Within this Chapter, the proportion of myeloid cells/microglia expressing MHCII mimics expression trends of Ly6C throughout several timepoints in EAE. Upon

further investigation into specific immune cell subsets, MHCII was expressed highest in infiltrating macrophages within the CNS compared to microglia and neutrophils, suggesting greater proportions of macrophages are exerting phagocytic and/or antigen presenting abilities. Grajchen et al. described dual effector roles of macrophages, either facilitating inflammation and contributing to demyelination, or assisting with myelin debris clearance and promoting oligodendrocyte progenitor cell differentiation (Grajchen, Jerome J. A. Hendriks and Bogie, 2018). Relating this finding to MHCII expression data from this Chapter, it would suggest that macrophages upregulating MHCII could either be facilitating demyelination or promoting repair by phagocytosis myelin debris, therefore further studies specifically investigating these processes could provide further insights.

CCR2 is an essential cytokine for immune cell trafficking into the CNS during EAE disease progression. (Mazzon *et al.*, 2016). In the context of EAE, Croxford et al. describes GM-CSF as an essential promoter of CCR2, and $CCR2^{+}$ monocytes are reliant on GM-CSF to mediate CNS tissue damage (Croxford *et al.*, 2015). Phenotypic analysis from this Chapter reported CCR2 was expressed by almost half the population of infiltrating myeloid cells and microglia within the CNS at day 14, more specifically >90% of infiltrating macrophages but not neutrophils were expressing this chemokine receptor. Several reports have identified chemokines to play a role in macrophage and microglia polarisation in addition to cell-trafficking (Ruytinx *et al.*, 2018). Morganti et al. has described infiltrating $CCR2^{+}$ monocytes to corroborate with neurotoxicity abilities in monocyte derived macrophages within the CNS in the context of traumatic brain injury (Morganti *et al.*, 2015). It was suggested by Lewis et el. that macrophages upregulate activation markers to a higher extent than microglia, indicating monocyte-derived macrophages are more involved in co-stimulating autoreactive T cells mediated by these surface molecules (Lewis *et al.*, 2014). This suggestion correlates with phenotypic analysis from this Chapter as most proinflammatory and antigen presenting markers are present on infiltrating macrophages compared to CNS resident microglia.

Whilst investigating gene markers of polarisation, myeloid cells/microglia displayed increased proinflammatory markers identified as *Inos* and *Tnfα* during middle stages of disease course, whereas during later stages of EAE a polarisation switch appeared with

increased anti-inflammatory marker *Arg1*. This finding was corroborated in an elegant study performed by Locatelli et al, who used reporter mice to establish that spontaneous alterations to macrophage phenotypes throughout an EAE time course were dependent on their microenvironment (Locatelli, Theodorou, Kendirli, Jordão, *et al.*, 2018). Reporter mice used in this study labelled distinct macrophage phenotypes: classical inflammatory (iNOS), and anti-inflammatory (ARG1), to identify distinct polarisation properties. These classic polarisation markers were used to track the conversion of macrophage plasticity states in EAE. Importantly, Locatelli et al. demonstrated that depending on EAE timepoints and the location of entry points into the CNS, distinct macrophage phenotypes existed. Additionally, there were evident occurrences of mixed iNOS/ARG1 heterogeneous populations, further supported by data generated from this Chapter. Increasing research efforts are directed towards understanding the regulation of inflammatory macrophage polarisation; if this plasticity could be controlled, macrophage inflammatory phenotypes could be suppressed and directed towards those that facilitate debris clearance and CNS remyelination (Rawji and Yong, 2013; Pitt *et al.*, 2017). Miron et al. reported a myeloid derived macrophage and microglia polarisation switch from proinflammatory towards anti-inflammatory phenotypes at initial stages of remyelinating processes in a lysolecithin mouse model of demyelination (Veronique E. Miron *et al.*, 2013). This study further correlated enhanced oligodendrocyte differentiation with anti-inflammatory conditioned media generated from IL-10 treated microglia, highlighting phagocytes as important players in CNS repair processes when in an anti-inflammatory state. Ultimately, Miron et al. demonstrated that macrophages and microglia polarised to anti-inflammatory phenotypes are crucial for effective remyelinating processes and driving oligodendrocyte differentiation at lesion sites.

EAE is an invaluable tool in understanding the pathogenesis of MS. However, certain limitations using EAE as a mouse model of MS was brought to light when discrepancies arose between this study and a separate study performed by Moore et al. (Moore, Vijayaraghava T.S. Rao, *et al.*, 2013a). Moore's research group importantly identified miR-155 as a crucial regulator of polarisation properties in macrophages and microglia in human MS. However, miR-155 was found significantly induced in blood derived monocytes from human relapsing remitting patients, opposing striking data from this study where no miR-155 induction in monocytes was observed. A separate study confirmed miR-155 induction in PBMCs from RRMS patients (Mameli *et al.*, 2016),

while another study demonstrated a higher induction of miR-155 in MS sera at disease relapse (Zhang *et al.*, 2014). Additionally, the EAE mouse model used in this Chapter resembles a primary progressive disease course, whereas MS samples utilised in the Moore et al. study represented miR-155 induction in monocytes derived from a relapsing remitting disease. To address this discrepancy, a relapsing-remitting EAE model could be used to track the induction of miR-155 at different stages of disease.

Single cell RNA sequencing has proven to be an excellent tool to assess infiltrating macrophages and microglia within the CNS during health and disease (Ajami *et al.*, 2018; Hammond *et al.*, 2019). Moreover, it is now possible to examine expression of miRNAs at the single cell level, which would be instrumental in defining the precise role of miR-155 in specific cell types during MS. Understanding the diversity of cell states and correlating their molecular signatures with their function during pathological processes will aid in the development of biomarkers and identify specific mechanistic pathways that could be targeted therapeutically with limited off-target affects.

In summary, it is undeniable that miR-155 plays a prominent role in immune cells during EAE. Results from this Chapter support a role for miR-155 in influencing $CD4^+$ T cells but additionally identifies a unique role for this microRNA in regulating macrophages within the CNS that is not yet fully elucidated. Valuable information was obtained from this Chapter by tracking gene expression and phenotypic markers alongside miR-155 throughout EAE. Correlating these data with published studies, there is an evident shift of macrophage polarisation from an inflammatory phenotype to an immunoregulatory state as EAE progresses. Further research utilising advanced visualisation techniques and next generation sequencing could fully elucidate the role of miR-155 in this immune cell subset. Ultimately, understanding the regulation of macrophages at the molecular level allows for the prospect of harnessing the plasticity of macrophages to promote CNS tissue repair.

Chapter 4

The role of miR-155 *in vitro*

4.1 Introduction

Macrophages are a heterogeneous phagocytic immune cell population that play an essential role in homeostasis, host defence and tissue repair. The plasticity of macrophages allows them to exist along a spectrum of activation states where they have a range of inflammatory and regulatory functions depending on their local environment (Barros *et al.*, 2013; Murray *et al.*, 2014). *In vitro* systems that expose macrophages to different stimuli have been incredibly useful in studying the diverse functions of these cells. For example, macrophages are highly receptive and swift responders to TLR agonists and cytokines (such as LPS, Poly I:C, IFN-γ) (Oneissi Martinez *et al.*, 2008), adopting a 'classically activated' state reminiscent of their *in vivo* role in sensing and responding to exogenous or endogenous danger signals. In addition to responding to inflammatory agonists, macrophages promote immune tolerance and the resolution phase of inflammation when alternatively activated and exposed to immunoregulatory agonists (such as IL-4, IL-13 and IL-10) (Murray *et al.*, 2014).

Macrophage polarisation can be typically delineated by a multitude of properties. These properties include changes to transcription factor activation, gene expression, and cytokine/ chemokine production. Additionally, during polarisation macrophages exhibit altered surface markers and changes in metabolism (Murray *et al.*, 2014). For example, LPS, a component of *E. coli* and PAMP, promotes an inflammatory immune response via TLR4 signalling in macrophages (Billack, 2006), induces the transcription factor NF-kB to produce proinflammatory cytokines (TNF) and chemokines (CXCL10, IL-8), enhance surface markers (CD11b, Ly6C), and metabolic enzymes (iNOS). Alternatively activated macrophages, particularly those exposed to IL-10, signal through STAT3 to attenuate proinflammatory cytokines and chemokines, along with inducing anti-inflammatory cytokines (IL-10), regulatory proteins (SOCS3), surface markers (MHCII, CD206), and metabolic enzymes including (ARG1) (Murray, 2006).

The switching of macrophages between different activation states has been implicated in numerous human diseases ranging from autoimmunity to cancers. For instance, monocyte-derived macrophages are abundantly located at CNS lesion sites in the EAE model of MS, where they facilitate demyelinating processes whilst exhibiting proinflammatory and

phagocytic properties (Croxford, Spath and Becher, 2015). As disease progresses, signals from the lesion microenvironment induce a phenotypic switch in monocyte-derived macrophages and the inflammatory responses gravitates towards a resolution phase (Locatelli, Theodorou, Kendirli, Jordão, *et al.*, 2018). The exact mechanisms and control of this polarisation process, however, remains to be fully understood.

There is growing evidence that miR-155 is involved in regulating macrophage polarisation. O' Connell et al. firstly described miR-155 induction in response to IFN-β via TRIF and MyD88-dependent signalling pathways within mouse macrophages (O'Connell *et al.*, 2007). MiR-155 induction was found to promote TNF-α autocrine signalling and was an initial finding implicating miR-155 in polarising macrophages to inflammatory phenotypes. Furthermore, McCoy et al. determined IL-10 potently inhibits miR-155, resulting in increased expression of the immunoregulatory gene SHIP1. This was the first observation that miR-155 inhibition may assist in promoting anti-inflammatory gene expression within murine macrophages (Claire E McCoy *et al.*, 2010). More recently, Jablonski et al. revealed almost half of the macrophage inflammatory signature is significantly dependent on miR-155. Almost 650 inflammatory genes were altered when macrophages were challenged with LPS and IFN-γ in miR-155 KO mice compared to WT controls (Kyle A Jablonski *et al.*, 2016). Even with accumulating evidence of miR-155 skewing macrophage polarisation, a detailed understanding of how miR-155 directly influences the molecular programme of macrophages and their polarisation is limited.

Data generated from Chapter 3 investigating the role of miR-155 in WT mice throughout EAE clearly suggested that miR-155 plays a critical role in macrophages and likely contributes to chronic neuroinflammation and disease progression. Thus, to further understand the direct impact of miR-155 on macrophage polarisation states, *in vitro* studies investigating BMDM and peritoneal macrophages derived from a novel transgenic strain where miR-155 was specifically deleted from the myeloid lineage, were assessed under unstimulated and LPS treated conditions.

The cre/lox system was applied to C57BL/6 mice to specifically delete miR-155 from immune cells of the myeloid lineage. Cyclization recombinase, also termed Cre, was originally derived from bacteriophage P1 and recognises loxP sites where it exerts its recombinase activity and removes DNA between loxP sites (Gewin, 2019). Mice utilised in this Chapter contained Cre recombinase inserted at the translational start site of the myeloid cell exclusive LysM promoter ($LysM^{cre}$). The second strain of mice utilised in this Chapter contained loxP sites located at the miR-155 HG ($miR\text{-}155^{fl/fl}$) and when crossed with LysMCre mice resulted in Cre deleting flanked loxP sites at the miR-155 HG. The data in this Chapter involves BMDMs and peritoneal macrophages derived from experimental mice ($miR\text{-}155^{fl/fl}$ x LysMCre) and $LysM^{Cre}$ mice as comparable controls. BMDMs and peritoneal macrophages from $miR\text{-}155^{fl/fl}$ x $LysM^{Cre}$ mice (miR-155 deleted) are expected to lack miR-155 and will be fully tested in this Chapter.

In summary, the objective of this Chapter was to assess how miR-155 deletion mediated by the cre/lox system may affect macrophage polarisation and functional characteristics during *in vitro* inflammatory conditions through the following experimental aims:

1. To validate that miR-155 is deleted in BMDM and peritoneal macrophages from $miR\text{-}155^{fl/fl}$ x $LysM^{Cre}$ mice.
2. To evaluate if miR-155 deletion impacts BMDM and peritoneal macrophage cytokine production.
3. To investigate if miR-155 deletion influences inflammatory and immunoregulatory gene expression in BMDMs and peritoneal macrophages.
4. To determine which miR-155 target genes are significantly impacted by miR-155 deletion in BMDMs and peritoneal macrophages.
5. To assess phenotypical markers of BMDMs and peritoneal macrophages in the absence of miR-155.

4.2 Results

4.2.1 LPS induces miR-155 expression in BMDMs.

Elevated miR-155 expression fine-tunes macrophages to a pro-inflammatory activation state, causing an increase of inflammatory cytokines, gene expression, and phenotypic markers (Li *et al.*, 2018). To investigate the role of miR-155 *in vitro,* initial studies utilised primary BMDMs. Expression of miR-155 in BMDMs was assessed after stimulation with LPS, a component of *Escherichia coli* and PAMP that promotes an inflammatory immune response via TLR signalling (Billack, 2006). As shown in Figure 4.1, miR-155 expression was significantly induced in BMDMs to 97.26-fold ($P<0.0001$) when cultured in the presence of LPS for 18-20 hours. Overall this demonstrates how an *in vitro* inflammatory stimulus results in a highly significant increase in miR-155 expression in macrophages.

4.2.2 IL-10 reduces miR-155 expression in BMDMs.

IL-10 is a classic immunoregulatory cytokine that polarises macrophages to an anti-inflammatory activation state, leading to attenuation of an inflammatory immune response. Moreover, this immunoregulatory cytokine can directly inhibit miR-155 expression from the *BIC* gene and mature miR-155 *in vitro* (Claire E. McCoy *et al.*, 2010). To confirm the suppressive effects of IL-10 on miR-155 expression, BMDMs were treated with IL-10 and/or LPS. Figure 4.2 represents miR-155 expression in BMDMs in the presence of LPS, IL-10, and LPS plus IL-10 for 18-20 hours. As expected, in the presence of LPS, miR-155 induction significantly increased to 124.36-fold ($P<0.0001$). In contrast, BMDMs treated with LPS in the presence of IL-10 had significantly reduced expression of miR-155 expression at 43.64-fold (P value<0.0001), compared to LPS alone. IL-10 alone had no effect on miR-155 expression in BMDMs. Overall, these results confirm the suppressive effects of IL-10 on miR-155 induction in LPS treated BMDMs.

4.2.3 miR-155 cannot be induced in miR-155 deleted BMDMs.

To understand how miR-155 expression impacts macrophage inflammatory properties, the Cre-lox recombination system was used to generate a novel transgenic mouse strain in which miR-155 was genetically deleted in macrophages. As a first step, miR-155 deletion in

macrophages needed to be validated and compared to control macrophages derived from LysMCre mice. MiR-155 deletion was initially assessed using control BMDMs and miR-155 deleted BMDMs in the absence and presence of LPS. As demonstrated in Figure 4.3, miR-155 expression was significantly induced in control BMDMs when treated with LPS to 43.59-fold (P<0.0001), whereas miR-155 expression could not be induced by LPS in miR-155 deleted BMDMs. Overall, this data validates that miR-155 expression cannot be induced in BMDMs from miR-155$^{fl/fl}$ x LysMCre mice in the presence of an inflammatory agonist.

4.2.4 miR-155 deletion in BMDMs does not affect cytokine production.

Analysis of cytokine secretion profiles can provide significant insight into how specific stimuli influence the activation state of macrophages. To investigate if miR-155 expression influenced cytokine production in BMDMs, inflammatory and anti-inflammatory cytokines were measured in culture supernatants harvested from control and miR-155 deleted BMDMs under unstimulated and LPS-treated conditions. A cytokine bead array (CBA) kit was used to quantify inflammatory cytokines: TNFα, IL-6, IFN-γ, anti-inflammatory cytokine: IL-10, Th1 promoting cytokine: IL-12p70, and chemokine: MCP-1 (CCL2).

As shown in Figure 4.4A, LPS significantly increased TNFα production in control BMDMs (81.83 pg/ml to 3988.56 pg/ml) and miR-155 deleted BMDMs (90.30 pg/ml to 3646.84 pg/ml) (P<0.0001). The induction of TNFα secretion by LPS was higher in control BMDMs, although this did not reach statistical significance. Figure 4.4B shows that LPS significantly increased IL-10 production in control BMDMs from 3.36 pg/ml to 2363.09 pg/ml (P value 0.0002), and in miR-155 deleted BMDMs from 5.14 pg/ml to 3127.21 pg/ml (P<0.0001). In this case, induction of the anti-inflammatory cytokine IL-10 was higher in miR-155 deleted BMDMs than control BMDMs, but again no statistically significant difference was observed. LPS caused significant production of IL-6 in both control BMDMs (9.73 pg/ml to 2088.14 pg/ml) and miR-155 deleted BMDMs (4.62 pg/ml to 2603.10 pg/ml) (P<0.0001) (Figure 4.4C). Figure 4.4D shows LPS could not significantly promote IL-12p70 production in either control BMDMs or miR-155 deleted BMDMs. Significantly increased IFNγ production, from 0.47 pg/ml to 9.07 pg/ml in control BMDMs (P value 0.0099) and from 0.67 pg/ml to 9.20 pg/ml in miR-155 deleted BMDMs (P value 0.0105) was observed in response to LPS (Figure 4.4E), although the levels of this cytokine in culture supernatants were much lower compared to other cytokines tested. Figure 4.4F shows MCP-1 production

was not significantly influenced by LPS stimulation. However, MCP-1 was the only cytokine that had significantly high production levels under unstimulated conditions. Levels of MCP-1 only slightly increased from 5316.79 pg/ml to 6443.25 pg/ml in control BMDMs and increased from 5628.76 pg/ml to 5782.28 pg/ml in miR-155 deleted BMDMs.

Overall LPS stimulation increased the levels of inflammatory cytokines TNFα, IL-6, and IFNγ, and the anti-inflammatory cytokine IL-10, but did not influence IL-12 or MCP-1, with the latter cytokine being constitutively expressed at high levels. When comparing BMDMs that either expressed miR-155 or were deficient in miR-155, the production of TNF is lower whereas IL-10 is higher upon stimulation, suggesting a potential shift towards an anti-inflammatory polarisation state.

4.2.5 miR-155 deletion in BMDMs does not affect proinflammatory cytokine ratios to IL-10.

The ratio of proinflammatory (TNF-α, IL-6, IFN-γ, IL-12p70)) to anti-inflammatory (IL-10) cytokines secreted by BMDMs were analysed using the data in Figure 4.4 in order to investigate how miR-155 deletion may affect the overall cytokine milieu and downstream responses in lymphocytes, such as polarisation of CD4 T cells to different Th cell subsets. This method of cytokine ratio analysis was adapted from Bar-Or et al. (Bar-Or *et al.*, 2010).

Figure 4.5A demonstrated that miR-155 deletion resulted in a trend of increased TNFα ratios to IL-10 in control BMDMs (2.15) compared to miR-155 deleted BMDMs (1.01), suggesting control macrophages may be skewed towards a proinflammatory state to a higher extent compared to when miR-155 is deleted. As shown in Figure 4.5B, there were relatively no changes in IL-6 to IL-10 ratios upon LPS treatment in either control BMDMs (1.16) or miR-155 deleted BMDMs (0.86). Figure 4.5C outlined a slight increase of IFNγ ratios to IL-10 in control BMDMs (0.0059) in comparison to miR-155 deleted BMDMs (0.0029), once more indicating that in the presence of miR-155, BMDMs are polarised to an activated state to a greater extent than when miR-155 is absent. As shown in Figure 4.5D, there were relatively no changes in IL12p70 ratios to IL-10 between control BMDMs (0.0091) and miR-155 deleted BMDMs (0.0014).

Collectively, miR-155 appears to play a slight role in skewing BMDMs towards a proinflammatory state.

4.2.6 miR-155 deletion affects inflammatory gene expression in BMDMs.

Transcriptional changes, such as the upregulation of inflammatory genes (*Inos* and *Tnfα*) or immunoregulatory genes (*Il-10m* and *Arg1*), occurs during polarisation of macrophages to inflammatory or regulatory activation states. To further understand how miR-155 deletion affects macrophage polarisation, control BMDMs and miR-155 deleted BMDMs were stimulated with LPS to investigate if miR-155 expression alters their molecular profile. Specifically, induction of *Inos*, *Tnfα*, *Il-10m*, and *Arg1* was assessed to determine if miR-155 deleted BMDMs adopted a regulatory polarisation state when compared to controls.

As shown in Figure 4.6A, LPS significantly induced *Inos* in control BMDMs to 2941.05-fold ($P<0.0001$), while *Inos* was induced 868.74-fold in miR-155 deleted BMDMs. A direct comparison between the two groups demonstrates that *Inos* induction was significantly higher in control BMDMs compared to miR-155 deleted BMDMs (P value 0.0021).

Figure 4.6B represents *Tnfα* induction in BMDMs. As expected, this inflammatory gene was significantly induced by LPS in control BMDMs to 7.17-fold (P value 0.0014) but was only slightly increased in miR-155 deleted BMDMs to 3.76-fold (not significant). This mirrors the trend observed in TNFα protein levels measured in supernatants (Figure 4.4A).

As shown in Figure 4.6C, the immunoregulatory gene *Il-10m* was significantly induced by LPS in both control BMDMs and miR-155 deleted BMDMs to 36.73-fold and 31.57-fold, respectively ($P<0.001$), again correlating with previous cytokine data (Figure 4.4B).

Interestingly, as shown in Figure 4.6D, the classic immunoregulatory gene *Arg1* was significantly induced in miR-155 deleted BMDMs to 29.88-fold but not in control BMDMs (14.06-fold). Despite the evident difference in *Arg1* induction between the two BMDM groups, no statistical significance could be determined.

Overall, LPS significantly induced inflammatory genes (*Inos* and *Tnfα*) in control BMDMs, whereas this induction was reduced in miR-155 deleted BMDMs. *Inos* gene expression particularly displayed a more significant reduction. When investigating anti-inflammatory genes, there was little difference between LPS-treated control BMDMs and miR-155 deleted BMDMs for *Il-10m* gene expression, whereas *Arg1* gene expression was more significantly induced in miR-155 deleted BMDMs compared to controls. Collectively this data suggests

that miR-155 deleted BMDMs become polarised to a less inflammatory state when stimulated with LPS *in vitro*.

4.2.7 miR-155 deletion affects *Ets2* and *Arg2* gene expression in BMDMs.

Investigating miR-155 targets and transcription factors allows the further evaluation of miR-155s role in BMDM inflammatory abilities *in vitro*. MiR-155 gene targets *(Ship1*, and *Arg2*) and transcription factor (*Ets2)* were investigated in control BMDMs and miR-155 deleted BMDMs in the absence and presence of LPS.

As previously mentioned in Chapter 3, *Ets2* is an established and essential transcriptional inducer of miR-155 (Quinn *et al.*, 2014) and would therefore be expected to follow similar trends to miR-155 expression. Figure 4.7A represents the induction of *Ets2* in response to LPS. *Ets2* gene expression was significantly induced to 3.26-fold in control BMDMs ($P<0.0001$) and to 2.07-fold in miR-155 deleted BMDMs (P value 0.0103). *Ets2* induction was, however, significantly lower in miR-155 deleted BMDMs by 1.19-fold (P value 0.0054), correlating with the trend of reduced miR-155 expression in miR-155 deleted BMDMs.

The immunoregulatory gene *Ship1* is a known miR-155 target that is involved in dampening the immune response (O'Connell *et al.*, 2009). Figure 4.7B represents the induction of Ship1 in response to LPS in control BMDMs and miR-155 deleted BMDMs. As expected, LPS did not significantly induce *Ship1* gene expression, however there was also no significant differences between control BMDMs and miR-155 deleted BMDMs.

Arg2, a novel anti-inflammatory/immunoregulatory gene marker and target of miR-155 (Dunand-Sauthier *et al.*, 2014) was also investigated in the absence and presence of LPS. As shown in Figure 4.7C, *Arg2* gene expression was significantly induced upon LPS stimulation to 52.43-fold in control BMDMs (P value 0.0033) and to 174.32-fold in miR-155 deleted BMDMs ($P<0.0001$). Strikingly, *Arg2* was significantly higher in miR-155 deleted BMDMs compared to control BMDMs ($P<0.0001$).

Collectively, these data outline how gene expression of miR-155 targets differ between control BMDMs and miR-155 deleted macrophages when stimulated with LPS. Expectedly, *Ets2* expression is supressed in miR-155 deleted BMDMs, but there was no evident change in *Ship1* expression. Interestingly, significantly higher *Arg2* gene induction suggested miR-

155 deleted BMDMs are more immunoregulatory than controls, further correlating with classic anti-inflammatory marker, *Arg1* gene expression (Figure 4.5D).

4.2.8 miR-155 deletion does not significantly affect Ly6C or MHCII expression on BMDMs.

To further characterise how miR-155 expression influences the phenotype of BMDMs, control BMDMs and miR-155 deleted BMDMs were stimulated with LPS and phenotypically assessed for proinflammatory (Ly6C) and antigen presenting (MHCII) phenotypic markers on the surface of BMDMs. Figure 4.8A represents the gating strategy used to delineate BMDMs for phenotypic analysis of surface Ly6C, and MHCII within intact $CD45^{+}CD11b^{+}$ cells.

As shown in Figure 4.8B, LPS slightly increased the proportion of $Ly6C^{+}$ BMDMs from 3.74% to 10.36% in control BMDMs, and 3.60% to 15.43% in miR-155 deleted BMDMs (not significant). Additionally, there was a slightly higher proportion of $Ly6C^{+}$ cells in miR-155 deleted BMDMs compared to control BMDMs, but no statistically significant difference was determined. To further investigate how miR-155 deletion affected the proportion of BMDMs expressing Ly6C under the inflammatory stress of LPS, BMDMs were analysed to determine the percentage difference between unstimulated and LPS conditions amongst LysMCre controls and $miR\text{-}155^{fl/fl}$ x LysMCre mice. Figure 4.8C showed there was a significant increase in BMDMs expressing Ly6C after miR-155 deletion (6.68% for control BMDMs, 11.80% for miR-155 deleted BMDMs) (P value 0.0052). This overall suggested miR-155 deletion enhances this marker of cell activation in response to LPS.

Figure 3.8D represents expression of MHCII in BMDMs in response to LPS. $MHCII^{+}$ proportions slightly increased from 7.41% to 10.72% in control BMDMs and increased from 5.91% to 10.4% in miR-155 deleted macrophages. Overall there was no change in the proportions of $MHCII^{+}$ expressing cells in miR-155 deleted BMDMs compared to control BMDMs (not significant). Figure 3.8E displays MHCII changes between controls and miR-155 deleted BMDMs stimulated with LPS relative to unstimulated conditions. ΔMHCII did not significantly differ between both groups but a slight trend of increased ΔMHCII was observed in controls (3.31%) compared to miR-155 deleted BMDMs (4.47%).

In summary, there was no significant difference in the surface expression of Ly6C and MHCII between LPS treated control BMDMs and miR-155 deleted BMDMs. However, there was a significantly increased proportion of $Ly6C^+$ miR-155 deleted BMDMs upon LPS stimulation relative to controls.

4.2.9 miR-155 deletion affects intracellular iNOS expression in BMDMs.

Intracellular iNOS and CD206 (mannose receptor C) expression were investigated to understand how miR-155 plays a role in regulating these classical proinflammatory and anti-inflammatory markers in BMDMs. Figure 4.9A represents the gating strategy used to delineate BMDMs for phenotypic analysis of intracellular iNOS, and CD206 within viable intact cells.

As shown in Figure 4.9B, intracellular iNOS expression was significantly increased by LPS in both control BMDMs and miR-155 deleted BMDMs. INOS proportions increased from 0.32% to 7.75% in control BMDMs (P value 0.0114), and 0.29% to 5.31% in miR-155 deleted BMDMs (P value 0.0049) Although no statistical significance was determined between these two groups, there is a trend of lower iNOS expression in miR-155 deleted BMDMs treated with LPS compared to control BMDMs, similarly mirroring iNOS gene expression in Figure 4.7A. Figure 4.9C represents ΔiNOS expression between unstimulated and LPS conditions in control BMDMs and miR-155 deleted BMDMs. There is an evident shift of ΔiNOS (8.73%) in control BMDMs compared to miR-155 deleted BMDMs (5.01%) (not significant), suggesting control BMDMs can upregulate iNOS expression to a higher extent in the presence of miR-155.

Figure 4.9D represents the proportions of anti-inflammatory marker CD206 within BMDMs. Interestingly, LPS did not significantly affect CD206 expression on either control BMDMs or miR-155 deleted BMDMs. Both groups of BMDMs had a high proportional range of CD206 expression from 71.13% to 61.42%. Figure 4.9E represents ΔCD206 expression changes in response to LPS between control BMDMs and miR-155 deleted BMDMs. Control BMDMs displayed relatively the same Δ change in CD206 expression (-8.45%) compared to miR-155 deleted BMDMs (-7.92%), suggesting CD206 expression was unaffected by miR-155 deletion.

Collectively, there was no significant differences of intracellular iNOS and CD206 expression between LPS treated controls BMDMs and miR-155 deleted BMDMs. However, there were slight trends of decreased iNOS proportions of LPS treated miR-155 deleted BMDMs compared to control BMDMs, suggesting miR-155 deletion may play a role in BMDM phenotypes under stress *in vitro.*

4.2.10 miR-155 cannot be induced in miR-155 deleted peritoneal macrophages.

Peritoneal macrophages are a useful comparative tool to investigate alongside BMDMs. They are a specific subset of differentiated tissue resident macrophages used in this research project to understand how the role of miR-155 may the polarisation of mature macrophages. Prior to understanding how miR-155 expression could affect peritoneal macrophages, miR-155 deletion needed to be verified. MiR-155 deletion was evaluated in control peritoneal macrophages and miR-155 deleted macrophages under unstimulated and LPS-treated conditions. As shown in Figure 4.10, LPS significantly induced miR-155 expression to 21.14-fold in control peritoneal macrophages ($P<0.0001$), whereas LPS could not induce miR-155 expression in miR-155 deleted peritoneal macrophages. Overall, these results validated that Cre recombination has efficiently prevented miR-155 induction in miR-155 deleted peritoneal macrophages in the presence of the inflammatory agonist LPS.

4.2.11 miR-155 deletion in peritoneal macrophages affects TNFα and IL-10 production.

To investigate how miR-155 expression may affect macrophage inflammatory states, inflammatory and anti-inflammatory cytokines were measured in supernatants from control peritoneal macrophages and miR-155 deleted peritoneal macrophages cultured under unstimulated and LPS-stimulated conditions. A cytokine bead array (CBA) kit was used to measure inflammatory cytokines: TNFα, IL-6, and IFN-γ, anti-inflammatory cytokine: IL-10, Th1 promoting cytokine: IL-12p70, and chemokine: MCP-1 (CCL2).

As shown in Figure 4.11A, LPS significantly increased inflammatory TNFα production from 55.64 pg/ml to 1447.20 pg/ml (P value 0.0490) in control peritoneal macrophages and could increase TNFα production in miR-155 deleted peritoneal macrophages (45.17 pg/ml to 1307.56 pg/ml) (not significant). There was no significant change in TNFα induction between the LPS-treated groups.

Figure 4.11B represents immunoregulatory IL-10 production in response to LPS from controls and miR-155 deleted peritoneal macrophages. LPS significantly increased IL-10 in both control peritoneal macrophages (5.05 pg/ml to 410.18 pg/ml) ($P<0.0001$) and miR-155 deleted peritoneal macrophages (11.02 pg/ml to 297.94 pg/ml) ($P<0.0001$). Interestingly, IL-10 production was significantly higher in control peritoneal macrophages (410.18 pg/ml) in response to LPS compared to miR-155 deleted peritoneal macrophages (297.94 pg/ml) (P value 0.0402).

Inflammatory IL-6 production is represented in Figure 4.11C. LPS significantly increased IL-6 production in control peritoneal macrophages (90.83 pg/ml to 8026.88 pg/ml) and miR-155 deleted peritoneal macrophages (94.79 pg/ml to 8559.33 pg/ml), although no statistically significant difference was found between both LPS stimulated groups.

As shown in Figure 4.11D, the Th1 promoting cytokine IL-12p70 could not be significantly increased by LPS in either control or miR-155 deleted peritoneal macrophages. Although no significance was determined, miR-155 deleted peritoneal macrophages produced slightly less IL-12p70 in unstimulated and LPS conditions compared to controls.

Figure 4.11D represents IFNγ production in the absence and presence of LPS. No increase of IFNγ production was evident in the presence or absence of LPS, reaching < 3.35 pg/ml in all investigated conditions. As such, no difference between unstimulated and LPS stimulated control peritoneal macrophages and miR-155 deleted peritoneal macrophages was observed.

As shown in Figure 4.11F, chemokine MCP-1 production increased from 59.90 pg/ml to 502.62 pg/ml in control peritoneal macrophages and 55.08 pg/ml to 488.54 pg/ml in miR-155 deleted peritoneal macrophages, however there were no statistically significant difference in MCP-1 production between both LPS treated conditions.

Overall, miR-155 deletion in peritoneal macrophages only affected inflammatory TNFα production and immunoregulatory IL-10 production upon LPS stimulation. TNFα could not be significantly induced by LPS in the absence of miR-155, IL-10 production was significantly lower in miR-155 deleted peritoneal macrophages, in contrast to previous BMDM cytokine data (Figure 4.4B).

4.2.12 miR-155 deletion in peritoneal macrophages does not affect proinflammatory cytokine ratios to IL-10 in response to LPS.

The ratio of proinflammatory (TNF-α, IL-6, IFN-γ, IL-12p70)) to anti-inflammatory (IL-10) cytokines secreted by peritoneal macrophages were analysed using the data in Figure 4.13 to further evaluate how miR-155 deletion may affect cytokine profiles and downstream responses in adaptive immune cells, such as CD4 T cells differentiation towards Th cell subsets. These analyses were performed and adapted from Bar-Or's method of cytokine ratio method (Bar-Or *et al.*, 2010).

Figure 4.12A demonstrated that miR-155 deletion did not alter the TNFα to IL-10 ratio in controls (4.07) and miR-155 deleted macrophages (3.98). Similarly shown in Figure 4.12B, the IL-6 to IL-10 ratio relatively did not change under LPS conditions in controls (24.60) versus miR-155 deleted peritoneal macrophages (30.50). As shown in Figure 4.12C, IFNγ to IL-10 ratios appeared higher in controls (0.0027) compared to miR-155 deleted macrophages (0.00086), suggesting control macrophages are polarised to an inflammatory phenotype to a higher extent in the presence of miR-155. Additionally, Figure 4.12D identified control macrophages to have a slightly higher IL-12p70 to IL-10 ratio (0.04) in comparison to miR-155 deleted peritoneal macrophages (0.0055), further suggesting a role for miR-155 in macrophage polarisation towards a proinflammatory phenotype.

Collectively, a trend of increased IFNγ and IL-12p70 to IL-10 ratios within controls compared to miR-155 deleted peritoneal macrophages was identified, suggesting a proinflammatory role for miR-155 in tissue resident macrophages.

4.2.13 miR-155 deletion affects *Arg1* gene expression in peritoneal macrophages.

To further understand how miR-155 expression may affect peritoneal macrophage inflammatory characteristics and polarisation states, a panel of inflammatory and immunoregulatory genes were investigated under unstimulated and LPS stimulated conditions. Inflammatory genes assessed in control peritoneal macrophages and miR-155 deleted macrophages include*: Inos* and *Tnfα*, and immunoregulatory genes investigated include: *Il-10m* and *Arg1*.

As shown in Figure 4.13A, LPS induced *Inos* gene expression to 39.47-fold in controls and 48.63-fold in miR-155 deleted peritoneal macrophages, but no statistically significant difference was determined in LPS-treated conditions. This data indicated miR-155 deletion

does not significantly alter *Inos* expression levels in peritoneal macrophages, which interestingly opposed BMDM data from Figure 4.6A.

Figure 4.13B represents pro-inflammatory *Tnfα* gene expression when treated with LPS. Control and miR-155 deleted peritoneal macrophages demonstrated *Tnfα* induction to 1.53-fold and 1.62-fold, respectively (not significant). This data differs from macrophages derived from bone marrow, as *Tnfα* was significantly induced in control BMDMs (Figure 4.6B).

Il-10m gene expression is represented in Figure 4.13C. LPS slightly increased *Il-10m* expression by 7.95-fold in control peritoneal macrophages and 6.24-fold in miR-155 deleted peritoneal macrophages. Overall, no difference was determined in either LPS treated groups.

As shown in Figure 4.13D, *Arg1* gene expression was slightly induced by LPS to 6.87-fold in control peritoneal macrophages (not significant) but significantly increased to 13.03-fold in miR-155 deleted peritoneal macrophages. Despite the evident difference of 6.16-fold between these two LPS-treated groups, no significant difference could be determined.

In summary, there was no significant differences in inflammatory gene expression (*Inos* and *Tnfα*) in control peritoneal macrophages and miR-155 deleted peritoneal macrophages when treated with LPS. When investigating anti-inflammatory gene expression, the immunoregulatory gene *Il-10m* could not be significantly induced by LPS, unlike *Arg1*, which could only be significantly induced when miR-155 was deleted. Thus far, *Arg1* is the only indication of miR-155 deletion affecting macrophage polarisation towards an immunoregulatory phenotype in peritoneal macrophages. To further clarify how miR-155 expression affects macrophage functional characteristics *in vitro*, additional gene expression studies needed to be carried out.

4.2.14 miR-155 deletion affects *Arg2* gene expression in peritoneal macrophages.

Simultaneously investigating miR-155 target genes alongside inflammatory and immunoregulatory genes in response to an inflammatory agonist provides a greater insight into the functional polarisation state of peritoneal macrophage. To further assess the role of miR-155 in macrophages *in vitro*, miR-155 target genes: *Ets2*, *Ship1*, and *Arg2* were examined in peritoneal macrophages in unstimulated and LPS conditions.

As shown in Figure 4.14A, *Ets2* gene expression was induced by LPS in controls to 5.47-fold (not significant), but this gene could not be induced in miR-155 deleted peritoneal macrophages (1.80-fold increase). As *Ets2* is a known transcription factors of miR-155, *Ets2* expectedly mimicked the trend of miR-155 induction in peritoneal macrophages in Figure 4.10.

Figure 4.14B represents *Ship1* gene expression in response to LPS. *Ship1* was reduced in LPS treated control peritoneal macrophages in comparison to unstimulated conditions (2.08-fold to 0.47-fold). Interestingly, *Ship1* expression did not change between unstimulated and LPS conditions (0.55-fold to 0.44-fold) in miR-155 deleted macrophages.

As demonstrated in Figure 4.14C, when investigating the novel immunoregulatory gene *Arg2*, LPS could not induce *Arg2* expression in control peritoneal macrophages (0.90-fold to 0.72-fold). However, LPS caused a significant increase of *Arg2* expression in miR-155 deleted peritoneal macrophages to 5.00-fold (P value 0.0027). Furthermore, *Arg2* expression was significantly higher in miR-155 deleted macrophages compared to controls (P value 0.004).

Overall, the absence or presence of miR-155 did not significantly affect miR-155 targets: *Ets2* and *Ship1* when treated with LPS, suggesting miR-155 expression alone cannot significantly control these genes in peritoneal macrophages. However, the immunoregulatory miR-155 target *Arg2* was significantly higher in miR-155 deleted peritoneal macrophages, correlating with BMDM data from Figure 4.7C. This further suggests miR-155 deletion fine-tunes peritoneal macrophages to an immunoregulatory phenotype.

4.2.15 miR-155 deletion does not significantly affect surface phenotypes of peritoneal macrophages.

To further investigate if miR-155 influenced expression of surface phenotypic markers of macrophage polarisation, control peritoneal macrophages and miR-155 deleted peritoneal macrophages were left unstimulated or stimulated with the inflammatory agonist LPS. The following markers were assessed: Ly6C and MHCII. Figure 4.15A represents the gating strategy used to delineate peritoneal macrophages for phenotypic analysis of surface Ly6C and MHCII. Proportions were derived from intact $CD45^{+}CD11b^{+}$ cells.

As shown in Figures 4.15B, the proportion of $CD45^+CD11b^+$ peritoneal macrophages expressing the surface marker Ly6C slightly increased from 3.05% to 3.90% in response to LPS in control peritoneal macrophages and 4.71% to 6.4% in miR-155 deleted peritoneal macrophages. Although no statistical significance was determined, there was a trend of higher Ly6C expression in miR-155 deleted peritoneal macrophages in response to LPS compared to control peritoneal macrophages. The chance in the proportion of $Ly6C^+$ cells upon LPS stimulation relative to unstimulated conditions was for each genotype was determined in peritoneal macrophages. Figure 4.15C illustrates a greater ΔLy6C change under unstimulated and LPS conditions in miR-155 deleted peritoneal macrophages (1.52%) compared to controls (0.86%), although not statistically significant.

Figure 4.15D demonstrates the proportion MHCII expression on $CD45^+CD11b^+$ peritoneal macrophages. MHCII expression levels were not significantly impacted by LPS in either control peritoneal macrophages (from 4.76% to 4.99%) or miR-155 deleted macrophages (6.74% to 8.78%). As shown in Figure 4.15E, ΔMHCII was highest in miR-155 deleted peritoneal macrophages at 1.65% compared to 0.23% in controls (not significant).

Overall, no significant changes were observed when investigating cell surface polarisation phenotypic markers in controls or miR-155 deleted peritoneal macrophages. This suggests miR-155 alone cannot skew the above investigated phenotypic markers on this specific subset of tissue resident macrophages *in vitro* using LPS alone as a classical activation agonist.

4.2.16 MiR-155 deletion affects intracellular iNOS expression in peritoneal macrophages.

Intracellular iNOS and CD206 (mannose receptor C) expression were investigated in peritoneal macrophages to further evaluate how miR-155 plays a role in regulating proinflammatory and anti-inflammatory phenotypic markers within tissue resident macrophage populations. Figure 4.16A represents the gating strategy used to delineate peritoneal macrophages for phenotypic analysis of intracellular iNOS, and CD206 within viable intact cells.

Intracellular iNOS expression is shown in Figure 4.16B. INOS was not expressed in unstimulated control peritoneal macrophages but was significantly increased upon

stimulation with LPS from 0.29% to 2.33% (P value 0.0075). Likewise, no expression of iNOS was observed in unstimulated miR-155 deleted peritoneal macrophages but expression levels slightly increased from 0.58% to 1.45% when LPS-treated (not significant). As shown in Figure 4.16C, ΔiNOS expression was measured in peritoneal macrophages to investigate how miR-155 may affect the change in iNOS expression between LPS stimulated conditions relative to unstimulated for each genotype. ΔiNOS was highest in controls with 2.00% change and only 0.91% change in miR-155 deleted peritoneal macrophages (not significant), overall suggesting iNOS was not increased to the same extent when miR-155 was deleted in peritoneal macrophages.

Figure 4.16D represents expression of the scavenger receptor CD206 within peritoneal macrophages in unstimulated and LPS-treated conditions. Interestingly, LPS did not significantly affect CD206 expression in control peritoneal macrophages or miR-155 deleted macrophages. CD206 expression increased from 11.75% to 14.82% in controls and no relative change occurred in miR-155 deleted peritoneal macrophages (15.33% to 14.6%). Figure 4.16E demonstrates ΔCD206 expression between unstimulated and LPS conditions in controls and miR-155 deleted peritoneal macrophages. ΔCD206 was found higher in controls in comparison to miR-155 deleted peritoneal macrophages, with 3.08% change compared to 0.70%, respectively.

In summary, there was no statistically significant differences between controls and peritoneal macrophages in relation to intracellular iNOS and CD206 expression upon LPS-treatment. However, iNOS was significantly increased in controls unlike miR-155 deleted macrophages, suggesting miR-155 deletion may play a role in proinflammatory properties of peritoneal macrophages *in vitro.*

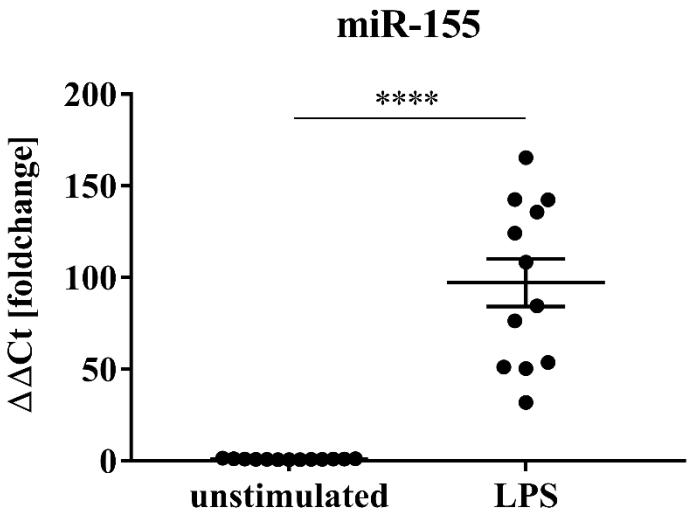

Figure 4.1 LPS induces miR-155 expression in BMDMs.

Primary BMDMs were plated at 5 x 10^5 cells per well in a 24 well plate and stimulated with 100ng/ml LPS or left unstimulated for 18-20 hours at 37°C. Total RNA was extracted and rtPCR and qPCR performed using Taqman probes to determine miR-155 expression. Data represent the ΔΔCT fold induction of miR-155 relative to unstimulated control, normalised against the average of three housekeeping genes sno-202, miR-191, and snU6, and expressed as mean ± S.EM. (n=13, 4 independent experiments). ****P<0.0001; unpaired t test with Welch's correction.

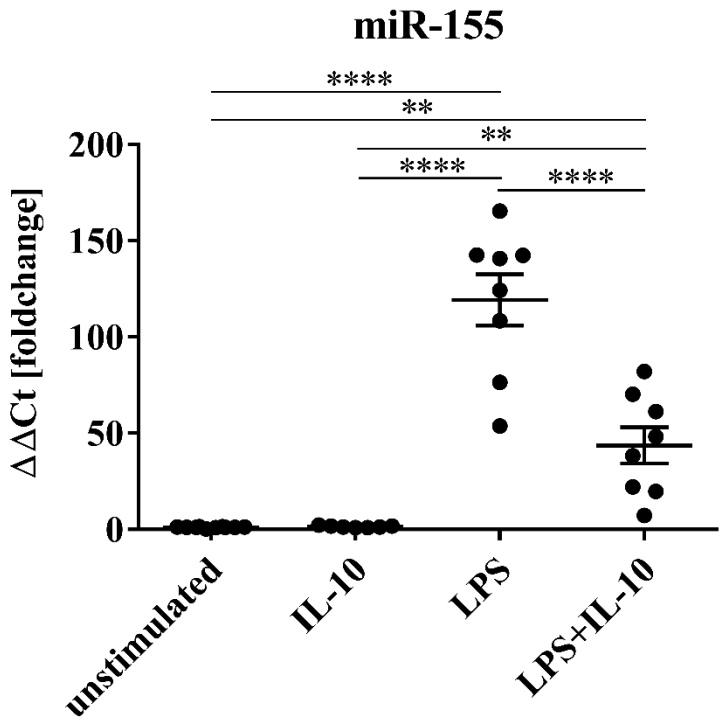

Figure 4.2 IL-10 reduces miR-155 expression in BMDMs.

Primary BMDMs were plated at 5 x 10^5 cells per well in a 24 well plate and stimulated with 100ng/ml LPS, and/or 20ng/ml IL-10, or left unstimulated for 18-20 hours at 37°C. Total RNA was extracted and rtPCR and qPCR performed using Taqman probes to determine miR-155 expression. Data represent the ΔΔCT fold induction of miR-155 relative to unstimulated control, normalised against the average of three housekeeping genes sno-202, miR-191, and snU6, and expressed as mean ± S.EM. (n=8, 3 independent experiments). **P<0.01, ****P<0.0001; one-way ANOVA with Bonferroni's correction.

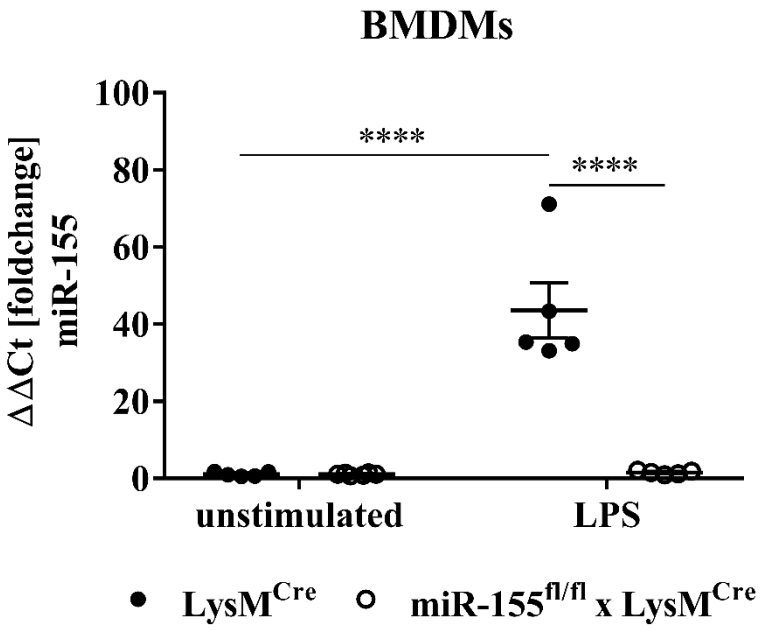

Figure 4.3 miR-155 cannot be induced in miR-155 deleted BMDMs.

Primary BMDMs from LysMCre controls and miR-155$^{fl/fl}$ x LysMCre mice were plated at 5 x 10^5 cells per well in a 24 well plate and stimulated with 100ng/ml LPS or left unstimulated for 18-20 hours at 37°C. Total RNA was extracted and rtPCR and qPCR performed using Taqman probes to determine miR-155 expression. Data represent the ΔΔCT fold induction of miR-155, relative to unstimulated control, normalised against the average of three housekeeping genes sno-202, miR-191, and snU6, and expressed as mean ± S.EM. (n=5, 2 independent experiments). ****P<0.0001; two-way ANOVA with Bonferroni's correction.

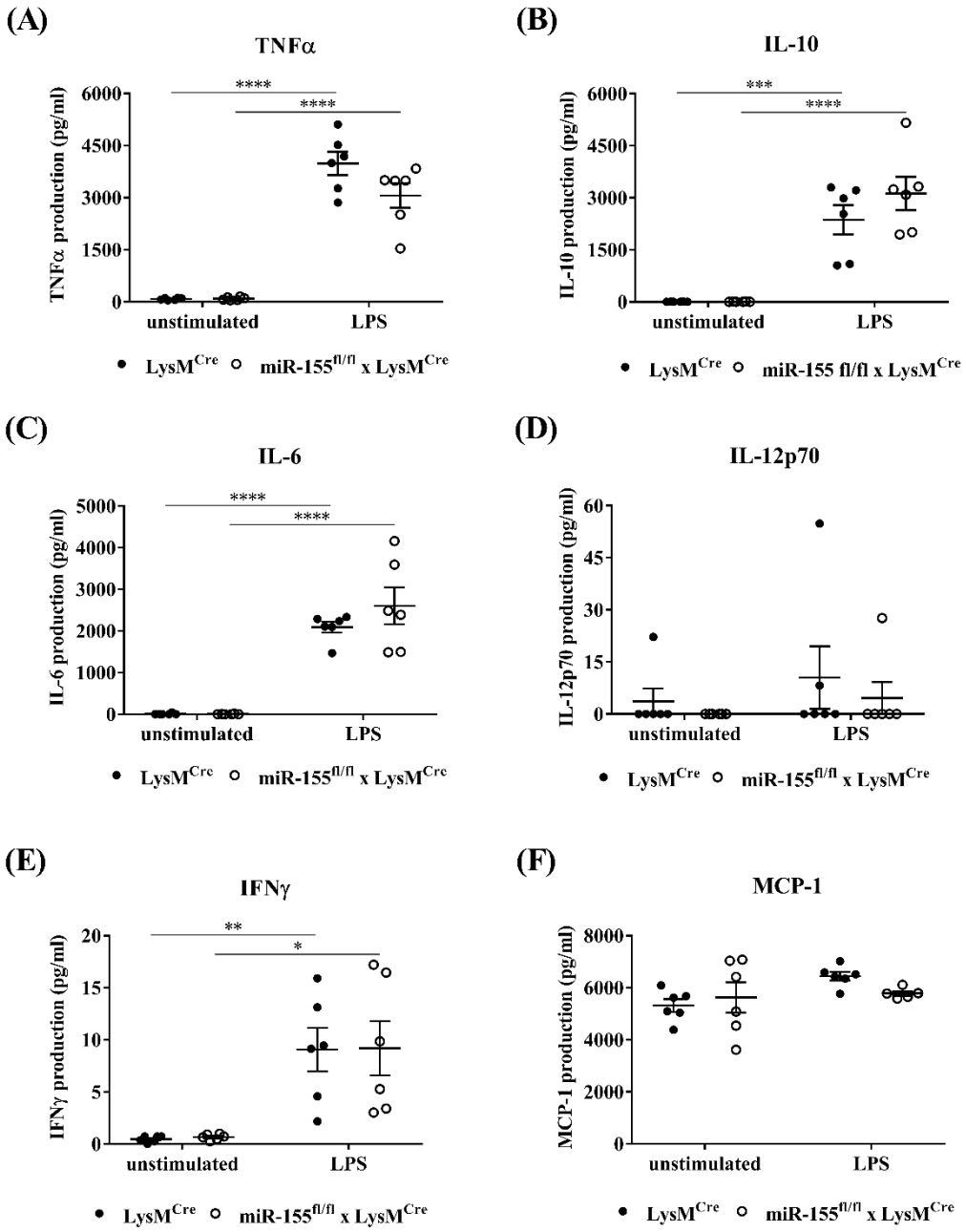

Figure 4.4 miR-155 deletion in BMDMs does not affect cytokine production.

Primary BMDMs from LysMCre controls and miR-155$^{fl/fl}$ x LysMCre mice were plated at 5 x 10^5 cells per well in a 24 well plate and stimulated with 100ng/ml LPS or left unstimulated for 18-20 hours at 37°C. Supernatants were collected and secreted cytokines were quantified using a BD™ Cytometric Bead Array (CBA) kit. Data represents mean ± S.EM. (n=6, 2 independent experiments). *P<0.05, **P<0.01, ***P<0.001, ****P<0.0001; two-way ANOVA with Bonferroni's multiple comparisons test.

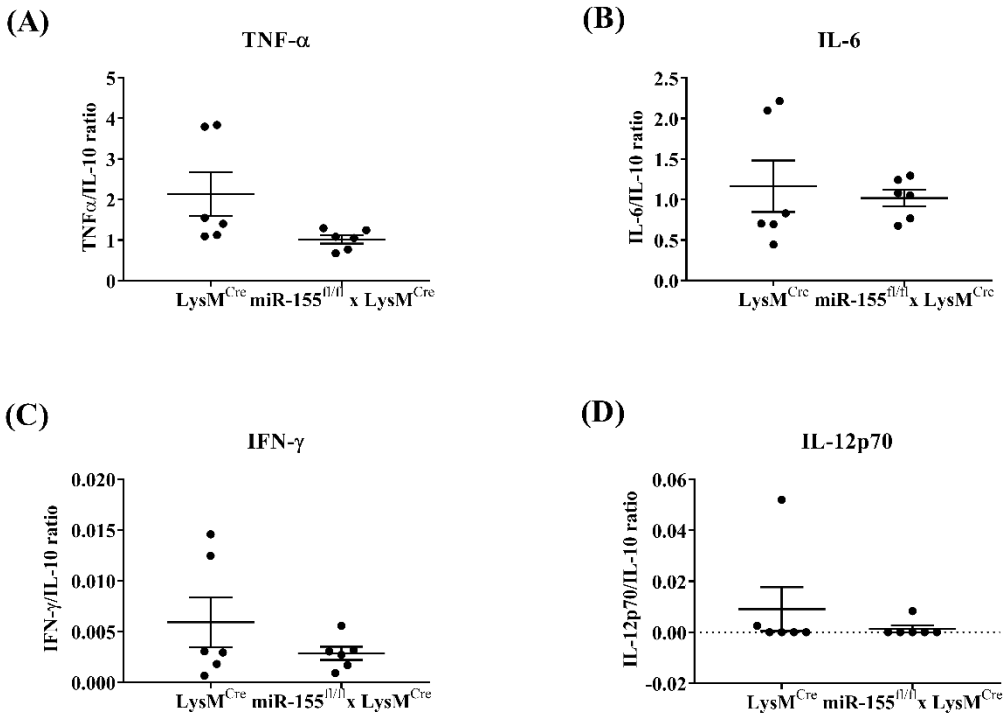

Figure 4.5 miR-155 deletion in BMDMs does not affect proinflammatory cytokine ratios to IL-10 in response to LPS.

Primary BMDMs from LysMCre controls and miR-155$^{fl/fl}$ x LysMCre mice were plated at 5 x 10^5 cells per well in a 24 well plate and stimulated with 100ng/ml LPS or left unstimulated for 18-20 hours at 37°C. Supernatants were collected and secreted cytokines were quantified using a BD™ Cytometric Bead Array (CBA) kit. Data represents mean ± S.EM. (n=6, 2 independent experiments).

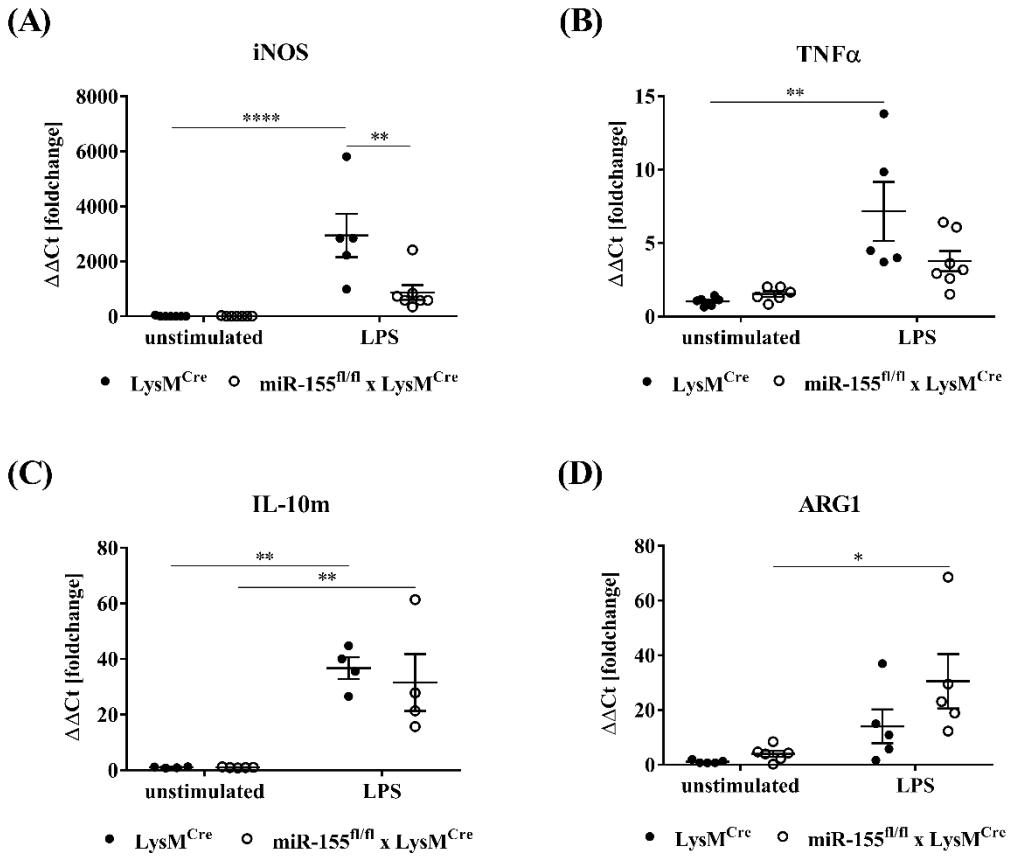

Figure 4.6 miR-155 deletion affects inflammatory gene expression in BMDMs.

Primary BMDMs from LysMCre controls and miR-155$^{fl/fl}$ x LysMCre mice were plated at 4.5-5 x 10^5 cells per well in a 24 well plate and stimulated with 100ng/ml LPS or left unstimulated for 18-20 hours at 37°C. Total RNA was extracted and rtPCR and qPCR performed to determine (A) *Inos* (B) *Tnfα* (C) *Il10m*, and (D) *Arg1* expression. Data represent the ΔΔCT fold induction relative to unstimulated control, normalised against the average of two housekeeping genes *m18s* and *Gapdh*, and expressed as mean ± S.EM. (n=4-7, 3 independent experiments). *P<0.05, **P<0.01; ****P<0.0001 two-way ANOVA with Bonferroni's correction.

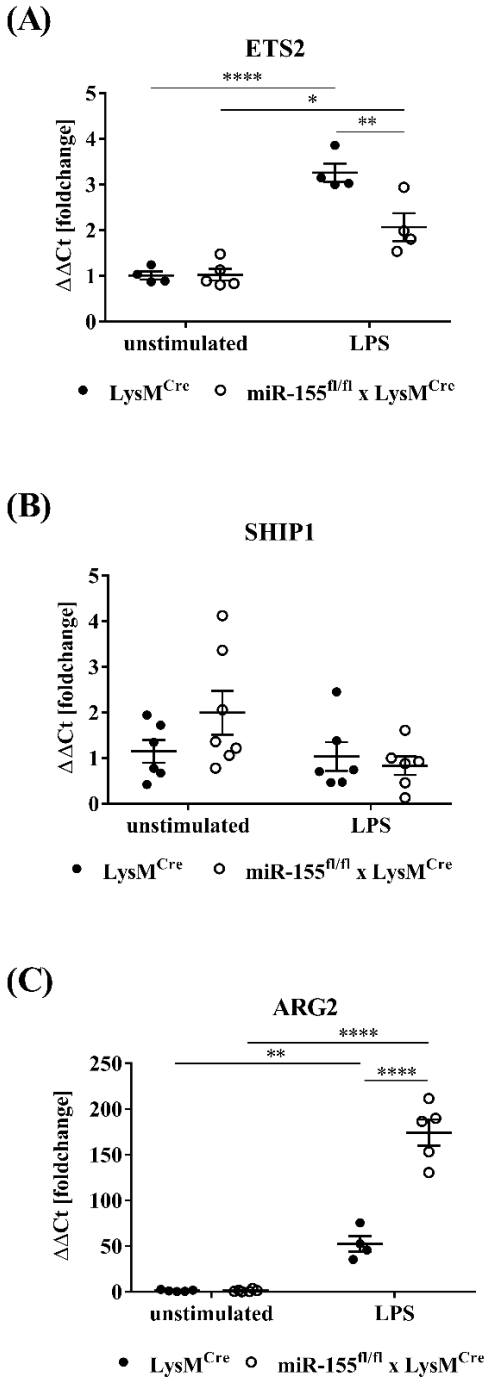

Figure 4.7 miR-155 deletion affects *Ets2* and *Arg2* gene expression in BMDMs.

Primary BMDMs from LysMCre controls and miR-155$^{fl/fl}$ x LysMCre mice were plated at 4.5-5 x 10^5 cells per well in a 24 well plate and stimulated with 100ng/ml LPS or left unstimulated for 18-20 hours at 37°C. Total RNA was extracted and rtPCR and qPCR performed to determine (A) *Ets2* (B) *Ship1* and (C) *Arg2* expression. Data represent the ΔΔCT fold induction relative to unstimulated control, normalised against the average of two housekeeping genes *m18s* and *Gapdh*, and expressed as mean ± S.EM. (n=4-7, 3 independent experiments). *P<0.05, **P<0.01, ****P<0.0001; two-way ANOVA with Bonferroni's correction.

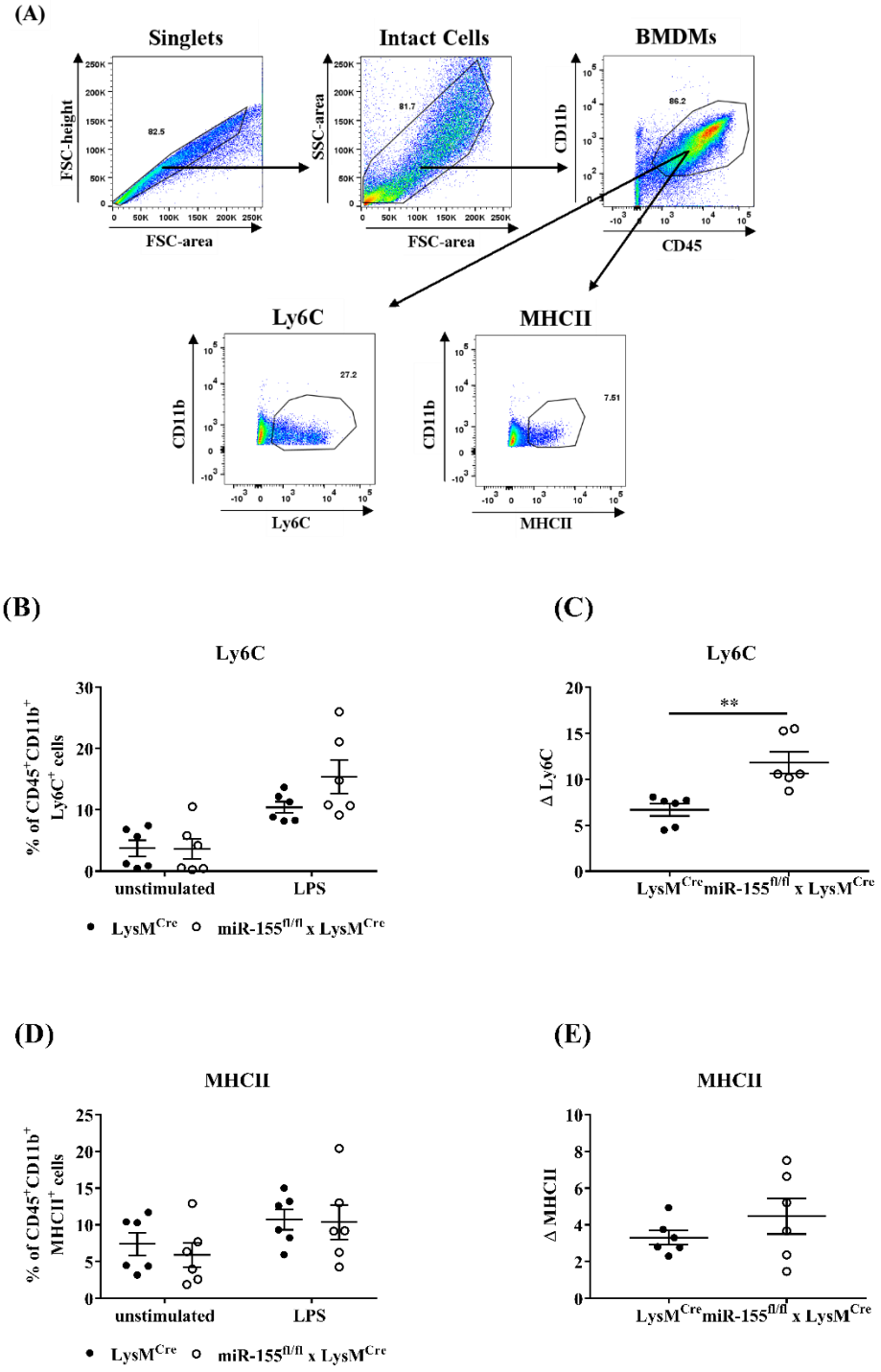

4.8 miR-155 deletion does not significantly affect surface phenotypes of BMDMs.

Primary BMDMs from LysMCre controls and miR-155$^{fl/fl}$ x LysM^{Cre} mice were plated at 5 x 10^5 cells per well in a 24 well plate and stimulated with 100ng/ml LPS or left unstimulated for 24 hours at 37°C. Cells were stained for surface CD45, CD11b, Ly6C, and MHCII. (A) Representative gating strategy for phenotypic analysis of BMDMs. (B-E) Quantification of the proportion of CD45$^+$CD11b$^+$ BMDMs expressing Ly6C (B,C) and MHCII (D,E). Data represents mean ± S.EM. (n=6, 2 independent experiments).

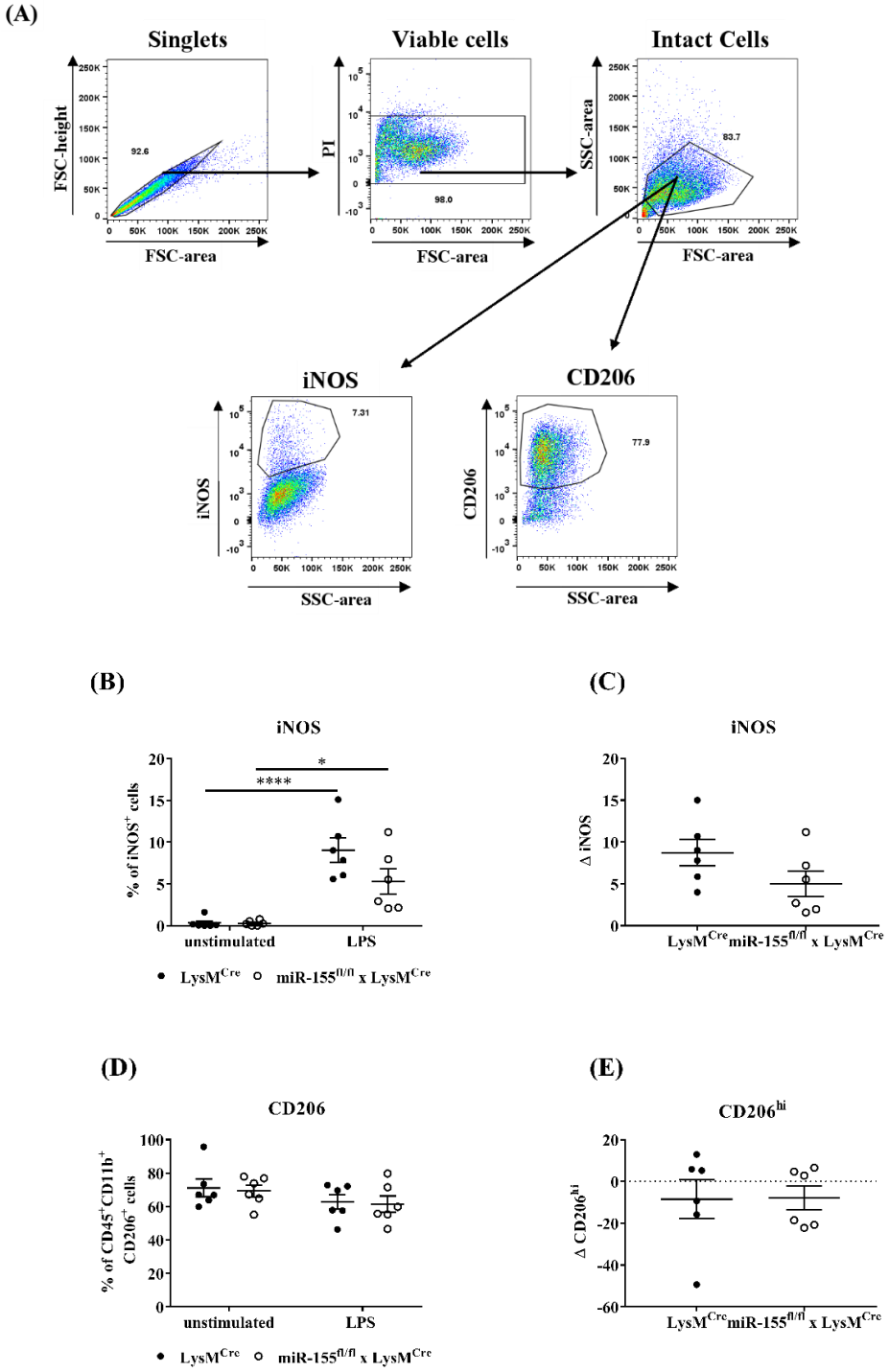

4.9 miR-155 deletion affects intracellular iNOS expression in BMDMs.

Primary BMDMs from LysM^{Cre} controls and miR-155$^{fl/fl}$ x LysM^{Cre} mice were plated at 5 x 10^5 cells per well in a 24 well plate and stimulated with 100ng/ml LPS or left unstimulated for 24 hours at 37°C. Cells were stained intracellularly for iNOS, and CD206. (A) Representative gating strategy for phenotypic analysis of BMDMs. (B-E) Quantification of the proportion of BMDMs expressing iNOS (B,C) and CD206 (D,E). Data represents mean ± S.EM. (n=6, 2 independent experiments). *P<0.05, ***P<0.001; two-way ANOVA with Bonferroni's correction.

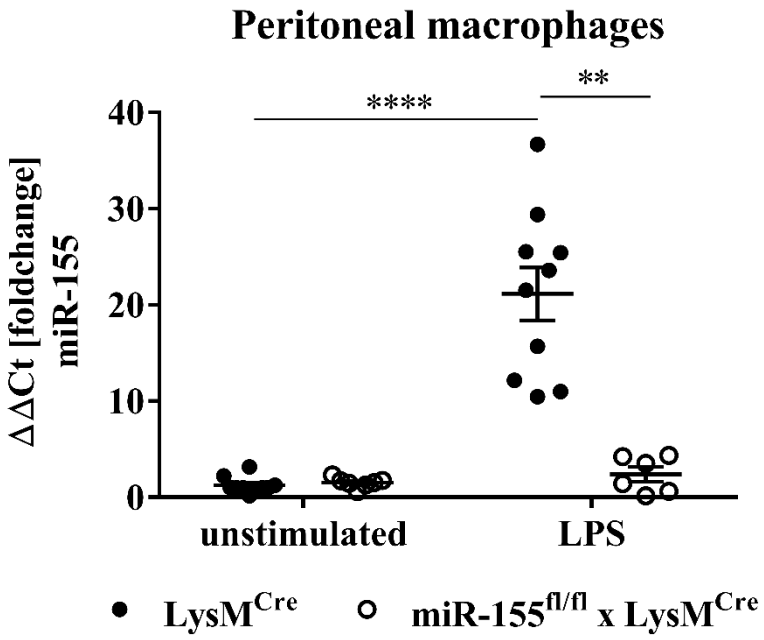

Figure 4.10 miR-155 cannot be induced in miR-155 deleted peritoneal macrophages.

Peritoneal macrophages from LysMCre controls and miR-155fl/fl x LysMCre mice were plated at 3 x 10^5 cells per well in a 24 well plate and stimulated with 100ng/ml LPS or left unstimulated for 18-20 hours at 37°C. Total RNA was extracted and rtPCR and qPCR performed using Taqman probes to determine miR-155 expression. Data represent the ΔΔCT fold induction of miR-155, relative to unstimulated control, normalised against the average of three housekeeping genes sno-202, miR-191, and snU6, and expressed as mean ± S.EM. (n=5-10, 2-4 independent experiments). ****P<0.0001; two-way ANOVA with Bonferroni's correction.

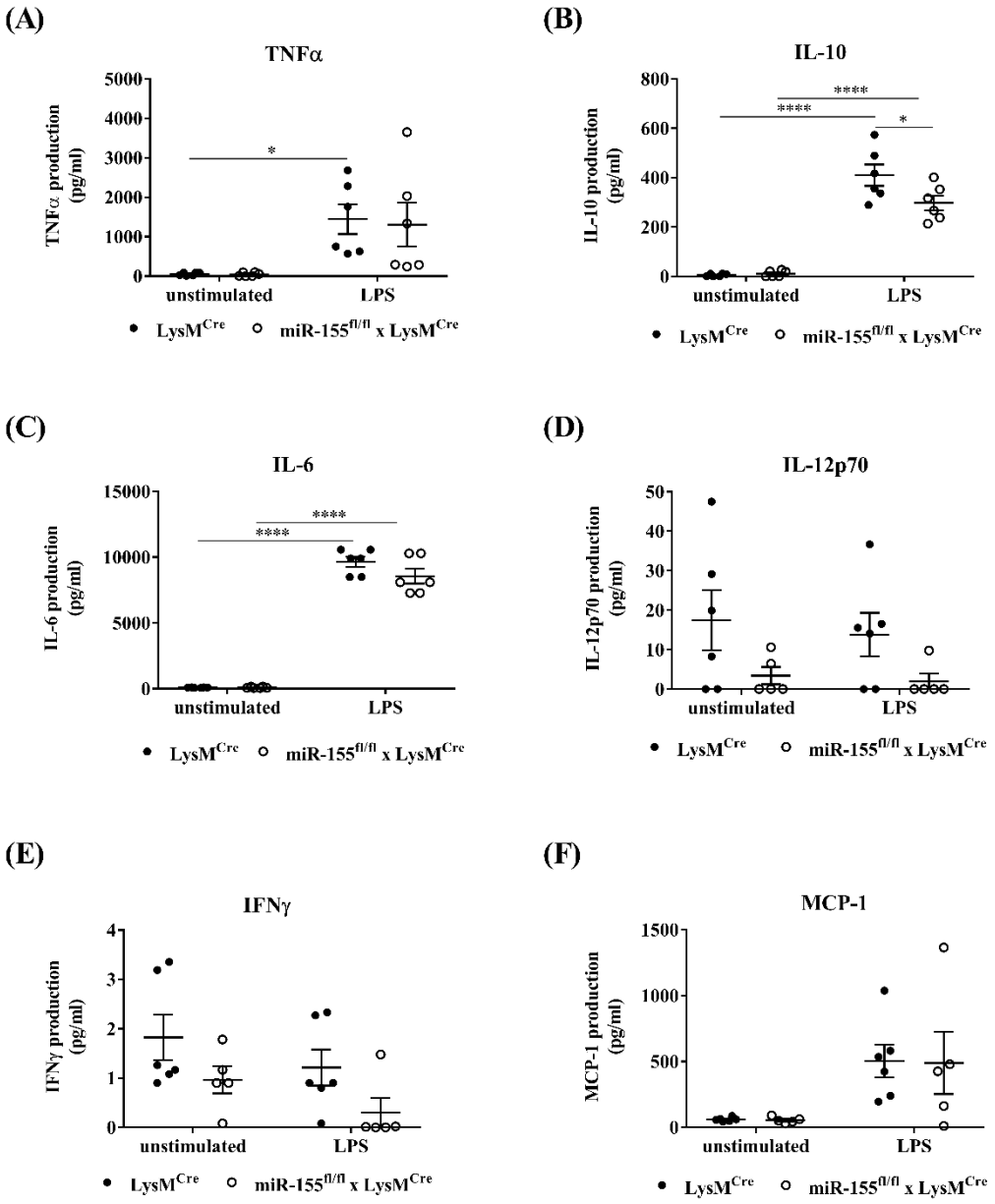

Figure 4.11 miR-155 deletion in peritoneal macrophages affects TNFα and IL-10 production.

Peritoneal macrophages from LysMCre controls and miR-155$^{fl/fl}$ x LysMCre mice were plated at 3 x 10^5 cells per well in a 24 well plate and stimulated with 100ng/ml LPS or left unstimulated for 18-20 hours at 37°C. Supernatants were collected and secreted cytokines were quantified using a BD™ Cytometric Bead Array (CBA) kit. Data represents mean ± S.EM. (n=6, 2 independent experiments). *P<0.05, ****P<0.0001; two-way ANOVA with Bonferroni's multiple comparisons test.

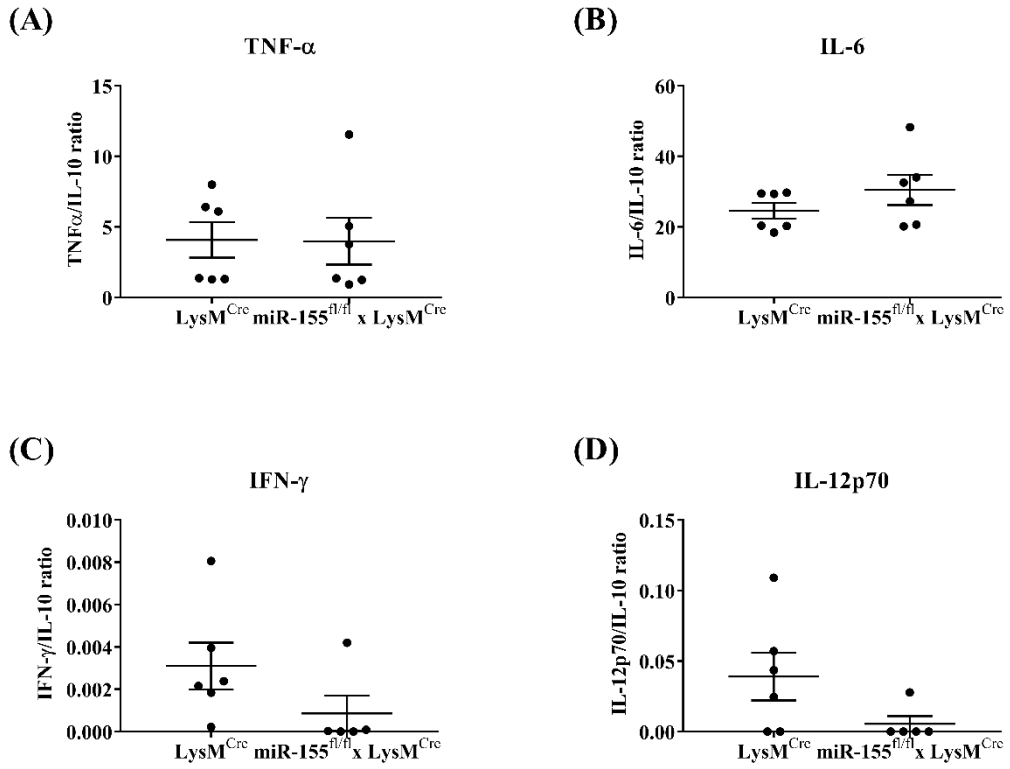

Figure 4.12 miR-155 deletion in peritoneal macrophages does not affect proinflammatory cytokine ratios to IL-10 in response to LPS.

Peritoneal macrophages from LysMCre controls and miR-155$^{fl/fl}$ x LysMCre mice were plated at 3 x 10^5 cells per well in a 24 well plate and stimulated with 100ng/ml LPS or left unstimulated for 18-20 hours at 37°C. Supernatants were collected and secreted cytokines were quantified using a BD™ Cytometric Bead Array (CBA) kit. Data represents mean ± S.EM. (n=5-6, 2 independent experiments).

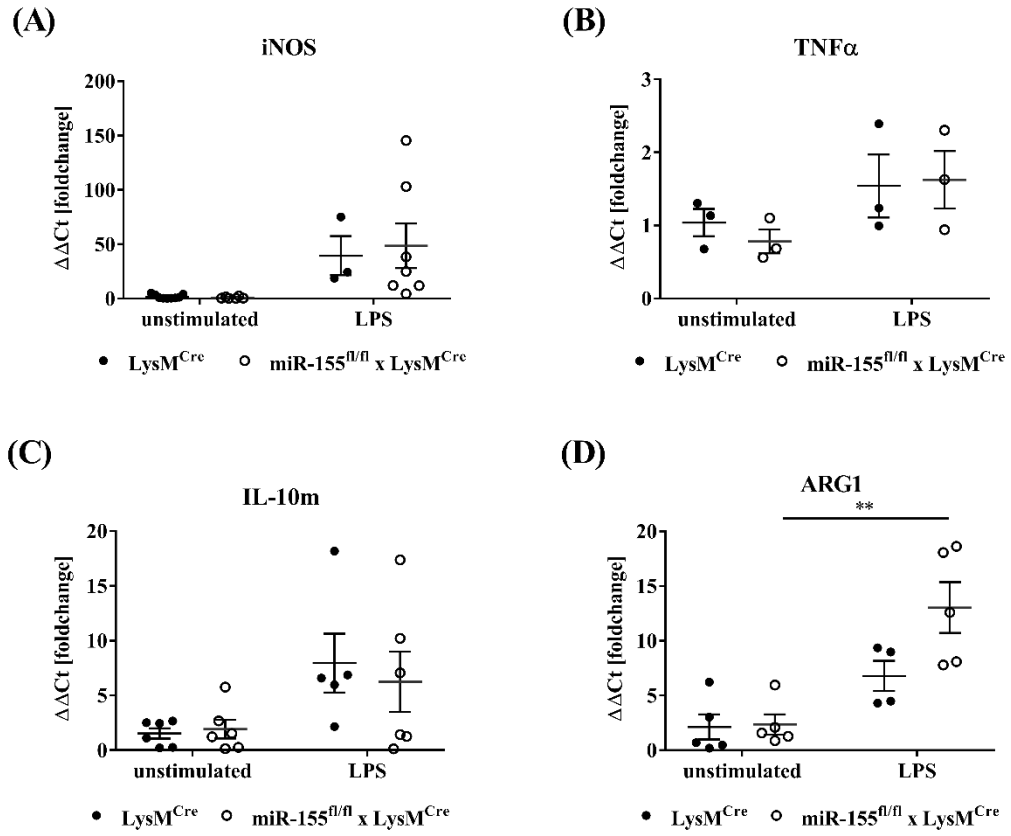

Figure 4.13 miR-155 deletion affects *Arg1* gene expression in peritoneal macrophages.

Peritoneal macrophages from LysMCre controls and miR-155$^{fl/fl}$ x LysMCre mice were plated at 3 x 10^5 cells per well in a 24 well plate and stimulated with 100ng/ml LPS or left unstimulated for 18-20 hours at 37°C. Total RNA was extracted and rtPCR and qPCR performed to determine (A) *Inos* (B) *Tnfα* (C) *Il10m* and (D) *Arg1* expression. Data represent the ΔΔCT fold induction relative to unstimulated control, normalised against the average of two housekeeping genes *m18s* and *Gapdh*, and expressed as mean ± S.EM. (n=3-7, 1-3 independent experiments).

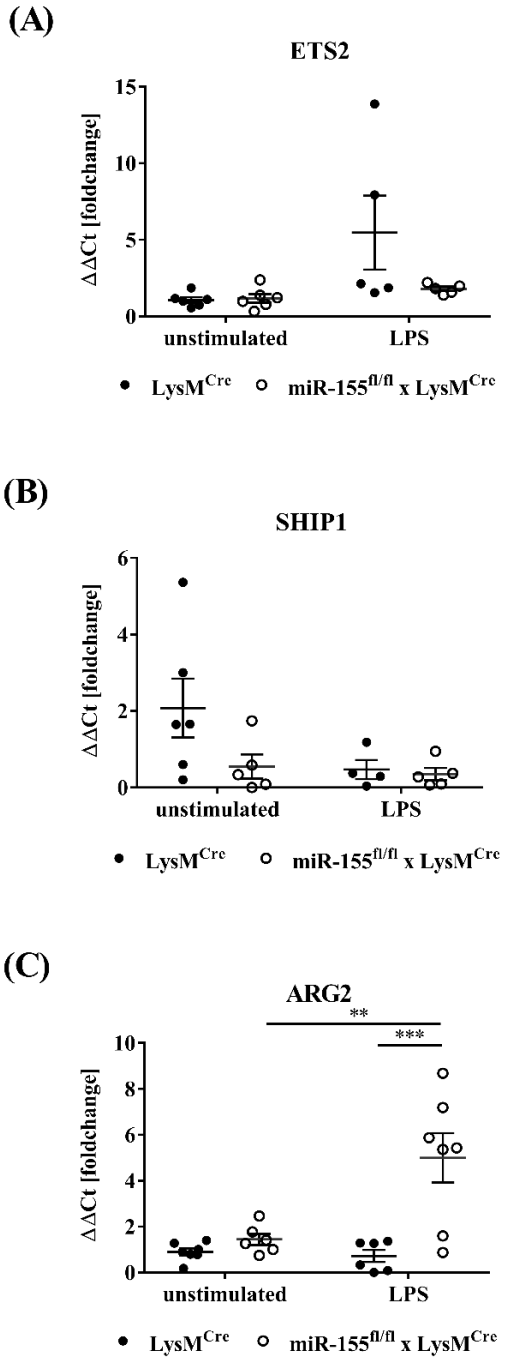

Figure 4.14 miR-155 deletion affects *Arg2* gene expression in peritoneal macrophages.

BMDMs from LysMCre controls and miR-155$^{fl/fl}$ x LysMCre mice were plated at 3 x 10^5 cells per well in a 24 well plate and stimulated with 100ng/ml LPS or left unstimulated for 18-20 hours at 37°C. Total RNA was extracted and rtPCR and qPCR performed to determine (A) *Arg1*, (B) *Arg2*, and (C) *Ship1* expression. Data represent the ΔΔCT fold induction relative to unstimulated control, normalised against the average of two housekeeping genes *GAPDH* and *m18s*, and expressed as mean ± S.EM. (n=4-7, 2-3 independent experiments). **P<0.001, ***P<0.001; two-way ANOVA with Bonferroni's correction.

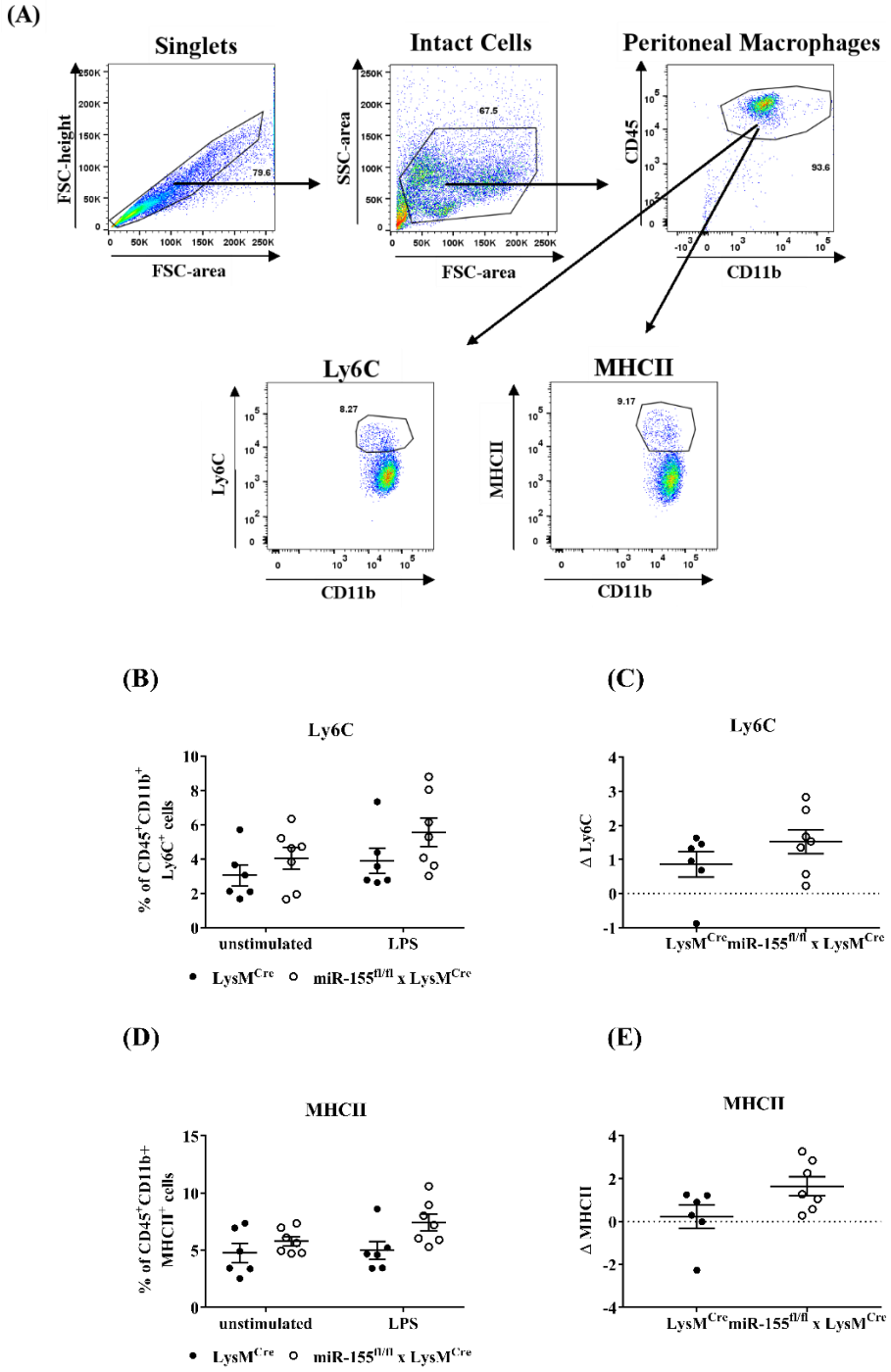

4.15 miR-155 deletion does not significantly affect surface phenotypes of peritoneal macrophages.

Peritoneal macrophages from LysMCre controls and miR-155$^{fl/fl}$ x LysM^{Cre} mice were plated at 3 x 10^5 cells per well in a 24 well plate and stimulated with 100ng/ml LPS or left unstimulated for 18 hours at 37°C. Cells were stained for surface CD45, CD11b, Ly6C, and MHCII. (A) Representative gating strategy for phenotypic analysis of peritoneal macrophages. (B-E) Quantification of the proportion of CD45$^+$CD11b$^+$cells expressing Ly6C (B,C) and MHCII (D,E). Data represents mean ± S.EM. (n=6-7, 2 independent experiments).

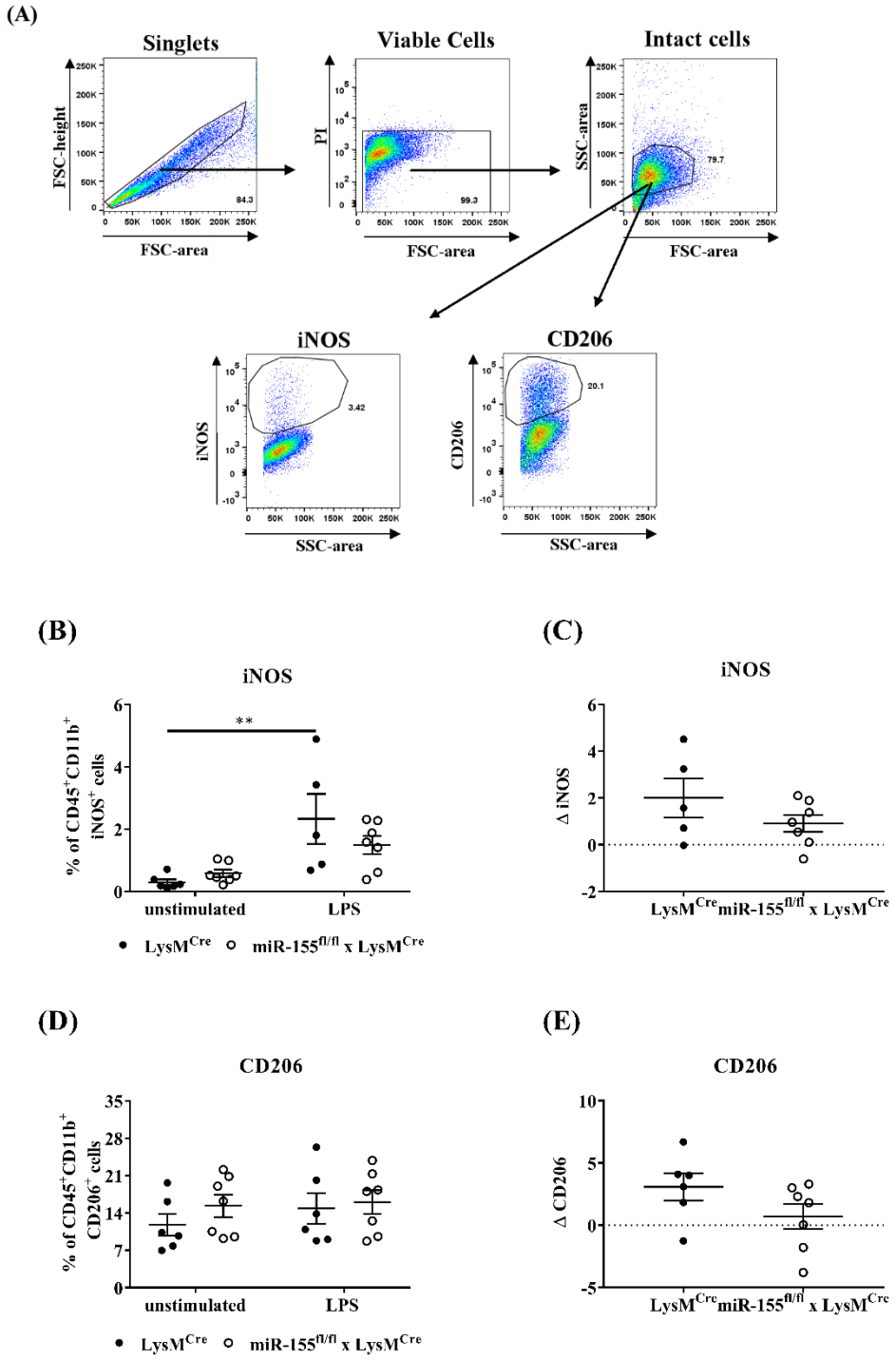

4.16 miR-155 deletion affects intracellular iNOS expression in peritoneal macrophages.

Peritoneal macrophages from LysM^{Cre} controls and miR-155$^{fl/fl}$ x LysM^{Cre} mice were plated at 3 x 10^5 cells per well in a 24 well plate and stimulated with 100ng/ml LPS or left unstimulated for 18 hours at 37°C. Cells were stained intracellularly for iNOS, and CD206. (A) Representative gating strategy for phenotypic analysis of peritoneal macrophages. (B-E) Quantification of the proportion cells expressing iNOS (B,C) and CD206 (D,E). Data represents mean ± S.EM. (n=6-7, 2 independent experiments). **P<0.005; two-way ANOVA with Bonferroni's correction.

4.3 Discussion

Macrophages are highly plastic and have the ability to switch functional activation states based on their exposure to environmental conditions. In the context of tissue injury, they have important roles in promoting the resolution phase of inflammation. Therefore, exploiting the regenerative properties of these immune cells appears to be a promising therapeutic opportunity for chronic inflammatory disorders (Y. Wang *et al.*, 2019). During the progression of MS, remyelination fails over time with increased age and lesion burden (Kuhlmann *et al.*, 2008). As evidenced by animal studies of MS, proinflammatory macrophages polarise towards anti-inflammatory and immunoregulatory phenotypes at initial stages of remyelination. Moreover, macrophages were confirmed as essential for efficient remyelination as depleting anti-inflammatory macrophage populations suppressed oligodendrocyte differentiation and limited repair (Veronique E. Miron *et al.*, 2013). Therefore, this Chapter explored whether miR-155 deletion could influence macrophage polarisation upon LPS stimulation and shift the activation state towards that of an anti-inflammatory phenotype.

To harness macrophages for tissue repair, it is important to understand the molecular basis for their dynamic changes in polarisation states during pathophysiological conditions. Specifically, elucidating how a critical microRNA of the immune system such as miR-155 plays a role in regulating macrophage plasticity, is invaluable information for developing strategies that promote pro-regenerative macrophage phenotypes in the context of MS. To further evaluate miR-155's role in macrophages, a novel mouse strain was generated where miR-155 was genetically deleted in cells of the myeloid lineage. Prior to exploring the impact of this deletion *in vivo*, it was essential to first establish preliminary evidence *in vitro*. Therefore, the objective of this Chapter was to investigate the role of miR-155 in macrophage polarisation by solely investigating two distinct macrophage populations: bone marrow derived macrophages (BMDMs) and peritoneal macrophages stimulated with a potent inflammatory agonist, LPS.

Monocytes circulating in the periphery during EAE infiltrate the CNS and are associated with enhanced disease severity. In the presence of GM-CSF, they are released from the bone

marrow to replenish the circulating monocytes pool (King, Dickendesher and Segal, 2009). BMDMs were used in this Chapter because it is a known occurrence during inflammatory stress that myeloid cells are produced in abundance from the bone marrow before being recruited to the CNS in EAE (King, Dickendesher and Segal, 2009; Julie M Rumble *et al.*, 2015). Therefore, it would be useful to study the effects of miR-155 deletion in BMDMs, since these cells give rise to the monocytes that traffic to and infiltrate the CNS and promoting inflammation.

Peritoneal macrophages are a distinct subset of tissue resident macrophages that patrol and communicate with other immune cell subsets under steady state conditions. It is valuable to study these fully differentiated macrophages alongside BMDMs considering the functional heterogeneity amongst macrophages, both in the steady state and under pathophysiological conditions. Moreover, examining peritoneal macrophages allows the investigation of miR-155 deletion in a mature tissue resident cell type that is maintained by localised proliferation rather than differentiation from precursors released from bone marrow during inflammatory stresses (Mosser and Edwards, 2008).

Once miR-155 deletion was validated in BMDMs and peritoneal macrophages, initial studies performed in this Chapter investigated how the absence of miR-155 impacted the cytokine secretion profile of BMDMs. No significant changes were evident from the six cytokines measured in BMDMs upon miR-155 deletion, although a trend of increased IL-10 and decreased TNF-α was observed in the presence of LPS. Separate studies support these findings as the first miR-155 transgenic KO model exhibited altered immune response, including a reduction in IFN-γ and increase in IL-10 production, along with increased IL-4 and IL-2 in $CD4^+$ T cells treated with anti-CD20 and CD28 (Rodriguez *et al.*, 2007b).

A study performed by Tili et al. utilising transgenic Eμ-miR-155 mice demonstrated that overexpression of miR-155 altered proinflammatory cytokine signatures (Tili *et al.*, 2007). Enhanced TNF-α production in the sera of Eμ-miR-155 was observed upon administering i.p LPS compared to WT controls (Tili *et al.*, 2007). This finding correlates with this research project where miR-155 expression was positively associated with TNF-α. For example, data

from this Chapter demonstrated that miR-155 deletion in BMDMs caused a reduction in TNF-α gene expression. Literature surrounding TNF-α in relation to MS and its animal model EAE are contradictory. The complexity of TNF-α in a pre-clinical setting is highlighted by a study performed by Frei et al. Frei demonstrated that SJL/J mice with inactivated *Tnf* and *Ita* genes backcrossed with C57BL/6 displayed a delayed onset of actively induced EAE clinical scores. However, these mice additionally progressed to develop enhanced EAE severity (Frei *et al.*, 1997). Corroborating this finding, previous MS clinical trials focussing on blocking TNF-α surprisingly exacerbated MS symptoms rather than alleviating disease progression (BGW, 1999). Due to conflicting correlations of TNF-α deletion with accelerating disease progression, further studies on how miR-155 deletion impacts TNF-α and if this impact is beneficial to assist attenuation of inflammatory processes are required.

IL-10 plays an important protective role during the pathogenesis of EAE. IL-$10^{-/-}$ mice induced with EAE display accelerated clinical scores (Samoilova, Horton and Chen, 1998). In contrast, mice injected with IL-10 producing Th2 cells post EAE induction were disease resistant (Cua *et al.*, 1999). More recently, Payne et al. demonstrated that human mesenchymal stem cells derived from adipose tissue constitutively expressing IL-10, termed Adi-IL-10-MSC, attenuated the ability of bone marrow derived DCs to antigen present, and produce inflammatory cytokines *in vitro*. Most importantly, Payne showed administration of Adi-IL-10-MSCs via i.p. caused ameliorated disease severity, in part due to a reduction in the priming of encephalitogenic T cells (Payne *et al.*, 2013). Therefore, increased IL-10 production from miR-155 deleted macrophages *in vitro*, and in *in vivo* animal models, suggests that therapeutic inhibition of miR-155 could contribute to the beneficial effects mediated by IL-10 in MS and its EAE animal model.

Intriguingly, cytokine profiles observed in peritoneal macrophages from this Chapter were not entirely consistent with BMDM cytokine profiles, whereby IL-10 production was decreased in the absence of miR-155 in peritoneal macrophages yet increased in BMDMs. This opposing effect of IL-10 production in BMDMs compared to peritoneal macrophages highlights the heterogeneity of macrophage subsets and their ability to respond to inflammatory stresses. A potential cause for this contrasting finding could be due to the

existence of diverse macrophage populations residing within the peritoneal cavity. A separate study surrounding the properties of peritoneal macrophages reported morphological differences between macrophage populations (Cassado, Lima and Bortoluci, 2015). Furthermore, Cassado et al. found two macrophage populations co-exist within the peritoneal cavity, which are theorised to originate from the macrophage granulocyte progenitor (GMP), and the common myeloid progenitor (CMP). Large peritoneal macrophages (LPM) are considered the most abundant subset and derived from the GMP. This subset expresses low MHCII expression and can be distinguished from small peritoneal macrophages (SPM) by higher expression levels of F4/80 and CD11b. SPMs are considered derivatives of the CMP and are the least abundant macrophage subset in steady state conditions. Upon in vivo inflammatory stresses, SPMs outnumber LPMs as they have greater capacity to upregulate MHCII, CD62L, and DC-sign (Cassado, Lima and Bortoluci, 2015). Considering two macrophage populations within the peritoneal cavity exert diverse properties during inflammation, it was possible that cytokine findings from this Chapter were predominantly derived from LPMs rather than SPMs. Moreover, miR-155 deletion elicited no significant differences in Ly6C or MHCII expression in peritoneal macrophages. Considering Cassado's findings surrounding LPMs and SPMs abilities to upregulate MHCII (Cassado, Lima and Bortoluci, 2015), it is possible that phenotypic analysis data are also relating to LPMs.

Future experiments should involve measuring proinflammatory cytokine IL-1β as it plays a prominent role in EAE progression (Lin and Edelson, 2017; Paré *et al.*, 2018). Literature supports a relationship between miR-155 and IL-1β where miR-155 is confirmed to be involved in a negative feedback loop in mature human DCs. Ceppi et al. demonstrated that DCs exhibited a reduction of IL-1β production that was reportedly mediated by miR-155 via targeting TAB2, a signal transducer (Ceppi, A. M. Pereira, *et al.*, 2009). Therefore, it would be interesting to evaluate the effects of miR-155 deletion on IL-1β production in the context of EAE, to determine whether this negative feedback-loop would exist in a pre-clinical model of MS.

Examining gene profiles of miR-155 deficient BMDMs revealed key polarisation characteristics of these cells, whereby both *Inos* and *Tnfα* gene expression were found

decreased in miR-155 deficient BMDMs. A separate study investigating *Inos* and *Tnfα* expression have previously observed a 72% downregulation of *Inos* and *Tnfα* in genetically deficient miR-155 BMDMs compared to WT controls (Kyle A Jablonski *et al.*, 2016). Although this Chapter corroborates these findings by Jablonski et al., there appears to be a larger decrease in *Inos* and *Tnfα* from this separate study. This could perhaps be due to Jablonski utilising total genetically deficient mice rather than miR-155$^{fl/fl}$ x LysMCre mice where separate studies report <100% deletion efficiency when using cre recombinase for gene deletion (Abram *et al.*, 2014). Jablonski et al. collectively established the importance of miR-155's effects on iNOS and TNF-α in macrophages via RT-PCR (Jablonski *et al.*, 2016). In the context of immune cells involved in the pathogenesis of EAE, myeloid derived macrophages and CNS resident macrophages (microglia), miR-155 was confirmed to exhibit increased IL-1, TNF-α, iNOS, and IL-6 in WT controls compared to miR-155$^{-/-}$ mice. Additionally, increased miR-155 was associated with decreased cell apoptosis, IL-10, ARG1, and TGF-βR (Ponomarev, Veremeyko and Weiner, 2013). More importantly, NO production, a by-product of *Inos* in macrophages, is confirmed to cause neurotoxicity within the CNS (Desai and Smith, 2017). Therefore, it would be interesting to measure NO production in miR-155 deleted BMDMs and peritoneal macrophages via a Greiss assay to determine the impact of miR-155 on NO production.

Although there were differences in cytokine production between BMDMs and peritoneal macrophages, there were striking similarities between immunoregulatory genes: *Arg1* and *Arg2*. ARG1 is an important gene in identifying immunoregulatory macrophage polarisation *in vitro* (Hannemann *et al.*, 2019). This gene was found to be upregulated in macrophages within the CNS during recovery stages of EAE (Greenhalgh *et al.*, 2016). Confirming with this finding, Giles et al. showed the presence of ARG1 expressing myeloid cells immediately prior to remission stages in EAE, and recognised the regenerative ability of these cells (David A Giles *et al.*, 2018). Within this Chapter, the correlation between *Arg1* induction in miR-155 deficient BMDMs and peritoneal macrophages, along with literature surrounding reparative phenotypes of macrophages exhibiting increased ARG1 within the CNS, strongly suggests an immunoregulatory role for these cells *in vitro* and potentially *in vivo.* Collectively, an increase in ARG1 supports the hypothesis that miR-155 deletion in BMDMs and peritoneal macrophages is associated with anti-inflammatory macrophage polarisation and a functional activation state that could potentially protect against chronic inflammation.

In relation to how miR-155 may affect ARG1 expression, there are currently no literature confirming ARG1 as a direct target of miR-155. However, the McCoy lab has performed analysis which suggests that the 3'UTR of ARG1 contains a miR-155 seed region, a preliminary finding that warrants further investigation. Additional potential avenues as to how miR-155 may affect ARG1 expression include interfering with STAT3. STAT3 is a known regulator of ARG1 expression (Vasquez-dunddel *et al.*, 2013), hence there is a possibility of miR-155 indirectly regulating ARG1 expression by directly targeting SOCS1, a downstream signalling molecule of STAT3 (L. Zhang *et al.*, 2017). Additionally, elevated IL-10 has strong associations with increased ARG1 expression (Deng *et al.*, 2012; Makita *et al.*, 2015), therefore perhaps enhanced IL-10 production mediated by miR-155 deletion is an indirect mechanism of increasing ARG1. Further investigation into signalling and targeted pathways of these anti-inflammatory markers is required to verify their positive feedback mechanisms. Interestingly, during neuroinflammation ARG1 exerts properties known to be reflective of anti-inflammatory macrophage phenotypes and is associated with enhanced recovery in EAE (Veronique E. Miron *et al.*, 2013). Furthermore, it is reportedly expressed solely on infiltrating myeloid cells and not microglia during certain timepoints in EAE (Greenhalgh *et al.*, 2016). It would also be worth investigating whether miR-155 deletion could impact tissue repair abilities mediated by an ARG1 mechanism.

In contrast to ARG1, the role of ARG2 in inflammatory disease has not yet been fully explored. Within this Chapter, this novel miR-155 target and immunoregulatory gene marker was highly induced in both BMDMs and peritoneal macrophages. Furthermore, results from Chapter 3 revealed that *Arg2* expression was repressed in myeloid cells/microglia throughout EAE in WT mice. Additionally, *Arg2* had an inverse correlation with miR-155 expression, which was increased and sustained at all EAE time-points. Collectively, data from this project suggest that ARG2 may be required for protection in EAE. In support of these findings, this is consistent with the reported role of ARG2 in osteoarthritis, hypertension, and *H. pylori* infection. For example, genetically deficient ARG2 mice exhibited enhanced disease pathology in osteoarthritis as macrophages were polarised towards a proinflammatory phenotype and facilitated in driving inflammation (Greenhalgh *et al.*, 2016). A separate study utilising *Arg2-/-* mice in a model of hypertension also demonstrated enhanced proinflammatory macrophage phenotypes during hypoxia-induced pulmonary hypertension (Johann *et al.*, 2007). In the context of bacterial infections, ARG2 deletion in

macrophages additionally promoted proinflammatory phenotypes, thus leading to improved clearance of infection when mice were challenged with *H. pylori*. This suggests the presence of ARG2 plays a protective role during bacterial infections in that it prevents clearance of the bacteria by the host immune response (Greenhalgh *et al.*, 2016). In contrast to these studies demonstrating enhanced proinflammatory responses upon ARG2 deletion, a separate study emerged surrounding the role of ARG2 in EAE. Choudry et al. reported amelioration of EAE disease scores and decreased demyelination upon global deletion of ARG2 through a null mutation, overall suggesting a role for ARG2 in driving inflammatory responses and demyelinating processes (Choudry *et al.*, 2018). Using a MOG peptide inducible model of EAE, Choudry et al. demonstrated ARG2 deficiency supressed IL-23 and IL-6 production by DCs, essential cytokines for Th17 differentiation within the spinal cord. Collectively, Choudry suggested ARG2 expression in DCs could facilitate Th17 differentiation, thus promoting EAE progression (Choudry *et al.*, 2018). This study conflicts with findings generated from this project and other disease models illustrating how ARG2 exhibits an anti-inflammatory and reparative phenotype in macrophages. This conflicting study highlights how further investigations surrounding ARG2 in disease models are required to fully elucidate the role of ARG2. Moreover, utilising conditional ARG2 deficient models would be beneficial where the role of ARG2 could be directly assessed in individual immune cell subsets. Although ARG2 mechanisms in macrophages are not yet fully understood in all disease model contexts, it is evidently clear from this Chapter that ARG2 is significantly upregulated in miR-155 deleted macrophages derived from both the bone marrow and peritoneal cavity during *in vitro* studies. This finding surrounding ARG2, in addition to the upregulation of ARG1, collectively suggests that macrophages are exhibiting immunoregulatory phenotypes in the absence of miR-155.

Collectively, gene expression data derived from miR-155 deleted BMDMs demonstrated a decrease in proinflammatory genes (*Tnf-α* and *Inos*). Additionally, anti-inflammatory genes were increased in both miR-155 deleted BMDMs and peritoneal macrophages (*Arg1,* and *Arg2*). Overall, strongly suggesting that miR-155 deletion in macrophage populations skew macrophage properties towards an anti-inflammatory phenotype.

LPS was used to stimulate macrophage populations in this Chapter as it is a potent agonist of miR-155 induction and is confirmed to polarise cells to proinflammatory phenotypes. Ample studies demonstrate the potent proinflammatory effect of LPS on monocytes and macrophages, resulting in excessive production of cytokines (IL-1, IL-6, TNF-α) mediated by the TLR4 signalling pathway (Fujihara *et al.*, 2003). Even though LPS signals through the same TLR4 pathway as M. Tuberculosis and Pertussis toxin, it is not a component of the active immunisation procedure for EAE induction, or directly involved in facilitating demyelination processes during EAE progression. Therefore, using this stimulant may be considered a limitation. Future studies aimed at further understanding how miR-155 deletion affects macrophage polarisation in the context of EAE could employ recombinant cytokines that drive neuroinflammation as stimulants. Such cytokines could include IFN-γ, TNF-α, GM-CSF, and IL-1β. These cytokines are all involved in the immunopathogenesis of EAE and could unveil new aspects of how miR-155 deletion in the presence of EAE related cytokines affects BMDM and peritoneal macrophage phenotypes.

Future investigations could be directed towards the functional consequences of deleting miR-155. For example, how miR-155 deletion could affect T cell priming towards specific T cell subsets and how this deletion may enhance phagocytosis abilities of macrophages to facilitate debris clearance and myelin. The clearance of myelin debris is an essential process for oligodendrocyte differentiation and remyelination at lesion sites (Lloyd and Miron, 2019). Investigating how miR-155 deletion affects the ability of macrophages to phagocytose myelin debris material *in vitro*, and thus potentially assist in remyelination, could offer great insight into how miR-155 affects functional properties of macrophages. Additional studies to further understand how miR-155 deletion in macrophages affects communication with the adaptive immune system during disease includes investigating T helper cell differentiation. O' Connell et al. verified that miR-155 was essential for LPS treated DCs to induce Th17 cell differentiation (O'Connell, Kahn, William S.J. Gibson, *et al.*, 2010). Moreover, Th17 cell differentiation is pivotal for onset of EAE (Jin *et al.*, 2009). Therefore, performing co-culture studies to measure naïve T cell differentiation, proliferation and cytokine production via co-culture experiments could contribute to understanding the involvement of miR-155 in MS.

In summary, investigating miR-155 deletion in two distinct macrophage populations provided useful information regarding the role of this inflammatory miRNA in macrophage polarisation *in vitro*. Although differential production and expression of TNF-α and *Il-10m* was observed between BMDMs and peritoneal macrophages respectively, it was clear that the arginase isoforms were consistently increased by LPS in miR-155 deleted conditions. Due to the role of these genes with macrophages *in vitro* and their protective roles *in vivo*, miR-155 deletion in this immune subset could prove promising as a therapeutic target in promoting immunoregulatory macrophage phenotypes. Lastly, due to the heterogeneity of macrophages *in vitro* and *in vivo*, it is essential that miR-155 deletion is explored in an *in vivo* model of EAE to characterise the role of miR-155 in CNS infiltrating myeloid-derived immune cells.

Chapter 5

The role of miR-155 in miR-155$^{fl/fl}$ x LysM^{Cre} mice

5.1 Introduction

MiR-155 plays a critical role in regulating inflammatory responses in all cells of the immune system. It is an essential miRNA for successful clearance of pathogens, but persistent overexpression of miR-155 is detrimental in chronic diseases such as MS (Thamilarasan *et al.*, 2012; Jevtić *et al.*, 2015). There have been numerous studies that support the importance of miR-155 in driving immune responses in MS. The first total miR-155 KO study carried out by O'Connell et al. in 2010 established miR-155 as a crucial player in EAE, by demonstrating total miR-155$^{-/-}$ mice are resistant to disease. Moreover, although O'Connell mainly focussed on T cell development and IL-17/IFN-γ producing CD4^{+} T cells, myeloid derived dendritic cells were proven necessary for production of Th17 polarising cytokines, emphasising the important role of myeloid cells in EAE (O'Connell *et al.*, 2010). Another study demonstrating that miR-155 antagomirs can alleviate clinical disease, further confirmed the importance of miR-155 in EAE, and most importantly highlighted that it can be targeted therapeutically (Murugaiyan et al., 2011).

The above pre-clinical evidence is strengthened by insightful studies surrounding miR-155 in human MS patients. One research group demonstrated relative miR-155 expression decreased in patients undergoing remission compared to relapsing patients, suggesting elevated miR-155 expression aids in disease progression (Zhang *et al.*, 2014). In terms of a potential role for miR-155 in the genetic predisposition to MS, a total of three SNPs were verified within the last exon of the BIC gene that correlated with MS (Paraboschi *et al.*, 2011). In the context of active MS lesions, Junker et al. demonstrated by using laser capture microdissections that astrocytes upregulated miR-155 expression within MS lesions (Junker *et al.*, 2009). Additionally, miR-155 was documented to target and significantly downregulate CD47 in active MS lesions when compared to normal white matter regions. Since CD47 is a macrophage marker of supressing cell activation, and a 'don't eat me' signal, Junker et al. suggested that miR-155 facilitated macrophage activation and phagocytosis by mediating CD47 downregulation (Junker *et al.*, 2009). Although these studies reveal the importance of miR-155 in MS, much information is yet to be explored surrounding its specific role in myeloid cells such as macrophages.

In the context of EAE pathogenesis, proinflammatory macrophages and microglia facilitate demyelination through their secretion of proinflammatory cytokines such as IFN-γ, TNF-α, GM-CSF, and IL-1β (Croxford, Spath and Becher, 2015; Chu *et al.*, 2018). Both macrophages and microglia have abilities to undergo polarisation and phenotypically switch into either a proinflammatory or anti-inflammatory phenotype, hence the garnered interest to harness anti-inflammatory properties of these immune cells for therapeutic options (Chu *et al.*, 2018). Although miR-155 is recognised to intervene with macrophages proinflammatory cytokine production, certain mechanisms surrounding the involvement of miR-155 in macrophages appear overlooked in previous studies utilising miR-155$^{-/-}$ mice. Moreover, there are major gaps in knowledge investigating the role of miR-155 in immune cells throughout an entire EAE time-course from early to late stages of disease progression. Tracking the role of miR-155 in macrophages proves important, as several studies verify a polarisation switch of macrophages towards an anti-inflammatory phenotype during middle to later stages of EAE, a plasticity switch deemed essential for CNS remyelinating process and repair (Kyle A Jablonski *et al.*, 2016). Investigating how and when miR-155 assists in controlling macrophages proinflammatory and immunoregulatory capabilities throughout EAE can exploit these mechanisms to promote CNS remyelination, an essential CNS repair process that is not promoted through any current FDA approved MS therapies (Baecher-Allan, Kaskow and Weiner, 2018). As illustrated in Chapter 4 where miR-155 deletion promotes an anti-inflammatory phenotype, along with separate studies highlighting miR-155 can influence macrophage polarisation (Li *et al.*, 2018), targeting miR-155 appears promising to suppress neuroinflammation during EAE. Therefore, utilising a novel approach of deleting miR-155 in myeloid with miR-155$^{fl/fl}$ x LysMCre mice creates an opportunistic window for exploring miR-155 mediated mechanisms exclusively in myeloid cells during EAE progression.

Collectively, the purpose of this Chapter is to evaluate how miR-155 deletion in immune cells of the myeloid lineage impacts the immunopathogenesis of EAE. Assessing miR-155 deletion in myeloid cells derived from miR-155$^{fl/fl}$ x LysM^{Cre} mice in rMOG induced EAE is a novel approach to understand how miR-155 influences macrophages, microglia and neutrophils. The overall objective of this chapter will be investigated by the following aims:

1. To confirm miR-155 deletion in CNS infiltrating myeloid cell subsets of miR-155$^{fl/fl}$ x LysM^{Cre} mice at critical time points during EAE.
2. To investigate the impact of miR-155 deletion in myeloid cells on CNS immune cell subset populations in miR-155$^{fl/fl}$ x LysM^{Cre} mice at key timepoints throughout EAE.
3. To assess if miR-155 deletion in myeloid cells alters the phenotype of CNS immune cell subsets from miR-155$^{fl/fl}$ x LysM^{Cre} mice at key stages in EAE.
4. To evaluate the impact of miR-155 deletion in myeloid cells on clinical progression and pathology in miR-155$^{fl/fl}$ x LysM^{Cre} mice compared to LysM^{Cre} controls throughout an EAE time course.

5.2 Results

5.2.1 Clinical scores of EAE using 65µg rMOG

To investigate the role of miR-155 in myeloid cells throughout EAE, C57BL/6 LysM^{Cre} controls and miR-155$^{fl/fl}$ x LysM^{Cre} mice were immunised with 65µg rodent recombinant MOG protein in CFA and 200ng *Pertussis* toxin to induce chronic progressive EAE. Initial studies investigated how miR-155 deletion in myeloid cells affected EAE progression through daily observations of clinical disease throughout a 26-day EAE time course. Mice were clinically scored by grading levels of paralysis via the same clinical scoring system previously utilised in Chapter 3 (1. Limp tail 2. Weak hind legs 3. Paralysed hind limbs 4. Weak forelimbs 5. Moribund/ dead).

Figure 5.1 shows the clinical scores of LysM^{Cre} controls and miR-155$^{fl/fl}$ x LysM^{Cre} mice throughout the 26-day time course. The mean onset of clinical disease occurred day 12 (S.E.M ± 0.89) in LysM^{Cre} controls. Clinical scores of EAE then plateaued from days 18-21 before slightly remitting in the chronic stages of EAE from days 22-26. LysM^{Cre} controls exhibited a mean clinical score of 1.84 (S.E.M ± 0.16), and cumulative score of 33 (S.E.M ± 2.91).

Whilst observing miR-155$^{fl/fl}$ x LysM^{Cre} mice, the mean onset of clinical scores occurred on day 9.67 (S.E.M ± 0.37). EAE clinical scores then sharply progressed from days 9-13 with scores ranging from 0.5-3, before plateauing between days 13-16. Lastly, clinical scores gradually remitted during chronic stages of EAE from days 17-26. Collectively, miR-155$^{fl/fl}$ x LysM^{Cre} mice had a mean clinical score of 2.37 (S.E.M ± 0.02), and cumulative score of 41 (S.E.M ± 0.79).

Overall, induction of EAE in miR-155$^{fl/fl}$ x LysM^{Cre} mice with 65µg resulted in accelerated clinical signs of disease when compared to LysM^{Cre} controls. MiR-155$^{fl/fl}$ x LysM^{Cre} mice displayed an earlier onset of clinical scores, accelerated clinical signs, and a higher maximum score and cumulative score, suggesting miR-155 deletion in myeloid cells may contribute to EAE progression in this mouse model when utilising 65µg rMOG.

5.2.2 Myeloid cell populations increase within the CNS at day 14 EAE.

To examine if miR-155 deletion in myeloid cells affected infiltration of immune cell populations within the CNS during EAE, tissue samples were collected from naïve LysM^{Cre} controls and miR-155$^{fl/fl}$ x LysM^{Cre} mice at day 14 post immunisation with 65µg rMOG. Day 14 EAE was chosen since this timepoint was investigated in WT C57BL/6 mice in chapter 3, but there were also marginal differences in the clinical scores between the two mouse strains (Figure 5.1). Figure 5.2A represents the gating strategy used to delineate and sort immune populations within the CNS. All immune cells were initially derived from singlets, viable, and intact cells, prior to being sorted into three immune cell subsets based on their cell surface marker expression. Macrophages were determined as CD45^{hi}Ly6G^{-} CD11b^{+}F4/80^{+} cells, microglia were identified as CD45^{int}Ly6G^{-}CD11b^{+}CX3CR1^{+} cells, and neutrophils were derived from CD45^{+}Ly6G^{+}CD11b^{+} cells.

Figure 5.2B represents the proportion of macrophages within the CNS. While macrophage proportions did increase from 0.44% in naïve samples to 3.31% at day 14 of EAE in LysM^{Cre} controls, this was not statistically significant. Interestingly, the proportion of miR-155 deleted macrophages significantly increased from 0.57% in naïve samples to 4.95% at day 14 EAE (P value 0.0251).

Microglia population proportions are shown in Figure 5.2C. There was a significant decrease in the proportion of microglia in both LysM^{Cre} controls and MiR-155$^{fl/fl}$ x LysM^{Cre} mice when comparing naïve to day 14 of EAE. LysM^{Cre} control microglia proportions significantly decreased from 80.08% to 37.69% (P value 0.0067). Similarly, miR-155$^{fl/fl}$ x LysM^{Cre} microglia significantly decreased from 84.25% to 25.09% (P value 0.0005).

As shown in Figure 5.2C, neutrophil proportions significantly increased from 1.69% in naïve LysM^{Cre} controls to 9.35% at day 14 EAE (P value 0.0013), whereas miR-155$^{fl/fl}$ x LysM^{Cre} neutrophil proportions only slightly increased from 1.53% in naïve samples to 6.14% at day 14 EAE (not significant).

Overall, infiltrating myeloid cell proportions evidently increased within the CNS at day 14 EAE, whereas microglia proportions significantly decreased in EAE. Additionally, there was a noticeable trend that miR-155 deletion in myeloid cells caused slight alterations to the proportion of macrophage, microglia, and neutrophil populations at day 14 EAE, where there were decreased proportions of macrophages but increased neutrophil proportions.

5.2.3 miR-155 cannot be induced in macrophages during EAE.

Population studies within the CNS suggested there were slight variations in myeloid cell populations between LysM^{Cre} controls and miR-155$^{fl/fl}$ x LysM^{Cre} mice at day 14 EAE. Therefore, all three immune populations from LysM^{Cre} controls and miR-155$^{fl/fl}$ x LysM^{Cre} mice were examined for miR-155 induction during EAE to assess if this deletion correlated with population variations. CNS samples were assessed for miR-155 expression in sorted immune cells (derived from section 5.2.2), and data was analysed using the ΔΔCT fold induction method to measure the fold-change of miR-155 in naïve and day 14 EAE immune cell subsets. This method of measuring miR-155 induction would determine how miR-155$^{fl/fl}$ x LysM^{Cre} immune cell subsets induce miR-155 during a timepoint in EAE when a sharp incline of clinical scores occurs in comparison to LysM^{Cre} controls.

As shown in Figure 5.3, macrophages from naïve mice show slight induction of miR-155. MiR-155 expression increased in LysM^{Cre} control macrophages from 1.28-fold in naïve samples to 19.93-fold at day 14 EAE (not significant). Importantly, miR-155 could not be induced in miR-155$^{fl/fl}$ x LysM^{Cre} mice (1.27-fold in naïve mice, 0.19-fold at day 14 of EAE). At this time point, LysM^{Cre} control macrophages displayed significantly higher fold changes of miR-155 compared to miR-155$^{fl/fl}$ x LysM^{Cre} macrophages (P value 0.0454). The induction of miR-155 in LysM^{Cre} controls correlated with that observed in WT C57BL/6 macrophages in Chapter 3 (Figure 3.14A).

MiR-155 fold-change in microglia is represented in Figure 5.3B. In LysM^{Cre} control microglia, there was a trend towards an increased miR-155 expression in naïve samples to day 14 EAE (2.95-fold - 8.00-fold) (not significant). In miR-155$^{fl/fl}$ x LysM^{Cre} microglia, there was relatively no induction of miR-155 in microglia when comparing naïve mice to day 14 EAE (1.74-fold to 3.51-fold). Although not statistically significant, induction of miR-155 was higher in LysM^{Cre} controls at day 14 of EAE compared to miR-155$^{fl/fl}$ x LysM^{Cre} mice.

As illustrated in Figure 5.3C, LysM^{Cre} controls and miR-155$^{fl/fl}$ x LysM^{Cre} neutrophils could not induce miR-155 at day 14 EAE when compared to naïve samples.

In summary, these data showed miR-155 could not be induced in miR-155$^{fl/fl}$ x LysM^{Cre} macrophages at day 14 EAE. Furthermore, miR-155 was relatively reduced in miR-155$^{fl/fl}$ x

LysM^{Cre} microglia when compared to LysM^{Cre} controls, possibly due to miR-155 deletion occurring in multiple cell types, including a percentage of microglia (Blank and Prinz, 2016).

5.2.4 miR-155 absolute values increased in macrophages and microglia in EAE.

Absolute miR-155 copy number values were next assessed in macrophages, microglia, and neutrophils at day 14 EAE. Sorted immune cells from the CNS (derived from Section 5.2.2A) were assessed for miR-155 absolute levels.

Figure 5.4A illustrates miR-155 expression levels in CNS infiltrating macrophages. Macrophages derived from naïve LysM^{Cre} controls demonstrated 127.38 x 10^4 miR-155 absolute number, which relatively increased at day 14 at 966.95 x 10^4. Corroborating with fold change data, miR-155 absolute values derived from miR-155$^{fl/fl}$ x LysM^{Cre} mice did not increase between naïve mice (430.92 x 10^4) to day 14 EAE (48.64 x 10^4).

As outlined in Figure 5.4B, miR-155 absolute values derived from LysM^{Cre} controls were increased from naïve mice at 483.26 x 10^4 to 1350.26 x 10^4 at day 14 EAE (not significant). MiR-155$^{fl/fl}$ x LysM^{Cre} microglia did not increase between naïve and day 14 EAE timepoints (49.03 x 10^4 to 100.75 x 10^4). Additionally, miR-155 expression values were determined significantly less in miR-155$^{fl/fl}$ x LysM^{Cre} mice compared to LysM^{Cre} controls at day 14 EAE (P value 0.0224).

Figure 5.4C represents miR-155 expression levels in neutrophils within the CNS of LysM^{Cre} controls and miR-155$^{fl/fl}$ x LysM^{Cre} mice. MiR-155 absolute values slightly decreased at day 14 EAE (5162.08 x 10^4) in LysM^{Cre} controls compared to naïve LysM^{cre} mice (847.17 x 10^4). Similarly, miR-155 expression derived from miR-155$^{fl/fl}$ x LysM^{Cre} mice slightly decreased at day 14 EAE (5548.67 x 10^4) compared to naïve mice (847.17 x 10^4).

In conclusion, this set of data suggests that the absolute level of miR-155 expression in macrophages and microglia was decreased in miR-155$^{fl/fl}$ x LysM^{Cre} mice at day 14 EAE compared LysM^{cre} controls.

5.2.5 Ly6C, MHCII, and CCR2 expression were increased on macrophages in EAE.

To investigate how miR-155 deletion in myeloid cell populations affect macrophage polarisation *in vivo*, total CNS immune cells isolated from LysM^{Cre} controls and miR-155$^{fl/fl}$

x Lys^{MCre} mice were surface stained to delineate macrophages from other immune cell subsets by: CD45^{hi}Ly6G^{-}CD11b^{+}F4/80^{+}, and stained for phenotypic markers: Ly6C, MHCII, and CCR2, to further illustrate the characteristics of miR-155 deleted macrophages at day 14 EAE.

Figure 5.5A represents the proportion of Ly6C expression on LysM^{Cre} controls and miR-155 deleted macrophages within the CNS. Ly6C expression was significantly increased from naïve LysM^{Cre} control macrophages to day 14 EAE (14.4% to 72.17%) (P value 0.0001), and significantly increased in miR-155 deleted macrophages from 7.22% to 72.5% (P<0.0001). Figure 5.5B represents Ly6C expression in a histogram format, there was a predominant shift of Ly6C expression in naïve macrophages compared to EAE samples when normalised to mode.

As shown in Figure 5.5C, MHCII expression was significantly increased in both LysM^{Cre} controls and miR-155 deleted macrophages at day 14 EAE compared to naïve samples, 3.97%-79.59% on LysM^{Cre} controls, and 7.33%-79.33% on miR-155 deleted macrophages (P<0.0001). Figure 5.5D displays MHCII expression as a histogram format when normalised to mode where an evident shift is present.

CCR2 expression of LysM^{Cre} controls and miR-155 deleted macrophages is shown in Figure 5.5E. CCR2 proportions was significantly increased on LysM^{Cre} controls from 25.92% to 70.8% at day 14 EAE within the CNS (P value 0.0115), whereas CCR2 expression was notably increased on miR-155 deleted macrophages but could not achieve statistical significance (34.13%-65.80%). Figure 5.5F demonstrates a visual representative of the increase in CCR2 expression as a histogram format normalised to mode.

Overall, no statistical significance could be determined between LysM^{Cre} controls and miR-155 deleted macrophages within the CNS at day 14 EAE, however there were notable trends of relative differences in Ly6C and CCR2 expression. Ly6C expression in miR-155 deleted macrophages obtained a higher statistical significance compared to LysM^{Cre} controls, and CCR2 was only significantly increased in LysM^{Cre} controls but not in miR-155 deleted macrophages.

5.2.6 Ly6C and MHCII, expression increase on microglia in EAE.

Previous microglia data generated from this chapter (population studies and miR-155 induction studies) suggests miR-155 deletion in myeloid cells (miR-155$^{fl/fl}$ x LysM^{Cre} mice) may relatively affect microglia proportions and functions. Therefore, to investigate how miR-155 deletion in myeloid cell subsets may affect phenotypic changes of microglia polarisation *in vivo* during EAE, total CNS immune cells were surface stained to delineate microglia from other immune cells by: CD45^{int}Ly6G^{-}CD11b^{+}CX3CR1^{+}, and stained for phenotypic markers: Ly6C and MHCII to further identify polarisation changes of microglia derived from miR-155$^{fl/fl}$ x LysM^{Cre} mice at day 14 EAE.

As shown in Figure 5.6A, Ly6C expression levels were relatively increased in LysM^{Cre} control microglia from 0.16% in naïve samples to 2.74% at day 14 EAE (not significant). Ly6C expression on naïve miR-155$^{fl/fl}$ x LysM^{Cre} microglia slightly increased from 0.18% to 1.36% at day 14 EAE. This relative shift of Ly6C expression on EAE microglia is evident in Figure 5.6B, whereby a histogram format was utilised to demonstrate the intensity of Ly6C expression when normalised to mode.

Figure 5.6C represents MHCII expression on microglia in naïve CNS samples and at day 14 EAE. As expected, MHCII expression levels were significantly increased from 0.29% in naïve LysM^{Cre} microglia to 69.40% at day 14 EAE ($P<0.0001$). Interestingly, MHCII expression in miR-155$^{fl/fl}$ x LysM^{Cre} microglia was also significantly increased from 0.50% in naïve samples to 62.33% at day 14 EAE ($P<0.0001$). Moreover, there was no statistical changes of MHCII expression between LysM^{Cre} controls and miR-155$^{fl/fl}$ x LysM^{Cre} microglia at day 14 EAE. Figure 5.6D illustrates MHCII expression on naïve and EAE microglia in a histogram format as a visual representative normalised to mode.

Collectively, no significant phenotypic changes occurred to miR-155$^{fl/fl}$ x LysM^{Cre} microglia in comparison to LysM^{Cre} controls regarding Ly6C and MHCII expression.

5.2.7 MHCII, and CCR2 expression are increased on neutrophils in EAE.

MiR-155$^{fl/fl}$ x LysM^{Cre} neutrophils are targets of the cre-lox system due to their myeloid lineage. To investigate how miR-155 deletion may impact neutrophil polarisation and characteristics relating to their function during EAE *in vivo*, total CNS immune cells were isolated in naïve and day 14 EAE mice. Total immune cells were surface stained to delineate

neutrophils from other immune subsets by: CD45^{+}Ly6G^{+}CD11b^{+}, and stained for phenotypic markers: Ly6C, MHCII, and CCR2.

As shown in Figure 5.7A, Ly6C expression levels were 80.90% and 95.83% in naïve LysM^{Cre} controls and miR-155 deleted neutrophils, respectively. Due to high expression levels in naïve samples, Ly6C expression did not significantly increase at day 14 EAE in either mouse strains, but rather slightly increased to 86.78% in LysM^{Cre} controls and 93.53% in miR-155 deleted neutrophils. Ly6C expression is visually represented as a histogram format in Figure 5.7B, there was an evident shift in Ly6C expression on EAE neutrophils compared to naïve samples when normalised to mode.

MHCII expression is represented in Figure 5.7C. MHCII expression levels were significantly increased in both LysM^{Cre} controls from 3.63% to 21.17% (P value 0.0023), and miR-155 deleted neutrophils from 3.03% to 23.40% (P value 0.0007). Overall, there was no evident change in MHCII expression levels amongst the two mouse strains investigated at day 14 EAE, however LysM^{Cre} controls could not increase MHCII expression to the same statistical significance as miR-155 deleted neutrophils ($P<0.01$ versus $P<0.001$). This increase of MHCII expression is visibly shown in Figure 5.7D as a histogram format normalised to mode.

As demonstrated in Figure 5.7E, CCR2 expression was significantly increased from 3.05% in naïve LysM^{Cre} control neutrophils to 48.20% at day 14 EAE (P value 0.0144). Moreover, miR-155 deleted neutrophils could also significantly increase CCR2 expression from 1.85% to 47.93% at day 14 EAE (P value 0.0133). As shown in Figure 5.7E, CCR2 expression increased in EAE neutrophils compared to naïve neutrophils when normalised to mode as a histogram format.

In summary, assessing LysM^{Cre} control and miR-155$^{fl/fl}$ x LysM^{Cre} CNS neutrophils demonstrated no significant changes between controls and miR-155$^{fl/fl}$ x LysM^{Cre} mouse strains at day 14 EAE.

5.2.8 Clinical scores of EAE using 32.5µg rMOG.

To further understand how miR-155 deletion in myeloid cells affect clinical outcomes of EAE, C57BL/6 LysM^{Cre} controls and miR-155$^{fl/fl}$ x LysM^{Cre} mice were immunised with a reduced dosage of rodent rMOG (32.5 µg) in CFA and 200ng Pertussis toxin to induce

chronic progressive EAE. As confirmed by Dr. Natalie Payne, when targeting singular pathways in specific immune subsets, such as the miR-155 pathway in myeloid cells, reducing EAE disease severity may be necessary to observe clinical, gene expression, or cytokine secretion differences during disease progression.

Initial studies focusing on miR-155 deletion in myeloid cells during EAE using a lower immunisation dosage of rMOG involved daily observations of clinical disease throughout a 28-day EAE time course. Mice were clinically scored by observing grading levels of paralysis using the clinical scoring system previously utilised in Figure 3.1 and Figure 5.1.

Figure 5.8 represents clinical scores of LysM^{Cre} controls and miR-155$^{fl/fl}$ x LysM^{Cre} mice throughout the 26-day EAE time course. When examining clinical scores of EAE in LysM^{Cre} control mice, the mean onset of clinical disease occurred on day 15.6 (S.E.M ± 1.03). EAE clinical signs of disease progressed from days 12-20 with scores ranging from 0.5-3.5 with 1 mortality (8% mortality rate). Clinical scores then slightly recovered from days 20-23 before plateauing between days 24-28 during chronic stages of EAE. Overall, LysM^{Cre} controls exhibited a maximum clinical score of 2.33 (S.E.M ± 0.31), and cumulative score of 15.04 (S.E.M ± 2.90) (As shown in Figure 5.8B). Additionally, in some instances miR-155$^{fl/fl}$ x LysM^{Cre} exhibited either disease resistance or atypical EAE, suggestively miR-155 deletion is attenuating inflammation or skewing inflammatory processes towards different mechanisms of pathogenesis.

When observing clinical scores of miR-155$^{fl/fl}$ x LysM^{Cre} mice, the mean onset of clinical disease occurred on day 17.5 (S.E.M ± 0.81). EAE symptoms progressed from days 15-20 with scores ranging from 0.5-3, clinical scores then plateaued from days 17-20 before recovering between days 20-21. Additionally, clinical signs of disease progressed once more at days 21-24 before gradually plateauing at days 24-26 before a final recovery stage was observed between days 26-28. Collectively, miR-155$^{fl/fl}$ x LysM^{Cre} mice had a maximum clinical score of 2.25 (S.E.M ± 0.27), and cumulative score of 10.38 (S.E.M ± 1.45).

In summary, induction of EAE in miR-155$^{fl/fl}$ x LysM^{Cre} mice with 32.5 µg rMOG resulted in ameliorated clinical signs of disease when compared to LysM^{Cre} controls. miR-155$^{fl/fl}$ x LysM^{Cre} mice displayed disease resistance, atypical EAE, a delayed onset of clinical scores, and a lower maximum score and cumulative score, suggesting miR-155 deletion in myeloid cells may contribute to EAE amelioration in this murine model.

5.2.9 miR-155 deletion in myeloid cells affect population proportions within the CNS during EAE.

To investigate the potential effects of miR-155 deletion in myeloid cells on immune cell population infiltration of the CNS during EAE, tissue samples were collected from naïve LysM^{Cre} controls and miR-155$^{fl/fl}$ x LysM^{Cre} mice at days 20/21 post immunisation with 32.5 µg rMOG. Days 20/21 of EAE were chosen because the difference in clinical signs of disease between these two mouse strains was greatest at this time point (Figure 5.8). All immune cell subsets assessed for population studies within the CNS (macrophages, neutrophils, and microglia) were delineated using the gating strategy outlined in Figure 5.2. All immune cells were derived from singlets, viable, and intact cells, before being sorted according to their population specific surface marker expression. Macrophages were delineated as CD45^{hi}Ly6G^{-}CD11b^{+}F4/80^{+} cells, microglia were sorted by CD45^{int}Ly6G^{-} CD11b^{+}CX3CR1^{+} cells, and neutrophils were identified as CD45^{+}Ly6G^{+}CD11b^{+} cells.

As shown in Figure 5.9A, macrophage proportions within the CNS significantly increased in LysM^{Cre} controls from 0.44% in naïve samples and 12.10% at days 20/21 EAE (P value 0.0088). In contrast, miR-155$^{fl/fl}$ x LysM^{Cre} macrophages only slightly increased from 0.57% in naïve samples to 5.62% at days 20/21 EAE (not significant).

Microglia proportions are represented in Figure 5.9B. LysM^{Cre} control microglia proportions significantly decreased from 80.08% to 25.86% at days 20/21 EAE (P<0.0001). Similarly, microglia proportions significantly decreased in miR-155$^{fl/fl}$ x LysM^{Cre} mice from 84.25% in naïve samples to 45.89% at days 20/21 EAE (P value 0.001). Furthermore, when comparing LysM^{Cre} control microglia with miR-155$^{fl/fl}$ x LysM^{Cre} microglia at day 20/21, miR-155$^{fl/fl}$ x LysM^{Cre} microglia had significantly higher proportions within the CNS (P value 0.0341), suggesting miR-155 deletion has affected population proportions of these innate CNS resident immune cells.

As demonstrated in Figure 5.9C, naïve LysM^{Cre} control neutrophils within the CNS relatively increased from 1.69% to 22.26% at days 20/21 EAE. MiR-155$^{fl/fl}$ x LysM^{Cre} neutrophils slightly increased from 1.69% in naïve miR-155 deleted neutrophils to 11.27% at days 20/21 EAE (not significant). Although no statistical significance could be determined

between two mouse strains at days 20/21 EAE, there was a 10.99% difference in neutrophil proportions when comparing LysMCre controls against miR-155$^{fl/fl}$ x LysM^{Cre}.

Collectively, there is an evident trend of decreased miR-155 deleted myeloid cell proportions within the CNS at days 20/21 EAE compared to LysM^{Cre} control immune cell subsets. Moreover, miR-155 deleted samples significantly affected microglial populations as shown by increased proportions relative to LysM^{Cre} controls.

5.2.10 miR-155 expression in macrophages, microglia, and neutrophils in EAE.

Previous data from population proportion studies within the CNS at days 20/21 demonstrated significant variations and/or relative proportion differences amongst LysM^{Cre} controls and miR-155$^{fl/fl}$ x LysM^{Cre} mice. Therefore, an investigation was carried out to determine miR-155 expression in each immune cell subset (macrophage, microglia, and neutrophils) from these CNS immune cells to confirm the inability of miR-155$^{fl/fl}$ x LysM^{Cre} myeloid cells to induce miR-155. Sorted CNS immune cells from Section 5.2.9 were analysed for miR-155 expression using the ΔΔCT fold induction method to determine the fold-change of miR-155 in naïve and days 20/21 EAE immune cell populations derived from LysM^{Cre} controls and miR-155$^{fl/fl}$ x LysM^{Cre} mice.

As demonstrated in Figure 5.10A, miR-155 induction in LysM^{Cre} control macrophages, there was a slight induction of miR-155 at days 20/21 EAE (3.55-fold) compared to naïve macrophages at 2.14-fold (not significant). When examining miR-155 induction in miR-155$^{fl/fl}$ x LysM^{Cre} macrophages, macrophages expectedly could not induce miR-155 (1.28-fold in naïve macrophages versus 0.58-fold at days 20/21 EAE).

Microglia fold change of miR-155 is outlined in Figure 5.10B. When assessing miR-155 induction in LysM^{Cre} control microglia, there was a relative fold-change in naïve samples from 2.95-fold to days 20/21 EAE samples at 6.28-fold (not significant). MiR-155$^{fl/fl}$ x LysM^{Cre} microglia evidently increased from 1.74-fold in naïve samples compared to 9.68-fold in days 20/21 EAE, although no statistical significance could be determined. Although not statistically significant, there was a notable trend of increased miR-155 induction in miR-155$^{fl/fl}$ x LysM^{Cre} microglia compared to LysM^{Cre} controls at days 20/21 EAE (3.40-fold difference).

As shown in Figure 5.10C, LysM^{Cre} control and miR-155$^{fl/fl}$ x LysM^{Cre} neutrophils could not increase miR-155 within the CNS at days 20/21 EAE. LysM^{Cre} control neutrophils exhibited no miR-155 induction, naïve samples and days 20/21 EAE had a fold change of 1.49-fold to 0.71-fold, respectively. As expected, miR-155$^{fl/fl}$ x LysM^{Cre} neutrophils displayed no miR-155 fold induction of miR-155 in naïve samples (1.16-fold) compared to 0.65-fold at days 20/21 EAE.

Overall, Figure 5.10 demonstrates the inability of miR-155 induction in myeloid cells at days 20/21 EAE from miR-155$^{fl/fl}$ x LysM^{Cre} CNS samples. Moreover, miR-155 induction in miR-155$^{fl/fl}$ x LysM^{Cre} microglia is relatively affected in comparison to LysM^{Cre} controls.

5.2.11 miR-155 absolute values at day 20 EAE.

Once fold changes of miR-155 were assessed at days 20/21 EAE, absolute miR-155 copy number values were next evaluated to obtain a broader insight of miR-155 expression levels at this timepoint. Sorted immune cells from the CNS (derived from Section 5.9.2A) were assessed for miR-155 absolute levels.

Figure 5.11A shows miR-155 absolute values in infiltrating macrophages. MiR-155 absolute values derived from naïve LysM^{Cre} control macrophages demonstrated relatively change from 127.38 x 10^4 to 115.78 x 10^4 at days 20/21 EAE. MiR-155$^{fl/fl}$ x LysM^{Cre} macrophages also did not increase between naïve mice (430.92 x 10^4) to day 14 EAE (177.32 x 10^4).

As demonstrated in Figure 5.11B, miR-155 expression levels derived from LysM^{Cre} control microglia increased between naïve and days 20/21 EAE timepoints (483.26 x 10^4 to 1303.22 x 10^4). MiR-155 absolute expression levels from miR-155$^{fl/fl}$ x LysM^{Cre} microglia exhibited a further increase from naïve mice at 49.02 x 10^4 to 2016.82 x 10^4 at days 20/21 EAE (not significant).

Figure 5.11C represents miR-155 expression levels in neutrophils within the CNS of LysM^{Cre} controls and 155$^{fl/fl}$ x LysM^{Cre} mice. miR-155 absolute values decreased at day 14 EAE (5162.08 x 10^4) in LysM^{Cre} controls compared to naïve (2037 x 10^4). Similarly, miR-155 expression derived from miR-155$^{fl/fl}$ x LysM^{Cre} neutrophils decreased at day 14 EAE (2131.70 x 10^4) compared to naïve samples (5548.67 x 10^4).

Collectively, this data suggests that miR-155 absolute values in macrophages and neutrophils relatively decreased between naïve and days 20/21 EAE in miR-155$^{fl/fl}$ x LysM^{Cre} mice.

5.2.12 Ly6C, MHCII, and CCR2 expression on macrophages at days 20/21 EAE.

To examine how miR-155 deletion in myeloid cell subsets affect macrophage polarisation characteristics at days 20/21 EAE, CNS immune cells were isolated from LysM^{Cre} controls and miR-155$^{fl/fl}$ x LysM^{Cre} mice. Total CNS immune cells were surface stained to delineate macrophages from other immune populations using: CD45^{hi}Ly6G^{-}CD11b^{+}F4/80^{+}, and stained for phenotypic markers: Ly6C, MHCII, and CCR2.

As shown in Figure 5.12A, the proportion of Ly6C expression is significantly increased on both LysM^{Cre} controls and miR-155$^{fl/fl}$ x LysM^{Cre} macrophages at days 20/21 EAE. Ly6C proportions significantly increased from 14.4% on naïve LysM^{Cre} controls to 75.38% at days 20/21 EAE ($P<0.0001$). Ly6C proportions also significantly increased from 7.22% on naïve miR-155 deleted macrophages to 71.4% at days 20/21 EAE ($P<0.0001$). Figure 5.12B visualises this significant increase of Ly6C expression as a histogram format normalised to mode.

Figure 5.12C represents MHCII expression proportions on LysM^{Cre} control macrophages and miR-155$^{fl/fl}$ LysM^{Cre} macrophages at days 20/21. LysM^{Cre} controls had increased MHCII expression proportions from 3.98% on naïve samples to 68.38% at days 20/21 EAE ($P<0.0001$). MiR-155$^{fl/fl}$ LysM^{Cre} macrophages had significantly increased MHCII expression from 7.33% on naïve samples to 54.12% at days 20/21 EAE ($P<0.0001$). Figure 5.12D outlines MHCII expression on miR-155$^{fl/fl}$ x LysM^{Cre} macrophages and LysM^{Cre} controls as a histogram format normalised to mode. However, there was no determined statistical significance between the two groups.

Figure 5.12E illustrates CCR2 proportions on LysM^{Cre} controls and miR-155$^{fl/fl}$ LysM^{Cre} macrophages. CCR2 expression proportions on LysM^{Cre} controls significantly increased from 25.93% to 68.75% at days 20/21 EAE (P value 0.0149), whereas CCR2 expression significantly increased on miR-155$^{fl/fl}$ x LysM^{Cre} mice from 34.13% to 66.80% at days 20/21 within the CNS (P value 0.0036). Although both and LysM^{Cre} controls and miR-155$^{fl/fl}$ x LysM^{Cre} macrophages had significantly increased CCR2 expression during EAE, the

statistical significance was greater in LysM^{Cre} controls compared to miR-155$^{fl/fl}$ x LysM^{Cre} mice. As shown in Figure 5.12F, CCR2 expression is visually represented via a histogram format normalised to mode.

Overall, there were no statistical or evident differences of Ly6C, MHCII, or CCR2 expression between LysM^{Cre} controls and miR-155$^{fl/fl}$ x LysM^{Cre} macrophages within the CNS at days 20/21 EAE.

5.2.13 Ly6C and MHCII expression on microglia at days 20/21 EAE.

To investigate if miR-155 deletion in myeloid cells may contribute to other aspects of microglia during EAE, such as changes in microglial polarisation and phenotypic characteristics, total CNS immune cells were obtained from naïve and days 20/21 EAE LysM^{Cre} controls and miR-155$^{fl/fl}$ x LysM^{Cre} mice. Microglia were delineated from other immune cell subsets by surface staining total CNS immune cells for: CD45^{int}Ly6G^{-} CD11b^{+}CX3CR1^{+}. Microglia were phenotypically analysed using surface markers: Ly6C, MHCII, to further assess if miR-155 deletion in myeloid cells influence microglia attributes in EAE.

Figure 5.13A represents Ly6C expression on microglia derived from LysM^{Cre} controls and miR-155$^{fl/fl}$ x LysM^{Cre} mice. When examining Ly6C expression on LysM^{Cre} controls, Ly6C proportions slightly increased from naïve samples to days 20/21 EAE (0.16% to 5.06. Ly6C expression levels did not increase on miR-155$^{fl/fl}$ x LysM^{Cre} microglia (0.18% on naïve samples to 1.23% on days 20/21 EAE samples). Ly6C expression is outlined in Figure 5.13B, whereby a slight positive shift in Ly6C expression on EAE samples was evident via a histogram format when normalised to mode.

MHCII expression levels are outlined in Figure 5.13C. MHCII expression strikingly increased on microglia at days 20/21 EAE. LysM^{Cre} control microglia also had a significant increase of MHCII expression levels from 0.29% in naïve samples to 71.98% at days 20/21 EAE ($P<0.0001$). Additionally, miR-155$^{fl/fl}$ x LysM^{Cre} microglia had significantly increased MHCII expression from 0.50% in naïve samples to 60.88% at days 20/21 EAE ($P<0.0001$). As shown in Figure 5.13D, a half-staggered histogram represents MHCII expression when normalised to mode.

In summary, even though miR-155 deletion significantly impacted certain characteristics of microglia (Figure 5.9B), no significant phenotypic changes were determined between LysM^{Cre} controls and miR-155$^{fl/fl}$ x LysM^{Cre} microglia when analysing Ly6C and MHCII expression at days 20/21 EAE.

5.2.14 Ly6C, MHCII, and CCR2 expression on neutrophils at day 20/21 EAE.

Although miR-155$^{fl/fl}$ x LysM^{Cre} mice have miR-155 deleted neutrophils, there were no significant alterations to neutrophil population proportions or miR-155 induction when immunised with 32.5ug rMOG at days 20/21 EAE. To further understand the role of miR-155 in neutrophils within the CNS during disease, neutrophils were isolated from LysM^{Cre} controls and miR-155$^{fl/fl}$ x LysM^{Cre} mice to assess phenotypic changes to this innate immune cell subset. Neutrophils were delineated from other immune cell populations within the CNS by cell surface staining with: CD45^{+}Ly6G^{-}CD11b^{+}, and phenotypically assessed by cell surface: Ly6C, MHCII, and CCR2.

Ly6C expression levels are represented in Figure 5.14A. Neutrophils did not exhibit significant changes in Ly6C expression at days 20/21 EAE. Whilst examining LysM^{Cre} controls, Ly6C expression relatively increased from 80.9% to 88.5% (not significant). However, miR-155$^{fl/fl}$ x LysM^{Cre} neutrophils had no evident changes in naïve samples and at days 20/21 EAE samples (86.78% to 85.1%). Figure 5.14B shows a visual representative of Ly6C expression as a histogram format normalised to mode.

As shown in Figure 5.14C, MHCII expression on neutrophils were significantly increased on naïve samples compared to days 20/21 EAE. LysM^{Cre} control neutrophils displayed an increase of MHCII expression from 3.63% to 24.73% (P value 0.0106). MiR-155$^{fl/fl}$ x LysM^{Cre} neutrophils additionally increased from 3.03% to 20.07% (P value 0.0255). Figure 5.14D displayed this evident shift in MHCII expression in EAE samples compared to naïve samples as a histogram normalised to mode.

CCR2 expression levels on neutrophils are outlined in Figure 5.14E. LysM^{Cre} control neutrophils exhibited an evident increase of CCR2 expression when comparing naïve samples (3.05%) to days 20/21 EAE (9.60%) (not significant). CCR2 expression also increased in miR-155$^{fl/fl}$ x LysM^{Cre} neutrophils from 1.85% on naïve samples to 7.31% at days 20/21 EAE samples, although this was not significant. Figure 5.14F illustrates CCR2

expression on neutrophils between these two mouse strains in naïve mice and at days 20/21 EAE as an off-staggered histogram format normalised to mode.

Collectively, CNS infiltrating neutrophils at days 20/21 EAE derived from LysM^{Cre} controls a and miR-155$^{fl/fl}$ x LysM^{Cre} mice displayed no significant changes to their phenotypic surface marker expression of Ly6C, MHCII, and CCR2 expression. This data suggests miR-155 may not play a crucial role in the expression of these specific markers on neutrophils at days 20/21 EAE.

5.2.15 H&E and IF staining of spinal cords at day 28 EAE

To investigate how miR-155 deletion in myeloid cells affects CNS inflammation and immune cell infiltration into spinal cord regions during later stages of EAE (day 28 EAE), histopathological analysis was performed on H&E stained sections from miR-155$^{fl/fl}$ x LysMCre mice and LysMCre controls. Immunofluorescent (IF) staining was also performed and observed in a highlighted region of interest. IF staining of CD68^{+}iNOS^{+} cells and CD68^{+}ARG1^{+} cells were used as characteristic markers of infiltrating macrophages, and whether these cells exhibited a classic proinflammatory phenotype (iNOS), a classic anti-inflammatory state (ARG1), or represent a heterogenous population by expressing both markers.

Figure 5.15A-B shows a summary of histopathological findings including the total number of lesions present in three randomly selected spinal cord sections, as determined by a blinded assessor. Overall, the presence of a lesions in the spinal cord correlated with mice that displayed higher clinical scores. Notably of the sections analysed, spinal cord lesions were only identified in one miR-155$^{fl/fl}$ x LysMCre mouse.

Spinal cord sections derived from LysM^{Cre} control mice that presented with different scores of EAE are demonstrated in Figures 5.16A-C. Figure 5.16A illustrates inflammation in spinal cord sections of a mouse at clinical score 2.5. Mass meningeal inflammation was observed surrounding <50% circumference of the spinal cord. There are several areas demonstrating parenchymal infiltration of immune cells (highlighted by black arrows) from the meninges that reach grey matter regions. Additionally, there are instances of immune cell infiltration at blood vessel regions. Due to the mass inflammation present in this section,

Figure 5.16Ai was chosen as a region of interest for further analysis under a higher magnification (highlighted by boxed region). Figure 5.16B demonstrates spinal cord inflammation of a mouse at clinical score 1.5. Visible immune cell accumulation was noted at the meninges in both dorsal and ventral regions of the spinal cord, leading into several areas of parenchyma inflammation (highlighted with black arrows). Additionally, there were immune cells present at the central canal. Figure 5.16C represents a spinal cord section derived from a mouse at EAE clinical score 0. Although no clinical signs of paralysis were observed, there were regions of immune cell accumulation around the perimeter of the section within the meninges.

As shown in Figure 5.16Aii, there were high levels of CD68^{+} cells at the parenchymal area of interest. Furthermore, CD68^{+} cells at this site expressed iNOS, suggesting infiltrating macrophages were exhibiting a proinflammatory phenotype. As shown in Figure 5.16Aiii, CD68^{+}ARG1^{+} cells were also observed at the same lesion site.

Collectively, LysM^{Cre} control mice exhibiting clinical scores of EAE visibly presented with mass immune cell accumulation at the meninges with several regions of immune cell infiltration into the parenchyma and formation of lesion sites. In relation to IF staining, there were observed CD68^{+}iNOS^{+} cells and CD68^{+}ARG1^{+} cell at immune cell infiltration sites in the parenchyma, indicating infiltrating macrophages within the CNS at sites of inflammation are expressing both iNOS and ARG1.

H&E staining of miR-155$^{fl/fl}$ x LysM^{Cre} spinal cord sections is shown in Figures 5.17A-C. As demonstrated by Figure 5.17A, both meningeal and parenchymal immune cell infiltration was present throughout several areas of the spinal cord section. However, it must be noted that this was the only miR-155$^{fl/fl}$ x LysM^{Cre} mouse in which parenchymal inflammation was observed, also presenting with the most sever clinical score (score 2). Figure 5.17B illustrates a spinal cord section derived from an EAE mouse at clinical score 1.5. There were no lesions or parenchymal infiltration observed, however there were instances of accumulating immune cells localised at meningeal locations surrounding the circumference of the spinal cord section. Due to a trend in the majority of miR-155$^{fl/fl}$ x LysM^{Cre} mice exhibiting immune cell accumulation at the meninges as opposed to parenchymal infiltration, this section was chosen for further investigation under high magnification, as

shown in Figure 5.17Bi. As demonstrated in Figure 5.17C, there are no lesion sites present within this spinal cord section. This is expected as this mouse was resistant to clinical signs of EAE, documented as exhibiting a clinical score of 0. Surrounding the circumference of the section, there were random areas of immune cell accumulation, though not as prominent as Figure 3.15C, the LysMCre control also exhibiting a clinical score of EAE at 0.

Investigating how miR-155 deletion affects the accumulation of CD68$^+$ cells within the spinal cord, and the expression of iNOS and ARG1 in a specific area of interest was performed with IF imaging Figure 3.16Bi. Figure 5.17Bii represents CD68$^+$iNOS$^+$ cells located at the meninges of the highlighted region of interest. DAPI positive cells and CD68$^+$iNOS$^+$ cells appeared to be less frequent compared to Figure 5.16Aii (LysMCre control). CD68$^+$ARG1$^+$ cells are represented in Figure 5.16Biii. ARG1 expressing cells were undoubtedly present at the meninges, collectively indicating both iNOS and ARG1 expressing cells are present at sites of immune cell accumulation at the meninges.

In summary, although parenchymal infiltration was observed in one mouse (Figure 5.17A), this was not a common occurrence in miR-155$^{fl/fl}$ x LysM^{Cre} spinal cord sections. In contrast, miR-155$^{fl/fl}$ x LysM^{Cre} spinal cords exhibited localised meningeal infiltration with minimal observations of immune cells within the parenchyma in comparison to LysMCre control spinal cord sections. In relation to IF staining, there were observed CD68$^+$iNOS$^+$ cells and CD68$^+$ARG1$^+$ in both LysMCre controls and miR-155$^{fl/fl}$ x LysM^{Cre} spinal cords, perhaps suggesting both mouse strains exhibited a mixed population of CD68$^+$ cells co-expressing proinflammatory and anti-inflammatory markers.

(A)

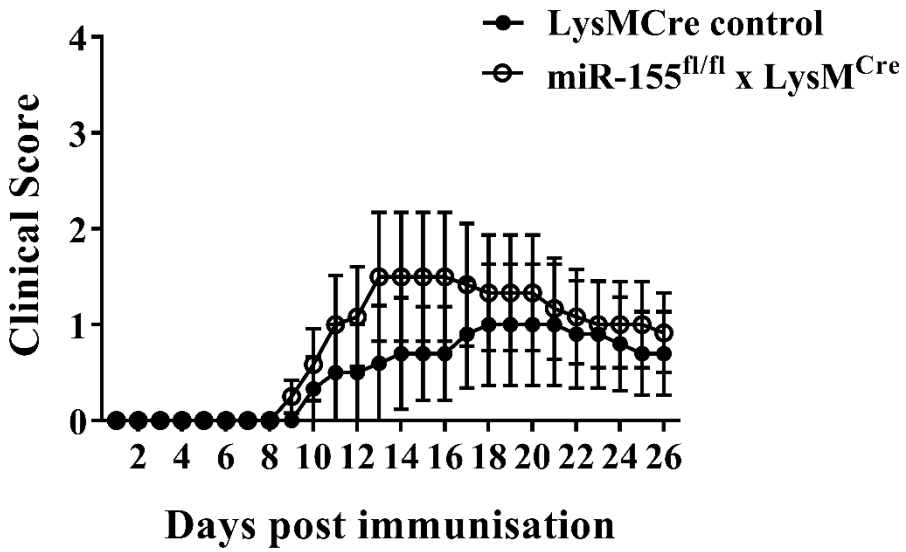

(B)

	LysM^{Cre} Controls	miR-155$^{fl/fl}$ x LysM^{Cre}
Day of disease onset	12 ± 0.89 (10-14)	9.67 ± 0.37 (9-11)
Maximum clinical score	1.84 ± 0.16 (1.49-2.19)	2.37 ± 0.02 (2.28-2.42)
Cumulative score	33 ± 2.91 (26.9-39.5)	41 ± 0.79 (28.5-43.5)

Figure 5.1 Clinical scores of EAE using 65µg rMOG.

LysM^{Cre} controls and miR-155$^{fl/fl}$ x LysM^{Cre} mice were actively induced with EAE using 65 µg rMOG on day 0 and 200 ng Pertussis toxin as an adjuvant on days 0 and 2. EAE was carried out for a total of 26 days. (A) Clinical scoring was carried out daily by measuring grade of paralysis. (B) Day of disease onset, mean clinical score, and cumulative score were derived from daily clinical scores. Data represents mean ± S.E.M, (n=6 per group, 1 independent experiment).

(A)

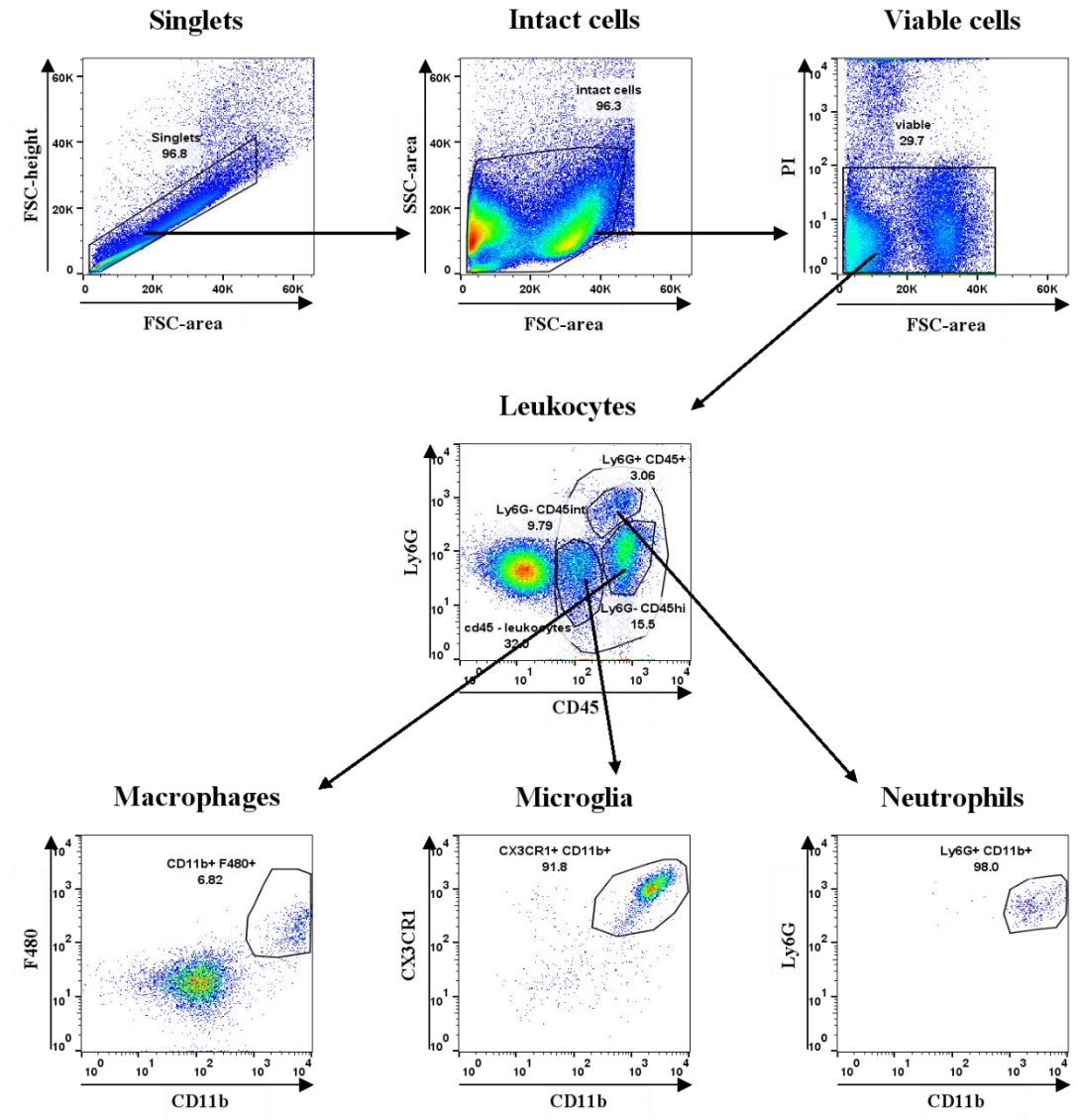
Singlets
Intact cells
Viable cells
FSC-height
FSC-area
Singlets
96.8
SSC-area
intact cells
96.3
PI
viable
29.7
Leukocytes
Ly6G
CD45
Ly6G+ CD45+
3.06
Ly6G- CD45int
9.79
Ly6G- CD45hi
15.5
cd45 - leukocytes
32.0
Macrophages
Microglia
Neutrophils
F480
CD11b
CD11b+ F480+
6.82
CX3CR1
CX3CR1+ CD11b+
91.8
Ly6G+ CD11b+
98.0

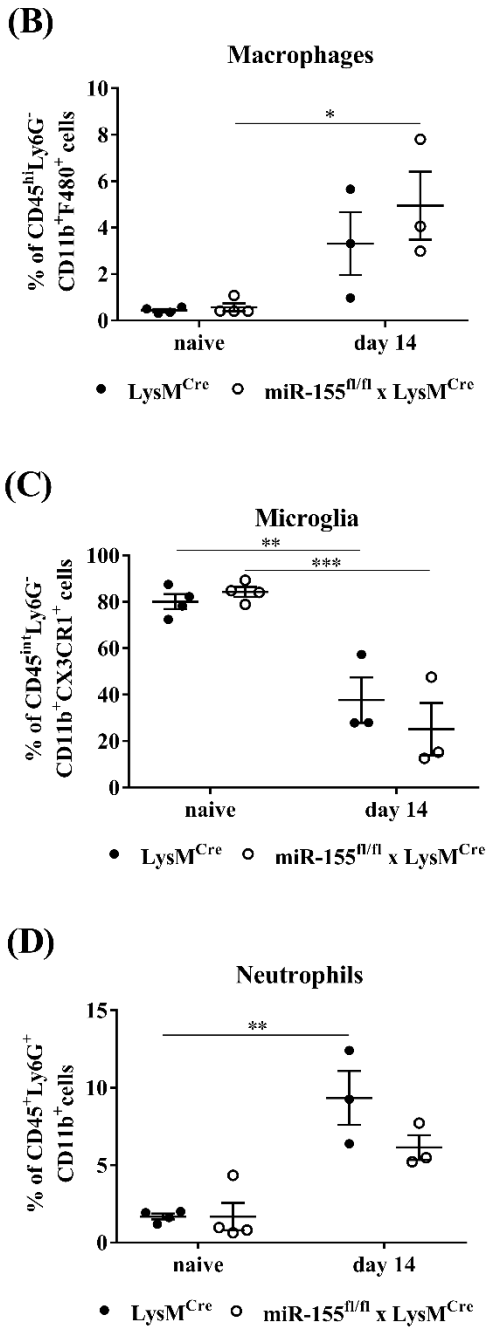

Figure 5.2 Myeloid cell populations increase within the CNS at day 14 EAE.

CNS samples from naïve and EAE induced LysM^{Cre} controls and miR-155$^{fl/fl}$ x LysM^{Cre} mice underwent immune cell isolation and cell sorting using flow cytometry. Cells were stained for surface CD45, CD11b, Ly6G, F4/80, and CX3CR1. (A) Representative gating strategy for immune cell population isolation. (B-D) Population proportions of macrophages (B), microglia (C), and neutrophils (D), in naïve mice and at day 14 EAE. Data represents the percentage of immune cells relative to intact viable cells and expressed as mean ± S.EM. (n=3-4, 1 independent experiment). *P<0.05, ** P<0.01, ***P<0.001; two-way ANOVA with Bonferroni's correction.

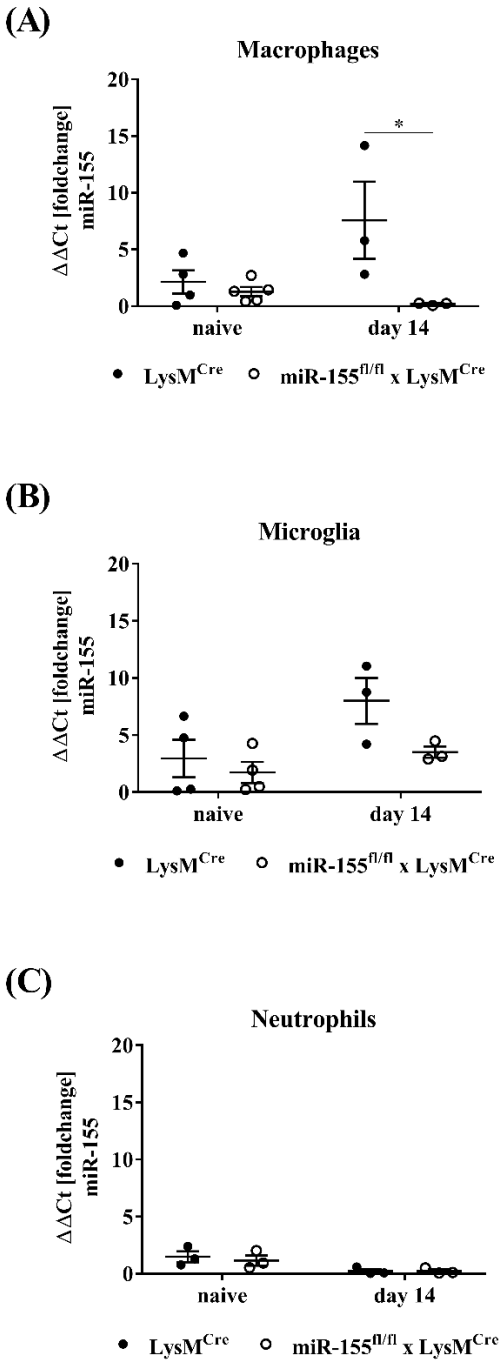

Figure 5.3 miR-155 is significantly reduced in macrophages during EAE.

CNS samples from naïve and day 14 EAE C57Bl/6 mice underwent immune cell isolation, cell sorting using flow cytometry into 3 immune cell populations, and lysis in TRIzol for total RNA isolation. Total RNA was extracted and rtPCR and qPCR was performed using Taqman probes to determine miR-155 expression in macrophages (A), microglia (B), and neutrophils (C). Data represent the ΔΔCT fold induction of miR-155 relative to naïve samples, normalised against the average of three housekeeping genes sno-202, miR-191, and snU6, and expressed as mean ± S.EM. (n=3-4, 1 independent experiment). *P<0.05; two-way ANOVA with Bonferroni's correction.

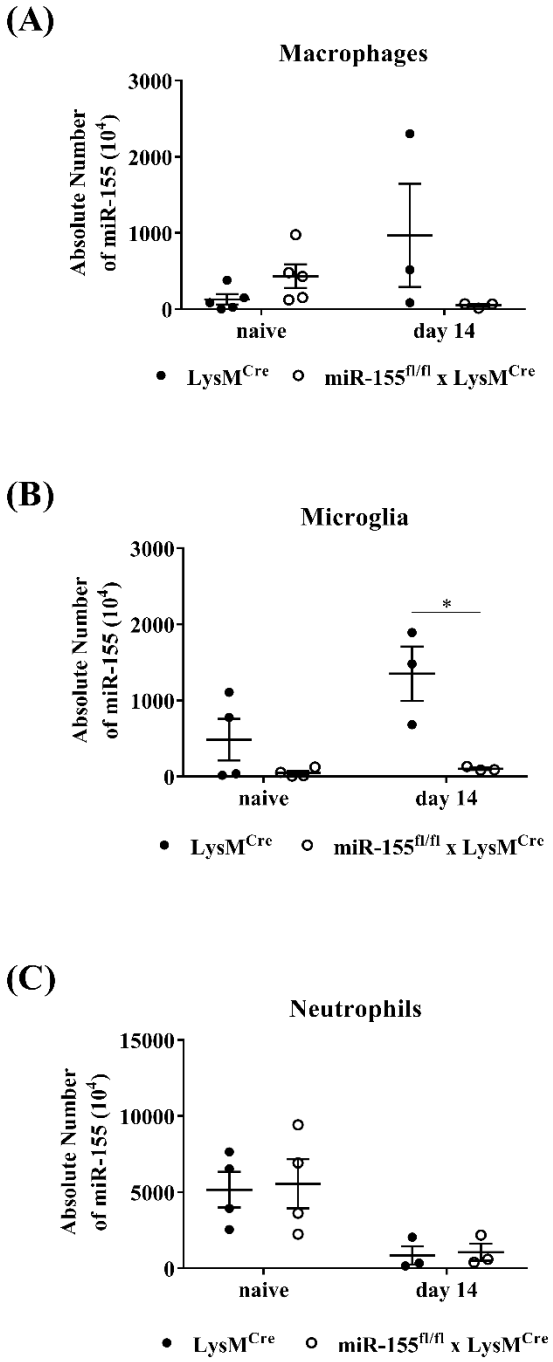

Figure 5.4 miR-155 absolute values increased in macrophages and microglia in EAE.

CNS samples from naïve and day 14 EAE C57BL/6 mice underwent immune cell isolation, cell sorting using flow cytometry into 3 immune cell populations, and lysis in TRIzol for total RNA isolation. Total RNA was extracted and rtPCR and qPCR was performed using Taqman probes to determine miR-155 expression in macrophages (A), microglia (B), and neutrophils (C). Data represent the absolute values of miR-155 normalised against the average of three housekeeping genes sno-202, miR-191, and snU6, and expressed as mean ± S.EM. (n=3-4, 1 independent experiment). *P<0.05; two-way ANOVA with Bonferroni's correction.

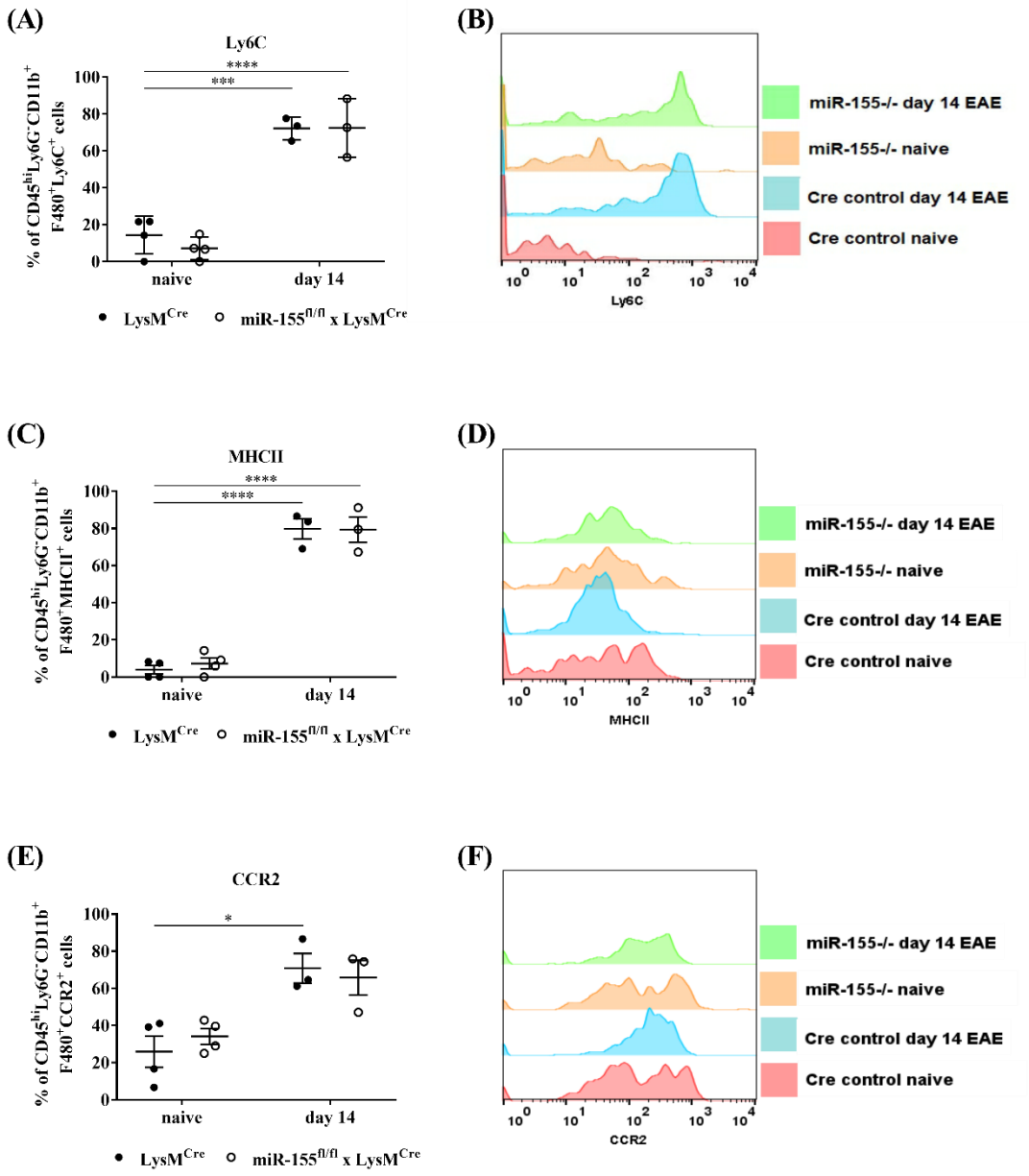

Figure 5.5 Ly6C, MHCII, and CCR2 expression are increased on macrophages in EAE.

CNS samples from naïve and day 14 EAE C57BL/6 LysM^{Cre} controls and miR-155$^{fl/fl}$ x LysM^{Cre} mice underwent immune cell isolation and cell sorting using flow cytometry. Cells were stained for surface CD45^{hi}, CD11b^{+}, F4/80^{+}, and Ly6G^{-} to delineate macrophages for phenotypic analysis. (A-F) Quantification of the proportion of macrophages expressing Ly6C (A,B), MHCII (C,D), and CCR2 (E,F). Data expressed as mean ± S.EM. (n=3-4, 1 independent experiment). *P<0.05, ***P<0.001, ****P<0.0001; two-way ANOVA with Bonferroni's correction.

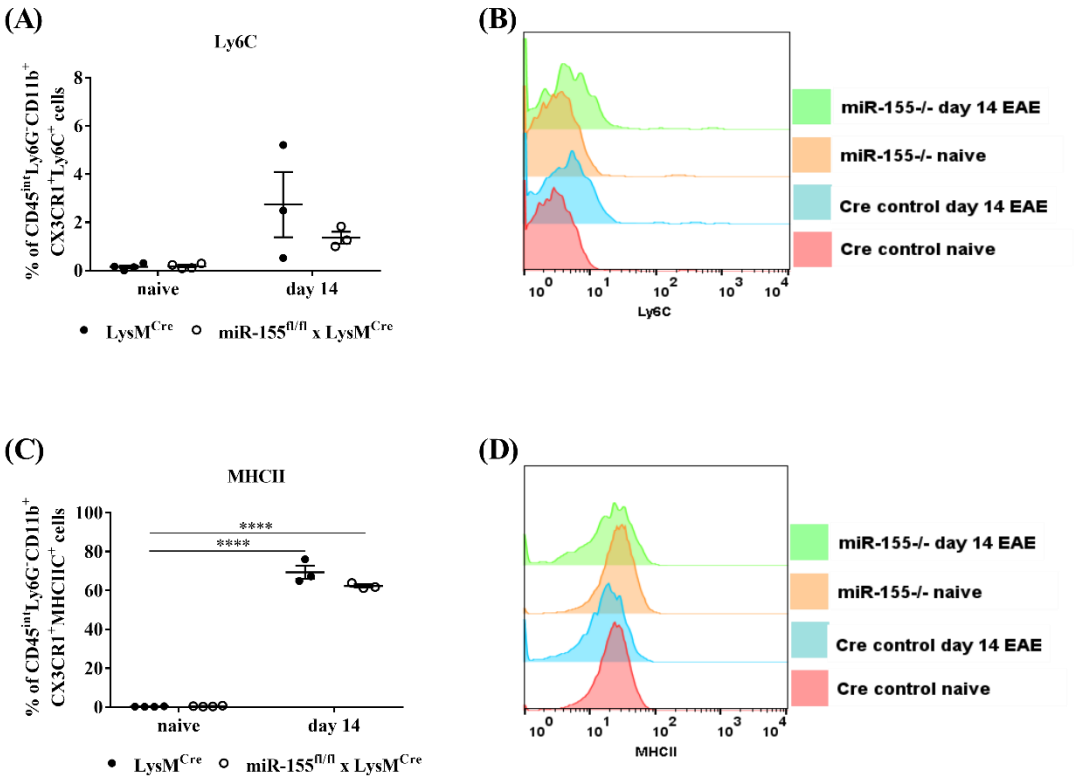

Figure 5.6 Ly6C and MHCII expression are increased on microglia in EAE.

CNS samples from naïve and day 14 EAE C57BL/6 LysM^{Cre} controls and miR-155$^{fl/fl}$ x LysM^{Cre} mice underwent immune cell isolation and cell sorting using flow cytometry. Cells were stained for surface CD45^{int}, CD11b^{+}, CX3CR1^{+}, and Ly6G^{-} to delineate microglia for phenotypic analysis. (A-F) Quantification of the proportion of microglia expressing Ly6C (A,B), and MHCII (C,D). Data expressed as mean ± S.EM. (n=3-4, 1 independent experiments). **P<0.01, ****P<0.0001; two-way ANOVA with Bonferroni's correction.

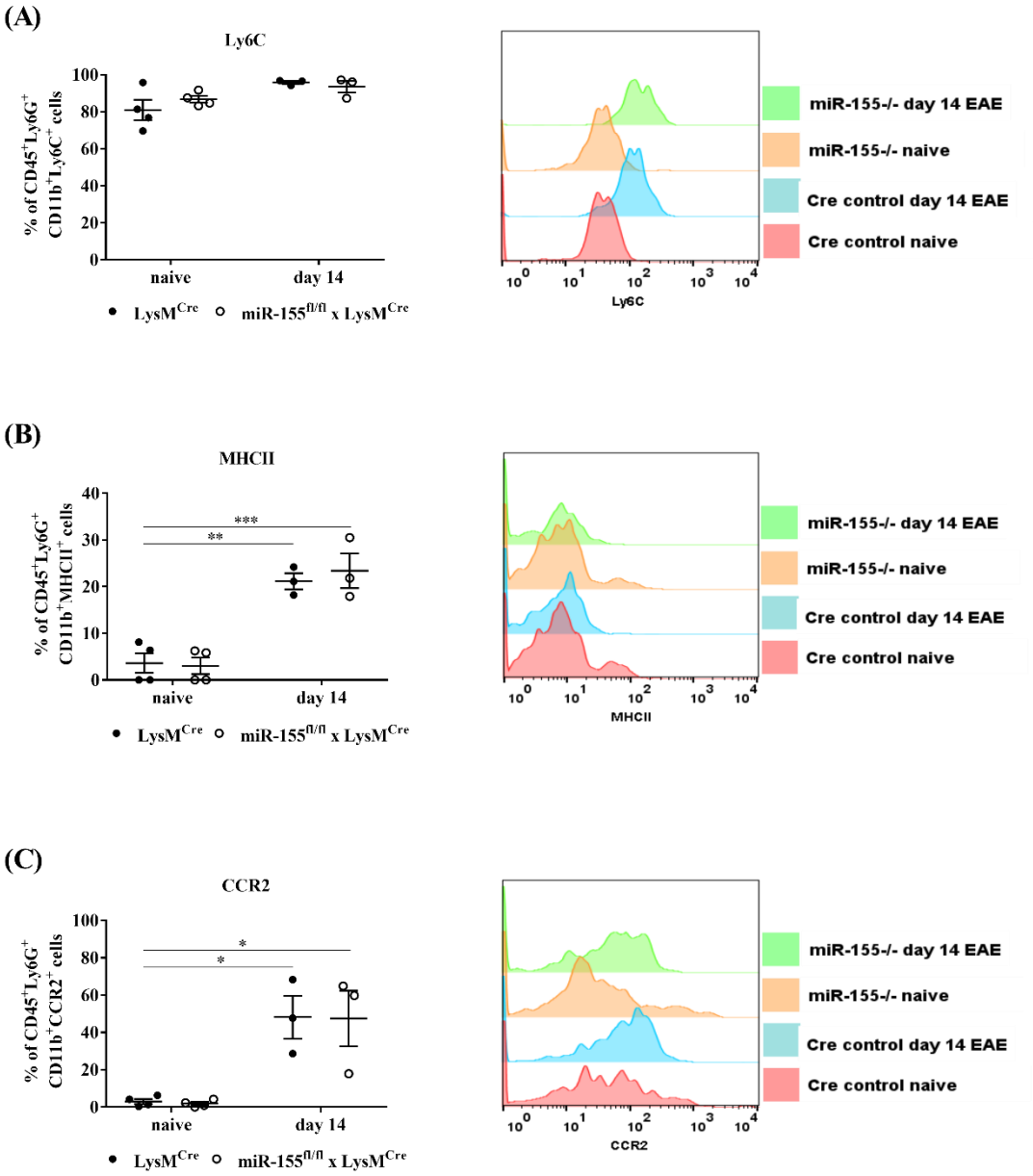

Figure 5.7 MHCII, and CCR2 expression are increased on neutrophils in EAE.

CNS samples from naïve and day 14 EAE C57BL/6 LysM^{Cre} controls and miR-155$^{fl/fl}$ x LysM^{Cre} mice underwent immune cell isolation and cell sorting using flow cytometry. Cells were stained for surface CD45^{+}, CD11b^{+}, and Ly6G^{+} to delineate neutrophils for phenotypic analysis. (A-F) Quantification of the proportion of neutrophils expressing Ly6C (A,B), MHCII (C,D), and CCR2 (E,F). Data expressed as mean ± S.EM. (n=3-4, 1 independent experiments). *P<0.05, **P<0.01; ***P<0.001, two-way ANOVA with Bonferroni's correction.

(A)

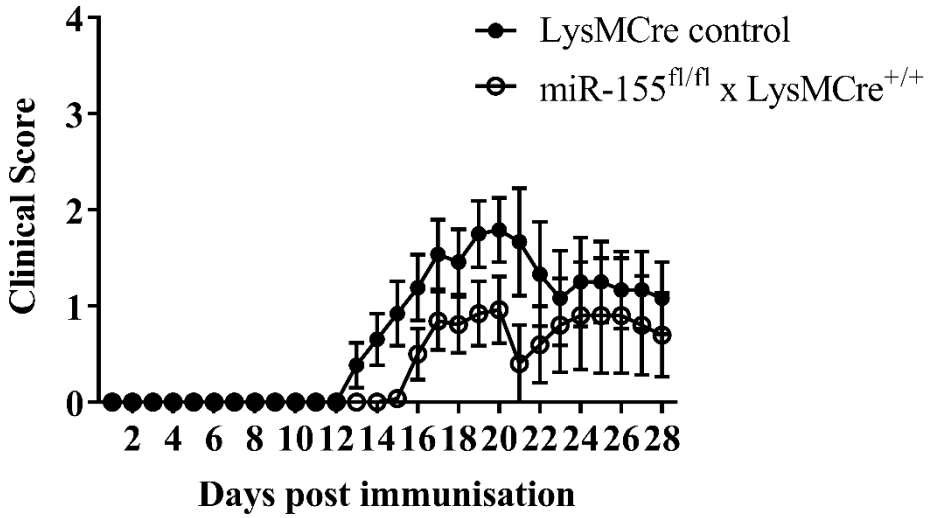

(B)

	LysM^{Cre} Controls	**miR-155$^{fl/fl}$ x LysM^{Cre}**
Day of disease onset	15.67 ± 1.03 (13-34)	17.5 ± 0.81 (10-14)
Maximum clinical score	2.33 ± 0.31 (0.5-3.5)	2.25 ± 0.27 (0.5-3)
Cumulative score	15.4 ± 2.90 (2.5-32.5)	10.38 ± 1.45 (2-16)

Figure 5.8 Clinical scores of EAE using 32.5µg rMOG.

LysM^{Cre} controls and miR-155$^{fl/fl}$ x LysM^{Cre} mice were actively induced with EAE using 32.5 µg rMOG on day 0 and 200 ng Pertussis toxin as an adjuvant on days 0 and 2. EAE was carried out for a total of 26 days. (A) Clinical scoring was carried out daily by measuring grade of paralysis. (B) Day of disease onset, mean clinical score, and cumulative score were derived from daily clinical scores. Data represents mean ± S.E.M, (n=12-13 per group, 2 independent experiments).

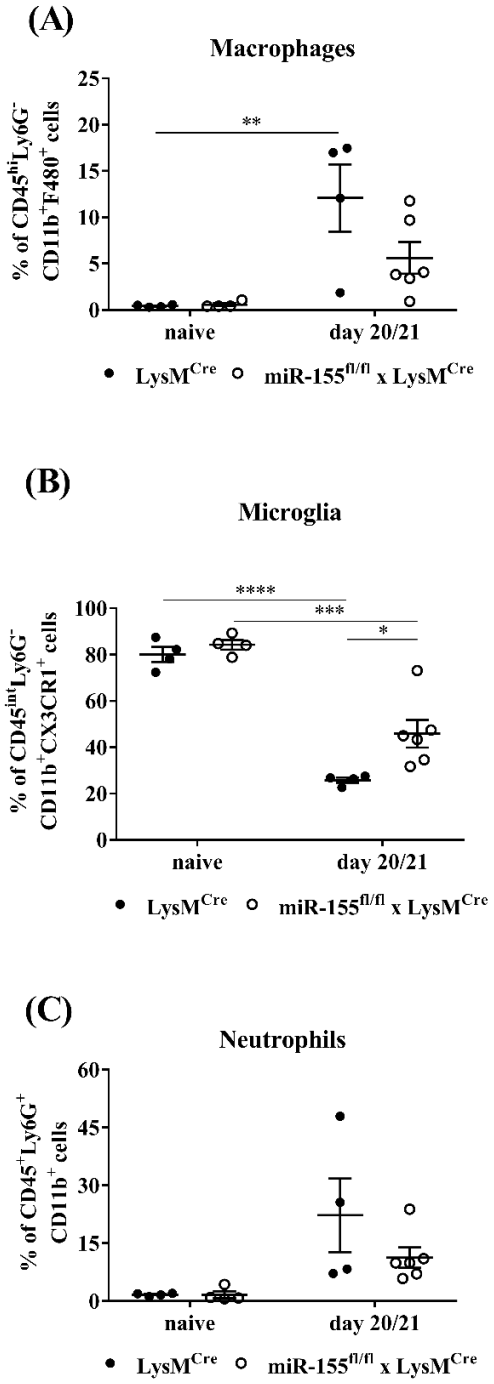

Figure 5.9 MiR-155 deletion in myeloid cells affect population proportions within the CNS during EAE.

CNS samples from naïve and EAE induced LysM^{Cre} controls and miR-155$^{fl/fl}$ x LysM^{Cre} mice underwent immune cell isolation and cell sorting using flow cytometry. Cells were stained for surface CD45, CD11b, Ly6G, F4/80, and CX3CR1. (A-C) Population proportions of macrophages (A), microglia (B), and neutrophils (C), in naïve mice and at days 20/21 EAE. Data represents the percentage of immune cells relative to intact viable cells and expressed as mean ± S.EM. (n=4-6, 2 independent experiments). *P<0.05, ** P<0.01, ***P<0.001, ****P<0.0001; two-way ANOVA with Bonferroni's correction.

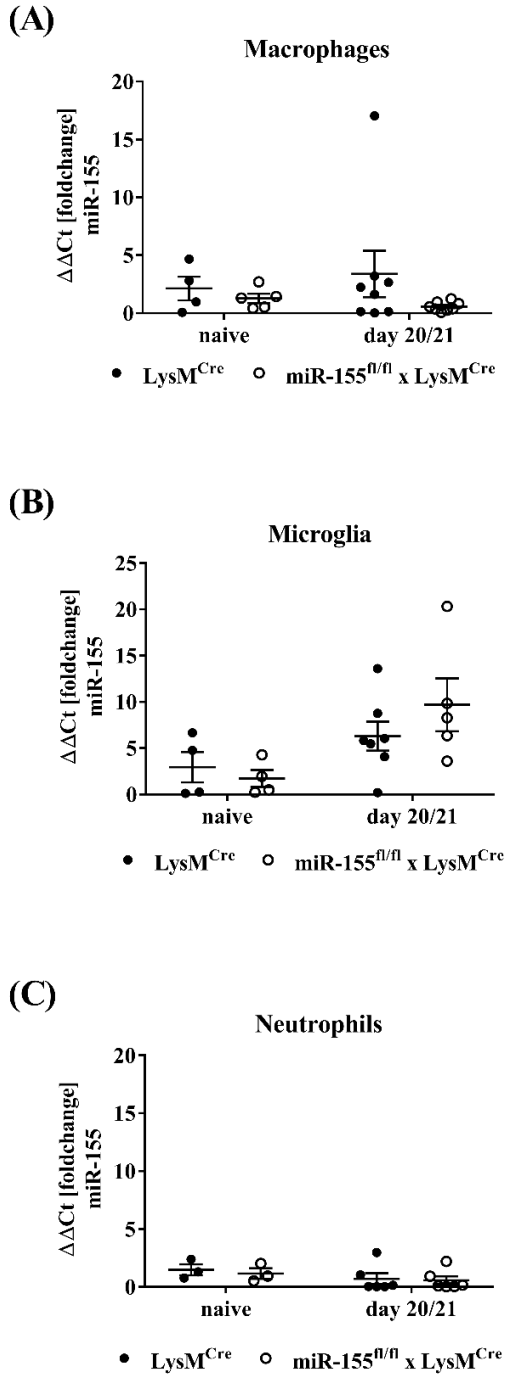

Figure 5.10 miR-155 expression in macrophages, microglia, and neutrophils in EAE.

CNS samples from naïve and day 20/21 EAE C57Bl/6 mice underwent immune cell isolation, cell sorting using flow cytometry into 3 immune cell populations, and lysis in TRIzol for total RNA isolation. Total RNA was extracted and rtPCR and qPCR was performed using Taqman probes to determine miR-155 expression in macrophages (A), microglia (B), and neutrophils (C). Data represent the ΔΔCT fold induction of miR-155 relative to naïve samples, normalised against the average of three housekeeping genes sno-202, miR-191, and snU6, and expressed as mean ± S.EM. (n=3-7, 2 independent experiments).

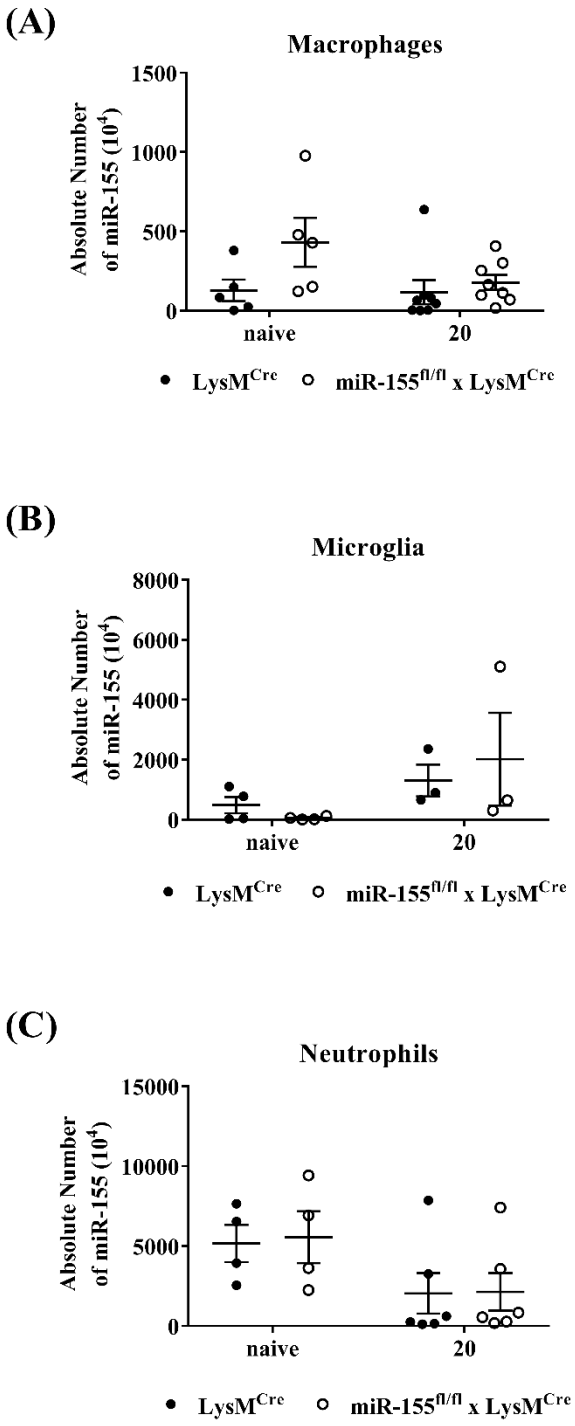

Figure 5.11 miR-155 absolute values at day 20 EAE.

CNS samples from naïve and day 20/21 EAE C57BL/6 mice underwent immune cell isolation, cell sorting using flow cytometry into 3 immune cell populations, and lysis in TRIzol for total RNA isolation. Total RNA was extracted and rtPCR and qPCR was performed using Taqman probes to determine miR-155 expression in macrophages (A), microglia (B), and neutrophils (C). Data represent the absolute values of miR-155 normalised against the average of three housekeeping genes sno-202, miR-191, and snU6, and expressed as mean ± S.EM. (n=3-8, 2 independent experiments).

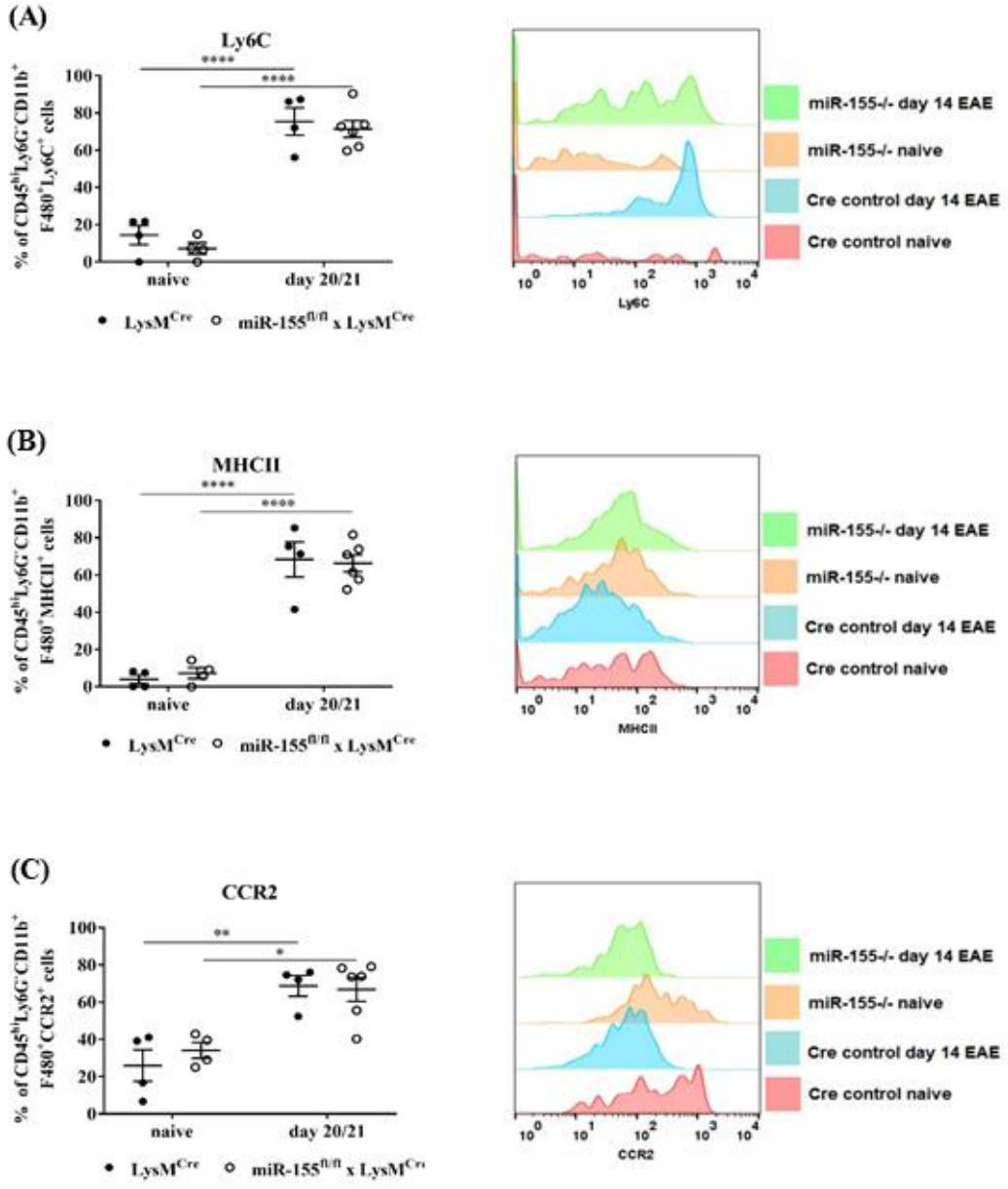

Figure 5.12 Ly6C, MHCII, and CCR2 expression on macrophages at day 20/21 EAE.

CNS samples from LysMCre controls and miR-155$^{fl/fl}$ x LysMCre$^{+/+}$ mice resistant to EAE underwent immune cell isolation followed by cell surface staining at day 20 EAE for flow cytometry analysis. CNS samples were cell surface stained with CD45-APCCy7, CD11b-APC, Ly6C-BV421, MHCII-510, CCR2-PE, Ly6G-PeCy7, and F480-BV605 to delineate macrophages for phenotypic analysis. The percentages of (A) Ly6C ns, P value 0.5874, (B) MHCII ns, P value 0.2067, and (C) CCR2 ns, P value 0.4821, were measured from CD45^{hi}Ly6G^{-}CD11b^{+}F480^{+} cells. Data represents mean ± S.EM. of n=3-4, 2 independent experiments. Statistical analysis was carried out using unpaired t-test with Welch's correction. Statistical significance was determined by $P < 0.05$.

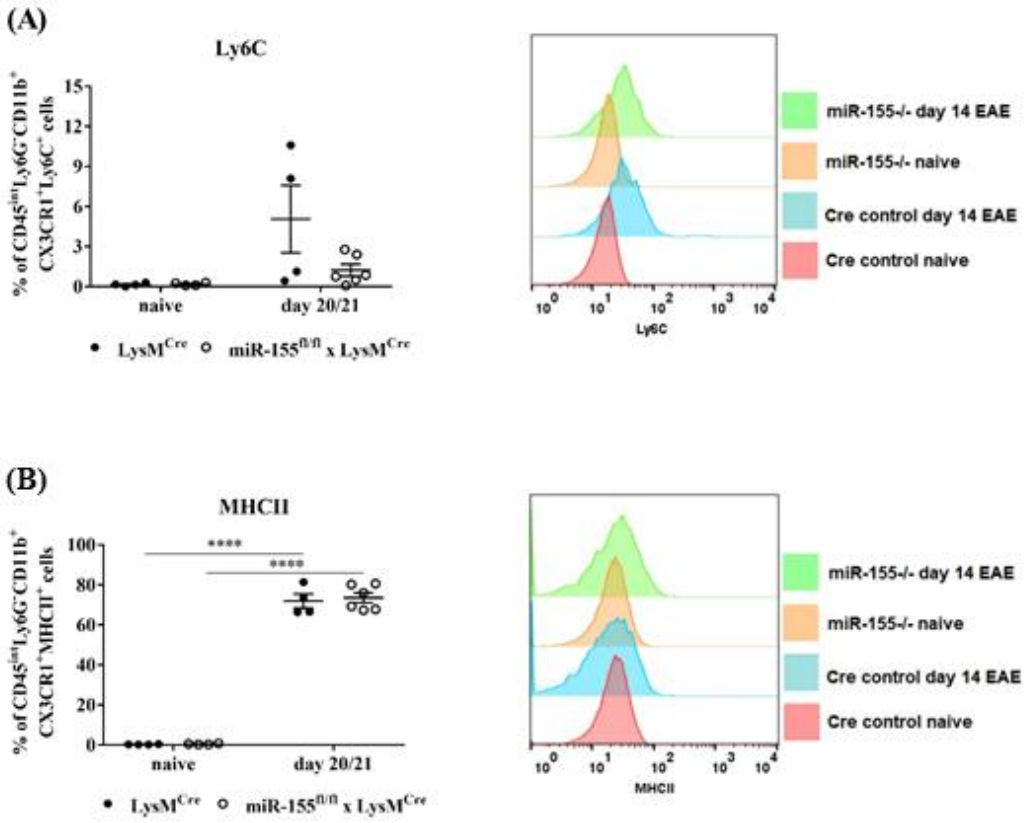

Figure 5.13 Ly6C and MHCII expression on microglia at day 20/21 EAE.

CNS samples from LysMCre controls and miR-155$^{fl/fl}$ x LysMCre$^{+/+}$ mice resistant to EAE underwent immune cell isolation followed by cell surface staining at day 20 EAE for flow cytometry analysis. CNS samples were cell surface stained with CD45-APCCy7, CD11b-APC, Ly6C-BV421, MHCII-510, Ly6G-PeCy7, and CX3CR1-FITC to delineate microglia for phenotypic analysis. The percentages of (A) Ly6C ns, P value 0.2617, and (B) MHCII ns, P value 0.3898, were measured from CD45^{int}Ly6G^{-}CD11b^{+}CX3CR1^{+} cells. Data represents mean ± S.EM. of n=3-4, 2 independent experiments. Statistical analysis was carried out using unpaired t-test with Welch's correction. Statistical significance was determined by $P < 0.05$.

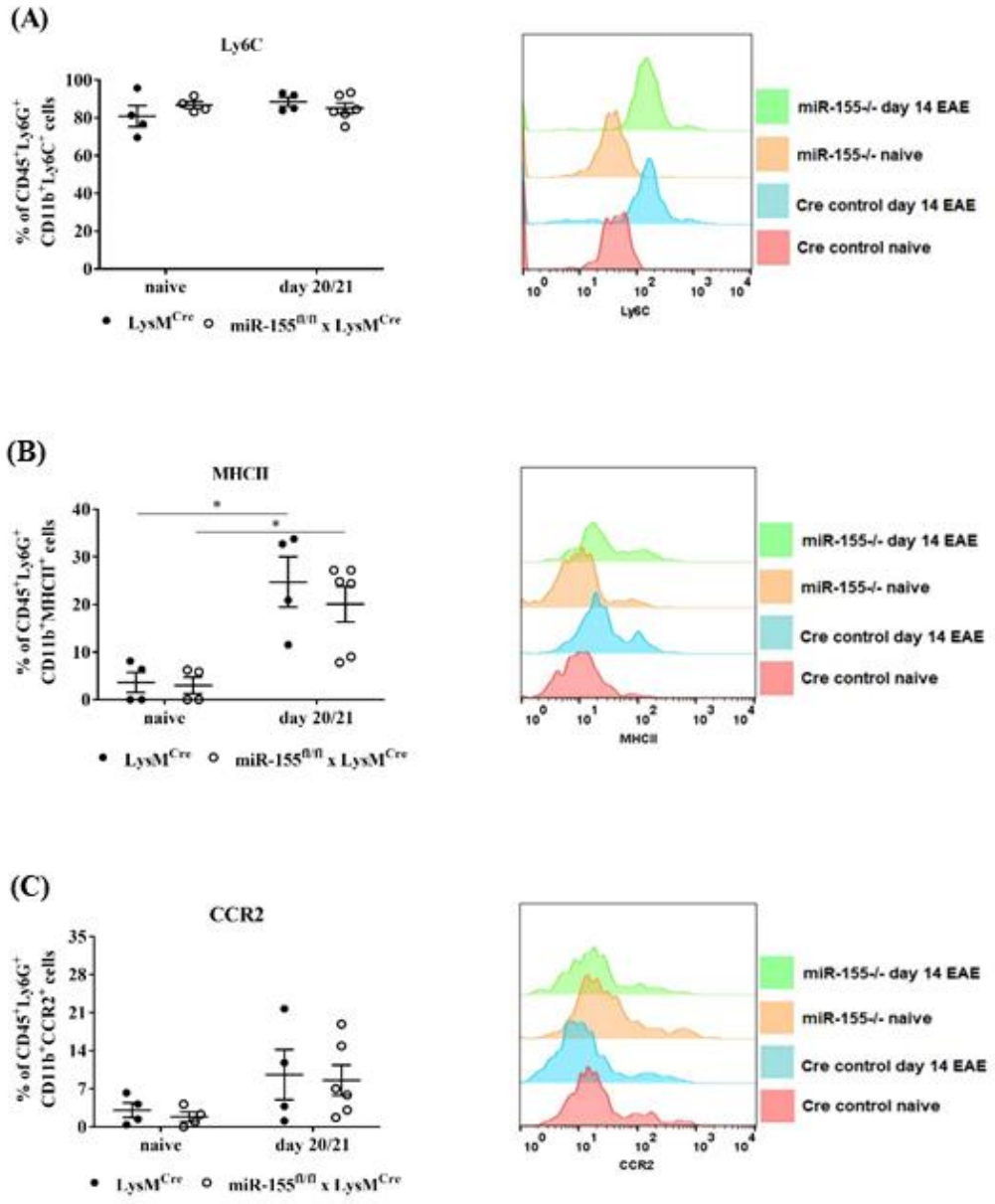

Figure 5.14 Ly6C, MHCII, and CCR2 expression on neutrophils at day 20/21 EAE.

CNS samples from LysMCre controls and miR-155$^{fl/fl}$ x LysMCre$^{+/+}$ mice resistant to EAE underwent immune cell isolation followed by cell surface staining at day 20 EAE for flow cytometry analysis. CNS samples were cell surface stained with CD45-APCCy7, CD11b-APC, Ly6C-BV421, MHCII-510, CCR2-PE, and Ly6G-PeCy7 to delineate neutrophils for phenotypic analysis. The percentages of (A) Ly6C ns, P value 0.4001, (B) MHCII ns, P value 0.2197, and (C) CCR2 ns, P value 0.2419, were measured from CD45^{+}Ly6G^{+}CD11b^{+} cells. Data represents mean ± S.EM. of n=3-6, 2 independent experiments. Statistical analysis was carried out using unpaired t-test with Welch's correction. Statistical significance was determined by $P < 0.05$.

(A)

Mouse Strain	Clinical score	Total Lesion Number	Brief Description
LyM^{Cre} Control 1	0	0	Immune cell accumulation at meninges though not dense. No signs of parenchyma infiltration.
LyM^{Cre} Control 2	0.5	0	Minor accumulation of cells at meninges. No parenchymal infiltration.
LyM^{Cre} Control 3	0.5	2	Immune cell accumulation at meninges, central canal, and blood vessels. Parenchymal infiltration from meninges.
LyM^{Cre} Control 4	1.5	5	Immune cell infiltration into parenchyma from meninges. Immune cells present at central canal, blood vessels, and meninges.
LyM^{Cre} Control 5	1.5	3	Immune cell accumulation at meninges, central canal, blood vessels. Parenchyma infiltration from meningeal regions.
LyM^{Cre} Control 6	2.5	5	Immune cell accumulation at meninges, central canal, and blood vessels. Mass parenchymal infiltration.
MiR-155$^{fl/fl}$ x LysM^{Cre} 1	0	0	Accumulation of immune cells at the meninges. Early signs of parenchymal infiltration.
MiR-155$^{fl/fl}$ x LysM^{Cre} 2	0	0	Accumulation of immune cells at the meninges. Early signs of parenchymal infiltration.
MiR-155$^{fl/fl}$ x LysM^{Cre} 3	0	0	Random immune cell accumulation at meninges, though not dense. No signs of parenchyma infiltration from meninges.
MiR-155$^{fl/fl}$ x LysM^{Cre} 4	1.5	0	Immune cell accumulation at meninges, central canal, and blood vessels. Slight immune cell infiltration into parenchyma.
MiR-155$^{fl/fl}$ x LysM^{Cre} 5	2	8	Immune cell accumulation at meninges. Parenchyma infiltration from meninges in white matter ventral and dorsal regions.

(B)

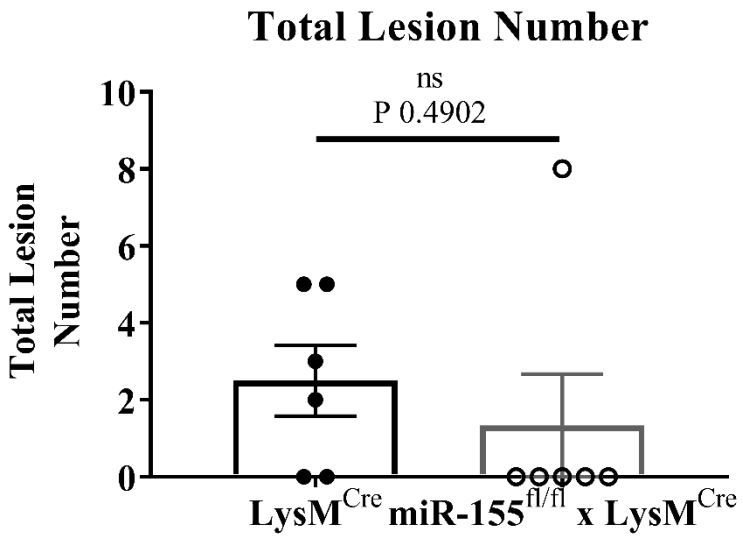

Figure 5.15 Descriptive histological analysis and lesion burden of miR-155$^{fl/fl}$ x LysMCre spinal cords.

LysMCre controls and miR-155$^{fl/fl}$ x LysMCre$^{+/+}$ mice were actively induced with EAE using 32.5 µg rMOG on day 0 and 200 ng Pertussis toxin as an adjuvant on days 0 and 2. EAE was carried out for a total of 28 days. Mice were perfused with PFA and spinal cord samples were fixed with PFA and sucrose protected. Spinal cord samples underwent OCT embedding and freezing prior to H&E staining. (A) A summary table containing clinical scores, total lesion number, and brief descriptions of LysMCre control and miR-155$^{fl/fl}$ x LysMCre$^{+/+}$spinal cord sections. Total lesion numbers and brief descriptions were derived from three randomly selected sections. (B) Total lesion numbers were derived from three randomly selected sections calculated per mouse strain. Total lesion numbers were derived from 3 sections throughout the spinal cord per mouse strain (n=6 LysMCre controls, n=5 miR-155$^{fl/fl}$ x LysMCre$^{+/+}$ mice, 1 independent experiment).

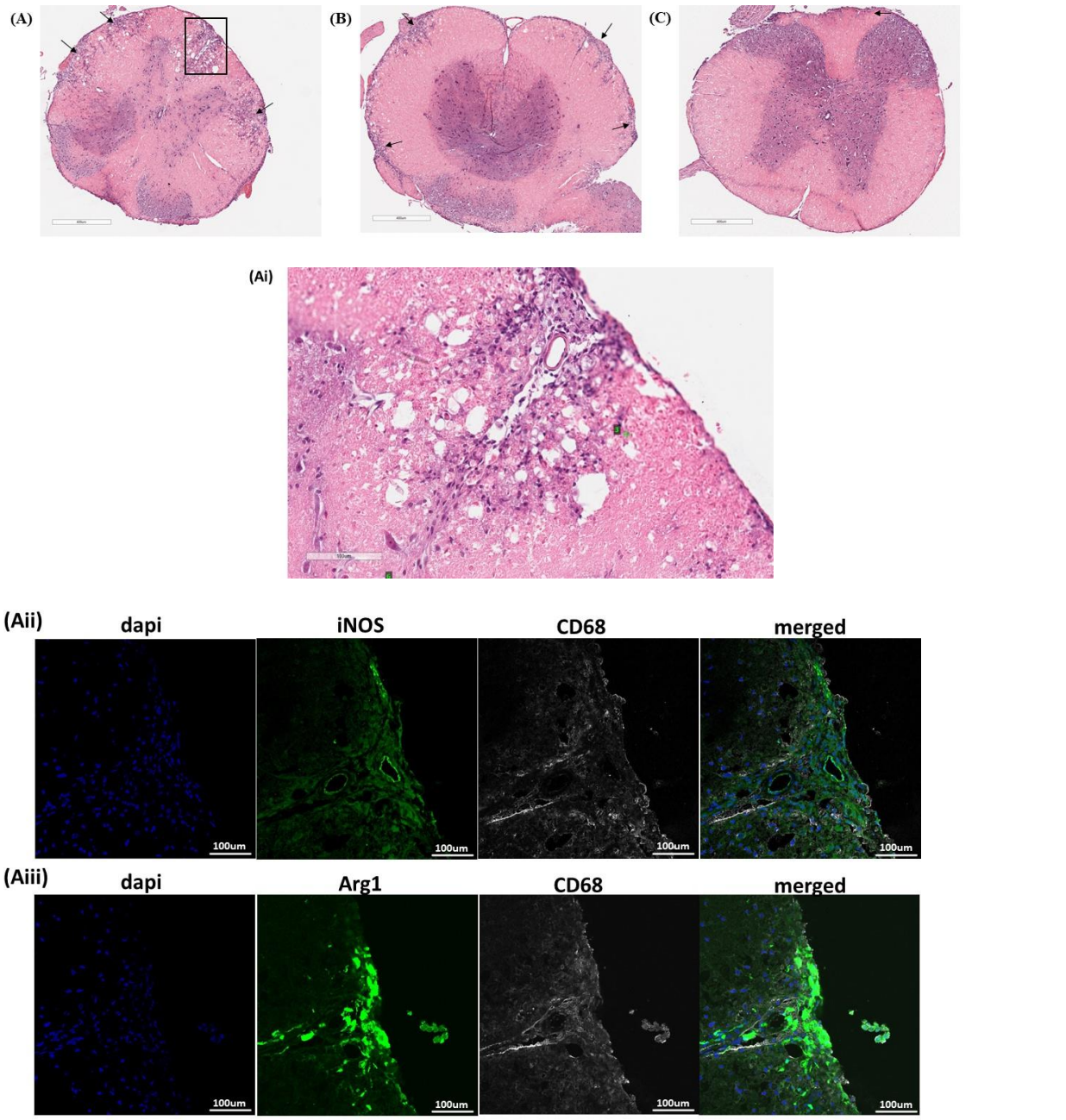

Figure 5.16 H&E and IF staining of LysMCre spinal cords at day 28 EAE.

LysMCre controls and miR-155$^{fl/fl}$ x LysMCre$^{+/+}$ mice were actively induced with EAE using 32.5 µg rMOG on day 0 and 200 ng Pertussis toxin as an adjuvant on days 0 and 2. EAE was carried out for a total of 28 days. Mice were perfused with PFA and spinal cord samples were fixed with PFA and sucrose protected. Spinal cord samples underwent OCT embedding and freezing prior to H&E staining. (A-C) H&E staining of LysMCre spinal cord sections, (Ai) magnified area of interest derived from boxed region in image (A), and (Aii-iii) IF staining for CD68, iNOS, and ARG1 of area derived from (Ai). Scale bar 400µm (A-C), 100µm (Ai-Aiii). Data represents mean descriptions of n=5 LysMCre control mice, 1 independent experiment.

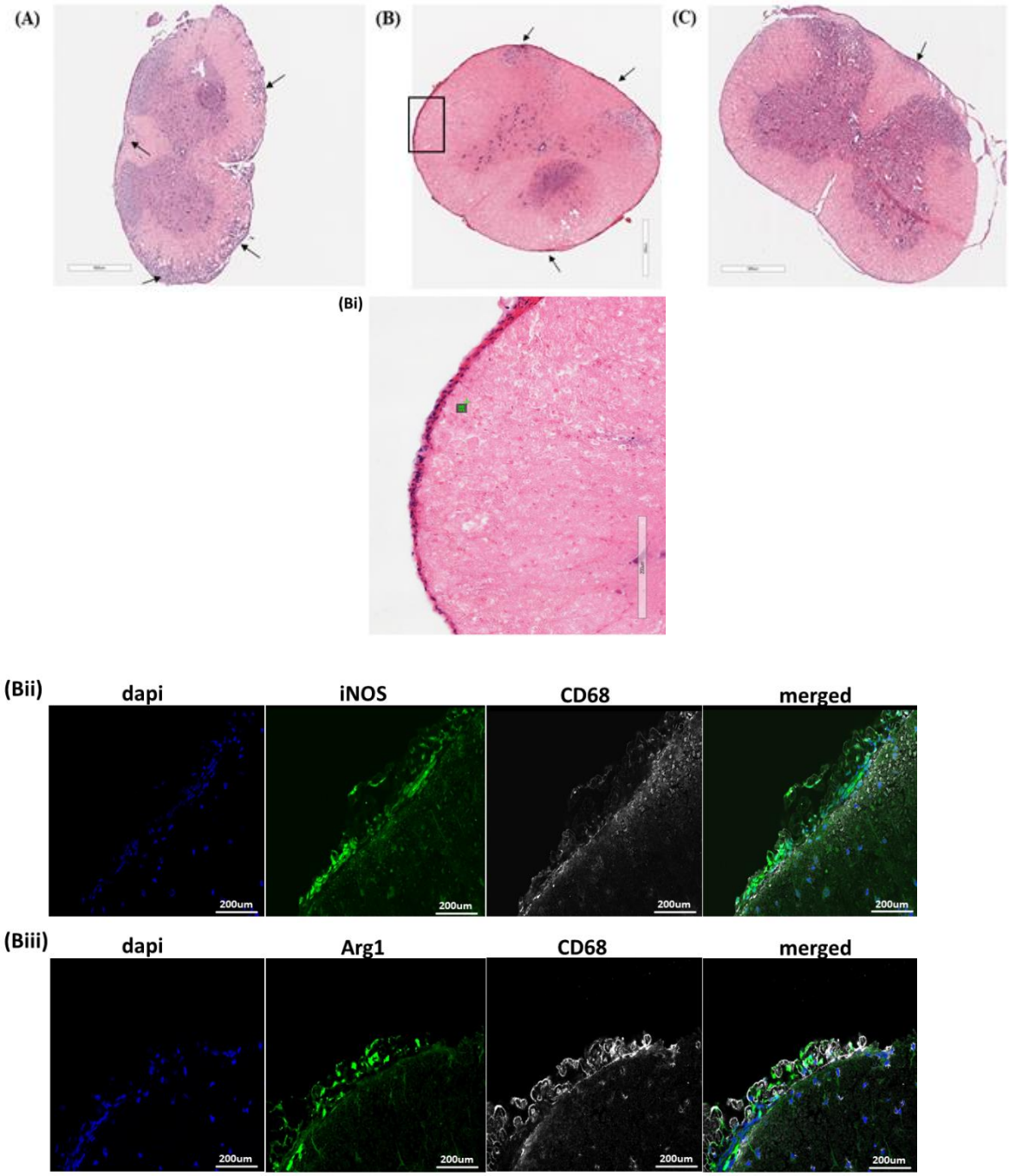

Figure 5.17 H&E and IF staining of miR-155$^{fl/fl}$ x LysMCre spinal cords at day 28 EAE.

LysMCre controls and miR-155$^{fl/fl}$ x LysMCre$^{+/+}$ mice were actively induced with EAE using 32.5 µg rMOG on day 0 and 200 ng Pertussis toxin as an adjuvant on days 0 and 2. EAE was carried out for a total of 28 days. Mice were perfused with PFA and spinal cord samples were fixed with PFA and sucrose protected. Spinal cord samples underwent OCT embedding and freezing prior to H&E staining. (A-C) H&E staining of miR-155$^{fl/fl}$ x LysMCre spinal cord sections, (Bi) magnified area of interest derived from boxed region in image (B), and (Bii-iii) IF staining for CD68, iNOS, and ARG1 of area derived from (Bi). Scale bar 600µm (A, C), 200µm (B, Bi-Biii). Data represents mean descriptions of n=6 miR-155$^{fl/fl}$ x LysMCre mice, 1 independent experiment.

5.3 Discussion

Growing evidence supporting the role of myeloid cells, particularly macrophages, in the pathogenesis of EAE allows opportunities for these immune cells to be potentiated for immunotherapy. Understanding how miR-155 in macrophages facilitates chronic inflammation and ultimately demyelination will enable the role of miR-155 in macrophages to be exploited and targeted to assist in CNS repair. This Chapter collectively demonstrates a unique approach at evaluating the role of miR-155 in myeloid cells throughout EAE by using novel miR-155$^{fl/fl}$ x LysM^{Cre} mice. In doing so, miR-155 deletion in macrophages can be explored on a functional level to determine how miR-155 deletion affects disease outcomes.

To test the hypothesis that miR-155 deletion attenuates proinflammatory properties of macrophages, EAE was initially induced in LysMCre control and miR-155$^{fl/fl}$ x LysMCre mice by immunising with 65µg rMOG. Unexpectedly, miR-155$^{fl/fl}$ x LysMCre mice exhibited exacerbated EAE clinical scores. This result was not anticipated as previous studies have shown total miR-155 deficient mice were completely resistant to EAE (O'connell *et al.*, 2010). Moreover, proinflammatory macrophages contribute to CNS demyelination (Ajami *et al.*, 2011), and high levels of miR-155 have been detected in immune cells during EAE and MS (Moore, Vijayaraghava T.S. Rao, *et al.*, 2013).

Neuroinflammatory processes during EAE are known to cause a significant increase in bone marrow production of myeloid cells that migrate towards the CNS environment. MiR-155 has been proven essential for myeloid cell differentiation (Moore, Vijayaraghava T.S. Rao, *et al.*, 2013), and if this differentiation role applies to EAE, deleting miR-155 could cause macrophages to exhibit a myeloid derived suppressor cell (MDSC) phenotype. Wang et al. performed a study focussing on global miR-155 deletion in mouse tumour models. Evidence supporting miR-155 deletion promotes an MDSC phenotype was prominent in these mice as Wang et al. reported an increase of MDSCs with enhanced recruitment abilities towards tumour sites, ultimately promoting solid tumour growth due to their suppressed proinflammatory response (Wang *et al.*, 2015). Environmental cues involved in promoting MDSC release from the bone marrow include proinflammatory cytokines such as IL-6, IL-

10, IL-1β, GM-CSF, and CCL2/MCP-1 (Groth *et al.*, 2019), all of which play a role in MS pathogenesis (Göbel, Ruck and Meuth, 2018). MDSCs exhibiting an immature anti-inflammatory phenotype can be identified by their co-expression of ARG1 and iNOS (Ostrand-Rosenberg and Fenselau, 2018), an observed finding from this Chapter focussing on spinal cord sections at day 28 EAE. Moreover, Ly6C is another indicative marker of an MDSC phenotype, and perhaps enhanced Ly6C expression from *in vitro* studies using miR-155$^{fl/fl}$ x LysMCre mice in Chapter 4 could additionally be correlating with MDSC characteristics. Accumulating evidence surrounding the role of MDSCs strongly suggests they play a role in miR-155$^{fl/fl}$ x LysMCre mice studied in this Chapter during EAE progression. However, future studies are required to provide confirmatory evidence of how these cells impact the ability of macrophages to mount an immune response. If macrophage precursor cells were in fact maintained in an MDSC phenotype, their ability to effectively elicit a proinflammatory response during active immunisation with tuberculosis and pertussis toxin to induce EAE would be greatly impaired.

To alternatively evaluate how miR-155 deletion in myeloid cells affect EAE progression, LysMCre control and miR-155$^{fl/fl}$ x LysMCre mice were induced with EAE by immunising with a lower dose of rMOG (32.5µg). By reducing the dosage of rMOG in active immunisation, it allows any impact of deleting a signalling pathway, such as miR-155 in macrophages, to be distinguished. Excitingly, while observing clinical scores of miR-155$^{fl/fl}$ x LysMCre mice undergoing EAE, they distinctly exhibited either disease resistance or overall attenuated clinical scores in comparison to LysMCre controls. In addition to miR-155$^{fl/fl}$ x LysMCre mice presenting with lower disease instance and severity, several mice exhibited atypical clinical signs of EAE. For example, tail paralysis may not have been observed but a prominent change to gait, where forward movement would be skewed to one direction, was documented. Separate studies additionally reported atypical signs of EAE, some of which suggested preferential trafficking of different immune cell types into the brain or spinal cord, or T cell differentiation, was responsible for this occurrence (Stromnes *et al.*, 2008). Findings from Liu et al. surrounding SOCS3 deletion in myeloid cells using the LysMCre system suggested that atypical EAE phenotypes were due to increased infiltrating neutrophil populations within the brain stem and cerebellum. Moreover, Liu et al. proved by suppressing neutrophil populations, atypical EAE phenotypes were replaced with classical signs of EAE (Liu *et al.*, 2015). However, relating these findings to miR-155$^{fl/fl}$ x LysMCre

data from this Chapter, there were decreased neutrophil and macrophage proportions within the CNS during EAE. An additional study performed by Kurte et al. observed atypical EAE upon administering MSCs in mid to late stages of EAE. Kurte et al. suggested atypical EAE was caused by an imbalanced ratio of Tregs to Th1/Th17 cells rather than an imbalanced ratio of Th1 to Th17 cells, however stated further confirmatory tests would need to verify this suggestion (Kurte *et al.*, 2015). It is possible that miR-155 deletion drives a Treg phenotype, as has been observed in studies outlined by Zhang et al. (Zhang *et al.*, 2011). However, this would need to be confirmed experimentally by measuring the impact on T cell phenotypes in miR-155$^{fl/fl}$ x LysMCre mice. Collectively these studies suggested either the accumulation of specific immune cell subsets within CNS compartments or T cell differentiation within the CNS are causative events of atypical EAE phenotypes.

Immune cell profiling could determine if clinical scores of miR-155$^{fl/fl}$ x LysMCre mice induced with EAE were possibly due to preferential immune cell proportions within the CNS. This Chapter demonstrated miR-155$^{fl/fl}$ x LysMCre mice at day 14 EAE (65µg rMOG) with enhanced disease severity and earlier disease onset displayed a trend of increased infiltrating macrophages and decreased microglia and neutrophil proportions within the CNS. These findings suggested that enhanced disease severity was associated with increased infiltrating macrophage proportions within the CNS and not neutrophils. Infiltrating macrophages are confirmed to enter the CNS and exert proinflammatory functions that contribute to the pathogenesis of EAE (Chu *et al.*, 2018). Macrophages have also been reported to re-activate microglia to sustain a chronically inflamed CNS and prolong proinflammatory cytokine production, therefore perhaps the presence of increased macrophage proportions in miR-155$^{fl/fl}$ x LysMCre mice are creating a heightened and sustainable proinflammatory environment. Whilst investigating immune cell populations in miR-155$^{fl/fl}$ x LysMCre mice at day 20 EAE (32.5µg rMOG) with resistant or ameliorated disease severity and delayed disease onset, mice contrastingly displayed a trend of decreased infiltrating macrophages and neutrophils and increased microglia proportions within the CNS. This finding identified a correlation between decreased macrophage infiltration into the CNS with attenuated clinical scores. Additionally, data from Chapter 4 demonstrated that miR-155 deleted macrophages failed to upregulate proinflammatory genes (iNOS, TNF-α) in response to inflammatory stress *in vitro*, but instead upregulated ARG1 and ARG2, markers of an anti-inflammatory state. Therefore, perhaps miR-155$^{fl/fl}$ x LysMCre

macrophages within the CNS at day 20 EAE exert attenuated inflammatory responses and cannot re-activate microglia to the same extent, thus indirectly dampening the overall inflammatory cascade within the CNS mediated by microglia.

Investigating surface markers on macrophages, microglia, and neutrophils, representing their functional properties in LysMCre controls and miR-155$^{fl/fl}$ x LysMCre mice may provide insight to how miR-155 deletion in myeloid cells functionally affects these immune cell subsets. Chosen cell surface markers were consistent with Chapter 3: Ly6C, MHCII, and CCR2, to identify cell activation states, antigen presentation processes, and the ability to upregulate an essential EAE chemokine. Interestingly, there were no significant differences in Ly6C or MHCII expression on macrophages, microglia, or neutrophils from both EAE experiments (65µg rMOG at day 14 EAE or 32.5µg rMOG at day 20 EAE). However, there was a notable trend of decreased CCR2 expression on macrophages and microglia at day 14 EAE in mice immunised with 65µg rMOG. As previously mentioned, CCR2 is crucial for macrophage entry into the CNS and contributes to EAE pathogenesis (Fife *et al.*, 2000). The presence of CCR2 on infiltrating monocyte derived macrophages is associated with proinflammatory phenotypes that invade the CNS tissue and facilitate demyelinating processes. Pare et al. confirmed that the transmigration of CCR2^{+} monocytes from the bloodstream into the CNS is reliant on IL-1β. Furthermore, Pare et al. shows how IL-1β grants access to CCR2^{+} monocytes prior to clinical onset of EAE by demonstrating an impediment of macrophage infiltration when interfering with the IL-1 β/IL-1R1 axis (Paré *et al.*, 2018). It would be interesting to measure IL-1β in miR-155$^{fl/fl}$ x LysMCre mice to further correlate how decreased CCR2 expression on macrophages from this Chapter is associated with the decreased proportions of macrophages within the CNS.

MiR-155 expression data in macrophages and neutrophils from this Chapter confirmed the failure of miR-155 induction at days 14 and 20 EAE in miR-155$^{fl/fl}$ x LysMCre mice. However, miR-155 expression in microglia also appeared impaired in miR-155$^{fl/fl}$ x LysMCre mice, where microglia had decreased miR-155 expression at day 14 EAE in mice immunised with 65µg rMOG. The LysMCre system is most likely responsible for this occurrence as separate studies provided similar findings of LysMCre targeting other cells within the CNS such as microglia (Abram *et al.*, 2014; Ferro *et al.*, 2018). Although there

have been reports of LysMCre targeting immune cells other than monocyte derived macrophages and neutrophils, it is one of the most reliable systems to conditionally target miR-155 deletion in monocyte derived macrophages in comparison to other Cre systems such as CD11b and F4/80 (Abram *et al.*, 2014; McCubbrey *et al.*, 2017). Another plausible cause why miR-155 expression was affected in miR-155$^{fl/fl}$ x LysMCre microglia could be indirectly due to miR-155 deletion in macrophages. Cross-talk between macrophages and microglia is known to occur during EAE (Chu *et al.*, 2018), therefore perhaps miR-155 deletion attenuated the ability of macrophages to exert proinflammatory effects thus indirectly dampening proinflammatory miR-155 induction in microglia.

Histological analyses of spinal cords derived from LysMCre control and miR-155$^{fl/fl}$ x LysMCre mice at day 28 EAE illustrated distinct differences in how immune cells were trafficked into the CNS. In concurrence with separate studies, there was a clear correlation of clinical scores reflecting immune cell pathology within the parenchyma regions of spinal cord sections (Jiang *et al.*, 2017; Shrestha *et al.*, 2017). There were notable trends of LysMCre control mice exhibiting clinical scores of EAE with heavy parenchymal infiltration and formation of spinal cord lesions. In comparison, the majority of miR-155$^{fl/fl}$ x LysMCre mice exhibited a decrease in disease severity, and a trend of immune cells accumulating in the meninges rather than heavy parenchymal infiltration.

In relation to how miR-155 deletion in myeloid cells affected immune cell trafficking into the CNS, there may be several plausible explanations for this occurrence. For example, miR-155 has been linked to facilitating T cell trafficking across the BBB into the CNS in a mouse model of acute encephalomyelitis (Dickey *et al.*, 2016). Dickey et al. used a virally induced encephalomyelitis model in miR-155$^{-/-}$ mice to confirm miR-155 was involved in suppressing T cell migration into the CNS and promoted antiviral activity of T cells. Interestingly, macrophage trafficking into the CNS was not affected in that disease model, a finding contrasting with this Chapter, but rather differences in observed disease severity was suggestively due to impaired T cell responses (Dickey *et al.*, 2016). Separate reports additionally identify miR-155 to affect myeloid cell migration. Cao et al. verified the involvement of miR-155 in neutrophil migration by demonstrating Rac1 suppression by miR-155 led to attenuated migration toward chemotactic agents, IL-8 and fMLF (Cao *et al.*,

2017). Interestingly, studies surrounding the role of Rac1 in macrophages did not confirm altered migration abilities in Rac1$^{-/-}$ mice, but rather observed an altered morphology resembling a 'ruffled membrane', indicating initial structural changes in macrophages. Additionally, Kim et al. reported phagocytosing macrophages exhibited an increase in Rac1 expression (Kim *et al.*, 2017). Therefore, perhaps miR-155 deletion in macrophages allowed migration towards the meninges, but due to an altered morphology or impaired phagocytosis abilities by miR-155 mediated Rac1 suppression, macrophages could not gain entry to the parenchyma. Overall, histology data generated in this Chapter illustrates a crucial trafficking role for miR-155 in immune cells in EAE that appears to reflect clinical scores of disease. However, further studies warrant investigation to identify how miR-155 deletion in myeloid cells affect cell migration from the meninges into the parenchyma, and if this specific communication checkpoint is mediated by a cytokine feedback loop involving miR-155, due to morphological changes in macrophages, or an altered ability in macrophages to phagocytose material at this location resulting in impaired entry.

Under further investigation, there was a prominent presence of CD68^{+} cells at sites of inflammation expressing both iNOS and ARG1 in both mouse strains, suggesting a heterogenous pool of infiltrating macrophage phenotypes (Kyle A Jablonski *et al.*, 2016). Evidence has shown classical polarisation markers ARG1 and iNOS are useful to distinguish phenotypical aspects of macrophages within CNS environment (Veronique E Miron *et al.*, 2013; Locatelli, Theodorou, Kendirli, Jordão, *et al.*, 2018). Immunofluorescent staining of CD68^{+} macrophages within spinal cords of miR-155$^{fl/fl}$ x LysMCre mice allowed visualisation of how miR-155 deleted macrophages are polarised at site specific locations within EAE spinal cords. Findings from this Chapter reported a heterogeneous population of CD68^{+} cells expressing iNOS, ARG1, or both, in LysMCre controls plus miR-155$^{fl/fl}$ x LysMCre spinal cord sections. These data correlated with a study performed by Locatelli et al. that verified macrophages underwent phenotypic changes at lesion depending on the environment within the CNS and the stage of inflammation (Locatelli, Theodorou, Kendirli, Jordão, *et al.*, 2018). Locatelli discussed how macrophages exhibited changes to their transcriptional profiles and most importantly confirmed that macrophages expressed iNOS at initiation stages of EAE prior to transitionally shifting towards a heterogeneous mix of iNOS and ARG1 expression before they predominantly expressed ARG1 at the later stages of disease. Additionally, the parenchyma compartment where macrophages enter the spinal

cord significantly affected their initial polarisation switches (Locatelli, Theodorou, Kendirli, Jordão, *et al.*, 2018). Furthermore, Miron et al. demonstrated how macrophage polarisation from proinflammatory to anti-inflammatory phenotypes occurred at initial stages of remyelination, and stated this occurrence was essential for efficient remyelination (Veronique E. Miron *et al.*, 2013). It would therefore be interesting to perform in situ hybridisation to visually identify miR-155 in CD68^{+} cells to assess how miR-155 directly impacts macrophages polarisation and location within specific compartments of the CNS, as well as its capacity for remyelination. Moreover, visually identifying miR-155 in other adaptive immune cells at specific lesion sites or meningeal areas displaying immune cell accumulation to determine if miR-155 deletion in myeloid cells indirectly affects T and B cell expression of miR-155 would provide a greater understanding.

Although preliminary IF staining of spinal cord sections in this Chapter strongly indicated the presence of heterogenous macrophage populations expressing iNOS and ARG1, future directions optimising IF staining would provide a greater and more accurate insight. The exact proportion of CD68^{+} macrophages expressing iNOS and ARG1 could be identified and visualised in specific spinal cord regions, a finding that could be directly correlative with Miron et al. and Locatelli at al. studies. Protocol areas for potential optimisation to enhance the visualisation of CD68^{+} macrophages expressing iNOS and ARG1 include the antigen retrieval technique. Efficiently restoring the immunoreactive epitope structures through optimised antigen retrieval techniques could result in enhanced binding of antibodies to tissue, and subsequently lead to improved visualisation of immunofluorescent labelled spinal cord sections (Shi *et al.*, 1995; Shi, Cote and Taylor, 1997). Citrate buffer antigen retrieval was utilised in this Chapter to retrieve immunoreactive epitopes for IF staining, therefore alterations to citrate buffer concentrations and incubation periods could minimise unspecific binding of antibodies and background staining. Preliminary attempts to identify the appropriate dilution factors of antibodies for IF staining were performed, however further optimisation to primary and secondary antibody dilutions could be applied to ensure optimal staining intensity.

Whilst invaluable information has been obtained from studying miR-155 in miR-155$^{fl/fl}$ x LysM^{Cre} mice throughout an inducible EAE time-course, it is important to acknowledge

certain limitations to this study, and how to overcome these limitations to further verify the role of miR-155 in myeloid cells during EAE. For instance, inducing EAE via active immunisation with pertussis toxin and TB involves the activation of TLR agonists such as TLR4 (Racke, Hu and Lovett-Racke, 2005). The lack of miR-155 in myeloid cells may impact the immune response to these adjuvants. One approach to overcome this limitation includes inducing EAE by adoptive transfer of MOG specific $CD4^+$ T cells into naïve mice to closer recapitulate MS (Robinson *et al.*, 2014).

Additional approaches to study the effects of miR-155 deletion in macrophages during EAE could include adoptively transferring miR-155 deleted macrophages that exhibit an anti-inflammatory phenotype into EAE mice. Ma et al. demonstrated that adoptive transfer of *in vitro* polarised anti-inflammatory macrophages derived from bone marrow into rats post spinal cord injury ameliorated overall spinal cord lesion volume (Ma *et al.*, 2015). Interestingly, Ma et al. confirmed this outcome was mediated by anti-inflammatory cytokine production from adoptively transferred macrophages. These anti-inflammatory macrophages were reportedly capable of producing IL-10, TGF-β, IL-13, subsequently skewing T cell differentiation from Th1 responses to Th2, in addition to polarising microglia and infiltrating macrophages to an anti-inflammatory phenotype. In the context of translationally approved therapies, adoptive transfer of primed T cells with anti-tumour properties have been successful for several human cancer treatments (Rosenberg and Restifo, 2015). Since *in vitro* studies from chapter 4 suggested that miR-155 deletion promoted an anti-inflammatory macrophage state, it would therefore be interesting to apply this adoptive transfer technique to the EAE mouse model used in this study to investigate how miR-155 deletion in macrophages affects disease progression and clinical outcome *in vivo*. By performing this approach as opposed to the LysMCre system of deleting miR-155 from macrophages, the therapeutic outcome of miR-155 deletion would solely be responsible for macrophages involvement in EAE, excluding the possibility of the LysMCre system affecting other immune cells subsets such as neutrophils and microglia.

Tamoxifen induced deletion of miR-155 in mature macrophages rather than developmental macrophages may be another avenue to consider investigating the role of miR-155 in macrophages during EAE. This chapter identified decreased proportions of myeloid derived

macrophages within the CNS of miR-155$^{fl/fl}$ x LysM^{Cre} mice immunised with 32.5 µg of rMOG. Therefore, it would be interesting to investigate the effect of inducing miR-155 deletion in macrophages post entry into the CNS. In doing so, it would allow a higher proportion of macrophages to enter the CNS that are subsequently switched to an anti-inflammatory phenotype upon miR-155 deletion, thus potentially enhancing the rate of repair processes and potentially alleviating clinical outcome. Leone et al. demonstrated a successful tamoxifen inducible Cre mouse model of EAE (Leone *et al.*, 2003). Leone's findings surrounded glial cells rather than macrophages but confirmed the possibility of selectively inducing cre recombinase activity in transgenic mice by fusing Cre to the human estrogen receptor ERT2 (CreERT2) to investigate Schwann cells and oligodendrocytes. If this crossbreeding technique was applied to mice in this Chapter containing miR-155 floxed regions and CreERT2 on myeloid-lineage cells, it would allow miR-155 deletion to be studied based on clinical scores and signs of paralysis. Deleting miR-155 in macrophages at distinct clinical stages of disease as opposed to 7-day interval timepoints would be an excellent tool to distinguish how miR-155 effects macrophage polarisation and demyelinating processes at distinct clinical stages of disease.

Population studies, miRNA expression, and cell surface marker analysis throughout this Chapter was performed utilising both the brain and spinal cord to gain a global overview of events occurring throughout the entire CNS. It could be additionally insightful to perform these analyses on brains and spinal cords separately, as data generated in this chapter may be representing diluted samples and not relaying information directly relating to lesion sites or specific areas of inflammation. Figures 5.15 and 5.16 attempted to overcome this by performing histological and IF imaging of sections throughout the spinal cord of EAE mice. Since the majority of lesions occur within the spinal cord in this mouse model of EAE (Gibson-Corley *et al.*, 2016), focusing on these regions allowed region specific comparative analysis between both mouse strains at an important later timepoint in EAE.

Harnessing miR-155 deletion in macrophages as a therapeutic option offers potential mechanisms of attenuating neuroinflammatory processes whilst assisting tissue repair. As current FDA approved MS therapies solely attenuate the inflammatory immune response, this approach would offer novel avenues surrounding the exploitation of macrophages for

their reparative features and not only at suppressing inflammation. Recent studies are however gravitating towards these important repair processes, some of which are under investigation in clinical trials attempting to promote remyelination in MS patients. This chapter undoubtedly identified the potential of deleting miR-155 in myeloid cells to attenuate immune cell infiltration within the spinal cord, and importantly demonstrated ameliorated disease severity. Controlling the ability to switch macrophages towards an anti-inflammatory phenotype and facilitate repair processes may offer exciting opportunities for investigating miR-155 deletion in a time and location dependent manner as a therapeutic option.

Chapter 6

General Discussion

6. General discussion

MiR-155 is an essential inflammatory regulator of all immune cell subsets within the immune system. Previous studies in the EAE model of MS suggest that the resistance of miR-155 knockout mice to EAE induction (Connell *et al.*, 2010) is predominantly $CD4^+$ T cell intrinsic (Gopal Murugaiyan, Beynon, Mittal, Joller and Howard L Weiner, 2011). Results from this research project have established, for the first time that, miR-155 is induced in macrophages during a chronic progressive EAE model. Importantly, miR-155 was only induced in this immune cell subset within the CNS, correlating with an inflammatory macrophage phenotype. *In vitro* studies that modelled monocyte-derived and tissue resident macrophages responses to a TLR4 agonist confirmed that miR-155 deficient macrophages highly upregulate ARG1 and ARG2 gene expression, indicative of a polarisation state associated with resolution of inflammation (Rath *et al.*, 2014; Choudry *et al.*, 2018). Novel *in vivo* studies utilising miR-$155^{fl/fl}$ x LysMCre mice exhibited a delayed onset of clinical scores and ameliorated disease severity, reflecting a distinct trend of immune cells accumulating at the meninges with less instances of parenchyma infiltration, and decreased infiltrating macrophage populations within the CNS. Collectively, these results support a role for miR-155 in regulating macrophage plasticity in EAE. Validation of these findings and an understanding of the molecular mechanisms involved are now crucial for harnessing the tissue reparative properties of macrophages in MS.

6.1 Relevance of studying other mouse models of CNS autoimmunity

Due to the diversity and multifaceted nature of MS, it proves extremely difficult to recapitulate the exact mechanisms involved in contributing to disease into animal models. In humans, there are four categories of MS dependent on clinical presentation of disease: primary progressive MS, secondary progressive MS, progressive relapsing MS, and the most abundant form relapsing remitting MS. Therefore, it is not surprising there are several animal models to study MS with distinct clinical disease courses.

Although RRMS is the most common form of MS in humans, the most studied animal model of this disease is chronic progressive EAE in mice. Results generated from this research project provided invaluable information implicating a pivotal role of miR-155 in

myeloid cells, particularly macrophages, throughout a progressive EAE disease time course. Concurring with multiple EAE studies, evidence from this project also acknowledged miR-155 as an important miRNA in contributing to EAE progression (Connell *et al.*, 2010; Gopal Murugaiyan, Beynon, Mittal, Joller and Howard L Weiner, 2011a; American Academy of Neurology. *et al.*, 2014). Expectedly, findings from Chapter 3 correlated with published findings surrounding $CD4^+$ T cells, but additionally uncovered a novel role for miR-155 in innate cells during EAE. In the context of translating these findings from EAE to MS, miR-155 induction in macrophages was confirmed in human MS studies performed by Moore et al. (Moore, Vijayaraghava T S Rao, *et al.*, 2013). Moore proved miR-155 induction was present in $CD68^+$ cells within untreated human MS brain samples, further supporting findings from Chapter 3 are translational from an EAE animal model to MS.

This research project used a novel approach to study miR-155 in EAE mice by utilising the entire recombinant MOG protein. Since rMOG contains multiple confirmed epitope sites involved in the pathogenesis of EAE (Delarasse *et al.*, 2013; Shetty *et al.*, 2014), this method would closer recapitulate human MS, and exhibit findings that would involve B cells and isotope class switching, which does not occur when using MOG peptide. As most studies surrounding miR-155 in EAE do not immunise with the extracellular domain of the MOG protein to induce disease, but instead use MOG^{35-55} peptide, findings surrounding miR-155 in macrophages during EAE would therefore be perhaps more relatable to pathogenic processes that occur in MS. This method of immunisation could additionally be the causative factor for certain discrepancies observed between data generated by Mycko et al. and findings from this research project.

The EAE mouse model chosen for this project is another aspect to consider when investigating the role of miR-155 in macrophages in disease progression. Active induction of EAE using rMOG and pertussis toxin in C57BL/6 mice resembles a chronic progressive disease course. Other EAE mouse models of MS which could provide insight to study a form of RRMS, would include the relapsing-remitting model of EAE mediated by immunising SJL mice with PLP (Croxford, Kurschus and Waisman, 2011; Al-Sabbagh and Weiner,

2014; Giralt, Molinero and Hidalgo, 2018). This mouse model initially undergoes a prominent progressive phase of EAE before clinical scores appear to remit several days later prior to a subsequent relapsing phase. CNS tissue damage occurring from the second wave of inflammation in this model is due to epitope spreading from the immunising epitope to another epitope of PLP (Marusic *et al.*, 2012). Therefore, understanding the correlation of miR-155 expression in myeloid cells during distinct remitting and relapsing stages of disease could expand current knowledge on miR-155 in macrophages. Additionally, the role of miR-155 in macrophage activation and antigen presentation during the subsequent waves of inflammation could provide insight to how miR-155 correlates with antigen presentation and polarisation markers in macrophages.

Active induction of EAE in C57BL/6 and SJL mice involves immunising with adjuvants containing agonists unrelated to self-antigens, such as Mycobacterium tuberculosis and Bordetella pertussis toxin. M. tuberculosis is a TLR agonist identified to promote NFkB translocation to the nucleus to promote inflammatory molecule production in macrophages and other myeloid cells (Faridgohar and Nikoueinejad, 2017). Moreover, B. Pertussis toxin reportedly affects activation of myeloid cells, such as monocytes, by directly stimulating inflammatory cytokine production and MHCII expression (Pradier *et al.*, 2002). As miR-155 exerts regulatory functions in all immune cell responses to pathogens, the clinical outcome of miR-155$^{fl/fl}$ x LysMCre mice used in this research project cannot exclude the possibility that these bacterial epitopes influenced observed clinical outcomes to some extent. Adoptive transfer EAE involves CD4^{+} T cell isolation from lymph nodes or spleen of EAE immunised mice, re-stimulation of CD4^{+} T cells with myelin protein *in vitro*, and subsequently adoptively transferring these reactivated CD4^{+} T cells specific for myelin protein into naïve mice to induce effector stages of EAE (Terry R.L. et al, 2014). Due to this model excluding the use of bacterial epitopes to induce EAE, and because CD4^{+} T cells in miR-155$^{fl/fl}$ x LysMCre mice would not be affected by the cre-lox system, this model would allow the mechanisms of miR-155 in macrophages to be explored using a closer recapitulating model to human MS. Therefore, adoptive EAE could be a great tool and alternative approach to identify the relationship between miR-155 and macrophages in EAE disease progression.

It would be interesting to investigate a spontaneous relapsing remitting disease course and study the role of miR-155 in macrophages throughout this form of EAE (Dunn *et al.*, 2009). Tracking and comparing the role of miR-155 expression in macrophage phenotypes throughout a spontaneous relapsing-remitting model of EAE could identify important differences and similarities between primary progressive EAE and relapsing remitting EAE, evident differences which are seen in human MS patients.

6.2 Macrophages can contribute to tissue repair depending on their polarisation state

MiR-155 expression plays a prominent role in regulating macrophage functions and characteristics. It is established that upregulation of miR-155 skews the polarisation of macrophages towards an inflammatory phenotype (Kyle A Jablonski *et al.*, 2016). Although inflammatory macrophages are implemented in promoting clinical EAE progression via inflammatory cytokine production and presenting autoantigens to $CD4^+$ T cells (Rawji and Yong, 2013), Miron et al. crucially determined a macrophage polarisation switch within the CNS. This research group observed a phenotypic switch from an inflammatory phenotype towards an immunoregulatory state at the initial stages of remyelination via identifying a dominant population of $CD68^+Arg1^+$ cells at remyelinating lesion sites (Veronique E Miron *et al.*, 2013). Interestingly, *In vitro* studies from this research project found an increase of ARG1 and ARG2 gene expression in miR-155 deficient macrophages treated with LPS, suggestive of immunoregulatory polarisation skewing. This finding was evident in two distinct macrophage population subsets: bone marrow derived macrophages, and fully differentiated tissue resident peritoneal macrophages, further emphasising the gravity of these results. These gene markers provide useful identification of macrophage polarisation and characteristic phenotypes, but unfortunately are not representatives of macrophage functional capabilities.

One mechanism by which macrophages prove beneficial in promoting remyelination is by phagocytosing myelin debris, thus allowing OPC differentiation. The importance of infiltrating macrophages in CNS repair is further highlighted by Kotter et al. findings of reduced remyelination upon deletion of monocytes in a rat model of demyelination using lysolecithin (Kotter *et al.*, 2005). As remyelination is a key mechanism for CNS repair, it

would be insightful to investigate the functional aspects of miR-155 deletion in macrophages regarding their ability to clear debris. Myelin debris clearance mediated by macrophage phagocytosis is an essential process for remyelination to commence (Yin *et al.*, 2017). Studying phagocytic abilities of miR-155 deficient macrophages could expand current knowledge surrounding the correlation of miR-155 in macrophage phagocytosis in the context of EAE and how it may promote remyelination. If miR-155 deletion in macrophages attenuates demyelinating processes whilst promote remyelination, neurodegeneration and disease progression would be limited. There is a correlation between age and decline in remyelination rates. This decline was suggestively related to the reduced ability of macrophages to phagocytose myelin material (Franklin and Ffrench-Constant, 2017). Moreover, Kotter et al. demonstrated that macrophages were critical for early remyelination processes, as macrophage depletion was documented to impair remyelination (Kotter *et al.*, 2001). Current FDA approved MS therapies aim at attenuating the inflammatory responses to limit demyelinating processes, however there are no therapies capable of remyelinating once demyelination occurs, hence CNS tissue damage does not get repaired. If miR-155 deletion promotes a reparative phenotype of macrophages, as suggested by gene analysis data from Chapter 4, tissue damage caused by demyelination may be reversible. Further evidence surrounding the functional properties of macrophages is required to verify that miR-155 deletion will facilitate CNS repair. Phagocytic capacity of macrophages could be assessed *in vitro* using fluorescently labelled myelin debris. Labelling myelin with pHrodo red allows a simplistic approach to measure myelin uptake into macrophages via flow cytometry to investigate if miR-155 deletion improves efficiency of phagocytosis (Rolfe *et al.*, 2017). Alternatively, macrophages deficient in miR-155 could be administered directly into the CNS to examine their role in promoting remyelination following cuprizone or lysolecithin-induced demyelination. Such an approach could examine not only their role in clearance of debris, but also in promoting OPC differentiation.

6.3 LysMCre studies is a novel approach to study miR-155 in EAE

Data generated from Chapter 3 strongly suggest miR-155 plays an important role in myeloid cells throughout EAE disease progression. Furthermore, Chapter 2 outlines how miR-155 deletion in macrophage populations promotes gene expression indicative of polarisation skewing towards an immunoregulatory phenotype. Therefore, LysMCre was chosen as a tool

to approach how the role of miR-155 in macrophages may affect EAE progression. The ability to target specific cell types using the Cre/loxP system has contributed to abundant information surrounding the roles of macrophages and other myeloid cells in autoimmune diseases since its establishment in 1999 (Clausen *et al.*, 1999). Although the target efficiency of the Cre/loxP system for macrophage studies has recently been debated due to Lyz2 been detected in additional cell subsets, the efficiency of monocytes/macrophages affected by Cre recombinase is approximately 83-100%, dependent on tissue location. Additionally, granulocytes such as neutrophils have reportedly 100% deletion efficiency, whereas splenic dendritic cells have 16%. Other frequently used Cre recombinase gene targets for macrophage studies include: CD11b, F4/80, and Csf1r (Shi *et al.*, 2018). However, all these targets vary in deletion efficacy and cell-specificity, and ultimately emphasises the struggle to perfectly target macrophages as a whole population using the approach of cre-recombinase. This is not surprising as macrophages are known to exhibit heterogeneous characteristics that are reliant on environmental cues to perform functional mechanisms.

Recent studies suggest a percentage of microglia proportions contain the Lyz2 gene and are consequently targeted by the cre/loxP system. The exact percentage of targeted microglia is unconfirmed, but it is suggested anywhere from 20% to 45% of microglia contain the Lyz2 gene (Blank and Prinz, 2016). Alongside macrophages, microglia exhibit abilities to promote CNS tissue repair through debris clearance and promoting remyelination (Miron *et al.*, 2013). Therefore, it cannot be excluded that these CNS resident cells contributed to clinical score data generated from Chapter 5 utilising miR-155$^{fl/fl}$ x LysMCre mice.

A neurodegenerative disease model more suitable to study miR-155 in microglia would be the cuprizone model. This mouse model of demyelination and remyelination allows functional mechanisms of miR-155 in microglia to be explored during demyelinating stages whilst excluding the involvement of the autoreactive immune response (Praet *et al.*, 2014). Furthermore, investigating the angle of miR-155's correlation with CNS tissue repair would be useful by studying miR-155 in microglia during spontaneous remyelinating stages to compare with miR-155 studies in CNS infiltrating macrophages during a remitting phase in EAE induced SJL mice. Another insightful approach to study miR-155 deletion in microglia would include using miR-155$^{fl/fl}$ x CX3CR1^{Cre} mice (Haimon *et al.*, 2018).

Overall, research studies have yet to define a robust model of specifically targeting genes within macrophages *in vivo*. Delays in identifying a robust model may be due to several possibilities; macrophages as a population are not entirely homogeneous like eosinophils or basophils, but rather they have acquired distinct compartmentalised macrophage populations, and the constant change of macrophage phenotypes in response to environmental signals. Therefore, utilising currently available gene recombination techniques to target the transcriptional profile of macrophages is a hurdle yet to be entirely overcome.

6.4 MiR-155 as a target candidate for immunotherapy

MiRNAs are emerging as promising therapeutic options for immunotherapy and biomarkers of autoimmune diseases. MiRNAs appear attractive candidates to resolve pathogenic processes in diseases due to their pleiotropic abilities and complex network signalling involved in skewing immune cell functional properties (Hanna, Hossain and Kocerha, 2019). In the context of prospectively using miRNAs for immunotherapy, the FDA approved its first small-interfering RNA (siRNA) drug termed Patisiran, in a polyneuropathic disease in 2018. Moreover, several therapies surrounding miRNAs are currently in Phase I and II clinical trials. Excitingly, an LNA based anti-miR of miR-155 is amongst such miRNAs undergoing trials under the drug name: MRG-106. Thus far, results using MRG-106 in T cell lymphoma and mycosis fungoides patients appear promising, offering potential for using an inhibitor of miR-155 in other disease applications involving immune cells such as MS.

The BBB provides difficulties for drug delivery systems required to infiltrate the CNS to ameliorate pathogenic processes during disease progression. RRMS patients are usually responsive to FDA approved MS DMTs with mechanisms directed towards limiting further relapses, however progressive MS patients are not as receptive to therapies that require entry into the CNS. Limited success in therapy appropriated for progressive MS, with Ocrelizumab as the exception, may be due to the lack of BBB permeability. Drug delivery systems using small RNA molecules are an opportune avenue to overcome entry into the CNS using nanoparticle delivery systems to deliver a miRNA inhibitor such as liposomes or

polymeric nanoparticles (Bors and Erdö, 2019). Inhibiting miR-155 in a specific immune cell subset during active stages of neuroinflammation in MS could offer potential to ameliorate inflammation directly inside the CNS whilst avoiding invasive technique.

6.5 Summary

In summary, data generated from this research project identified miR-155 playing a proinflammatory role in macrophages at specific stages of EAE, correlating with proinflammatory phenotypes. Additionally, miR-155$^{fl/fl}$ x LysMCre macrophage populations exhibited properties indicative of polarisation switching towards an anti-inflammatory phenotype upon exposure to an inflammatory agonist *in vitro.* Upon further investigation in pre-clinical studies, miR-155 deletion in myeloid cells affected spinal cord inflammation processes and attenuated clinical scores of EAE. Collectively these findings confirm miR-155 is playing a pathogenic role in macrophages during EAE and strongly suggests a role for miR-155 in facilitating chronic inflammation within the CNS. Further studies applying miR-155 deletion in macrophages to other models of MS at specific stages of disease, will offer greater insight to the mechanisms of miR-155 and how it may be harnessed for immunotherapy.

Chapter 7

Bibliography

Abram, C. L. *et al.* (2014) 'Comparative analysis of the efficiency and specificity of myeloid-Cre deleting strains using ROSA-EYFP reporter mice', *Journal of immunological methods*, (408), pp. 89–100. doi: 10.1016/j.jim.2014.05.009.Comparative.

Afrasiabi, A. *et al.* (2019) 'Evidence from genome wide association studies implicates reduced control of Epstein-Barr virus infection in multiple sclerosis susceptibility', *Genome Medicine*, 11(1). doi: 10.1186/s13073-019-0640-z.

Agarwal, V. *et al.* (2015) 'Predicting effective microRNA targets in mammalian mRNAs.pdf', *Research article Computational and systems biology | Genomics and evolutionary biology*. doi: 10.7554/eLife.05005.001.

Ahmad, A. S., Shah, Z. A. and Doré, S. (2016) 'Protective Role of Arginase II in Cerebral Ischemia and Excitotoxicity.', *Journal of neurology and neuroscience*, 7(2). Available at: http://www.ncbi.nlm.nih.gov/pubmed/27308186 (Accessed: 26 April 2019).

Airas, L., Nylund, M. and Rissanen, E. (2018) 'Evaluation of Microglial Activation in Multiple Sclerosis Patients Using Positron Emission Tomography.', *Frontiers in neurology*. Frontiers Media SA, 9, p. 181. doi: 10.3389/fneur.2018.00181.

Ajami, B. *et al.* (2011) 'Infiltrating monocytes trigger EAE progression, but do not contribute to the resident microglia pool.', *Nature neuroscience*, 14(9), pp. 1142–9. doi: 10.1038/nn.2887.

Ajami, B. *et al.* (2018) 'Single-cell mass cytometry reveals distinct populations of brain myeloid cells in mouse neuroinflammation and neurodegeneration models', *Nature Neuroscience*, 21(4), pp. 541–551. doi: 10.1038/s41593-018-0100-x.

Al-Sabbagh, A. and Weiner, H. L. (2014) 'Rat Experimental Autoimmune Encephalomyelitis', *Autoimmune Disease Models*, pp. 15–22. doi: 10.1016/b978-0-08-091736-8.50006-4.

Alivernini, S. *et al.* (2018) 'MicroRNA-155—at the Critical Interface of Innate and Adaptive Immunity in Arthritis', *Frontiers in Immunology*. Frontiers, 8, p. 1932. doi: 10.3389/fimmu.2017.01932.

Alizadeh, A., Dyck, S. M. and Karimi-Abdolrezaee, S. (2015) 'Myelin damage and repair in pathologic CNS: challenges and prospects.', *Frontiers in molecular neuroscience*. Frontiers Media SA, 8, p. 35. doi: 10.3389/fnmol.2015.00035.

American Academy of Neurology., M. *et al.* (2014) *Neurology., Neurology*. Advanstar Communications. Available at: https://n.neurology.org/content/82/10_Supplement/P1.184 (Accessed: 20 March 2019).

Amici, S. A., Dong, J. and Guerau-de-Arellano, M. (2017) 'Molecular mechanisms modulating the phenotype of macrophages and microglia', *Frontiers in Immunology*, 8(NOV), pp. 1–18. doi: 10.3389/fimmu.2017.01520.

Antel, J. P. *et al.* (2018) 'Immunology of oligodendrocyte precursor cells in vivo and in vitro', *Journal of Neuroimmunology*. Elsevier, (March), pp. 0–1. doi: 10.1016/j.jneuroim.2018.03.006.

Aram, J. *et al.* (2019) 'Granulocyte-Macrophage Colony-Stimulating Factor as a Therapeutic Target in Multiple Sclerosis', *Neurology and Therapy*, 8(1), pp. 45–57. doi: 10.1007/s40120-018-0120-1.

Arbour, N. *et al.* (2015) 'CD8 + T-Cells as immune Regulators of Multiple Sclerosis', *Article*, 6, p. 1. doi: 10.3389/fimmu.2015.00619.

Arcuri, C. *et al.* (2019) 'Parenchymal and non-parenchymal immune cells in the brain: A critical role in regulating CNS functions', *International Journal of Developmental Neuroscience*. doi: 10.1016/j.ijdevneu.2019.04.005.

Arellano, G. *et al.* (2015) 'Stage-specific role of interferon-gamma in experimental autoimmune encephalomyelitis and multiple sclerosis', *Frontiers in Immunology*, 6(SEP), p. 29. doi: 10.3389/fimmu.2015.00492.

Aung, L. L. *et al.* (2010) 'Plasmacytoid dendritic cells in multiple sclerosis: chemokine and chemokine receptor modulation by interferon-beta.', *Journal of neuroimmunology*. NIH Public Access, 226(1–2), pp. 158–64. doi: 10.1016/j.jneuroim.2010.06.008.

Baecher-Allan, C., Kaskow, B. J. and Weiner, H. L. (2018) 'Review Multiple Sclerosis: Mechanisms and Immunotherapy'. doi: 10.1016/j.neuron.2018.01.021.

Bahareh Ajami, Jame L Bennett, Charles Krieger, Kelly M McNagny, F. M. V. R. (2011) 'Infiltrating monocytes trigger EAE progression, but do not contribute to the resident microglia pool', *Nature Neuroscience*, 14(9).

Bala, S. *et al.* (2015) 'Biodistribution and function of extracellular miRNA-155 in mice OPEN', *Nature Publishing Group*. doi: 10.1038/srep10721.

Bar-Or, A. *et al.* (2010) 'Abnormal B-cell cytokine responses a trigger of T-cell-mediated disease in MS?', *Annals of Neurology*, 67(4), pp. 452–461. doi: 10.1002/ana.21939.

Bar-Or, A. *et al.* (2014) 'Teriflunomide and Its Mechanism of Action in Multiple Sclerosis'. doi: 10.1007/s40265-014-0212-x.

Baran, C. P. *et al.* (2011) 'Transcription factor ets-2 plays an important role in the pathogenesis of pulmonary fibrosis.', *American journal of respiratory cell and molecular biology*. American Thoracic Society, 45(5), pp. 999–1006. doi: 10.1165/rcmb.2010-0490OC.

Baranzini, S. E. and Oksenberg, J. R. (2017) 'The Genetics of Multiple Sclerosis: From 0 to 200 in 50 Years', *Trends in Genetics*. Elsevier Ltd, 33(12), pp. 960–970. doi: 10.1016/j.tig.2017.09.004.

Barca-Mayo, O. and Richard Lu, Q. (2012) 'Fine-tuning oligodendrocyte development by micrornas', *Frontiers in Neuroscience*, 6(FEB), pp. 1–7. doi: 10.3389/fnins.2012.00013.

Bardoel, B. W. *et al.* (2014) 'The Balancing Act of Neutrophils', *Cell Host & Microbe*. Cell Press, 15(5), pp. 526–536. doi: 10.1016/J.CHOM.2014.04.011.

Barros, M. H. M. *et al.* (2013) 'Macrophage polarisation: An immunohistochemical approach for identifying M1 and M2 macrophages', *PLoS ONE*. doi: 10.1371/journal.pone.0080908.

Bartel, D. P. (2004) *Review MicroRNAs: Genomics, Biogenesis, Mechanism, and Function*

ulation of hematopoietic lineage differentiation in mam-mals (Chen et al., 2004), and control of leaf and flower development in plants (Aukerman and Sakai, 2003, Cell. Available at: https://www.cell.com/action/showPdf?pii=S0092-8674%2804%2900045-5 (Accessed: 22 May 2019).

Bartholomäus I, Kawakami N, Odoardi F, Schläger C, Miljkovic D, Ellwart JW, et al. (2009) 'Effector T cells interactions with meningeal vascular structures in nascent autoimmune CNS lesions', *nature*, 462(5).

Basso, A. S., Cheroutre, H. and Mucida, D. (2009) 'More stories on Th17 cells.', *Cell research*. NIH Public Access, 19(4), pp. 399–411. doi: 10.1038/cr.2009.26.

Batoulis, H. *et al.* (2013) 'Blockade of tumour necrosis factor-α in experimental autoimmune encephalomyelitis reveals differential effects on the antigen-specific immune response and central nervous system histopathology'. doi: 10.1111/cei.12209.

Baulina, N. M., Kulakova, O. G. and Favorova, O. O. (2016) *MicroRNAs: The Role in Autoimmune Inflammation*, *REVIEWS*. Available at: https://www.ncbi.nlm.nih.gov/pmc/articles/PMC4837569/pdf/AN20758251-28-021.pdf (Accessed: 29 April 2019).

Baumjohann, D. and Ansel, K. M. (2013) 'MicroRNA-mediated regulation of T helper cell differentiation and plasticity', *Nature Reviews Immunology*. Nature Publishing Group, 13(9), pp. 666–678. doi: 10.1038/nri3494.

Beecham, A. H. *et al.* (2013) 'Analysis of immune-related loci identifies 48 new susceptibility variants for multiple sclerosis', *Nature Genetics*, 45(11), pp. 1353–1362. doi: 10.1038/ng.2770.

Ben-Nun, A. *et al.* (2014) 'From classic to spontaneous and humanized models of multiple sclerosis: Impact on understanding pathogenesis and drug development', *Journal of Autoimmunity*. doi: 10.1016/j.jaut.2014.06.004.

Berard, J. L. *et al.* (2010) 'Differential expression of SOCS1 in macrophages in relapsing-remitting and chronic EAE and its role in disease severity', *Glia*, 58(15), pp. 1816–1826. doi: 10.1002/glia.21051.

Bernardes-Silva, M. *et al.* (2001) 'Recruitment of neutrophils across the blood-brain barrier: The role of E- and P-selectins', *Journal of Cerebral Blood Flow and Metabolism*, 21(9), pp. 1115–1124. doi: 10.1097/00004647-200109000-00009.

Bettelli, E. *et al.* (1998) 'IL-10 is critical in the regulation of autoimmune encephalomyelitis as demonstrated by studies of IL-10- and IL-4-deficient and transgenic mice.', *Journal of immunology (Baltimore, Md. : 1950)*, 161(7), pp. 3299–306. Available at: http://www.ncbi.nlm.nih.gov/pubmed/9759845 (Accessed: 26 April 2019).

Bettelli, E. *et al.* (2004) 'Loss of T-bet, But Not STAT1, Prevents the Development of Experimental Autoimmune Encephalomyelitis', *The Journal of Experimental Medicine*, 200(1), pp. 79–87. doi: 10.1084/jem.20031819.

BGW, A. (1999) *TNF neutralization in MS: Results of a randomized, placebo-controlled multicenter study.*, *Neurology*. Available at: http://ovidsp.ovid.com/ovidweb.cgi?T=JS&PAGE=reference&D=cctr&NEWS=N&AN=CN-00414309 (Accessed: 26 August 2019).

Billack, B. (2006) 'Macrophage activation: role of toll-like receptors, nitric oxide, and nuclear factor kappa B.', *American journal of pharmaceutical education*. American Association of Colleges of Pharmacy, 70(5), p. 102. Available at: http://www.ncbi.nlm.nih.gov/pubmed/17149431 (Accessed: 15 February 2019).

Biphenyls, C. P. (2015) 'HHS Public Access', 91(2), pp. 165–171. doi: 10.1016/j.chemosphere.2012.12.037.Reactivity.

Bitsch, A. *et al.* (2000) 'Acute axonal injury in multiple sclerosis. Correlation with demyelination and inflammation.', *Brain : a journal of neurology*, 123 (Pt 6, pp. 1174–83. Available at: http://www.ncbi.nlm.nih.gov/pubmed/10825356.

Bjarnadóttir, K. *et al.* (2016) 'B cell-derived transforming growth factor-β1 expression limits the induction phase of autoimmune neuroinflammation', *Scientific Reports*. Nature Publishing Group, 6(1), p. 34594. doi: 10.1038/srep34594.

Bjelobaba, I. *et al.* (2018) 'Animal models of multiple sclerosis: Focus on experimental autoimmune encephalomyelitis', *Journal of Neuroscience Research*, 96(6), pp. 1021–1042. doi: 10.1002/jnr.24224.

Blank, T. and Prinz, M. (2016) 'CatacLysMic specificity when targeting myeloid cells?', *European Journal of Immunology*. John Wiley & Sons, Ltd, 46(6), pp. 1340–1342. doi: 10.1002/eji.201646437.

Blüml, S. *et al.* (2011) 'Essential role of microRNA-155 in the pathogenesis of autoimmune arthritis in mice', *Arthritis and Rheumatism*. doi: 10.1002/art.30281.

Bomprezzi, R. (2015) 'Dimethyl fumarate in the treatment of relapsing-remitting multiple sclerosis: An overview', *Therapeutic Advances in Neurological Disorders*, 8(1), pp. 20–30. doi: 10.1177/1756285614564152.

Borjini, N. *et al.* (2016) 'Cytokine and chemokine alterations in tissue, CSF, and plasma in early presymptomatic phase of experimental allergic encephalomyelitis (EAE), in a rat model of multiple sclerosis', *Journal of Neuroinflammation*, 13(1). doi: 10.1186/s12974-016-0757-6.

Bors, L. A. and Erdö, F. (2019) 'Overcoming the blood-brain barrier. Challenges and tricks for CNS drug delivery', *Scientia Pharmaceutica*, 87(1). doi: 10.3390/scipharm87010006.

Boven, L. A. *et al.* (2006) 'Myelin-laden macrophages are anti-inflammatory, consistent with foam cells in multiple sclerosis', *Brain*, 129(2), pp. 517–526. doi: 10.1093/brain/awh707.

Brodersen, P. and Voinnet, O. (2009) 'Target Recognition and Mode of Action', *Nature Reviews. Molecular Cell Biology*, 10(February), pp. 141–148. doi: 10.1038/nrm2619.

Bruck, W. *et al.* (1995) 'Monocyte/Macrophage Differentiation in Early Multiple Sclerosis Lesions Materials and Methods Biopsy Material and Clinical Data', *Ann Neurol*, 38, pp. 788–796.

Bruck, W. *et al.* (1996) 'Macrophages in Multiple Sclerosis', *Immunobiology*, 195, pp. 588–600. (Accessed: 5 August 2019).

Burfoot, R. K. *et al.* (2007) 'SNP mapping and candidate gene sequencing in the class I

region of the HLA complex: searching for multiple sclerosis susceptibility genes in Tasmanians', *Tissue Antigens*, 0(0), pp. 071030182930002-??? doi: 10.1111/j.1399-0039.2007.00962.x.

Burt, R. K. *et al.* (2015) 'Association of Nonmyeloablative Hematopoietic Stem Cell Transplantation With Neurological Disability in Patients With Relapsing-Remitting Multiple Sclerosis', *JAMA*. American Medical Association, 313(3), p. 275. doi: 10.1001/jama.2014.17986.

Butovsky, O. *et al.* (2015) 'Targeting miR-155 restores abnormal microglia and attenuates disease in SOD1 mice', *Annals of Neurology*, 77(1), pp. 75–99. doi: 10.1002/ana.24304.

Cai, X. *et al.* (2012) 'Re-polarization of tumor-associated macrophages to pro-inflammatory M1 macrophages by microRNA-155', *Journal of Molecular Cell Biology*, 4(5), pp. 341–343. doi: 10.1093/jmcb/mjs044.

Caldeira, C. *et al.* (2017) 'Key aging-associated alterations in primary microglia response to beta-amyloid stimulation', *Frontiers in Aging Neuroscience*. doi: 10.3389/fnagi.2017.00277.

Caldwell, R. B. *et al.* (2015) 'Arginase: an old enzyme with new tricks', *Trends in pharmacological sciences*. NIH Public Access, 36(6), p. 395. doi: 10.1016/J.TIPS.2015.03.006.

Cao, M. *et al.* (2017a) 'Mechanisms of Impaired Neutrophil Migration by MicroRNAs in Myelodysplastic Syndromes', *The Journal of Immunology*, 198(5), pp. 1887–1899. doi: 10.4049/jimmunol.1600622.

Cao, M. *et al.* (2017b) 'Mechanisms of Impaired Neutrophil Migration by MicroRNAs in Myelodysplastic Syndromes', *The Journal of Immunology*, 198(5), pp. 1887–1899. doi: 10.4049/jimmunol.1600622.

Caravagna, C. *et al.* (2018) 'Diversity of innate immune cell subsets across spatial and temporal scales in an EAE mouse model', *Scientific Reports*, 8(1). doi: 10.1038/s41598-018-22872-y.

Cardoso, A. L. *et al.* (2012) 'miR-155 modulates microglia-mediated immune response by down-regulating SOCS-1 and promoting cytokine and nitric oxide production', *Immunology*, 135(1), pp. 73–88. doi: 10.1111/j.1365-2567.2011.03514.x.

Carstensen Gjelstrup, M. *et al.* (2018) 'Subsets of activated monocytes and markers of inflammation in incipient and progressed multiple sclerosis', *Immunology & Cell Biology*, 96, pp. 160–174. doi: 10.1111/imcb.1025.

Cassado, A. dos A., Lima, M. R. D. and Bortoluci, K. R. (2015) 'Revisiting Mouse Peritoneal Macrophages: Heterogeneity, Development, and Function', *Frontiers in Immunology*. Frontiers, 6, p. 225. doi: 10.3389/fimmu.2015.00225.

Ceppi, M., Pereira, P. M., *et al.* (2009a) *MicroRNA-155 modulates the interleukin-1 signaling pathway in activated human monocyte-derived dendritic cells, Proceedings of the National Academy of Sciences*. doi: 10.1073/pnas.0811073106.

Ceppi, M., Pereira, P. M., *et al.* (2009b) *MicroRNA-155 modulates the interleukin-1 signaling pathway in activated human monocyte-derived dendritic cells, Proceedings*

of the National Academy of Sciences. doi: 10.1073/pnas.0811073106.

Ceppi, M., Pereira, A. M., *et al.* (2009) *MicroRNA-155 modulates the interleukin-1 signaling pathway in activated human monocyte-derived dendritic cells, Proceedings of the National Academy of Sciences of the United States of America*. doi: 10.1073/pnas.0811073106.

Chakraborty, C. *et al.* (2017) 'Therapeutic miRNA and siRNA: Moving from Bench to Clinic as Next Generation Medicine', *Molecular Therapy - Nucleic Acids*, 8, pp. 132–143. doi: 10.1016/j.omtn.2017.06.005.

Chandraratna, R. A. S., Noelle, R. J. and Nowak, E. C. (2016) 'Treatment with retinoid X receptor agonist IRX4204 ameliorates experimental autoimmune encephalomyelitis', *American Journal of Translational Research*, 8(2), pp. 1016–1026.

Chari, D. M. (2007) 'Remyelination In Multiple Sclerosis', *International Review of Neurobiology*, pp. 589–620. doi: 10.1016/S0074-7742(07)79026-8.

Chen, D., Yu, S. P. and Wei, L. (2014) 'Ion Channels in Regulation of Neuronal Regenerative Activities', *Translational Stroke Research*, 5(1), pp. 156–162. doi: 10.1007/s12975-013-0320-z.

Chernajovsky, Y. and Robbins, P. D. (2010) *Gene therapy for autoimmune and inflammatory diseases*. Birkhäuser. Available at: https://books.google.com.au/books?id= (Accessed: 30 April 2019).

Cheung, S. T. *et al.* (2013) 'Interleukin-10 Inhibits Lipopolysaccharide Induced miR-155 Precursor Stability and Maturation', *PLoS ONE*. Edited by G. Das. Public Library of Science, 8(8), p. e71336. doi: 10.1371/journal.pone.0071336.

Choudry, M. *et al.* (2018a) 'Deficient arginase II expression without alteration in arginase I expression attenuated experimental autoimmune encephalomyelitis in mice', *Immunology*, 155(1), pp. 85–98. doi: 10.1111/imm.12926.

Choudry, M. *et al.* (2018b) 'Deficient arginase II expression without alteration in arginase I expression attenuated experimental autoimmune encephalomyelitis in mice', *Immunology*, 155(1), pp. 85–98. doi: 10.1111/imm.12926.

Choudry, M. *et al.* (2018c) 'Deficient arginase II expression without alteration in arginase I expression attenuated experimental autoimmune encephalomyelitis in mice', *Immunology*. John Wiley & Sons, Ltd (10.1111), 155(1), pp. 85–98. doi: 10.1111/imm.12926.

Chu, F. *et al.* (2018a) 'The roles of macrophages and microglia in multiple sclerosis and experimental autoimmune encephalomyelitis', *Journal of Neuroimmunology*. Elsevier, 318(December 2017), pp. 1–7. doi: 10.1016/j.jneuroim.2018.02.015.

Chu, F. *et al.* (2018b) 'The roles of macrophages and microglia in multiple sclerosis and experimental autoimmune encephalomyelitis', *Journal of Neuroimmunology*, 318, pp. 1–7. doi: 10.1016/j.jneuroim.2018.02.015.

Chu, F. *et al.* (2018c) 'The roles of macrophages and microglia in multiple sclerosis and experimental autoimmune encephalomyelitis', *Journal of Neuroimmunology*. Elsevier, 318(December 2017), pp. 1–7. doi: 10.1016/j.jneuroim.2018.02.015.

Chun, J. and Hartung, H. P. (2010) 'Mechanism of action of oral fingolimod (FTY720) in multiple sclerosis', *Clinical Neuropharmacology*, 33(2), pp. 91–101. doi: 10.1097/WNF.0b013e3181cbf825.

Chung, Y. *et al.* (2009) 'Critical Regulation of Early Th17 Cell Differentiation by Interleukin-1 Signaling', *Immunity*, 30(4), pp. 576–587. doi: 10.1016/j.immuni.2009.02.007.

Clausen, B. E. *et al.* (1999) 'Conditional gene targeting in macrophages and granulocytes using LysMcre mice.', *Transgenic research*, 8(4), pp. 265–77. Available at: http://www.ncbi.nlm.nih.gov/pubmed/10621974 (Accessed: 25 March 2019).

Cohen-Poradosu, R. *et al.* (2011) 'Bacteroides fragilis - Stimulated interleukin-10 contains expanding disease', *Journal of Infectious Diseases*, 204(3), pp. 363–371. doi: 10.1093/infdis/jir277.

Cohen, F. *et al.* (2003) 'Synuclein β Induced by T Cell Immunity to Self Autoimmune Encephalomyelitis and Uveitis', *J Immunol References*, 170, pp. 628–634. doi: 10.4049/jimmunol.170.1.628.

Coles, A. J. *et al.* (2006) 'The window of therapeutic opportunity in multiple sclerosis', *Journal of Neurology*, 253(1), pp. 98–108. doi: 10.1007/s00415-005-0934-5.

Comi, G. *et al.* (2012) 'Placebo-Controlled Trial of Oral Laquinimod for Multiple Sclerosis', *New England Journal of Medicine*. Massachusetts Medical Society , 366(11), pp. 1000–1009. doi: 10.1056/NEJMoa1104318.

Connell, R. M. O. *et al.* (2010) 'Article MicroRNA-155 Promotes Autoimmune Inflammation by Enhancing Inflammatory T Cell Development', *Immunity*. Elsevier Inc., 33(4), pp. 607–619. doi: 10.1016/j.immuni.2010.09.009.

Constantinescu, C. S. *et al.* (2011) 'Experimental autoimmune encephalomyelitis (EAE) as a model for multiple sclerosis (MS)', *British Journal of Pharmacology*, pp. 1079–1106. doi: 10.1111/j.1476-5381.2011.01302.x.

Craggs, R. I., King, R. H. M. and Thomas, P. K. (1984) 'The effect of suppression of macrophage activity on the development of experimental allergic neuritis', *Acta Neuropathologica*, 62(4), pp. 316–323. doi: 10.1007/BF00687614.

Crawford, M. P. *et al.* (2004) 'High prevalence of autoreactive, neuroantigen-specific CD8+ T cells in multiple sclerosis revealed by novel flow cytometric assay', *Blood*, 103(11), pp. 4222–4231. doi: 10.1182/blood-2003-11-4025.

Croxford, A. L. *et al.* (2015) 'The Cytokine GM-CSF Drives the Inflammatory Signature of CCR2+ Monocytes and Licenses Autoimmunity', *Immunity*, 43(3), pp. 502–514. doi: 10.1016/j.immuni.2015.08.010.

Croxford, A. L., Kurschus, F. C. and Waisman, A. (2011) 'Mouse models for multiple sclerosis: Historical facts and future implications', *Biochimica et Biophysica Acta - Molecular Basis of Disease*. Elsevier, 1812(2), pp. 177–183. doi: 10.1016/j.bbadis.2010.06.010.

Croxford, A. L., Spath, S. and Becher, B. (2015a) 'GM-CSF in Neuroin fl ammation : Licensing Myeloid Cells for Tissue Damage', *Trends in Immunology*. Elsevier Ltd, 36(10), pp. 651–662. doi: 10.1016/j.it.2015.08.004.

Croxford, A. L., Spath, S. and Becher, B. (2015b) 'GM-CSF in Neuroinflammation: Licensing Myeloid Cells for Tissue Damage'. doi: 10.1016/j.it.2015.08.004.

Cua, D. J. *et al.* (1999) 'Transgenic interleukin 10 prevents induction of experimental autoimmune encephalomyelitis', *Journal of Experimental Medicine*, 189(6), pp. 1005–1010. doi: 10.1084/jem.189.6.1005.

Czarnek, M. and Bereta, J. (2017) 'SmartFlares fail to reflect their target transcripts levels', *Scientific Reports*. Springer US, 7(1), pp. 1–10. doi: 10.1038/s41598-017-11067-6.

Danger, R. *et al.* (2014) 'MicroRNAs, major players in B cells homeostasis and function', *Frontiers in Immunology*, 5(MAR). doi: 10.3389/fimmu.2014.00098.

Danikowski, K. M., Jayaraman, S. and Prabhakar, B. S. (2017) 'Regulatory T cells in multiple sclerosis and myasthenia gravis.', *Journal of neuroinflammation*. BioMed Central, 14(1), p. 117. doi: 10.1186/s12974-017-0892-8.

Delarasse, C. *et al.* (2013) 'Novel pathogenic epitopes of myelin oligodendrocyte glycoprotein induce experimental autoimmune encephalomyelitis in C57BL/6 mice.', *Immunology*. Wiley-Blackwell, 140(4), pp. 456–64. doi: 10.1111/imm.12155.

Dendroue CA, Fugger L, F. M. (2015) 'Immunopathology of Multiple Sclerosis', *Nature Reviews Immunology*, 15, pp. 545–58.

Deng, B. *et al.* (2012) 'Interleukin-10 triggers changes in macrophage phenotype that promote muscle growth and regeneration', *Journal of immunology*, 189(7), pp. 3669–3680. doi: 10.1038/jid.2014.371.

Desai, R. A. and Smith, K. J. (2017) 'Experimental autoimmune encephalomyelitis from a tissue energy perspective', *F1000Research*, 6, p. 1973. doi: 10.12688/f1000research.11839.1.

Dickey, L. L. *et al.* (2016) 'MicroRNA-155 enhances T cell trafficking and antiviral effector function in a model of coronavirus-induced neurologic disease', *Journal of Neuroinflammation*, 13(1), pp. 1–12. doi: 10.1186/s12974-016-0699-z.

Diebold, S. S. (2008) 'Determination of T-cell fate by dendritic cells', *Immunology and Cell Biology*, 86(5), pp. 389–397. doi: 10.1038/icb.2008.26.

Dunand-Sauthier, I. *et al.* (2011) 'Silencing of c-Fos expression by microRNA-155 is critical for dendritic cell maturation and function', *Blood*, 117(17), pp. 4490–4500. doi: 10.1182/blood-2010.

Dunand-Sauthier, I. *et al.* (2014) 'Repression of Arginase-2 Expression in Dendritic Cells by MicroRNA-155 Is Critical for Promoting T Cell Proliferation', *The Journal of Immunology*, 193(4), pp. 1690–1700. doi: 10.4049/jimmunol.1301913.

Dunn, R. *et al.* (2009) 'Spontaneous relapsing-remitting EAE in the SJL/J mouse: MOG-reactive transgenic T cells recruit endogenous MOG-specific B cells', *The Journal of Experimental Medicine*, 206(6), pp. 1303–1316. doi: 10.1084/jem.20090299.

Eis, P. S. *et al.* (2005) 'Accumulation of miR-155 and BIC RNA in human B cell lymphomas', *Proceedings of the National Academy of Sciences*, 102(10), pp. 3627–3632. doi: 10.1073/pnas.0500613102.

Eltayeb, S. *et al.* (2007) 'Temporal expression and cellular origin of CC chemokine receptors CCR1, CCR2 and CCR5 in the central nervous system: Insight into mechanisms of MOG-induced EAE', *Journal of Neuroinflammation*, 4. doi: 10.1186/1742-2094-4-14.

Elton, T. S. *et al.* (2013) 'Regulation of the MIR155 host gene in physiological and pathological processes', *Gene*, 532, pp. 1–12. doi: 10.1016/j.gene.2012.12.009.

Falcão, A. M. *et al.* (2018) 'Disease-specific oligodendrocyte lineage cells arise in multiple sclerosis', *Nature Medicine*, 24(12), pp. 1837–1844. doi: 10.1038/s41591-018-0236-y.

Faraoni, I. *et al.* (2009) 'miR-155 gene: A typical multifunctional microRNA', *Biochimica et Biophysica Acta - Molecular Basis of Disease*, pp. 497–505. doi: 10.1016/j.bbadis.2009.02.013.

Farias, A. S. *et al.* (2007) 'Nitric oxide and TNFα effects in experimental autoimmune encephalomyelitis demyelination', *NeuroImmunoModulation*, 14(1), pp. 32–38. doi: 10.1159/000107286.

Farias, A. S. *et al.* (2014) 'Ten years of proteomics in multiple sclerosis', *Proteomics*, 14(4–5), pp. 467–480. doi: 10.1002/pmic.201300268.

Faridgohar, M. and Nikoueinejad, H. (2017) 'New findings of Toll-like receptors involved in Mycobacterium tuberculosis infection.', *Pathogens and global health*. Taylor & Francis, 111(5), pp. 256–264. doi: 10.1080/20477724.2017.1351080.

Ferber, I. A. *et al.* (1996) 'Mice with a disrupted IFN-gamma gene are susceptible to the induction of experimental autoimmune encephalomyelitis (EAE).', *Journal of immunology (Baltimore, Md.: 1950)*, 156(1), pp. 5–7. Available at: http://www.ncbi.nlm.nih.gov/pubmed/8598493 (Accessed: 16 April 2019).

Ferro, A. *et al.* (2018) 'Inhibition of NF-κB signaling in IKKβF/F;LysM Cre mice causes motor deficits but does not alter pathogenesis of Spinocerebellar ataxia type 1', *PLoS ONE*, 13(7), pp. 1–22. doi: 10.1371/journal.pone.0200013.

Fife, B. T. *et al.* (2000) 'CC chemokine receptor 2 is critical for induction of experimental autoimmune encephalomyelitis.', *The Journal of experimental medicine*. The Rockefeller University Press, 192(6), pp. 899–905. Available at: http://www.ncbi.nlm.nih.gov/pubmed/10993920 (Accessed: 7 February 2019).

Fiorentino, D. F. *et al.* (1991) 'IL-10 inhibits cytokine production by activated macrophages.', *Journal of immunology (Baltimore, Md.: 1950)*. American Association of Immunologists, 147(11), pp. 3815–22. Available at: http://www.ncbi.nlm.nih.gov/pubmed/1940369 (Accessed: 27 February 2019).

Fletcher, J. M. *et al.* (2010) 'T cells in multiple sclerosis and experimental autoimmune encephalomyelitis', *Clinical and Experimental Immunology*, pp. 1–11. doi: 10.1111/j.1365-2249.2010.04143.x.

Fontana, L. *et al.* (2007) 'MicroRNAs 17-5p-20a-106a control monocytopoiesis through AML1 targeting and M-CSF receptor upregulation', *Nature Cell Biology*, 9(7), pp. 775–787. doi: 10.1038/ncb1613.

Fordham, J. *et al.* (1998) 'Autoimmune Encephalomyelitis Inhibits the Effector Phase of

Experimental Treatment with Anti-Granulocyte Antibodies', *Journal of Immunology*. Available at: http://www.jimmunol.org/content/161/11/6421 (Accessed: 29 April 2019).

Forster, S. C., Tate, M. D. and Hertzog, P. J. (2015) 'MicroRNA as Type I Interferon-Regulated Transcripts and Modulators of the Innate Immune Response.', *Frontiers in immunology*. Frontiers Media SA, 6, p. 334. doi: 10.3389/fimmu.2015.00334.

Foss, F. M. *et al.* (2018) 'Ph 1 study of MRG-106, an inhibitor of miR-155, in CTCL.', *Journal of Clinical Oncology*. American Society of Clinical Oncology, 36(15_suppl), pp. 2511–2511. doi: 10.1200/JCO.2018.36.15_suppl.2511.

Fouda, A. Y. *et al.* (2018) 'Arginase 1 promotes retinal neurovascular protection from ischemia through suppression of macrophage inflammatory responses', *Cell Death & Disease*. Nature Publishing Group, 9(10), p. 1001. doi: 10.1038/s41419-018-1051-6.

Fox, E. J. (2004) 'Mechanism of action of mitoxantrone.', *Neurology*, 63(12 Suppl 6), pp. S15-8. doi: 10.1212/wnl.63.12_suppl_6.s15.

Franklin, R. J. M. and Ffrench-Constant, C. (2017) 'Regenerating CNS myelin - From mechanisms to experimental medicines', *Nature Reviews Neuroscience*, 18(12), pp. 753–769. doi: 10.1038/nrn.2017.136.

Frei, K. *et al.* (1997) *Tumor necrosis factor α and lymphotoxin α are not required for induction of acute experimental autoimmune encephalomyelitis*, *Journal of Experimental Medicine*. doi: 10.1084/jem.185.12.2177.

Freilich, R. W., Woodbury, M. E. and Ikezu, T. (2013) 'Integrated expression profiles of mRNA and miRNA in polarized primary murine microglia', *PLoS ONE*. doi: 10.1371/journal.pone.0079416.

Friedman, R. C. *et al.* (2009) 'Most mammalian mRNAs are conserved targets of microRNAs', *Genome Research*, 19(1), pp. 92–105. doi: 10.1101/gr.082701.108.

Friese, M. A. *et al.* (2008) 'Opposing effects of HLA class I molecules in tuning autoreactive CD8+ T cells in multiple sclerosis', *Nature Medicine*, 14(11), pp. 1227–1235. doi: 10.1038/nm.1881.

Fujihara, M. *et al.* (2003) 'Molecular mechanisms of macrophage activation and deactivation by lipopolysaccharide: Roles of the receptor complex', *Pharmacology and Therapeutics*, 100(2), pp. 171–194. doi: 10.1016/j.pharmthera.2003.08.003.

Gaidatzis, D. *et al.* (2007) 'Inference of miRNA targets using evolutionary conservation and pathway analysis', *BMC Bioinformatics*, 8. doi: 10.1186/1471-2105-8-69.

Gallo, P., Centonze, D. and Marrosu, M. G. (2017) 'Alemtuzumab for multiple sclerosis: the new concept of immunomodulation', *Multiple Sclerosis and Demyelinating Disorders*, 2(1). doi: 10.1186/s40893-017-0024-4.

Galloway, D. A. and Moore, C. S. (2016) 'miRNAs As Emerging Regulators of Oligodendrocyte Development and Differentiation', *Frontiers in Cell and Developmental Biology*, 4(June), pp. 1–8. doi: 10.3389/fcell.2016.00059.

Garg, N. and Smith, T. W. (2015) 'An update on immunopathogenesis, diagnosis, and treatment of multiple sclerosis', *Brain and Behavior*, 5(9), pp. 1–13. doi:

10.1002/brb3.362.

Gebert, L. F. R. and MacRae, I. J. (2019) 'Regulation of microRNA function in animals', *Nature Reviews Molecular Cell Biology*, 20(1), pp. 21–37. doi: 10.1038/s41580-018-0045-7.

Geginat, J. *et al.* (2017) 'The Enigmatic Role of Viruses in Multiple Sclerosis: Molecular Mimicry or Disturbed Immune Surveillance?', *Trends in Immunology*. Elsevier Ltd, 38(7), pp. 498–512. doi: 10.1016/j.it.2017.04.006.

Gewin, L. S. (2019) 'The cre/lox system: Cre-ating unintended damage', *American Journal of Physiology - Renal Physiology*, 316(5), pp. F873–F874. doi: 10.1152/ajprenal.00428.2018.

Ghasemi, Nazem(Sidiropoulou, Pissadaki, & Poirazi, 2006) Sidiropoulou, K., Pissadaki, E. K., & Poirazi, P. (2006). Inside the brain of a neuron. EMBO Reports, 7(9), 886–892. https://doi.org/10.1038/sj.embor.7400789, Razavi, S. and Nikzad, E. (2017) *Multiple Sclerosis: Pathogenesis, Symptoms, Diagnoses and Cell-Based Therapy Citation: Ghasemi N, Razavi Sh, Nikzad E. Multiple sclerosis: pathogenesis, symptoms, diagnoses and cell-based therapy, Cell J.* doi: 10.22074/cellj.2016.4867.

Gibson-Corley, K. N. *et al.* (2016) 'A method for histopathological study of the multifocal nature of spinal cord lesions in murine experimental autoimmune encephalomyelitis', *PeerJ*, 2016(1). doi: 10.7717/peerj.1600.

Giles, David A. *et al.* (2018) 'CNS-resident classical DCs play a critical role in CNS autoimmune disease', *Journal of Clinical Investigation*, 128(12), pp. 5322–5334. doi: 10.1172/JCI123708.

Giles, David A *et al.* (2018) 'Myeloid cell plasticity in the evolution of central nervous system autoimmunity HHS Public Access', *Ann Neurol*, 83(1), pp. 131–141. doi: 10.1002/ana.25128.

Gillen, K. M. *et al.* (2018) 'Significance and in vivo detection of iron-laden microglia in white matter multiple sclerosis lesions', *Frontiers in Immunology*, 9(FEB), pp. 1–8. doi: 10.3389/fimmu.2018.00255.

Giralt, M., Molinero, A. and Hidalgo, J. (2018) 'Active induction of experimental autoimmune encephalomyelitis (EAE) with MOG35-55 in the mouse', *Methods in Molecular Biology*. Springer Science+Business Media, 1791, pp. 227–232. doi: 10.1007/978-1-4939-7862-5_17.

Girvin, A. M., Dal Canto, M. C. and Miller, S. D. (2002) 'CD40/CD40L Interaction is Essential for the Induction of EAE in the Absence of CD28-Mediated Co-stimulation', *Journal of Autoimmunity*, 18, pp. 83–94. doi: 10.1006/jaut.2001.0573.

Göbel, K., Ruck, T. and Meuth, S. G. (2018a) 'Cytokine signaling in multiple sclerosis: Lost in translation', *Multiple Sclerosis Journal*, 24(4), pp. 432–439. doi: 10.1177/1352458518763094.

Göbel, K., Ruck, T. and Meuth, S. G. (2018b) 'Cytokine signaling in multiple sclerosis: Lost in translation', *Multiple Sclerosis Journal*, 24(4), pp. 432–439. doi: 10.1177/1352458518763094.

Goodin, D. S. *et al.* (2016) 'Relapses in multiple sclerosis: Relationship to disability',

Multiple Sclerosis and Related Disorders, 6, pp. 10–20. doi: 10.1016/j.msard.2015.09.002.

Goverman, J. (2009) 'Autoimmune T cell responses in the central nervous system.', *Nature reviews. Immunology*. NIH Public Access, 9(6), pp. 393–407. doi: 10.1038/nri2550.

Goverman, J., Perchellet, A. and Huseby, E. S. (2005) 'The role of CD8(+) T cells in multiple sclerosis and its animal models.', *Current drug targets. Inflammation and allergy*, 4(2), pp. 239–45. Available at: http://www.ncbi.nlm.nih.gov/pubmed/15853746 (Accessed: 17 April 2019).

Graeber, M. B. and Streit, W. J. (2010) 'Microglia: Biology and pathology', *Acta Neuropathologica*, 119(1), pp. 89–105. doi: 10.1007/s00401-009-0622-0.

Grajchen, E., Hendriks, Jerome J. A. and Bogie, J. F. J. (2018) 'The physiology of foamy phagocytes in multiple sclerosis', *Acta Neuropathologica Communications*. BioMed Central, 6(1), p. 124. doi: 10.1186/s40478-018-0628-8.

Grajchen, E., Hendriks, Jerome J.A. and Bogie, J. F. J. (2018) 'The physiology of foamy phagocytes in multiple sclerosis', *Acta neuropathologica communications*, 6(1), p. 124. doi: 10.1186/s40478-018-0628-8.

Greenhalgh, A. D. *et al.* (2016a) 'Arginase-1 is expressed exclusively by infiltrating myeloid cells in CNS injury and disease', *Brain, Behavior, and Immunity*, 56, pp. 61–67. doi: 10.1016/j.bbi.2016.04.013.

Greenhalgh, A. D. *et al.* (2016b) 'Arginase-1 is expressed exclusively by infiltrating myeloid cells in CNS injury and disease', *Brain, Behavior, and Immunity*, 56, pp. 61–67. doi: 10.1016/j.bbi.2016.04.013.

Gregory, A. P. *et al.* (2012) 'TNF receptor 1 genetic risk mirrors outcome of anti-TNF therapy in multiple sclerosis.', *Nature*. Europe PMC Funders, 488(7412), pp. 508–511. doi: 10.1038/nature11307.

Groth, C. *et al.* (2019) 'Immunosuppression mediated by myeloid-derived suppressor cells (MDSCs) during tumour progression', *British Journal of Cancer*. Springer US, 120(1), pp. 16–25. doi: 10.1038/s41416-018-0333-1.

Haimon, Z. *et al.* (2018) 'Re-evaluating microglia expression profiles using RiboTag and cell isolation strategies.', *Nature immunology*. Europe PMC Funders, 19(6), pp. 636–644. doi: 10.1038/s41590-018-0110-6.

Hammond, T. R. *et al.* (2019) 'Single-Cell RNA Sequencing of Microglia throughout the Mouse Lifespan and in the Injured Brain Reveals Complex Cell-State Changes', *Immunity*, 50(1), pp. 253-271.e6. doi: 10.1016/j.immuni.2018.11.004.

Hanisch, U. K. (2002a) 'Microglia as a source and target of cytokines', *GLIA*, pp. 140–155. doi: 10.1002/glia.10161.

Hanisch, U. K. (2002b) 'Microglia as a source and target of cytokines', *Glia*, 40(2), pp. 140–155. doi: 10.1002/glia.10161.

Hanna, J., Hossain, G. S. and Kocerha, J. (2019) 'The Potential for microRNA Therapeutics and Clinical Research', *Frontiers in Genetics*, 10(May). doi: 10.3389/fgene.2019.00478.

Hannemann, N. *et al.* (2019) 'Transcription factor Fra-1 targets arginase-1 to enhance macrophage-mediated inflammation in arthritis', *Journal of Clinical Investigation*, 129(7), pp. 2669–2684. doi: 10.1172/JCI96832.

Harlow, D. E., Honce, J. M. and Miravalle, A. A. (2015) 'Remyelination therapy in multiple sclerosis', *Frontiers in Neurology*, 6(DEC), pp. 1–13. doi: 10.3389/fneur.2015.00257.

Harrington, L. E. *et al.* (2005) 'Interleukin 17-producing CD4 + effector T cells develop via a lineage distinct from the T helper type 1 and 2 lineages', *Nature Immunology*, 6(11), pp. 1123–1132. doi: 10.1038/ni1254.

Hart, P. H. *et al.* (2015) 'Ultraviolet radiation, vitamin D and multiple sclerosis', *Neurodegenerative Disease Management*, 5(5), pp. 413–424. doi: 10.2217/nmt.15.33.

Hauser, S. L. *et al.* (2008) 'B-Cell Depletion with Rituximab in Relapsing–Remitting Multiple Sclerosis', *New England Journal of Medicine*, 358(7), pp. 676–688. doi: 10.1056/NEJMoa0706383.

Häusler, D. *et al.* (2018) 'Functional characterization of reappearing B cells after anti-CD20 treatment of CNS autoimmune disease', *Proceedings of the National Academy of Sciences*, 115(39), pp. 9773–9778. doi: 10.1073/pnas.1810470115.

Hausser, J. and Zavolan, M. (2014) 'Identification and consequences of miRNA-target interactions-beyond repression of gene expression', *Nature Reviews Genetics*. Nature Publishing Group, 15(9), pp. 599–612. doi: 10.1038/nrg3765.

Hawkins, R. F. W. *et al.* (2017) 'ICAM1+ neutrophils promote chronic inflammation via ASPRV1 in B cell–dependent autoimmune encephalomyelitis', *JCI Insight*, 2(23). doi: 10.1172/jci.insight.96882.

Henderson, A. P. D. *et al.* (2009) 'Multiple sclerosis: Distribution of inflammatory cells in newly forming lesions', *Annals of Neurology*, 66(6), pp. 739–753. doi: 10.1002/ana.21800.

Henry, R. J. *et al.* (2018) 'Inhibition of miR-155 Limits Neuroinflammation and Improves Functional Recovery After Experimental Traumatic Brain Injury in Mice', *Neurotherapeutics*. Neurotherapeutics, (6), pp. 1–15. doi: 10.1007/s13311-018-0665-9.

Heon Park1, Zhaoxia Li, Xuexian O Yang, Seon Hee Chang, Roza Nurieva, Yi-Hong Wang, Ying Wang, Leroy Hood, Zhou Zhu, Qiang Tian, and C. D. (2005) 'A distinct lineage of CD4 T cells regulates tissue inflammation by producing interleukin 17', *Nature immunology*, 6(11), pp. 1133–1141. Available at: http://npg.nature.com/reprintsandpermissions/ (Accessed: 1 July 2019).

Heppner, F. L. *et al.* (2005) 'Experimental autoimmune encephalomyelitis repressed by microglial paralysis', *Nature Medicine*, 11(2), pp. 146–152. doi: 10.1038/nm1177.

Herz, J. *et al.* (2017) 'Myeloid Cells in the Central Nervous System'. doi: 10.1016/j.immuni.2017.06.007.

Hibbits, N. *et al.* (2009) 'Cuprizone demyelination of the corpus callosum in mice correlates with altered social interaction and impaired bilateral sensorimotor coordination.',

ASN neuro, 1(3). doi: 10.1042/AN20090032.

Hirbec, H. E., Noristani, H. N. and Perrin, F. E. (2017) 'Microglia responses in acute and chronic neurological diseases: What microglia-specific transcriptomic studies taught (and did not teach) Us', *Frontiers in Aging Neuroscience*, 9(JUL). doi: 10.3389/fnagi.2017.00227.

Holmøy, T., Kvale, E. Ø. and Vartdal, F. (2004) 'Cerebrospinal fluid CD4 $^{+}$ T cells from a multiple sclerosis patient cross-recognize Epstein-Barr virus and myelin basic protein', *Journal of Neurovirology*. Springer-Verlag, 10(5), pp. 278–283. doi: 10.1080/13550280490499524.

Hopp, A.-K., Rupp, A. and Lukacs-Kornek, V. (2014) 'Self-antigen presentation by dendritic cells in autoimmunity.', *Frontiers in immunology*. Frontiers Media SA, 5, p. 55. doi: 10.3389/fimmu.2014.00055.

Hsin, J.-P. *et al.* (2018) 'The effect of cellular context on miR-155-mediated gene regulation in four major immune cell types', *Nat Immunol*, 19(10), pp. 1137–1145. doi: 10.1038/s41590-018-0208-x.

Huang, Y. M. *et al.* (1999) 'Multiple sclerosis is associated with high levels of circulating dendritic cells secreting pro-inflammatory cytokines.', *Journal of neuroimmunology*, 99(1), pp. 82–90. Available at: http://www.ncbi.nlm.nih.gov/pubmed/10496180 (Accessed: 24 April 2019).

Huitinga, I., van Rooijen, N., de Groot, C. J., *et al.* (1990) 'Suppression of experimental allergic encephalomyelitis in Lewis rats after elimination of macrophages.', *The Journal of experimental medicine*, 172(4), pp. 1025–33. Available at: http://www.ncbi.nlm.nih.gov/pubmed/2145387%0Ahttp://www.pubmedcentral.nih.gov/articlerender.fcgi?artid=PMC2188611.

Huitinga, I., van Rooijen, N., de Groot, C. J. ., *et al.* (1990) 'Suppression of experimental allergic encephalomyelitis in Lewis rats after elimination of macrophages', *Journal of Experimental Medicine*, 172(4), pp. 1025–1033. doi: 10.1084/jem.172.4.1025.

Hume, D. A., Irvine, K. M. and Pridans, C. (2019) 'The Mononuclear Phagocyte System: The Relationship between Monocytes and Macrophages', *Trends in Immunology*, 40(2), pp. 98–112. doi: 10.1016/j.it.2018.11.007.

Hunter, S. F. (2016) 'Overview and diagnosis of multiple sclerosis.', *The American journal of managed care*, 22(6 Suppl), pp. s141-50. Available at: http://www.ncbi.nlm.nih.gov/pubmed/27356023 (Accessed: 29 March 2019).

Itoh, N. *et al.* (2018) 'Cell-specific and region-specific transcriptomics in the multiple sclerosis model: Focus on astrocytes', *Proceedings of the National Academy of Sciences*, 115(2), pp. E302–E309. doi: 10.1073/pnas.1716032115.

Izikson, L. *et al.* (2000) *Brief Definitive Report Resistance to Experimental Autoimmune Encephalomyelitis in Mice Lacking the CC Chemokine Receptor (CCR)2*, *J. Exp. Med*. Available at: http://www.jem.org/cgi/content/full/192/7/1075 (Accessed: 10 June 2019).

Jablonski, Kyle A. *et al.* (2016) 'Control of the inflammatory macrophage transcriptional signature by miR-155', *PLoS ONE*, 11(7). doi: 10.1371/journal.pone.0159724.

Jablonski, Kyle A *et al.* (2016) 'Control of the Inflammatory Macrophage Transcriptional Signature by miR-155', 1, pp. 1–21. doi: 10.1371/journal.pone.0159724.

Jäkel, S. *et al.* (2019) 'Altered human oligodendrocyte heterogeneity in multiple sclerosis', *Nature*, 566(7745), pp. 543–547. doi: 10.1038/s41586-019-0903-2.

Jeffrey Weidner, M. R. *et al.* (1998) *Gene NOS2 Exacerbated in Mice Lacking the Experimental Autoimmune Encephalomyelitis Is*. Available at: http://www.jimmunol.org/content/160/6/2940 (Accessed: 26 April 2019).

Jevtić, B. *et al.* (2015) 'Micro RNA-155 participates in re-activation of encephalitogenic T cells', *Biomedicine and Pharmacotherapy*, 74, pp. 206–210. doi: 10.1016/j.biopha.2015.08.011.

Jiang, H. *et al.* (2017) 'Amelioration of experimental autoimmune encephalomyelitis through transplantation of placental derived mesenchymal stem cells', *Scientific Reports*. Nature Publishing Group, 7(September 2016), pp. 1–16. doi: 10.1038/srep41837.

Jiang, Z., Jiang, J. X. and Zhang, G.-X. (2014) 'Macrophages: A double-edged sword in experimental autoimmune encephalomyelitis', *Immunology Letters*, 160(1), pp. 17–22. doi: 10.1016/j.imlet.2014.03.006.

Jiang, Z., Jiang, J. X. and Zhang, G. X. (2014) 'Macrophages: A double-edged sword in experimental autoimmune encephalomyelitis', *Immunology Letters*, 160(1), p. 17. doi: 10.1016/j.imlet.2014.03.006.

Jin, W.-N. *et al.* (2017) 'Depletion of microglia exacerbates postischemic inflammation and brain injury', *Journal of Cerebral Blood Flow & Metabolism*, 37(6), pp. 2224–2236. doi: 10.1177/0271678X17694185.

Jin, W. *et al.* (2009) 'Regulation of Th17 cell differentiation and EAE induction by MAP3K NIK.', *Blood*. The American Society of Hematology, 113(26), pp. 6603–10. doi: 10.1182/blood-2008-12-192914.

Jiyeon Yang, Lixiao Zhang, Caijia Yu, X.-F. Y. and H. W. (2014) 'Monocyte and macrophage differentiation: circulation inflammatory monocyte as biomarker for inflammatory diseases', *Biomarker Research*, 2(1). doi: 10.1126/science.312.5782.1868.

Johann, A. M. *et al.* (2007) 'Apoptotic cells induce arginase II in macrophages, thereby attenuating NO production', *The FASEB Journal*, 21(11), pp. 2704–2712. doi: 10.1096/fj.06-7815com.

Jonathan L. McQualter, 1 Rima Darwiche, 2 Christine Ewing, 1 Manabu Onuki, 1 Thomas W. Kay, 2 John A. Hamilton, 3 Hugh H. Reid, 1 and Claude C.A. Bernard 1 (2001) 'Granulocyte-macrophage colony-stimulating factor', *Journal of Experimental Medicine*, 194(7), pp. 503–524. doi: 10.1016/B978-012689663-3/50025-9.

Jr, O. de F. *et al.* (2013) 'MicroRNA dysregulation in multiple sclerosis', *Frontiers in Genetics*. Frontiers, 3, p. 311. doi: 10.3389/fgene.2012.00311.

Junker, A. *et al.* (2009) 'MicroRNA profiling of multiple sclerosis lesions identifies modulators of the regulatory protein CD47', *Brain*, 132(12), pp. 3342–3352. doi: 10.1093/brain/awp300.

Van Kaer, L. *et al.* (2019) 'Innate, innate-like and adaptive lymphocytes in the pathogenesis of MS and EAE', *Cellular & Molecular Immunology*. doi: 10.1038/s41423-019-0221-5.

Kappos, L. *et al.* (2014) 'Atacicept in multiple sclerosis (ATAMS): a randomised, placebo-controlled, double-blind, phase 2 trial', *The Lancet Neurology*, 13(4), pp. 353–363. doi: 10.1016/S1474-4422(14)70028-6.

Karceski, S., Frederick, M. C. and Bourdette, D. (2017) 'MS and bone marrow transplant Not for most patients'. doi: 10.1212/WNL.0000000000004001.

Kaskow, Belinda J and Baecher-Allan, C. (2018) 'Effector T Cells in Multiple Sclerosis.', *Cold Spring Harbor perspectives in medicine*. Cold Spring Harbor Laboratory Press, 8(4), p. a029025. doi: 10.1101/cshperspect.a029025.

Kaskow, Belinda J. and Baecher-Allan, C. (2018) 'Effector T Cells in Multiple Sclerosis', *Cold Spring Harbor Perspectives in Medicine*, 8(4), p. a029025. doi: 10.1101/cshperspect.a029025.

Kawachi, I. *et al.* (2018) 'Latitude, Vitamin D, Melatonin, and Gut Microbiota Act in Concert to Initiate Multiple Sclerosis: A New Mechanistic Pathway', *Frontiers in Immunology | www.frontiersin.org*, 9, p. 2484. doi: 10.3389/fimmu.2018.02484.

Kawakami, N. *et al.* (2004) 'The Activation Status of Neuroantigen-specific T Cells in the Target Organ Determines the Clinical Outcome of Autoimmune Encephalomyelitis', *The Journal of Experimental Medicine*, 199(2), pp. 185–197. doi: 10.1084/jem.20031064.

Kim, S. Y. *et al.* (2017) 'Coordinated balance of Rac1 and RhoA plays key roles in determining phagocytic appetite', *PLoS ONE*, 12(4), pp. 1–19. doi: 10.1371/journal.pone.0174603.

King, I. L., Dickendesher, T. L. and Segal, B. M. (2009a) 'Circulating Ly-6C+ myeloid precursors migrate to the CNS and play a pathogenic role during autoimmune demyelinating disease.', *Blood*. The American Society of Hematology, 113(14), pp. 3190–7. doi: 10.1182/blood-2008-07-168575.

King, I. L., Dickendesher, T. L. and Segal, B. M. (2009b) 'Circulating Ly-6C+ myeloid precursors migrate to the CNS and play a pathogenic role during autoimmune demyelinating disease.', *Blood*. The American Society of Hematology, 113(14), pp. 3190–7. doi: 10.1182/blood-2008-07-168575.

Kipp, M. *et al.* (2017) 'Multiple sclerosis animal models: a clinical and histopathological perspective', *Brain Pathology*, 27(2), pp. 123–137. doi: 10.1111/bpa.12454.

Kitz, A., Singer, E. and Hafler, D. (2018) 'Regulatory T Cells: From Discovery to Autoimmunity.', *Cold Spring Harbor perspectives in medicine*. Cold Spring Harbor Laboratory Press, 8(12), p. a029041. doi: 10.1101/cshperspect.a029041.

Kiyoshi Takeda1 and Shizuo Akira2, 3 (2005) 'Toll-like receptors in innate immunity', *The Japanese Society for Immunology*, 17(1). Available at: https://watermark.silverchair.com/dxh186.pdf?token=AQECAHi208BE49Ooan9kkhW_Ercy7Dm3ZL_9Cf3qfKAc485ysgAAAj8wggI7BgkqhkiG9w0BBwagggIsMIICKAIBADCCAiEGCSqGSIb3DQEHATAeBglghkgBZQMEAS4wEQQM0t-k4bc_vNAZugMQAgEQgIIB8nAdIgTT3aQQtcrMLlcrzp20b9K0UA16tpKuxSWlh

nk7bgkr (Accessed: 30 April 2019).

Klose, J. *et al.* (2013) *Suppression of experimental autoimmune encephalomyelitis by interleukin-10 transduced neural stem/progenitor cells*, *Journal of Neuroinflammation*. doi: 10.1186/1742-2094-10-117.

Kluiver, J. *et al.* (2007) 'Regulation of pri-microRNA BIC transcription and processing in Burkitt lymphoma', *Oncogene*, 26, pp. 3769–3776. doi: 10.1038/sj.onc.1210147.

Kohanbash, G. and Okada, H. (2012) 'MicroRNAs and STAT Interplay', *Semin Cancer Biol*, 22(1), pp. 70–75. doi: 10.1016/j.semcancer.2011.12.010.

Komuczki, J. *et al.* (2019) 'Fate-Mapping of GM-CSF Expression Identifies a Discrete Subset of Inflammation-Driving T Helper Article Fate-Mapping of GM-CSF Expression Identifies a Discrete Subset of Inflammation-Driving T Helper Cells Regulated by Cytokines IL-23 and IL-1 b', *Immunity*. Elsevier Inc., 50(5), pp. 1289-1304.e6. doi: 10.1016/j.immuni.2019.04.006.

Konishi, H. and Kiyama, H. (2018) 'Microglial TREM2/DAP12 Signaling: A Double-Edged Sword in Neural Diseases', *Frontiers in Cellular Neuroscience*, 12(August), pp. 1–14. doi: 10.3389/fncel.2018.00206.

Kopper, T. J. and Gensel, J. C. (2018) 'Myelin as an inflammatory mediator: Myelin interactions with complement, macrophages, and microglia in spinal cord injury', *Journal of Neuroscience Research*, 96(6), pp. 969–977. doi: 10.1002/jnr.24114.

Kostic, M. *et al.* (2018) 'Granulocyte-macrophage colony-stimulating factor as a mediator of autoimmunity in multiple sclerosis', *Journal of Neuroimmunology*, 323, pp. 1–9. doi: 10.1016/j.jneuroim.2018.07.002.

Kotter, M. R. *et al.* (2001) 'Macrophage depletion impairs oligodendrocyte remyelination following lysolecithin-induced demyelination', *Glia*, 35(3), pp. 204–212. doi: 10.1002/glia.1085.

Kotter, M. R. *et al.* (2005) 'Macrophage-depletion induced impairment of experimental CNS remyelination is associated with a reduced oligodendrocyte progenitor cell response and altered growth factor expression', *Neurobiology of Disease*, 18(1), pp. 166–175. doi: 10.1016/j.nbd.2004.09.019.

Kouwenhoven, M. *et al.* (2001) 'Monocytes in multiple sclerosis: phenotype and cytokine profile', *Journal of Neuroimmunology*, 112, pp. 197–205. Available at: www.elsevier.com/locate/jneuroinMonocytesinmultiplesclerosis:phenotypeandcytokineprofilë (Accessed: 10 June 2019).

Kozomara, A. and Griffiths-Jones, S. (2014) 'MiRBase: Annotating high confidence microRNAs using deep sequencing data', *Nucleic Acids Research*, 42(D1). doi: 10.1093/nar/gkt1181.

Krasemann, S. *et al.* (2017) 'The TREM2-APOE Pathway Drives the Transcriptional Phenotype of Dysfunctional Microglia in Neurodegenerative Diseases', *Immunity*. Elsevier Inc., 47(3), pp. 566-581.e9. doi: 10.1016/j.immuni.2017.08.008.

Kremer, D. *et al.* (2019) 'Current advancements in promoting remyelination in multiple sclerosis', *Multiple Sclerosis Journal*, 25(1), pp. 7–14. doi: 10.1177/1352458518800827.

Kuhlmann, T. (2002) *Acute axonal damage in multiple sclerosis is most extensive in early disease stages and decreases over time, Brain*. doi: 10.1093/brain/awf235.

Kuhlmann, T. *et al.* (2008) 'Differentiation block of oligodendroglial progenitor cells as a cause for remyelination failure in chronic multiple sclerosis', *Brain*, 131(7), pp. 1749–1758. doi: 10.1093/brain/awn096.

Kuo, G., Wu, C.-Y. and Yang, H.-Y. (2019) 'MiR-17-92 cluster and immunity', *Journal of the Formosan Medical Association*, 118(1), pp. 2–6. doi: 10.1016/j.jfma.2018.04.013.

Kurte, M. *et al.* (2015) 'Intravenous administration of bone marrow-derived mesenchymal stem cells induces a switch from classical to atypical symptoms in experimental autoimmune encephalomyelitis', *Stem Cells International*, 2015. doi: 10.1155/2015/140170.

Lagos-Quintana, M. *et al.* (2002) 'Identification of Tissue-Specific MicroRNAs from Mouse', *Current Biology*, 12, pp. 735–739. (Accessed: 27 May 2019).

Landgraf, P. *et al.* (2007) 'A Mammalian microRNA Expression Atlas Based on Small RNA Library Sequencing', *Cell*, 129(7), pp. 1401–1414. doi: 10.1016/j.cell.2007.04.040.

Langrish, C. L. *et al.* (2005) 'IL-23 drives a pathogenic T cell population that induces autoimmune inflammation', *The Journal of Experimental Medicine*, 201(2), pp. 233–240. doi: 10.1084/jem.20041257.

Larochelle, C., Alvarez, J. I. and Prat, A. (2011a) 'How do immune cells overcome the blood-brain barrier in multiple sclerosis?', *FEBS Letters*. Federation of European Biochemical Societies, 585(23), pp. 3770–3780. doi: 10.1016/j.febslet.2011.04.066.

Larochelle, C., Alvarez, J. I. and Prat, A. (2011b) 'How do immune cells overcome the blood–brain barrier in multiple sclerosis?', *FEBS Letters*. No longer published by Elsevier, 585(23), pp. 3770–3780. doi: 10.1016/J.FEBSLET.2011.04.066.

Lassmann, H. (2017) 'Targets of therapy in progressive MS', *Multiple Sclerosis*, 23(12), pp. 1593–1599. doi: 10.1177/1352458517729455.

Lassmann, H. (2018) 'Pathogenic Mechanisms Associated With Different Clinical Courses of Multiple Sclerosis', *Frontiers in immunology*, 9(January), p. 3116. doi: 10.3389/fimmu.2018.03116.

Lassmann, H. and Bradl, M. (2017) 'Multiple sclerosis: experimental models and reality Introduction: basic features of MS, which should be mirrored in experimental models', *Acta Neuropathol*, 3, pp. 223–244. doi: 10.1007/s00401-016-1631-4.

Lazibat, I. (2018) 'Multiple Sclerosis: New Aspects of Immunopathogenesis', *Acta Clinica Croatica*, 57(2), pp. 352–361. doi: 10.20471/acc.2018.57.02.17.

Lee, H.-M., Kim, T. S. and Jo, E.-K. (2016) 'MiR-146 and miR-125 in the regulation of innate immunity and inflammation', *BMB Rep*, 49(6), pp. 311–318. doi: 10.5483/BMBRep.2016.49.6.056.

Legroux, L. and Arbour, N. (2015) 'Multiple Sclerosis and T Lymphocytes: An Entangled Story', *Journal of Neuroimmune Pharmacology*, 10(4), pp. 528–546. doi: 10.1007/s11481-015-9614-0.

Leist, T. P. and Weissert, R. (2011) 'Cladribine: Mode of action and implications for treatment of multiple sclerosis', *Clinical Neuropharmacology*, 34(1), pp. 28–35. doi: 10.1097/WNF.0b013e318204cd90.

Leng, R. X. *et al.* (2011a) 'Role of microRNA-155 in autoimmunity', *Cytokine and Growth Factor Reviews*, pp. 141–147. doi: 10.1016/j.cytogfr.2011.05.002.

Leng, R. X. *et al.* (2011b) 'Role of microRNA-155 in autoimmunity', *Cytokine and Growth Factor Reviews*. doi: 10.1016/j.cytogfr.2011.05.002.

Leone, D. P. *et al.* (2003) 'Tamoxifen-inducible glia-specific Cre mice for somatic mutagenesis in oligodendrocytes and Schwann cells', *Molecular and Cellular Neuroscience*, 22(4), pp. 430–440. doi: 10.1016/S1044-7431(03)00029-0.

Lévesque, S. A. *et al.* (2016) 'Myeloid cell transmigration across the CNS vasculature triggers IL-1β–driven neuroinflammation during autoimmune encephalomyelitis in mice', *Journal of Experimental Medicine*. Rockefeller University Press, 213(6), pp. 929–949. doi: 10.1084/JEM.20151437.

Lewis, N. D. *et al.* (2014) 'RNA sequencing of microglia and monocyte-derived macrophages from mice with experimental autoimmune encephalomyelitis illustrates a changing phenotype with disease course', *Journal of Neuroimmunology*. Elsevier B.V., 277(1–2), pp. 26–38. doi: 10.1016/j.jneuroim.2014.09.014.

Li, D. *et al.* (2019) 'Cytokine Signaling 1 Immunity by Targeting Suppressor of Type I IFN Signaling in Antiviral Innate Inducible microRNA-155 Feedback Promotes', *J Immunol*, 185, pp. 6226–6233. doi: 10.4049/jimmunol.1000491.

Li, H. *et al.* (2018) 'Transcriptional Regulation of Macrophages Polarization by MicroRNAs.', *Frontiers in immunology*. Frontiers Media SA, 9, p. 1175. doi: 10.3389/fimmu.2018.01175.

Li, J. *et al.* (2013) 'The role of microRNAs in B-cell development and function', *Cellular and Molecular Immunology*, 10, pp. 107–112. doi: 10.1038/cmi.2012.62.

Liau, N. P. D. *et al.* (2018) 'The molecular basis of JAK/STAT inhibition by SOCS1', *Nature Communications*, 9(1). doi: 10.1038/s41467-018-04013-1.

Liddelow, S. A. *et al.* (2017) 'Neurotoxic reactive astrocytes are induced by activated microglia', *Nature*. Nature Publishing Group, 541(7638), pp. 481–487. doi: 10.1038/nature21029.

Lin, C.-C. and Edelson, B. T. (2017) 'Encephalomyelitis and Multiple Sclerosis Experimental Autoimmune in β New Insights into the Role of IL-1', *J Immunol References*, 198, pp. 4553–4560. doi: 10.4049/jimmunol.1700263.

Lindsay, M. A. (2009) 'microRNAs and the immune response', *Current Opinion in Pharmacology*, 9(4), pp. 514–520. doi: 10.1016/j.coph.2009.05.003.

Di Lisio, L. *et al.* (2012) 'The role of miRNAs in the pathogenesis and diagnosis of B-cell lymphomas', *Blood*, 120(9), pp. 1782–1790. doi: 10.1182/blood-2012-05-402784.

Liu, X. and Quan, N. (2018) 'Microglia and CNS Interleukin-1: Beyond Immunological Concepts.', *Frontiers in neurology*. Frontiers Media SA, 9, p. 8. doi: 10.3389/fneur.2018.00008.

Liu, Y.-C. *et al.* (2014) 'Macrophage Polarization in Inflammatory Diseases', *International Journal of Biological Sciences*, 10(5), pp. 520–529. doi: 10.7150/ijbs.8879.

Liu, Y. *et al.* (2015) 'Preferential Recruitment of Neutrophils into the Cerebellum and Brainstem Contributes to the Atypical Experimental Autoimmune Encephalomyelitis Phenotype', *The Journal of Immunology*, 195(3), pp. 841–852. doi: 10.4049/jimmunol.1403063.

Liu, Y., WMoore, K. and L-FMui, A. (1998) *IL-10 inhibits macrophage activation and proliferation by distinct signaling mechanisms: evidence for Stat3-dependent and-independent pathways*, *The EMBO Journal*. Available at: https://www.ncbi.nlm.nih.gov/pmc/articles/PMC1170450/pdf/001006.pdf (Accessed: 26 April 2019).

Lloyd, A. F. *et al.* (2019) 'Central nervous system regeneration is driven by microglia necroptosis and repopulation', *Nature Neuroscience*, 22(7), pp. 1046–1052. doi: 10.1038/s41593-019-0418-z.

Lloyd, A. F. and Miron, V. E. (2019) 'The pro-remyelination properties of microglia in the central nervous system', *Nature Reviews Neurology*. Nature Publishing Group. doi: 10.1038/s41582-019-0184-2.

Locatelli, G., Theodorou, D., Kendirli, A., Jordão, M. J. C., *et al.* (2018) 'Mononuclear phagocytes locally specify and adapt their phenotype in a multiple sclerosis model', *Nature Neuroscience*, 21(9), pp. 1196–1208. doi: 10.1038/s41593-018-0212-3.

Locatelli, G., Theodorou, D., Kendirli, A., Joana, M., *et al.* (2018) 'sclerosis model', *Nature Neuroscience*. Springer US, 21(September). doi: 10.1038/s41593-018-0212-3.

Lodygin, D. *et al.* (2019) 'β-Synuclein-reactive T cells induce autoimmune CNS grey matter degeneration', *Nature*, 566(7745), pp. 503–508. doi: 10.1038/s41586-019-0964-2.

Loeb, G. B. *et al.* (2012) 'Transcriptome-wide miR-155 binding map reveals widespread noncanonical microRNA targeting.', *Molecular cell*. NIH Public Access, 48(5), pp. 760–70. doi: 10.1016/j.molcel.2012.10.002.

Lu, D. *et al.* (2014) 'The miR-155–PU.1 axis acts on Pax5 to enable efficient terminal B cell differentiation', *The Journal of Experimental Medicine*, 211(11), pp. 2183–2198. doi: 10.1084/jem.20140338.

Lu, F. *et al.* (2008) 'Epstein-Barr Virus-Induced miR-155 Attenuates NF-B Signaling and Stabilizes Latent Virus Persistence †', *JOURNAL OF VIROLOGY*, 82(21), pp. 10436–10443. doi: 10.1128/JVI.00752-08.

Lublin, F. D. *et al.* (2014) 'Defining the clinical course of multiple sclerosis: The 2013 revisions', *Neurology*, 83(3), pp. 278–286. doi: 10.1212/WNL.0000000000000560.

Lucchinetti, C. *et al.* (2000) 'Heterogeneity of multiple sclerosis lesions', *Annals of Neurology*, 47(July), pp. 707–717. doi: 10.1002/1531-8249(200006)47.

Luo, C. *et al.* (2017a) 'The role of microglia in multiple sclerosis.', *Neuropsychiatric disease and treatment*. Dove Press, 13, pp. 1661–1667. doi: 10.2147/NDT.S140634.

Luo, C. *et al.* (2017b) 'The role of microglia in multiple sclerosis.', *Neuropsychiatric disease and treatment*. Dove Press, 13, pp. 1661–1667. doi: 10.2147/NDT.S140634.

Luo, C. *et al.* (2017c) 'The role of microglia in multiple sclerosis', *Neuropsychiatric Disease and Treatment*, 13, pp. 1661–1667. doi: 10.2147/NDT.S140634.

Ma, S. F. *et al.* (2015) 'Adoptive transfer of M2 macrophages promotes locomotor recovery in adult rats after spinal cord injury', *Brain, Behavior, and Immunity*. Elsevier Inc., 45, pp. 157–170. doi: 10.1016/j.bbi.2014.11.007.

Makita, N. *et al.* (2015) 'IL-10 enhances the phenotype of M2 macrophages induced by IL-4 and confers the ability to increase eosinophil migration', *International Immunology*, 27(3), pp. 131–141. doi: 10.1093/intimm/dxu090.

Mameli, G. *et al.* (2016) 'Natalizumab Therapy Modulates miR-155, miR-26a and Proinflammatory Cytokine Expression in MS Patients', *PLOS ONE*. Edited by R. Rota. Public Library of Science, 11(6), p. e0157153. doi: 10.1371/journal.pone.0157153.

Mann, Monica K *et al.* (2012) 'Pathogenic and regulatory roles for B cells in experimental autoimmune encephalomyelitis.', *Autoimmunity*. NIH Public Access, 45(5), pp. 388–99. doi: 10.3109/08916934.2012.665523.

Mann, Monica K. *et al.* (2012) 'Pathogenic and regulatory roles for B cells in experimental autoimmune encephalomyelitis', *Autoimmunity*, 45(5), pp. 388–399. doi: 10.3109/08916934.2012.665523.

Mantovani, A. *et al.* (2011) 'Neutrophils in the activation and regulation of innate and adaptive immunity', *Nature Reviews Immunology*. Nature Publishing Group, 11(8), pp. 519–531. doi: 10.1038/nri3024.

Markopoulos, G. *et al.* (2018) 'Roles of NF-κB Signaling in the Regulation of miRNAs Impacting on Inflammation in Cancer', *Biomedicines*, 6(2), p. 40. doi: 10.3390/biomedicines6020040.

Martin, R. *et al.* (2016a) 'Current multiple sclerosis treatments have improved our understanding of MS autoimmune pathogenesis', pp. 2078–2090. doi: 10.1002/eji.201646485.

Martin, R. *et al.* (2016b) 'Current multiple sclerosis treatments have improved our understanding of MS autoimmune pathogenesis', *European Journal of Immunology*, 46(9), pp. 2078–2090. doi: 10.1002/eji.201646485.

Marusic, S. *et al.* (2012) 'Immunization method influences EAE relapse rate in SJL mice (171.6)', *The Journal of Immunology*, 188(1 Supplement).

Mashima, R. (2015a) 'Physiological roles of miR-155', *Immunology*, 145(3), pp. 323–333. doi: 10.1111/imm.12468.

Mashima, R. (2015b) 'Physiological roles of miR-155', *Immunology*. doi: 10.1111/imm.12468.

Mazzon, C. *et al.* (2016) 'CCRL2 regulates M1/M2 polarization during EAE recovery phase', *Journal of Leukocyte Biology*, 99(6), pp. 1027–1033. doi: 10.1189/jlb.3ma0915-444rr.

Mccoy, C. E. (2011) 'The role of miRNAs in cytokine signaling Claire', *Frontiers in Bioscience*, (3), pp. 2161–2171.

McCoy, Claire E *et al.* (2010a) 'IL-10 inhibits miR-155 induction by toll-like receptors.', *The Journal of biological chemistry*. American Society for Biochemistry and Molecular Biology, 285(27), pp. 20492–8. doi: 10.1074/jbc.M110.102111.

McCoy, Claire E *et al.* (2010b) 'IL-10 inhibits miR-155 induction by toll-like receptors.', *The Journal of biological chemistry*. American Society for Biochemistry and Molecular Biology, 285(27), pp. 20492–8. doi: 10.1074/jbc.M110.102111.

McCoy, Claire E *et al.* (2010c) 'IL-10 inhibits miR-155 induction by toll-like receptors.', *The Journal of biological chemistry*. American Society for Biochemistry and Molecular Biology, 285(27), pp. 20492–8. doi: 10.1074/jbc.M110.102111.

McCoy, Claire E. *et al.* (2010) 'IL-10 inhibits miR-155 induction by toll-like receptors', *Journal of Biological Chemistry*, 285(27), pp. 20492–20498. doi: 10.1074/jbc.M110.102111.

McCubbrey, A. L. *et al.* (2017) 'Promoter specificity and efficacy in conditional and inducible transgenic targeting of lung macrophages', *Frontiers in Immunology*, 8(NOV). doi: 10.3389/fimmu.2017.01618.

McKay, K. A. *et al.* (2015) 'Risk factors associated with the onset of relapsing-remitting and primary progressive multiple sclerosis: A systematic review', *BioMed Research International*, 2015. doi: 10.1155/2015/817238.

McQualter, J. L. *et al.* (2001) 'Granulocyte macrophage colony-stimulating factor : a new putative therapeutic target in multiple sclerosis. IF14.588', *Journal of Experimental Medicine*, 194(7), pp. 873–882.

Mildner, A. *et al.* (2009) 'CCR2 + Ly-6C hi monocytes are crucial for the effector phase of autoimmunity in the central nervous system', *Brain*, 132(9), pp. 2487–2500. doi: 10.1093/brain/awp144.

Miller, N. M. *et al.* (2015) 'Anti-inflammatory mechanisms of IFN-γ studied in experimental autoimmune encephalomyelitis reveal neutrophils as a potential target in multiple sclerosis', *Frontiers in Neuroscience*. Frontiers, 9, p. 287. doi: 10.3389/fnins.2015.00287.

Miller, S. D. *et al.* (2008) 'Autoimmune Encephalomyelitis Severity of Relapsing Experimental Plasmacytoid Dendritic Cells Regulate the Cutting Edge: Central Nervous System', *J Immunol References*, 180, pp. 6457–6461. doi: 10.4049/jimmunol.180.10.6457.

Miller, S. D., Karpus, W. J. and Davidson, T. S. (2007) 'Experimental Autoimmune Encephalomyelitis in the Mouse', *Current Protocols in Immunology*, 15.1(3), pp. 1–26. doi: 10.1002/0471142735.im1501s77.Experimental.

Minton, K. (2017) 'Immune regulation: IL-10 targets macrophage metabolism', *Nature Publishing Group*, 17. doi: 10.1038/nri.2017.57.

Miron, Veronique E *et al.* (2013) 'M2 microglia and macrophages drive oligodendrocyte differentiation during CNS remyelination.', *Nature neuroscience*, 16(9), pp. 1211–8. doi: 10.1038/nn.3469.

Miron, Veronique E. *et al.* (2013) 'M2 microglia and macrophages drive oligodendrocyte differentiation during CNS remyelination', *Nature Neuroscience*, 16(9), pp. 1211–

1218. doi: 10.1038/nn.3469.

Miron, V. E., Kuhlmann, T. and Antel Jack P., J. P. (2011) 'Cells of the oligodendroglial lineage, myelination, and remyelination', *Biochimica et Biophysica Acta - Molecular Basis of Disease*. Elsevier B.V., 1812(2), pp. 184–193. doi: 10.1016/j.bbadis.2010.09.010.

Mishra, M. K. and Wee Yong, V. (2016) 'Myeloid cells — targets of medication in multiple sclerosis'. doi: 10.1038/nrneurol.2016.110.

Mitrovič, M. *et al.* (2018) 'Low-Frequency and Rare-Coding Variation Contributes to Multiple Sclerosis Risk', *Cell*. Cell Press, 175(6), pp. 1679-1687.e7. doi: 10.1016/J.CELL.2018.09.049.

Mitsdoerffer, M. and Peters, A. (2016) 'Tertiary Lymphoid Organs in Central Nervous System Autoimmunity.', *Frontiers in immunology*. Frontiers Media SA, 7, p. 451. doi: 10.3389/fimmu.2016.00451.

Mohammed, E. M. (2019) 'Multiple Sclerosis and the Pathogenicity of Mir-155', *Biomedical Journal of Scientific & Technical Research*, 9(4). doi: 10.26717/bjstr.2018.09.001841.

Montes-Cobos, E. *et al.* (2017) 'Targeted delivery of glucocorticoids to macrophages in a mouse model of multiple sclerosis using inorganic-organic hybrid nanoparticles', *Journal of Controlled Release*, 245, pp. 157–169. doi: 10.1016/j.jconrel.2016.12.003.

Moore, C. S., Rao, Vijayaraghava T.S., *et al.* (2013a) 'miR-155 as a multiple sclerosis-relevant regulator of myeloid cell polarization', *Annals of Neurology*. John Wiley & Sons, Ltd, 74(5), pp. 709–720. doi: 10.1002/ana.23967.

Moore, C. S., Rao, Vijayaraghava T.S., *et al.* (2013b) 'miR-155 as a multiple sclerosis-relevant regulator of myeloid cell polarization', *Annals of Neurology*, 74(5), pp. 709–720. doi: 10.1002/ana.23967.

Moore, C. S., Rao, Vijayaraghava T S, *et al.* (2013) 'MiR-155 as a multiple sclerosis-relevant regulator of myeloid cell polarization', *Annals of Neurology*. doi: 10.1002/ana.23967.

Moreno, M. A. *et al.* (2016) 'Therapeutic depletion of monocyte-derived cells protects from long-term axonal loss in experimental autoimmune encephalomyelitis', *Journal of Neuroimmunology*. Elsevier B.V., 290, pp. 36–46. doi: 10.1016/j.jneuroim.2015.11.004.

Morganti, J. M. *et al.* (2015) 'CCR2 Antagonism Alters Brain Macrophage Polarization and Ameliorates Cognitive Dysfunction Induced by Traumatic Brain Injury', *Neurobiology of Disease* , 35(2). doi: 10.1523/JNEUROSCI.2405-14.2015.

Mosser, D. M. and Edwards, J. P. (2008) 'Exploring the full spectrum of macrophage activation', *Nature Reviews Immunology*, 8(12), pp. 958–969. doi: 10.1038/nri2448.

Mrdjen, D. *et al.* (2018) 'High-Dimensional Single-Cell Mapping of Central Nervous System Immune Cells Reveals Distinct Myeloid Subsets in Health, Aging, and Disease', *Immunity*. Elsevier, 48(2), pp. 380-395.e6. doi: 10.1016/j.immuni.2018.01.011.

Mulero, P., Midaglia, L. and Montalban, X. (2018) 'Ocrelizumab: a new milestone in multiple sclerosis therapy', *Therapeutic Advances in Neurological Disorders*, 11, pp. 1–6. doi: 10.1177/1756286418773025.

Murray, P. J. (2006) 'Understanding and exploiting the endogenous interleukin-10/STAT3-mediated anti-inflammatory response', *Current Opinion in Pharmacology*, 6(4), pp. 379–386. doi: 10.1016/j.coph.2006.01.010.

Murray, P. J. *et al.* (2014) 'Macrophage activation and polarization: nomenclature and experimental guidelines', *Immunity*, 41(1), pp. 14–20. doi: 10.1016/j.immuni.2014.06.008.

Murugaiyan, Gopal, Beynon, V., Mittal, A., Joller, N. and Weiner, Howard L (2011a) 'Silencing MicroRNA-155 Ameliorates Experimental Autoimmune Encephalomyelitis.', *Journal of immunology (Baltimore, Md. : 1950)*, 187(5), pp. 2213–2221. doi: 10.4049/jimmunol.1003952.

Murugaiyan, G. *et al.* (2011) 'Silencing MicroRNA-155 Ameliorates Experimental Autoimmune Encephalomyelitis', *The Journal of Immunology*. doi: 10.4049/jimmunol.1003952.

Murugaiyan, Gopal, Beynon, V., Mittal, A., Joller, N. and Weiner, Howard L (2011b) 'Silencing MicroRNA-155 Ameliorates Experimental Autoimmune Encephalomyelitis', *J Immunol*, 187(5), pp. 2213–2221. doi: 10.4049/jimmunol.1003952.

Murugaiyan, Gopal, Beynon, V., Mittal, A., Joller, N. and Weiner, Howard L. (2011) 'Silencing MicroRNA-155 Ameliorates Experimental Autoimmune Encephalomyelitis', *The Journal of Immunology*, 187(5), pp. 2213–2221. doi: 10.4049/jimmunol.1003952.

Mycko, M. P. *et al.* (2015) 'miR-155-3p Drives the Development of Autoimmune Demyelination by Regulation of Heat Shock Protein 40', *Journal of Neuroscience*, 35(50), pp. 16504–16515. doi: 10.1523/jneurosci.2830-15.2015.

Naegele, M. *et al.* (2012) 'Neutrophils in multiple sclerosis are characterized by a primed phenotype', *Journal of Neuroimmunology*. Elsevier B.V., 242(1–2), pp. 60–71. doi: 10.1016/j.jneuroim.2011.11.009.

Neumann, H., Kotter, M. R. and Franklin, R. J. M. (2009) 'Debris clearance by microglia: an essential link between degeneration and regeneration.', *Brain : a journal of neurology*. Oxford University Press, 132(Pt 2), pp. 288–95. doi: 10.1093/brain/awn109.

Neumann, J. T. *et al.* (2013) 'Local APCs Nervous System Infiltrates by Maturing Neutrophils Amplify Autoimmune Central', *Journal of Immunology*. doi: 10.4049/jimmunol.1202613.

Nichols, F. C. *et al.* (2009) 'Unique Lipids from a Common Human Bacterium Represent a New Class of Toll-Like Receptor 2 Ligands Capable of Enhancing Autoimmunity', *The American Journal of Pathology*, 175(6), pp. 2430–2438. doi: 10.2353/ajpath.2009.090544.

Niu, J. *et al.* (2019) 'Aberrant oligodendroglial–vascular interactions disrupt the blood–brain barrier, triggering CNS inflammation', *Nature Neuroscience*, 22(5), pp. 709–718.

doi: 10.1038/s41593-019-0369-4.

Niwald, M. *et al.* (2017) 'Evaluation of Selected MicroRNAs Expression in Remission Phase of Multiple Sclerosis and Their Potential Link to Cognition, Depression, and Disability', *Journal of Molecular Neuroscience*, 63(3–4), pp. 275–282. doi: 10.1007/s12031-017-0977-y.

Nuyts, A. *et al.* (2013) 'Dendritic cells in multiple sclerosis: key players in the immunopathogenesis, key players for new cellular immunotherapies?', *Multiple Sclerosis Journal*, 19(8), pp. 995–1002. doi: 10.1177/1352458512473189.

O'Carroll, D. *et al.* (2007) 'A Slicer-independent role for Argonaute 2 in hematopoiesis and the microRNA pathway', *Genes & Development*, 21(16), pp. 1999–2004. doi: 10.1101/gad.1565607.

O'connell, R. M. *et al.* (2010) 'Article MicroRNA-155 Promotes Autoimmune Inflammation by Enhancing Inflammatory T Cell Development', *Immunity*, 33, pp. 607–619. doi: 10.1016/j.immuni.2010.09.009.

O'Connell, R. M. *et al.* (2007) 'MicroRNA-155 is induced during the macrophage inflammatory response', *Proceedings of the National Academy of Sciences*, 104(5), pp. 1604–1609. doi: 10.1073/pnas.0610731104.

O'Connell, R. M. *et al.* (2008) 'Sustained expression of microRNA-155 in hematopoietic stem cells causes a myeloproliferative disorder', *The Journal of Experimental Medicine*, 205(3), pp. 585–594. doi: 10.1084/jem.20072108.

O'Connell, R. M. *et al.* (2009) 'Inositol phosphatase SHIP1 is a primary target of miR-155.', *Proceedings of the National Academy of Sciences of the United States of America*. National Academy of Sciences, 106(17), pp. 7113–8. doi: 10.1073/pnas.0902636106.

O'Connell, R. M., Kahn, D., Gibson, William S J, *et al.* (2010) 'MicroRNA-155 promotes autoimmune inflammation by enhancing inflammatory T cell development', *Immunity*, 33(4), pp. 607–619. doi: 10.1016/j.immuni.2010.09.009.

O'connell, R. M., Zhao, J. L. and Rao, D. S. (2011) 'MicroRNA function in myeloid biology', *Blood*. doi: 10.1182/blood-2011-03-291971.

O'Connor, R. A. *et al.* (2008) 'Cutting edge: Th1 cells facilitate the entry of Th17 cells to the central nervous system during experimental autoimmune encephalomyelitis.', *Journal of immunology (Baltimore, Md. : 1950)*, 181(6), pp. 3750–4. Available at: http://www.ncbi.nlm.nih.gov/pubmed/18768826 (Accessed: 17 April 2019).

O'Neill, J. K. *et al.* (1998) 'Optic neuritis in chronic relapsing experimental allergic encephalomyelitis in Biozzi ABH mice: demyelination and fast axonal transport changes in disease.', *Journal of neuroimmunology*. Elsevier, 82(2), pp. 210–8.

O'Neill, L. A., Sheedy, F. J. and McCoy, C. E. (2011) 'MicroRNAs: The fine-tuners of Toll-like receptor signalling', *Nature Reviews Immunology*, 11(3), pp. 163–175. doi: 10.1038/nri2957.

Ochoa-Repáraz, J., Kirby, T. O. and Kasper, L. H. (2018) 'The gut microbiome and multiple sclerosis', *Cold Spring Harbor Perspectives in Medicine*, 8(6), pp. 1–16. doi: 10.1101/cshperspect.a029017.

Oikawa, T. and Yamada, T. (2003) 'Molecular biology of the Ets family of transcription factors', *Gene*. Elsevier, 303, pp. 11–34. doi: 10.1016/S0378-1119(02)01156-3.

Oishi, Y. and Manabe, I. (2018) 'Macrophages in inflammation, repair and regeneration', *International Immunology*. Narnia, 30(11), pp. 511–528. doi: 10.1093/intimm/dxy054.

Okoye, I. S. *et al.* (2014) 'Transcriptomics identified a critical role for Th2 cell-intrinsic miR-155 in mediating allergy and antihelminth immunity', *Proceedings of the National Academy of Sciences*, 111(30), pp. E3081–E3090. doi: 10.1073/pnas.1406322111.

Oneissi Martinez, F. *et al.* (2008) *Macrophage activation and polarization*, *Frontiers in Bioscience*. (Accessed: 27 February 2019).

van Oosten, B. W. *et al.* (1997) 'Treatment of multiple sclerosis with the monoclonal anti-CD4 antibody cM-T412: results of a randomized, double-blind, placebo-controlled, MR-monitored phase II trial.', *Neurology*, 49(2), pp. 351–7. doi: 10.1212/wnl.49.2.351.

Oreja-Guevara, C. *et al.* (2012) 'TH1/TH2 Cytokine profile in relapsing-remitting multiple sclerosis patients treated with Glatiramer acetate or Natalizumab.', *BMC neurology*. BioMed Central, 12, p. 95. doi: 10.1186/1471-2377-12-95.

Ostrand-Rosenberg, S. and Fenselau, C. (2018) 'Myeloid-Derived Suppressor Cells: Immune-Suppressive Cells That Impair Antitumor Immunity and Are Sculpted by Their Environment', *The Journal of Immunology*, 200(2), pp. 422–431. doi: 10.4049/jimmunol.1701019.

Owens, T., Bechmann, I. and Engelhardt, B. (2008) 'Perivascular Spaces and the Two Steps to Neuroinflammation', *Journal of Neuropathology & Experimental Neurology*. Narnia, 67(12), pp. 1113–1121. doi: 10.1097/NEN.0b013e31818f9ca8.

Panitch, H. S. *et al.* (1987) 'Exacerbations of multiple sclerosis in patients treated with gamma interferon.', *Lancet (London, England)*, 1(8538), pp. 893–5. Available at: http://www.ncbi.nlm.nih.gov/pubmed/2882294 (Accessed: 16 April 2019).

Papayannopoulos, V. (2018) 'Neutrophil extracellular traps in immunity and disease', *Nature Reviews Immunology*, 18(2), pp. 134–147. doi: 10.1038/nri.2017.105.

Paraboschi, E. M. *et al.* (2011) 'Genetic Association and Altered Gene Expression of Mir-155 in Multiple Sclerosis Patients', *Int. J. Mol. Sci*, 12, pp. 8695–8712. doi: 10.3390/ijms12128695.

Parameswaran, N. and Patial, S. (2010) *Tumor Necrosis Factor-α Signaling in Macrophages*.

Paré, A. *et al.* (2018) ' IL-1β enables CNS access to CCR2 hi monocytes and the generation of pathogenic cells through GM-CSF released by CNS endothelial cells ', *Proceedings of the National Academy of Sciences*, 115(6), pp. E1194–E1203. doi: 10.1073/pnas.1714948115.

Pareek, S. *et al.* (2014) 'MiR-155 induction in microglial cells suppresses Japanese encephalitis virus replication and negatively modulates innate immune responses', *Journal of Neuroinflammation*. doi: 10.1186/1742-2094-11-97.

Pashenkov, M. *et al.* (2002) 'Elevated expression of CCR5 by myeloid (CD11c +) blood dendritic cells', *Clinical and Experimental Immunology*, pp. 519–526.

Pasquinelli, A. E. (2012) 'MicroRNAs and their targets: Recognition, regulation and an emerging reciprocal relationship', *Nature Reviews Genetics*. Nature Publishing Group, 13(4), pp. 271–282. doi: 10.1038/nrg3162.

Patel, A. R. *et al.* (2013) 'Microglia and ischemic stroke: A double-edged sword', *International Journal of Physiology, Pathophysiology and Pharmacology*, 5(2), pp. 73–90.

Patrikios, P. *et al.* (2006) 'Remyelination is extensive in a subset of multiple sclerosis patients', *Brain*. Narnia, 129(12), pp. 3165–3172. doi: 10.1093/brain/awl217.

Pauls, S. D. and Marshall, A. J. (2017) 'Regulation of immune cell signaling by SHIP1: A phosphatase, scaffold protein, and potential therapeutic target', *European Journal of Immunology*, 47(6), pp. 932–945. doi: 10.1002/eji.201646795.

Payne, N. L. *et al.* (2013) 'Human adipose-derived mesenchymal stem cells engineered to secrete IL-10 inhibit APC function and limit CNS autoimmunity', *Brain Behavior and Immunity*, 30, pp. 103–114. doi: 10.1016/j.bbi.2013.01.079.

Pena-Philippides, J. C. *et al.* (2016) 'In vivo inhibition of miR-155 significantly alters post-stroke inflammatory response', *Journal of Neuroinflammation*. Journal of Neuroinflammation, 13(1), pp. 1–16. doi: 10.1186/s12974-016-0753-x.

Pierson, Emily R, Stromnes, I. M. and Goverman, J. M. (2014) 'B cells promote induction of experimental autoimmune encephalomyelitis by facilitating reactivation of T cells in the central nervous system.', *Journal of immunology (Baltimore, Md. : 1950)*. NIH Public Access, 192(3), pp. 929–39. doi: 10.4049/jimmunol.1302171.

Pierson, Emily R., Stromnes, I. M. and Goverman, J. M. (2014) 'B Cells Promote Induction of Experimental Autoimmune Encephalomyelitis by Facilitating Reactivation of T Cells in the Central Nervous System', *The Journal of Immunology*, 192(3), pp. 929–939. doi: 10.4049/jimmunol.1302171.

Pierson, E. R., Wagner, C. A. and Goverman, J. M. (2018) 'The contribution of neutrophils to CNS autoimmunity', *Clinical Immunology*. Academic Press, 189, pp. 23–28. doi: 10.1016/J.CLIM.2016.06.017.

Pitt, D. *et al.* (2017) 'Myeloid cell plasticity in the evolution of central nervous system autoimmunity', *Annals of Neurology*, 83(1), pp. 131–141. doi: 10.1002/ana.25128.

Pizzorusso, T. *et al.* (2015) 'An updated role of microRNA-124 in central nervous system disorders: a review'. doi: 10.3389/fncel.2015.00193.

Ponath, G. *et al.* (2018) 'Enhanced astrocyte responses are driven by a genetic risk allele associated with multiple sclerosis', *Nature Communications*, 9(1). doi: 10.1038/s41467-018-07785-8.

Ponath, G., Park, C. and Pitt, D. (2018) 'The role of astrocytes in multiple sclerosis', *Frontiers in Immunology*, 9(FEB), p. 1. doi: 10.3389/fimmu.2018.00217.

Ponomarev, E. D., Veremeyko, T. and Weiner, H. L. (2013) 'MicroRNAs are universal regulators of differentiation, activation, and polarization of microglia and macrophages in normal and diseased CNS', *Glia*, 61(1), pp. 91–103. doi:

10.1002/glia.22363.

Pradier, O. *et al.* (2002) 'Bordetella pertussis toxin induces the release of inflammatory cytokines and dendritic cell activation in whole blood: impaired responses in human newborns', *European Journal of Immunology*, 32(11), pp. 3118–3125. doi: 10.1002/1521-4141(200211)32:11<3118::aid-immu3118>3.0.co;2-b.

Praet, J. *et al.* (2014a) 'Cellular and molecular neuropathology of the cuprizone mouse model: Clinical relevance for multiple sclerosis', *Neuroscience & Biobehavioral Reviews*, 47, pp. 485–505. doi: 10.1016/j.neubiorev.2014.10.004.

Praet, J. *et al.* (2014b) 'Cellular and molecular neuropathology of the cuprizone mouse model: Clinical relevance for multiple sclerosis', *Neuroscience & Biobehavioral Reviews*, 47, pp. 485–505. doi: 10.1016/j.neubiorev.2014.10.004.

Prajnya Ranganath (2015) 'MicroRNA-155 and Its Role in Malignant Hematopoiesis', *Libertas Academica*. doi: 10.4137/Bmi.s27676.

Qin, Z. *et al.* (2016) 'miRNA-124 in immune system and immune disorders', *Frontiers in Immunology*, 7(OCT), p. 406. doi: 10.3389/fimmu.2016.00406.

Quinn, S. R. *et al.* (2014) 'The role of Ets2 transcription factor in the induction of microRNA-155 by LPS, and its targeting by IL-10.', *Journal of Biological Chemistry*, 289(7), pp. 4316–4325. doi: 10.1074/jbc.M113.522730.

Racke, M. K., Hu, W. and Lovett-Racke, A. E. (2005) 'PTX cruiser: Driving autoimmunity via TLR4', *Trends in Immunology*. doi: 10.1016/j.it.2005.03.012.

Ramadan, A. *et al.* (2016) 'In situ expansion of T cells that recognize distinct self-antigens sustains autoimmunity in the CNS', *Brain*, 139(5), pp. 1433–1446. doi: 10.1093/brain/aww032.

RAMESH S. PILLAI (2005) 'MicroRNA function : Multiple mechanisms for a tiny RNA ?', *Rna*, 11(Bartel 2004), pp. 1753–1761. doi: 10.1261/rna.2248605.that.

Ransohoff, R. M. (2012) 'Animal models of multiple sclerosis: The good, the bad and the bottom line', *Nature Neuroscience*. Nature Publishing Group, 15(8), pp. 1074–1077. doi: 10.1038/nn.3168.

Rath, M. *et al.* (2014) 'Metabolism via arginase or nitric oxide synthase: two competing arginine pathways in macrophages'. doi: 10.3389/fimmu.2014.00532.

Rawji, K. S., Mishra, M. K. and Vw, Y. (2016) 'Regenerative Capacity of Macrophages for Remyelination', *Frontiers in Cell and Developmental Biology | www.frontiersin.org*, 1, p. 47. doi: 10.3389/fcell.2016.00047.

Rawji, K. S. and Yong, V. W. (2013a) 'The benefits and detriments of macrophages/microglia in models of multiple sclerosis.', *Clinical & developmental immunology*. Hindawi, 2013, p. 948976. doi: 10.1155/2013/948976.

Rawji, K. S. and Yong, V. W. (2013b) 'The benefits and detriments of macrophages/microglia in models of multiple sclerosis.', *Clinical & developmental immunology*. Hindawi Limited, 2013, p. 948976. doi: 10.1155/2013/948976.

Rice, R. A. *et al.* (2017) 'Microglial repopulation resolves inflammation and promotes brain recovery after injury HHS Public Access', *Glia*, 65(6), pp. 931–944. doi:

10.1002/glia.23135.

Rittchen, S. *et al.* (2015) 'Myelin repair invivo is increased by targeting oligodendrocyte precursor cells with nanoparticles encapsulating leukaemia inhibitory factor (LIF)', *Biomaterials*. Elsevier Ltd, 56, pp. 78–85. doi: 10.1016/j.biomaterials.2015.03.044.

Robinson, A. P. *et al.* (2014) *The experimental autoimmune encephalomyelitis (EAE) model of MS. utility for understanding disease pathophysiology and treatment.*, *Handbook of Clinical Neurology*. Elsevier B.V. doi: 10.1016/B978-0-444-52001-2.00008-X.

Rodriguez, A. *et al.* (2007) 'Requirement of bic/microRNA-155 for Normal Immune Function', *Science*, 316(5824), pp. 608–611. doi: 10.1126/science.1139253.

Rojas, M. *et al.* (2018) 'Molecular mimicry and autoimmunity', *Journal of Autoimmunity*. Elsevier, 95(September), pp. 100–123. doi: 10.1016/j.jaut.2018.10.012.

Rolfe, A. J. *et al.* (2017) 'In vitro phagocytosis of myelin debris by bone marrow-derived macrophages', *Journal of Visualized Experiments*, 2017(130), pp. 1–8. doi: 10.3791/56322.

Rosenberg, S. A. and Restifo, N. P. (2015) 'Adoptive cell transfer as personalized immunotherapy for human cancer.', *Science (New York, N.Y.)*. American Association for the Advancement of Science, 348(6230), pp. 62–8. doi: 10.1126/science.aaa4967.

Rothhammer, V. *et al.* (2018) 'Microglial control of astrocytes in response to microbial metabolites', *Nature*, 557.

Rowshanravan, B., Halliday, N. and Sansom, D. M. (2018) 'CTLA-4: A moving target in immunotherapy', *Blood*, 131(1), pp. 58–67. doi: 10.1182/blood-2017-06-741033.

Rubino, S. J. *et al.* (2018) 'Acute microglia ablation induces neurodegeneration in the somatosensory system', *Nature communications*, 9(1), p. 4578. doi: 10.1038/s41467-018-05929-4.

Rui-Xue Leng 1, Hai-Feng Pan 1 and Wei-Zi Qin, Gui-Mei Chen, D.-Q. (2011) 'Role of microRNA-155 in autoimmunity', *Cytokine and Growth Factors*. Available at: https://pdf.sciencedirectassets.com.

Rumble, Julie M *et al.* (2015a) 'Neutrophil-related factors as biomarkers in EAE and MS.', *The Journal of experimental medicine*. Rockefeller University Press, 212(1), pp. 23–35. doi: 10.1084/jem.20141015.

Rumble, Julie M *et al.* (2015b) 'Neutrophil-related factors as biomarkers in EAE and MS.', *The Journal of experimental medicine*. Rockefeller University Press, 212(1), pp. 23–35. doi: 10.1084/jem.20141015.

Rumble, Julie M. *et al.* (2015) 'Neutrophil-related factors as biomarkers in EAE and MS', *Journal of Experimental Medicine*, 212(1), pp. 23–35. doi: 10.1084/jem.20141015.

Ruytinx, P. *et al.* (2018) 'Chemokine-Induced Macrophage Polarization in Inflammatory Conditions', *Frontiers in Immunology*. Frontiers, 9, p. 1930. doi: 10.3389/fimmu.2018.01930.

Sagar, D. *et al.* (2012) *Dendritic cell CNS recruitment correlates with disease severity in EAE via CCL2 chemotaxis at the blood-brain barrier through paracellular transmigration and ERK activation*, *Journal of Neuroinflammation*. doi:

10.1186/1742-2094-9-245.

Samoilova, E. B., Horton, J. L. and Chen, Y. (1998) 'Acceleration of Experimental Autoimmune Encephalomyelitis in Interleukin-10-Deficient Mice: Roles of Interleukin-10 in Disease Progression and Recovery', *Cellular Immunology*. Academic Press, 188(2), pp. 118–124. doi: 10.1006/CIMM.1998.1365.

Sarah Hewer, Robyn Lucas, Ingrid van der Mei, B. V. T. (2013) 'Vitamin D and multiple sclerosis', *Journal of Clinical Neuroscience*. Churchill Livingstone, 20(5), pp. 634–641. doi: 10.1016/J.JOCN.2012.10.005.

Savarin, C., Dutta, R. and Bergmann, C. C. (2018) 'Distinct gene profiles of bone marrow-derived macrophages and microglia during neurotropic coronavirus-induced demyelination', *Frontiers in Immunology*, 9(JUN). doi: 10.3389/fimmu.2018.01325.

Sawcer, S., Franklin, R. J. M. and Ban, M. (2014) 'Multiple sclerosis genetics', *The Lancet Neurology*, 13(7), pp. 700–709. doi: 10.1016/S1474-4422(14)70041-9.

Saxena, A. *et al.* (2015) 'Interleukin-10 paradox: A potent immunoregulatory cytokine that has been difficult to harness for immunotherapy', *Cytokine*. Academic Press, 74(1), pp. 27–34. doi: 10.1016/J.CYTO.2014.10.031.

Schilling, S. *et al.* (2006) 'Clinical and Experimental Immunology Fumaric acid esters are effective in chronic experimental autoimmune encephalomyelitis and suppress macrophage infiltration', *Clinical and Experimental Immunology*, 145, pp. 101–107. doi: 10.1111/j.1365-2249.2006.03094.x.

Schonberg, D. L. *et al.* (2012) 'Development/Plasticity/Repair Ferritin Stimulates Oligodendrocyte Genesis in the Adult Spinal Cord and Can Be Transferred from Macrophages to NG2 Cells In Vivo', *the journal of neuroscience*. doi: 10.1523/JNEUROSCI.3517-11.2012.

Schrempf, W. and Ziemssen, T. (2007) 'Glatiramer acetate: Mechanisms of action in multiple sclerosis', *Autoimmunity Reviews*, 6(7), pp. 469–475. doi: 10.1016/j.autrev.2007.02.003.

Seddiki, N. *et al.* (2014) 'Role of miR-155 in the regulation of lymphocyte immune function and disease', *Immunology*, 142(1), pp. 32–38. doi: 10.1111/imm.12227.

Sellebjerg, F. *et al.* (2016) 'Exploring potential mechanisms of action of natalizumab in secondary progressive multiple sclerosis', *Therapeutic Advances in Neurological Disorders*, 9(1), pp. 31–43. doi: 10.1177/1756285615615257.

Shah, M. Y. *et al.* (2016) 'microRNA Therapeutics in Cancer — An Emerging Concept', *EBioMedicine*, 12, pp. 34–42. doi: 10.1016/j.ebiom.2016.09.017.

Shahi, S. K., Freedman, S. N. and Mangalam, A. K. (2017) 'Gut microbiome in multiple sclerosis: The players involved and the roles they play', *Gut Microbes*, 8(6), pp. 607–615. doi: 10.1080/19490976.2017.1349041.

Shetty, A. *et al.* (2014) 'Immunodominant T-cell epitopes of MOG reside in its transmembrane and cytoplasmic domains in EAE.', *Neurology(R) neuroimmunology & neuroinflammation*. American Academy of Neurology, 1(2), p. e22. doi: 10.1212/NXI.0000000000000022.

Shi, J. *et al.* (2018) 'Cre driver mice targeting macrophages', *Methods in Molecular Biology*,

1784, pp. 263–275. doi: 10.1007/978-1-4939-7837-3_24.

Shi, S. R. *et al.* (1995) 'Antigen retrieval immunohistochemistry under the influence of pH using monoclonal antibodies', *Journal of Histochemistry and Cytochemistry*, 43(2), pp. 193–201. doi: 10.1177/43.2.7822775.

Shi, S. R., Cote, R. J. and Taylor, C. R. (1997) 'Antigen retrieval immunohistochemistry: Past, present, and future', *Journal of Histochemistry and Cytochemistry*, 45(3), pp. 327–343. doi: 10.1177/002215549704500301.

Shrestha, B. *et al.* (2017) 'Spatiotemporal resolution of spinal meningeal and parenchymal inflammation during experimental autoimmune encephalomyelitis', *Neurobiology of Disease*. Elsevier Inc., 108, pp. 159–172. doi: 10.1016/j.nbd.2017.08.010.

Silva, J. S. *et al.* (2017) 'Multiple Phenotypic Changes Define Neutrophil Priming', *Frontiers in Cellular and Infection Microbiology | www.frontiersin.org*, 1, p. 217. doi: 10.3389/fcimb.2017.00217.

Sonar, S. A. and Lal, G. (2019) 'The iNOS Activity During an Immune Response Controls the CNS Pathology in Experimental Autoimmune Encephalomyelitis', *Frontiers in Immunology*. Frontiers, 10, p. 710. doi: 10.3389/fimmu.2019.00710.

Song, W. M. and Colonna, M. (2018) 'The identity and function of microglia in neurodegeneration', *Nature Immunology*. Springer US, 19(October). doi: 10.1038/s41590-018-0212-1.

Sonkoly, E. *et al.* (2010) 'MiR-155 is overexpressed in patients with atopic dermatitis and modulates T-cell proliferative responses by targeting cytotoxic T lymphocyte-associated antigen 4', *Journal of Allergy and Clinical Immunology*, 126(3). doi: 10.1016/j.jaci.2010.05.045.

Sonkoly, E., Ståhle, M. and Pivarcsi, A. (2008) 'MicroRNAs and immunity: Novel players in the regulation of normal immune function and inflammation', *Seminars in Cancer Biology*. doi: 10.1016/j.semcancer.2008.01.005.

Sospedra, M. (2018) 'B cells in multiple sclerosis', *Current Opinion in Neurology*. Informa UK Limited, trading as Taylor & Francis Group, 31(3), pp. 256–262. doi: 10.1097/WCO.000000000000563.

Sousa, C., Biber, K. and Michelucci, A. (2017) 'Cellular and molecular characterization of microglia: A unique immune cell population', *Frontiers in Immunology*, 8(MAR). doi: 10.3389/fimmu.2017.00198.

Spath, S. *et al.* (2017) 'Dysregulation of the Cytokine GM-CSF Induces Spontaneous Phagocyte Invasion and Immunopathology in the Central Nervous System'. doi: 10.1016/j.immuni.2017.01.007.

Springer, T. A. (1990) *Adhesion Receptors of the Immune System, Nature*. Available at: https://search-proquest-com.ezproxy.lib.monash.edu.au/docview/15877996?accountid=12528&rfr_id=info%3Axri%2Fsid%3Aprimo (Accessed: 9 August 2019).

Staedel, C. and Darfeuille, F. (2013) 'MicroRNAs and bacterial infection', *Cellular Microbiology*, 15(9), pp. 1496–1507. doi: 10.1111/cmi.12159.

Stromnes, I. M. *et al.* (2008) 'Differential regulation of central nervous system autoimmunity

by T H1 and TH17 cells', *Nature Medicine*, 14(3), pp. 337–342. doi: 10.1038/nm1715.

Stromnes, I. M. and Goverman, J. M. (2006) 'Passive induction of experimental allergic encephalomyelitis', *Nature Protocols*, 1(4), pp. 1952–1960. doi: 10.1038/nprot.2006.284.

Sun, X. *et al.* (2018) 'Inhibition of microRNA-155 modulates endotoxin tolerance by upregulating suppressor of cytokine signaling 1 in microglia', *Experimental and Therapeutic Medicine*, 15(6), pp. 4709–4716. doi: 10.3892/etm.2018.6032.

Svensson, L. *et al.* (2002) 'A comparative analysis of B cell-mediated myelin oligodendrocyte glycoprotein-experimental autoimmune encephalomyelitis pathogenesis in B cell-deficient mice reveals an effect on demyelination', *European Journal of Immunology*, 32(7), p. 1939. doi: 10.1002/1521-4141(200207)32:7<1939::AID-IMMU1939>3.0.CO;2-S.

Tam, W. *et al.* (1997) 'bic, a Novel Gene Activated by Proviral Insertions in Avian Leukosis Virus-Induced Lymphomas, Is Likely To Function through Its Noncoding RNA', *MOLECULAR AND CELLULAR BIOLOGY*, 17(3), pp. 1490–1502. Available at: https://www.ncbi.nlm.nih.gov/pmc/articles/PMC231875/pdf/171490.pdf (Accessed: 27 May 2019).

Taoufik, E. *et al.* (2011) 'Transmembrane tumour necrosis factor is neuroprotective and regulates experimental autoimmune encephalomyelitis via neuronal nuclear factor-κB', *Brain*, 134(9), pp. 2722–2735. doi: 10.1093/brain/awr203.

Terry, R., Ifergan, I. and Miller, S. D. (2016) 'Experimental Autoimmune Encephalomyelitis in Mice Rachael', *Methods in Molecular Biology*, (1341), pp. 257–284. doi: 10.1007/7651.

Testa, U. *et al.* (2017) 'miR-146 and miR-155: Two Key Modulators of Immune Response and Tumor Development', *Non-Coding RNA*, 3(3), p. 22. doi: 10.3390/ncrna3030022.

Thai, T. H. *et al.* (2007) 'Regulation of the germinal center response by MicroRNA-155', *Science*, 316(5824), pp. 604–608. doi: 10.1126/science.1141229.

Thakker, P. *et al.* (2014) 'IL-23 Is Critical in the Induction but Not in the Effector Phase of Experimental Autoimmune Encephalomyelitis', *The Journal of Immunology*. American Association of Immunologists, 178(4), pp. 2589–2598. doi: 10.4049/jimmunol.178.4.2589.

Thamilarasan, M. *et al.* (2012) 'MicroRNAs in multiple sclerosis and experimental autoimmune encephalomyelitis', *Autoimmunity Reviews*, pp. 174–179. doi: 10.1016/j.autrev.2011.05.009.

Thomas, K. *et al.* (2017) 'Fingolimod additionally acts as immunomodulator focused on the innate immune system beyond its prominent effects on lymphocyte recirculation', *Journal of Neuroinflammation*, 14(1). doi: 10.1186/s12974-017-0817-6.

Thome, A. D. *et al.* (2016) 'microRNA-155 Regulates Alpha-Synuclein-Induced Inflammatory Responses in Models of Parkinson Disease', *Journal of Neuroscience*. doi: 10.1523/JNEUROSCI.3900-15.2016.

Thompson, A. J. *et al.* (2018) 'Diagnosis of multiple sclerosis: 2017 revisions of the McDonald criteria', *The Lancet Neurology*, 17, pp. 162–173. doi: 10.1016/S1474-4422(17)30470-2.

Thompson, K. K. and Tsirka, S. E. (2017) 'The diverse roles of microglia in the neurodegenerative aspects of central nervous system (CNS) autoimmunity', *International Journal of Molecular Sciences*, 18(3). doi: 10.3390/ijms18030504.

Thompson, K. and Tsirka, S. (2017) 'The Diverse Roles of Microglia in the Neurodegenerative Aspects of Central Nervous System (CNS) Autoimmunity', *International Journal of Molecular Sciences*, 18(3), p. 504. doi: 10.3390/ijms18030504.

Thompson, R. C., Vardinogiannis, I. and Gilmore, T. D. (2013) *Identification of an NF-κB p50/p65-responsive site in the human MIR155HG promoter*, *BMC Molecular Biology*. doi: 10.1186/1471-2199-14-24.

Tili, E. *et al.* (2007) 'Modulation of miR-155 and miR-125b Levels following Lipopolysaccharide/TNF-α Stimulation and Their Possible Roles in Regulating the Response to Endotoxin Shock', *The Journal of Immunology*, 179(8), pp. 5082–5089. doi: 10.4049/jimmunol.179.8.5082.

'TNF neutralization in MS: results of a randomized, placebo-controlled multicenter study. The Lenercept Multiple Sclerosis Study Group and The University of British Columbia MS/MRI Analysis Group.' (1999) *Neurology*, 53(3), pp. 457–65. Available at: http://www.ncbi.nlm.nih.gov/pubmed/10449104 (Accessed: 26 April 2019).

Tran, Elise H, Prince, E. N. and Owens, T. (2000) 'Chemokines Central Nervous System Via Regulation of Shapes Immune Invasion of the γ IFN', *J Immunol References*, 164, pp. 2759–2768. doi: 10.4049/jimmunol.164.5.2759.

Tran, E. H., Prince, E. N. and Owens, T. (2000) 'IFN- Shapes Immune Invasion of the Central Nervous System Via Regulation of Chemokines', *The Journal of Immunology*, 164(5), pp. 2759–2768. doi: 10.4049/jimmunol.164.5.2759.

Treiber, T., Treiber, N. and Meister, G. (2012) 'Regulation of microRNA biogenesis and function.', *Thrombosis and haemostasis*, 107(4), pp. 605–10. doi: 10.1160/TH11-12-0836.

Treiber, T., Treiber, N. and Meister, G. (2019) 'Regulation of microRNA biogenesis and its crosstalk with other cellular pathways', *Nature Reviews Molecular Cell Biology*, 20(1), pp. 5–20. doi: 10.1038/s41580-018-0059-1.

Trotta, T. *et al.* (2018) 'Microglia-derived extracellular vesicles in Alzheimer's Disease: A double-edged sword', *Biochemical Pharmacology*. Elsevier Inc., 148, pp. 184–192. doi: 10.1016/j.bcp.2017.12.020.

Tsai, H.-C. *et al.* (2019) 'Myeloid sphingosine-1-phosphate receptor 1 is important for CNS autoimmunity and neuroinflammation', *Journal of Autoimmunity*. doi: 10.1016/j.jaut.2019.06.001.

Tsiperson, V. *et al.* (2015) 'Brain-derived neurotrophic factor deficiency restricts proliferation of oligodendrocyte progenitors following cuprizone-induced demyelination', *ASN Neuro*, 7(1). doi: 10.1177/1759091414566878.

Tsitsiou, E. and Lindsay, M. A. (2009) 'microRNAs and the immune response', *Current Opinion in Pharmacology*, 9(4), pp. 514–520. doi: 10.1016/j.coph.2009.05.003.

Tzartos, J. S. *et al.* (2008) 'Interleukin-17 Production in Central Nervous System-Infiltrating T Cells and Glial Cells Is Associated with Active Disease in Multiple Sclerosis', *The American Journal of Pathology*, 172(1), pp. 146–155. doi: 10.2353/ajpath.2008.070690.

Umazume, A. *et al.* (2018) 'Role of PU.1 Expression as an Inflammatory Marker in Experimental Autoimmune Uveoretinitis', *Ocular Immunology and Inflammation*, 26(6), pp. 951–963. doi: 10.1080/09273948.2017.1299867.

Valentin-Torres, A. *et al.* (2016) 'Sustained TNF production by central nervous system infiltrating macrophages promotes progressive autoimmune encephalomyelitis', *Journal of Neuroinflammation*, 13(1), p. 46. doi: 10.1186/s12974-016-0513-y.

Vasquez-dunddel, D. *et al.* (2013) 'STAT3 regulates arginase-I in myeloid-derived suppressor cells from cancer patients', *The Journal of clinical investigation*, 123(4), pp. 1580–1589. doi: 10.1172/JCI60083.1580.

Vickers, S. P., Jackson, H. C. and Cheetham, S. C. (2011) 'Themed Issue: Translational Neuropharmacology-Using Appropriate Animal Models to Guide Clinical Drug Development The utility of animal models to evaluate novel anti-obesity agents LINKED ARTICLES'. doi: 10.1111/bph.2011.164.issue-4.

Vidigal, J. A. and Ventura, A. (2014) 'The biological functions of miRNAs: lessons from in vivo studies An elusive role for microRNAs', *Trends in Cell Biology*. doi: 10.1016/j.tcb.2014.11.004.

Vidigal, J. A. and Ventura, A. (2015) 'The biological functions of miRNAs: Lessons from in vivo studies', *Trends in Cell Biology*, 25(3), pp. 137–147. doi: 10.1016/j.tcb.2014.11.004.

Vigorito, E. *et al.* (2013) 'miR-155: An ancient regulator of the immune system', *Immunological Reviews*, pp. 146–157. doi: 10.1111/imr.12057.

Vincent, F. B. *et al.* (2014) 'The BAFF/APRIL system in SLE pathogenesis', *Nature Reviews Rheumatology*, 10(6), pp. 365–373. doi: 10.1038/nrrheum.2014.33.

Virtue, A., Wang, H. and Yang, X.-F. (2012) *MicroRNAs and Toll-like Receptor/Interleukin-1 Receptor Signaling*, *Journal of Hematology & Oncology*. doi: 10.1186/1756-8722-5-66.

Voß, E. V. *et al.* (2012) 'Characterisation of microglia during de- and remyelination: Can they create a repair promoting environment?', *Neurobiology of Disease*, 45(1), pp. 519–528. doi: 10.1016/j.nbd.2011.09.008.

Vukusic, S. and Confavreux, C. (2003) *Prognostic factors for progression of disability in the secondary progressive phase of multiple sclerosis.*, *Journal of the neurological sciences*. Available at: http://www.ncbi.nlm.nih.gov/pubmed/12559500 (Accessed: 15 May 2019).

Waisman, A. and Johann, L. (2018) 'Antigen-presenting cell diversity for T cell reactivation in central nervous system autoimmunity', *Journal of Molecular Medicine*, 96(12), pp. 1279–1292. doi: 10.1007/s00109-018-1709-7.

Wang, J. *et al.* (2015) 'microRNA-155 Deficiency Enhances the Recruitment and Functions of Myeloid-Derived Suppressor Cells in Tumor Microenvironment and Promotes Solid Tumor Growth', *Journal of Investigative Dermatology*, 136(6), pp. 602–613. doi: 10.1038/jid.2014.371.

Wang, J. *et al.* (2019) 'Targeting Microglia and Macrophages: A Potential Treatment Strategy for Multiple Sclerosis', *Frontiers in Pharmacology*, 10. doi: 10.3389/fphar.2019.00286.

Wang, S., Wan, X. and Ruan, Q. (2016) 'The microRNA-21 in autoimmune diseases', *International Journal of Molecular Sciences*, 17(6). doi: 10.3390/ijms17060864.

Wang, Y. *et al.* (2019) 'M1 and M2 macrophage polarization and potentially therapeutic naturally occurring compounds', *International Immunopharmacology*, 70, pp. 459–466. doi: 10.1016/j.intimp.2019.02.050.

Waschbisch, A. *et al.* (2016) ' Pivotal Role for CD16 + Monocytes in Immune Surveillance of the Central Nervous System ', *The Journal of Immunology*, 196(4), pp. 1558–1567. doi: 10.4049/jimmunol.1501960.

Weinstock-Guttman, B. *et al.* (2017) 'Two decades of glatiramer acetate: From initial discovery to the current development of generics'. doi: 10.1016/j.jns.2017.03.030.

Wergeland, S. *et al.* (2011) 'Dietary Vitamin D3 Supplements Reduce Demyelination in the Cuprizone Model', *PLoS ONE*. Edited by M. Reindl. Public Library of Science, 6(10), p. e26262. doi: 10.1371/journal.pone.0026262.

Winger, R. C. and Zamvil, S. S. (2016) 'IL-10-dependent Tr1 cells attenuate astrocyte activation and ameliorate chronic central nervous system inflammation', *Brain*, 139(7), pp. 1866–1869. doi: 10.1093/brain/aww121.

Wlodarczyk, A. *et al.* (2015) 'Pathologic and protective roles for microglial subsets and bone marrow- and blood-derived myeloid cells in central nervous system inflammation', *Frontiers in Immunology*, 6(SEP). doi: 10.3389/fimmu.2015.00463.

Woodberry, T. *et al.* (2018) 'The Emerging Role of Neutrophil Granulocytes in Multiple Sclerosis.', *Journal of clinical medicine*. Multidisciplinary Digital Publishing Institute (MDPI), 7(12). doi: 10.3390/jcm7120511.

X., H., Z., J. and G., C. (2014) 'MicroRNAs: New regulators of toll-like receptor signalling pathways', *BioMed Research International*, 2014. doi: 10.1155/2014/945169.

Xie, G. B. *et al.* (2014) 'Evolution of the Mir-155 family and possible targets in cancers and the immune system', *Asian Pacific Journal of Cancer Prevention*, 15(18), pp. 7547–7552. doi: 10.7314/APJCP.2014.15.18.7547.

Xie, Z.-X. *et al.* (2015) 'Role of the Immunogenic and Tolerogenic Subsets of Dendritic Cells in Multiple Sclerosis'. doi: 10.1155/2015/513295.

Xu, L. *et al.* (2003) 'Arginase and autoimmune inflammation in the central nervous system.', *Immunology*. Wiley-Blackwell, 110(1), pp. 141–8. doi: 10.1046/J.1365-2567.2003.01713.X.

Xu, W. *et al.* (2006) 'IL-10–producing macrophages preferentially clear early apoptotic cells', pp. 1–5. doi: 10.1182/blood-2005-10.

Xu, W. D. *et al.* (2012) 'Association of microRNA-146a with autoimmune diseases', *Inflammation*, 35(4), pp. 1525–1529. doi: 10.1007/s10753-012-9467-0.

Yang, Y. *et al.* (2009) 'T-bet is essential for encephalitogenicity of both Th1 and Th17 cells.', *The Journal of experimental medicine*. Rockefeller University Press, 206(7), pp. 1549–64. doi: 10.1084/jem.20082584.

Yang, Z. and Ming, X.-F. (2013) 'Arginase: The Emerging Therapeutic Target for Vascular Oxidative Stress and Inflammation', *Frontiers in Immunology*. Frontiers, 4, p. 149. doi: 10.3389/fimmu.2013.00149.

Yao, Y. *et al.* (2015) 'Neutrophil priming occurs in a sequential manner and can be visualized in living animals by monitoring IL-1β promoter activation', *Journal of immunology (Baltimore, Md. : 1950)*. NIH Public Access, 194(3), p. 1211. doi: 10.4049/JIMMUNOL.1402018.

de Yébenes, V. G., Bartolomé-Izquierdo, N. and Ramiro, A. R. (2013) 'Regulation of B-cell development and function by microRNAs', *Immunological Reviews*, 253(1), pp. 25–39. doi: 10.1111/imr.12046.

Yee, D. *et al.* (2017a) 'MicroRNA-155 induction via TNF-α and IFN-γ suppresses expression of programmed death ligand-1 (PD-L1) in human primary cells', *Journal of Biological Chemistry*, 292(50), pp. 20683–20693. doi: 10.1074/jbc.M117.809053.

Yee, D. *et al.* (2017b) 'MicroRNA-155 induction via TNF-α and IFN-γ suppresses expression of programmed death ligand-1 (PD-L1) in human primary cells', *Journal of Biological Chemistry*, 292(50), pp. 20683–20693. doi: 10.1074/jbc.M117.809053.

Yeung, M. S. Y. *et al.* (2019) 'Dynamics of oligodendrocyte generation in multiple sclerosis', *Nature*, 566(7745), pp. 538–542. doi: 10.1038/s41586-018-0842-3.

Yin, J. *et al.* (2017) 'The Role of Microglia and Macrophages in CNS Homeostasis, Autoimmunity, and Cancer', *Journal of Immunology Research*. Hindawi, 2017. doi: 10.1155/2017/5150678.

Yin, Q. *et al.* (2008) 'B-cell receptor activation induces BIC/miR-155 expression through a conserved AP-1 element.', *The Journal of biological chemistry*. NIH Public Access, 283(5), pp. 2654–62. doi: 10.1074/jbc.M708218200.

Yogev, N. *et al.* (2012) 'Dendritic Cells Ameliorate Autoimmunity in the CNS by Controlling the Homeostasis of PD-1 Receptor+ Regulatory T Cells', *Immunity*, 37(2), pp. 264–275. doi: 10.1016/j.immuni.2012.05.025.

Yong, H. Y. F. *et al.* (2019) 'The benefits of neuroinflammation for the repair of the injured central nervous system', *Cellular & Molecular Immunology*. Nature Publishing Group, p. 1. doi: 10.1038/s41423-019-0223-3.

Zhang, D. *et al.* (2017) 'A comparative study of the characterization of miR-155 in knockout mice', *PLoS ONE*, 12(3). doi: 10.1371/journal.pone.0173487.

Zhang, H. *et al.* (2017) 'Silencing c-Rel in macrophages dampens Th1 and Th17 immune responses and alleviates experimental autoimmune encephalomyelitis in mice', *Immunology and Cell Biology*, 95, pp. 593–600. doi: 10.1038/icb.2017.11.

Zhang, J. *et al.* (2014a) 'MicroRNA-155 modulates Th1 and Th17 cell differentiation and is associated with multiple sclerosis and experimental autoimmune

encephalomyelitis.', *Journal of neuroimmunology*. Elsevier, 266(1–2), pp. 56–63. doi: 10.1016/j.jneuroim.2013.09.019.

Zhang, L. *et al.* (2017) 'The relationship between microRNAs and the STAT3-related signaling pathway in cancer', *Tumor Biology*, 39(7), pp. 1–11. doi: 10.1177/1010428317719869.

Zhang, M. *et al.* (2011) 'MicroRNA-155 may affect allograft survival by regulating the expression of suppressor of cytokine signaling 1', *Medical Hypotheses*, 77(4), pp. 682–684. doi: 10.1016/j.mehy.2011.07.016.

Zhou, H. *et al.* (2010) 'MiR-155 and its star-form partner miR-155* cooperatively regulate type I interferon production by human plasmacytoid dendritic cells', *Blood*, 116(26), pp. 5885–5894. doi: 10.1182/blood-2010-04-280156.

Zhou, X., Li, X. and Wu, M. (2018) 'miRNAs reshape immunity and inflammatory responses in bacterial infection', *Signal Transduction and Targeted Therapy*, 3(1). doi: 10.1038/s41392-018-0006-9.

Zhuang, G. *et al.* (2017) 'A tiny RNA that packs a big punch: The critical role of a viral miR-155 ortholog in Lymphomagenesis in Marek's disease', *Frontiers in Microbiology*, 8(JUN), pp. 1–8. doi: 10.3389/fmicb.2017.01169.

Zostawa, J. *et al.* (2017) 'The influence of sodium on pathophysiology of multiple sclerosis', *Neurological Sciences*. Springer Milan, 38(3), pp. 389–398. doi: 10.1007/s10072-016-2802-8.

van Zwam, M. *et al.* (2011) 'Myelin ingestion alters macrophage antigen-presenting function in vitro and in vivo', *Journal of Leukocyte Biology*, 90(1), pp. 123–132. doi: 10.1189/jlb.1209813.

Chapter 8

Appendix

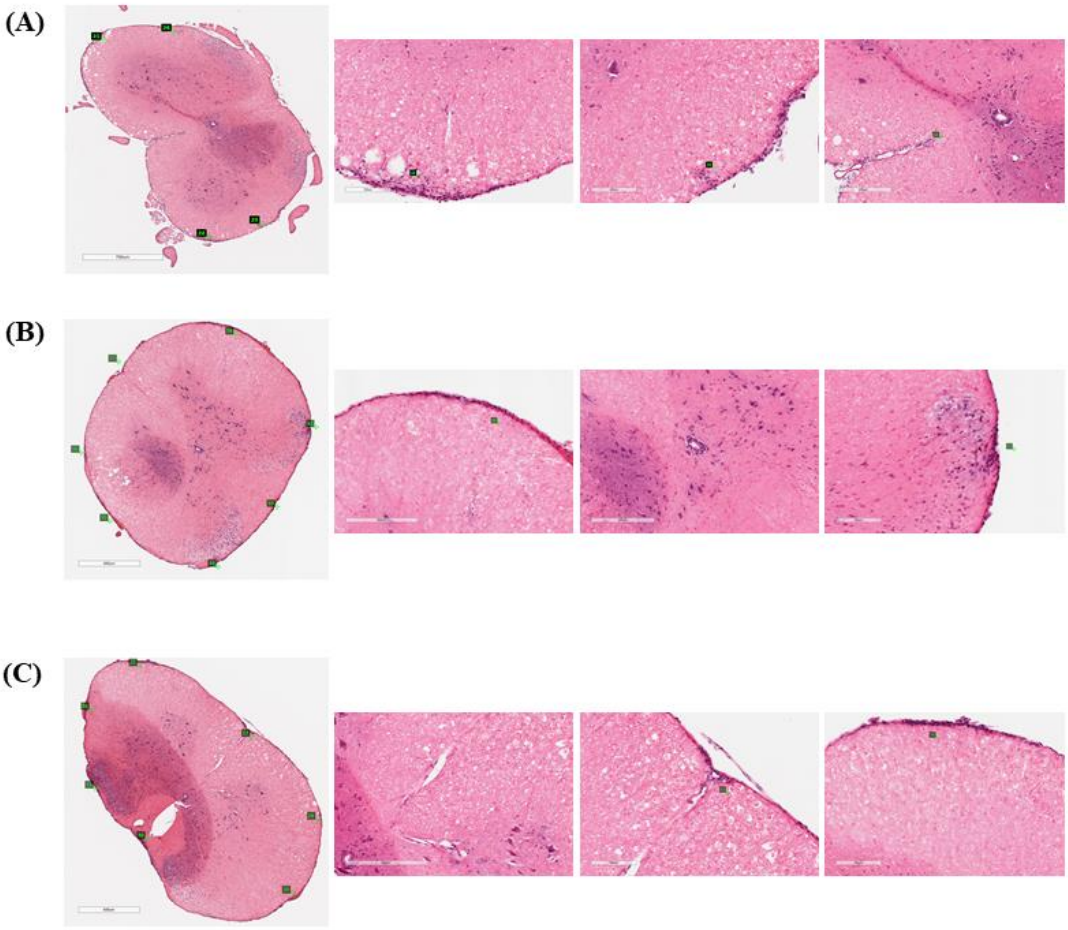
(A)
(B)
(C)

Mouse Strain	Mouse number	Clinical score	Section number	Description
MiR-155$^{fl/fl}$ x LysMCre	4	1.5	A	<50% spinal cord circumference displays immune cell accumulation at meninges Immune cell infiltration at the central canal and anterior blood vessels Slight immune cell infiltration into parenchyma white matter regions
			B	Immune cell accumulation in meninges surrounding the entire section Slight infiltration into parenchyma at dorsal white matter regions Immune cells present at central canal
			C	Spinal cord circumference displays immune cell accumulation at meninges Immune cell infiltration at the central canal and anterior blood vessels Immune cell into parenchyma at dorsal white matter regions

Supplementary figure 1: Histological analysis of miR-155$^{fl/fl}$ x LysMCre 4 spinal cord section.

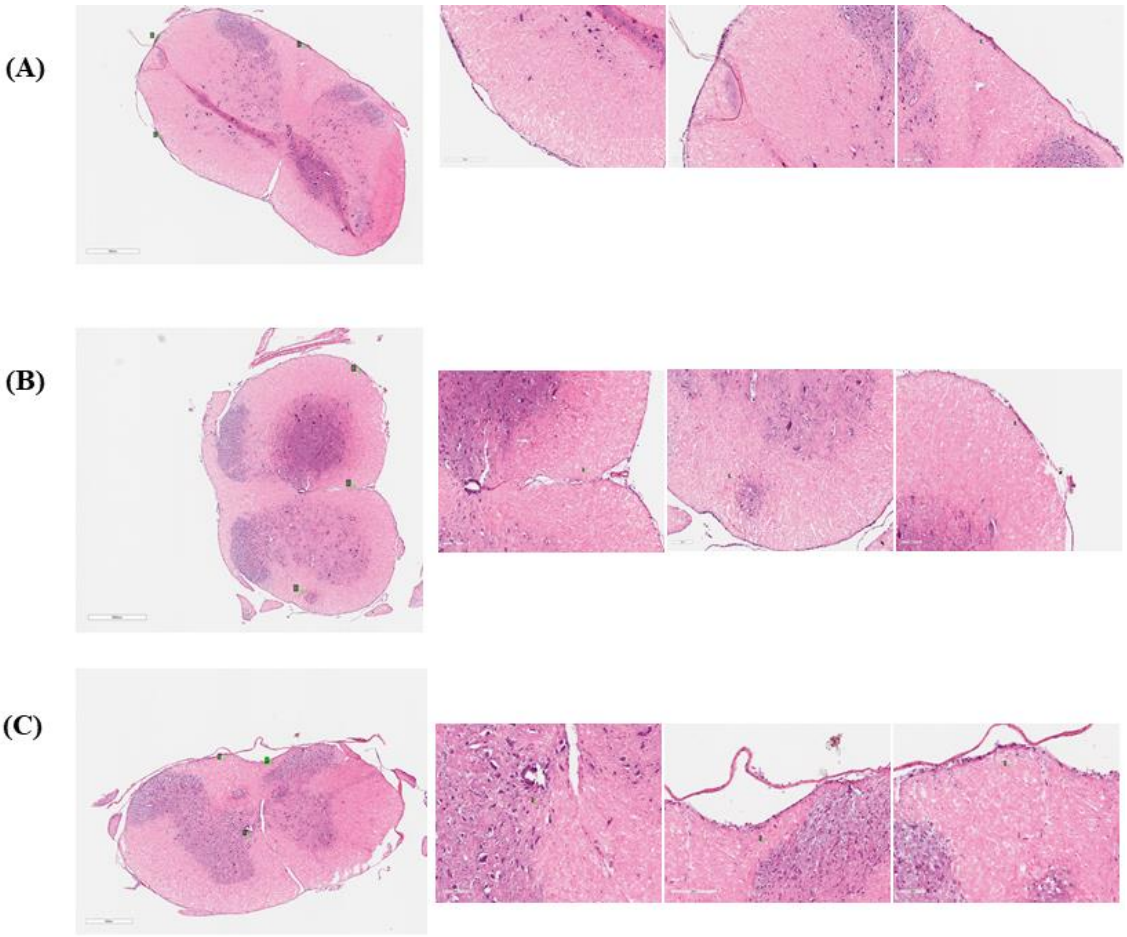
(A)
(B)
(C)

Mouse Strain	Mouse number	Clinical score	Section number	Description
MiR-155$^{fl/fl}$ x LysMCre	1	0	A	Spinal cord circumference displays immune cell accumulation at meninges Meningeal accumulation of white blood cells Slight immune cell infiltration at white matter parenchyma regions
			B	Immune cell accumulation in meninges surrounding <50% of section Immune cells accumulating at blood vessels located in ventral region – immune cells at central canal Need to confirm with LFB as out of focus
			C	Spinal cord circumference displays immune cell accumulation at meninges Immune cell infiltration at the central canal

Supplementary figure 2: Histological analysis of miR-155$^{fl/fl}$ x LysMCre 1 spinal cord section.

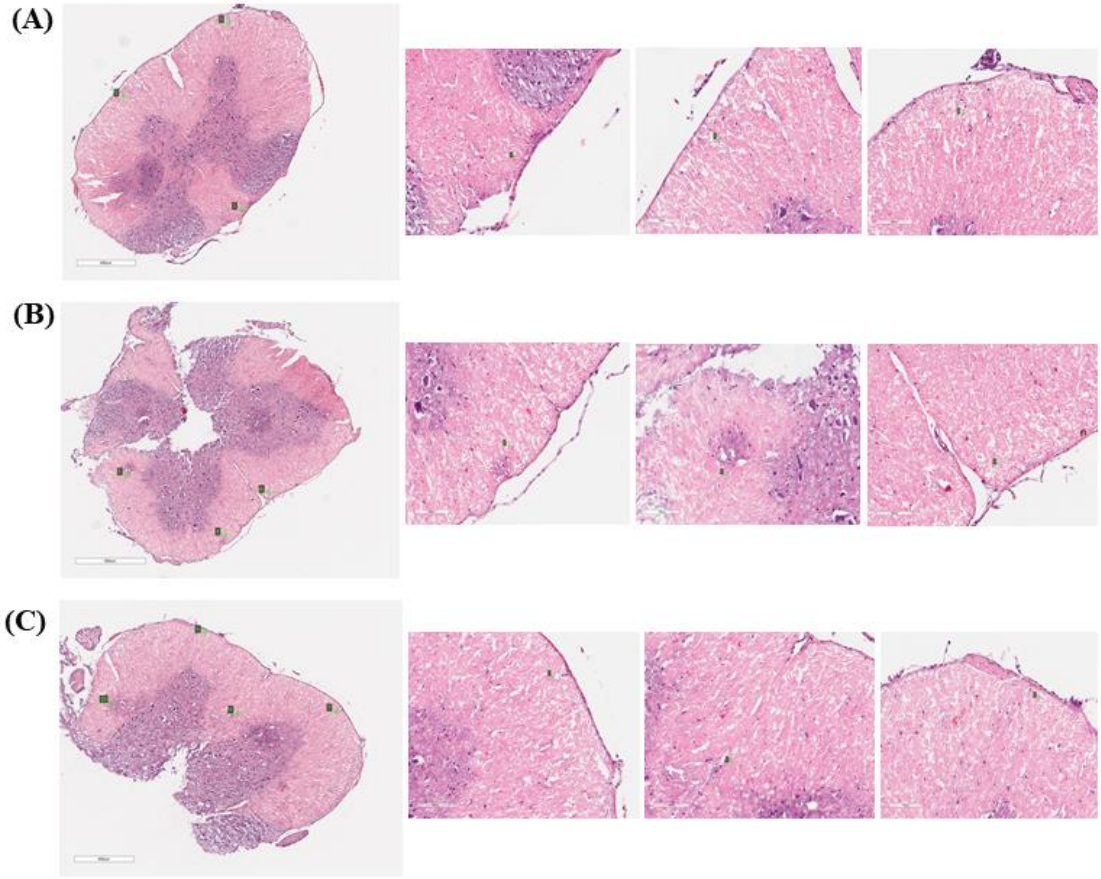
(A)
(B)
(C)

Mouse Strain	Mouse number	Clinical score	Section number	Description
MiR-155$^{fl/fl}$ x LysMCre	2	0	A	Spinal cord circumference displays <50% immune cell accumulation at meninges No early signs of parenchyma infiltration from meningeal regions
			B	Immune cell accumulation in meninges Early signs of parenchyma infiltration from meninges Suspected lesion located in white matter between dorsal and ventral region Immune cells accumulating at blood vessels located in ventral region
			C	<50% Immune cell accumulation in meninges Early signs of parenchyma infiltration from meninges Immune cells accumulating at blood vessels located in ventral region Lesion located in white matter dorsal region adjacent to grey matter

Supplementary figure 3: Histological analysis of miR-155$^{fl/fl}$ x LysMCre 2 spinal cord section.

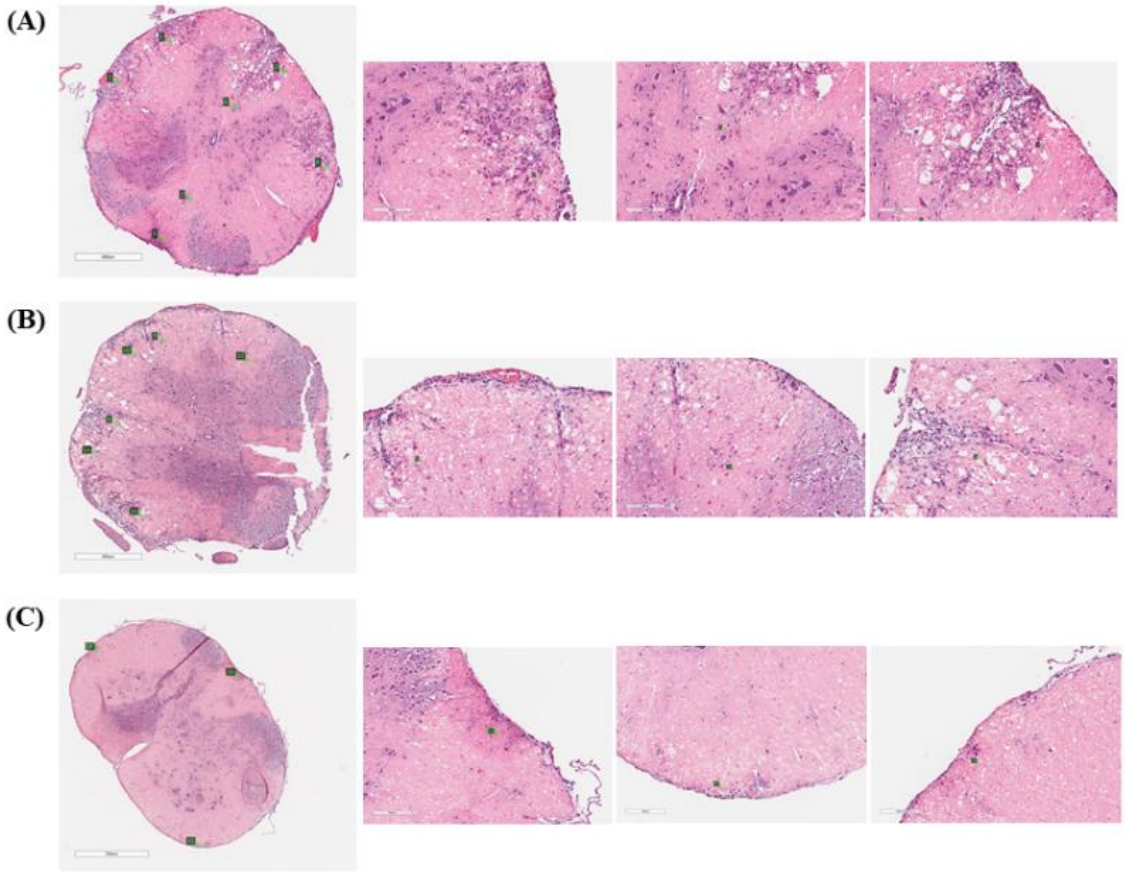
(A)
(B)
(C)

Mouse Strain	Mouse number	Clinical score	Section number	Description
LysMCre control	6	2.5	A	Spinal cord circumference displays immune cell accumulation at meninges in entire section Mass signs of parenchyma infiltration from meningeal regions – certain areas reaching grey matter Abundant immune cell infiltration at blood vessels and central canal
			B	Immune cell accumulation at meninges in entire section Mass signs of parenchyma infiltration from meninges Suspected lesions located in white matter Infiltrating immune cells at blood vessels accumulating at into parenchyma regions from grasile fascic and vent med fiss
			C	<50% Immune cell accumulation in meninges Early signs of parenchyma infiltration from meninges Evident immune cells accumulating at blood vessels located in ventral region

Supplementary figure 4: Histological analysis of LysMCre control 6 spinal cord section.

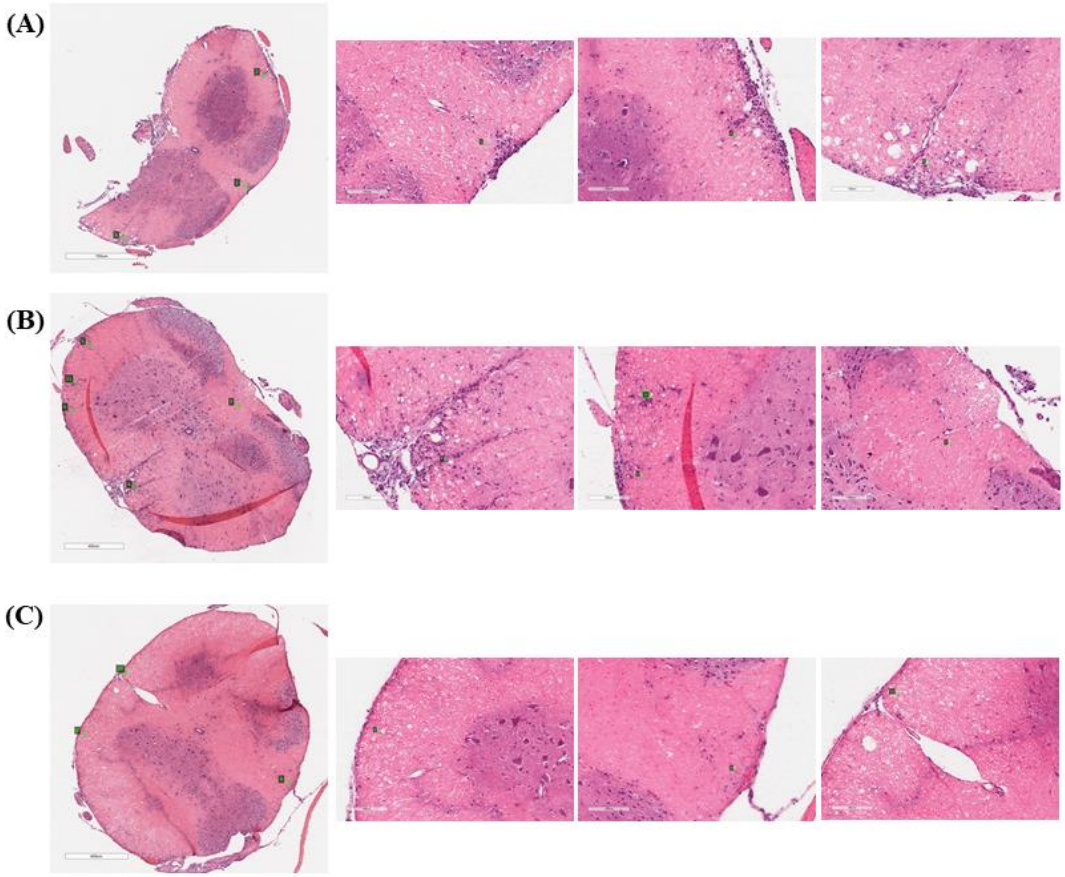
(A)
(B)
(C)

Mouse Strain	Mouse number	Clinical score	Section number	Description
LysMCre control	4	1.5	A	Spinal cord circumference displays immune cell accumulation at meninges Parenchyma infiltration from meningeal regions Immune cell accumulation at blood vessels and central canal
			B	Immune cell accumulation at meninges in <50% Mass signs of parenchyma infiltration from meninges Suspected lesion located in white matter ventral Infiltrating immune cells at blood vessels Accumulating immune cells infiltrating into parenchyma regions from vent med fiss and ventral funiculus regions
			C	Entire section contains immune cell accumulation in meninges Early parenchyma infiltration from meninges – suspect lesion

Supplementary figure 5: Histological analysis of LysMCre control 4 spinal cord section.

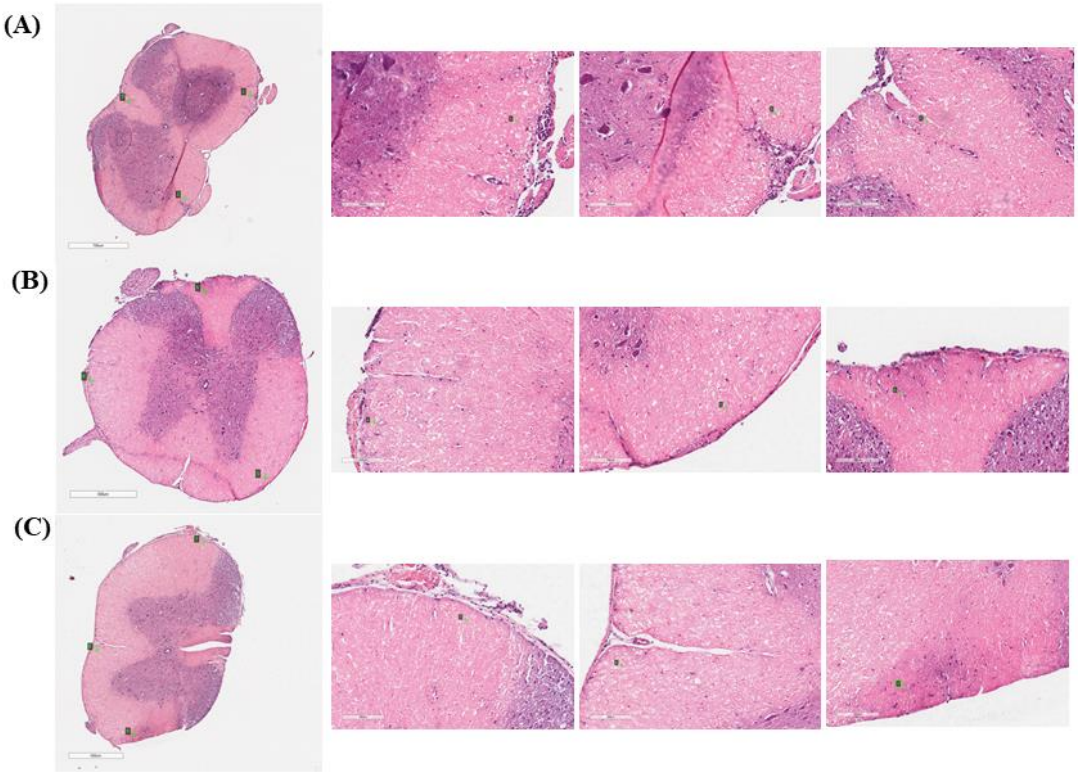
(A)
(B)
(C)

Mouse Strain	Mouse number	Clinical score	Section number	Description
LysMCre control	1	0	A	Spinal cord circumference displays immune cell accumulation at meninges <50% Parenchyma infiltration from meninges in ventral region Immune cell present at blood vessels at ventral funiculus and central canal
			B	Immune cell accumulation at meninges <50% - however not dense No signs of parenchyma infiltration from meninges
			C	Immune cell accumulation in meninges present though not dense No signs of parenchyma infiltration from meninges

Supplementary figure 6: Histological analysis of LysMCre control 1 spinal cord section.

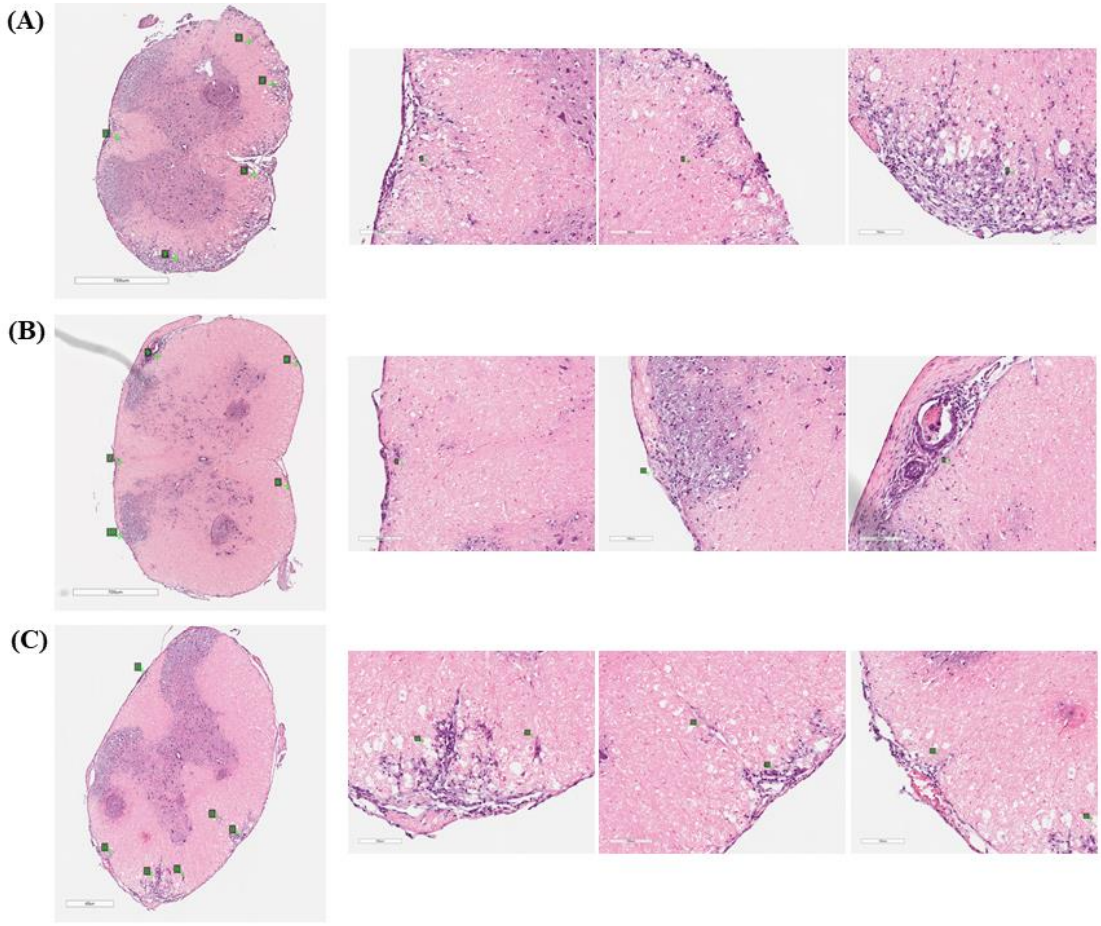
(A)
(B)
(C)

Mouse Strain	Mouse number	Clinical score	Section number	Description
MiR-155$^{fl/fl}$ x LysMCre	5	2	A	Entire Spinal cord circumference displays immune cell accumulation at meninges
				Parenchyma infiltration from meninges in multiple white matter ventral and dorsal regions
				Immune cell present at blood vessels at ventral funiculus and central canal
				Lesion at ventral white matter
			B	Immune cell accumulation at meninges <50%
				Parenchyma infiltration from meninges white matter
				Parenchyma infiltration from meninges at white matter towards grey matter located at dorsal regions
				Mass infiltration at dorsal root and parenchyma in ventral region
			C	Immune cell accumulation in meninges present over entire section
				Multiple signs of parenchyma infiltration from meninges in both dorsal and ventral regions
				Suspected lesion in white matter ventral region
				Accumulating immune cells at blood vessels and central canal

Supplementary figure 7: Histological analysis of miR-155$^{fl/fl}$ x LysMCre control 5 spinal cord section.

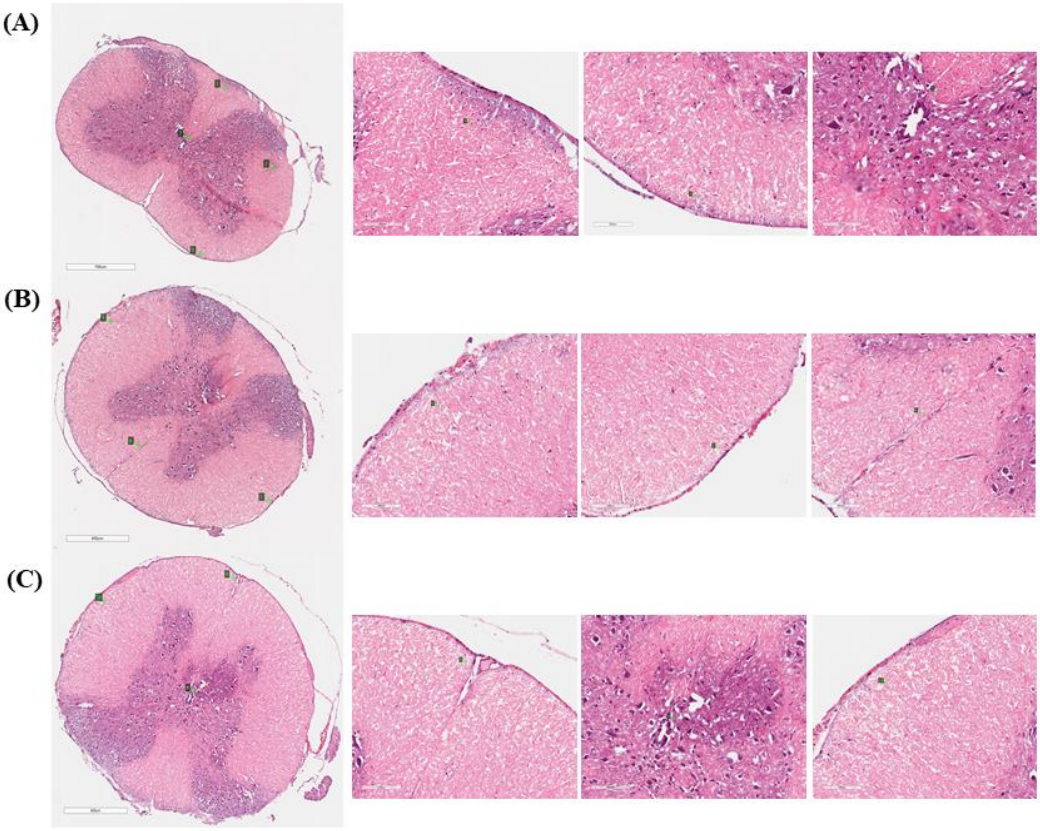
(A)
(B)
(C)

Mouse Strain	Mouse number	Clinical score	Section number	Description
MiR-155$^{fl/fl}$ x LysMCre	3	0	A	Spinal cord circumference displays random immune cell accumulation at meninges – though not dense No signs of parenchyma infiltration from meninges Immune cells present at central canal
			B	Spinal cord circumference displays immune cell accumulation at meninges – though not dense No signs of parenchyma infiltration from meninges Immune cells present at central canal Cells present at vent med fiss region
			C	Spinal cord circumference displays immune cell accumulation at meninges – though not dense No signs of parenchyma infiltration from meninges Immune cells present at central canal Cells present at vent med fiss region

Supplementary figure 8: Histological analysis of miR-155$^{fl/fl}$ x LysMCre 3 spinal cord section.

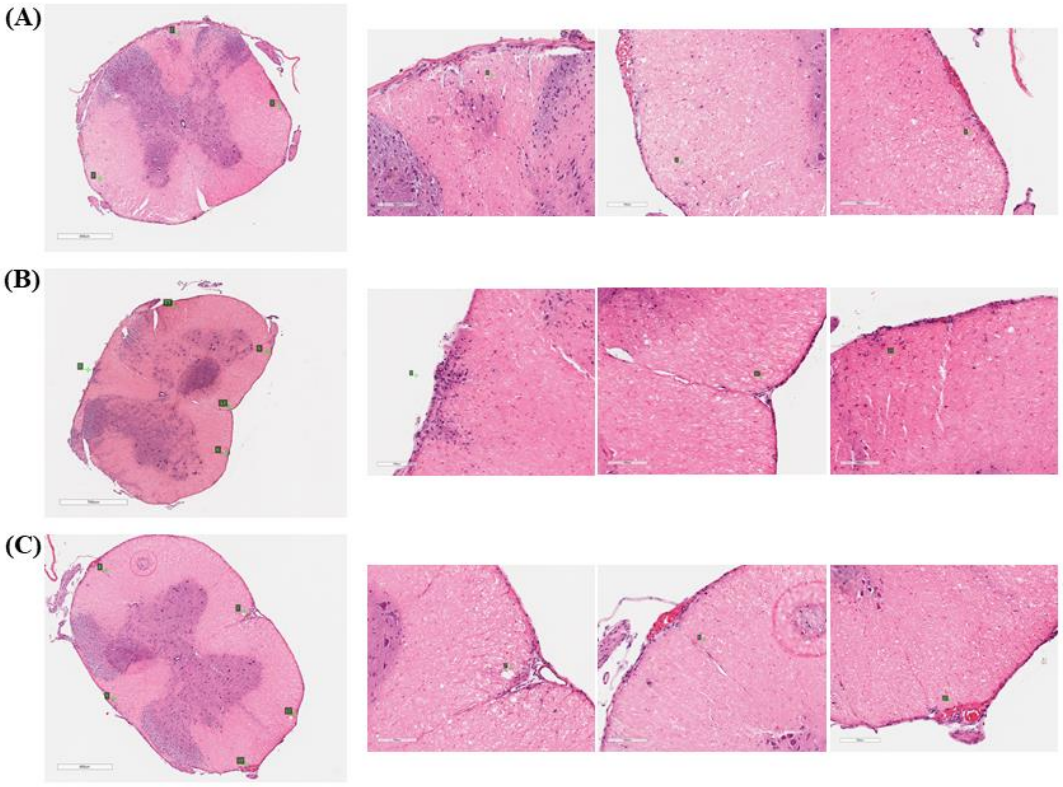
(A)
(B)
(C)

Mouse Strain	Mouse number	Clinical score	Section number	Description
LysMCre control	3	0.5	A	Spinal cord contains immune cell accumulation at meninges Lesion in parenchyma white matter dorsal region Slight/early signs of parenchyma infiltration from meninges Immune cells present at central canal
			B	Spinal cord circumference displays immune cell accumulation at meninges Multiple signs of parenchyma infiltration from meninges Immune cells present at central canal Possible lesion next to meninges in ventral region
			C	Spinal cord circumference displays immune cell accumulation at meninges Immune cell infiltration into parenchyma from vent med fiss Immune cells accumulating in blood vessel between dorsal and ventral region Early/slight signs of cell infiltration from meninges into parenchyma Cell infiltration into parenchyma from meninges

Supplementary figure 9: Histological analysis of LysMCre control 3 spinal cord section.

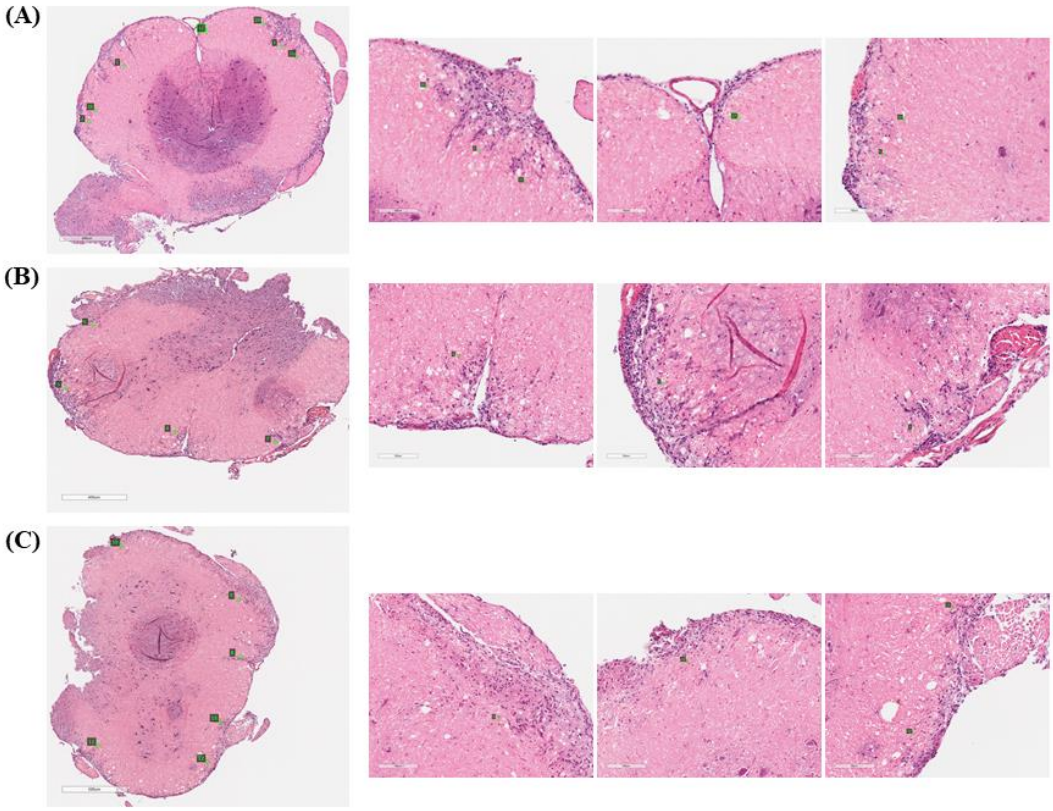
(A)
(B)
(C)

Mouse Strain	Mouse number	Clinical score	Section number	Description
LysMCre control	4	1.5	A	Mass infiltration into parenchyma from meninges surrounding both dorsal and ventral regions of spinal cord section Suspected lesions in parenchyma white matter – difficult to differentiate from parenchyma infiltration Slight signs of parenchyma infiltration from vent med fiss region Immune cells present at central canal
			B	Suspect lesion from meningeal derived parenchyma infiltration in dorsal region Multiple signs of parenchyma infiltration from meninges No. 5, 6 Immune cells present at central canal Vent med fiss infiltration into parenchyma
			C	Spinal cord circumference displays immune cell accumulation at meninges Immune cell infiltration into parenchyma from vent med fiss Immune cells accumulating in blood vessel between dorsal and ventral region Early/slight signs of cell infiltration from meninges into parenchyma Cell infiltration into parenchyma from meninges

Supplementary figure 10: Histological analysis of LysMCre control 4 spinal cord section.

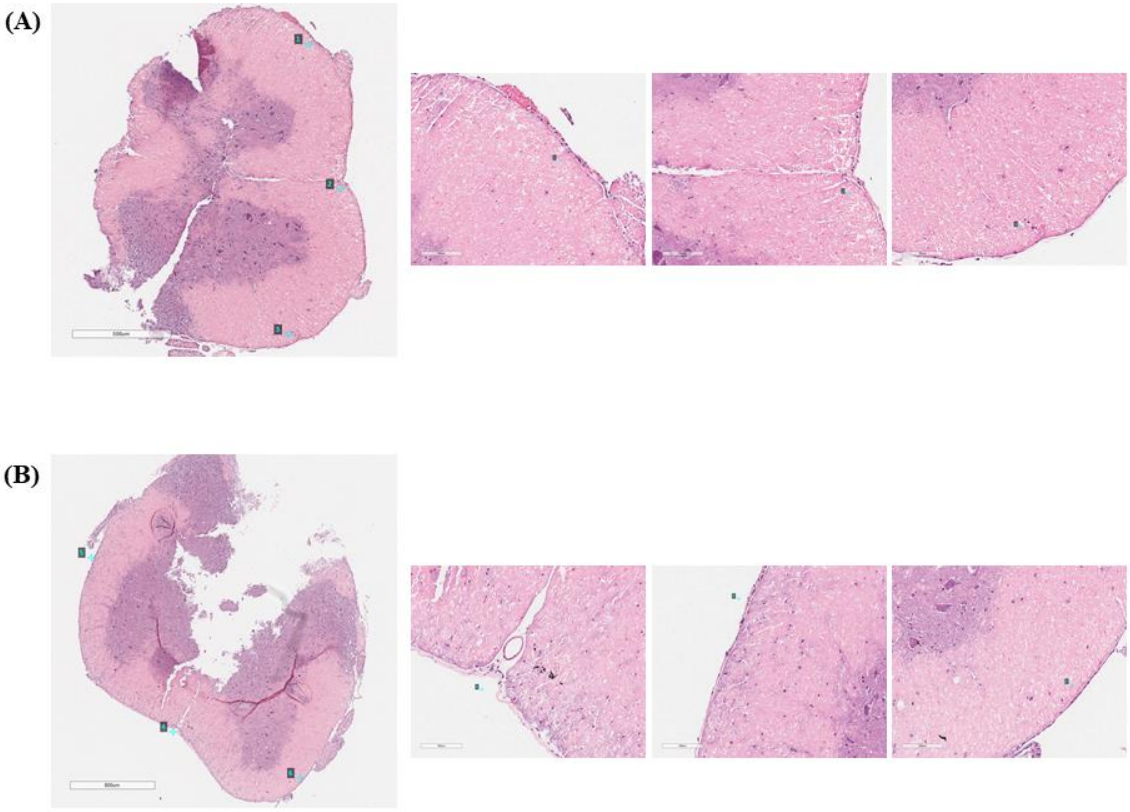
(A)
(B)

Mouse Strain	Mouse number	Clinical score	Section number	Description
LysMCre control	2	0.5	A	Minor accumulation of cells at meninges – random locations surrounding spinal cord No parenchyma region infiltration
			B	Accumulation of immune cells at meninges – though not dense Immune cells present at meninges near vent med fiss but no signs of infiltration into parenchyma

Supplementary figure 11: Histological analysis of LysMCre control 2 spinal cord section.